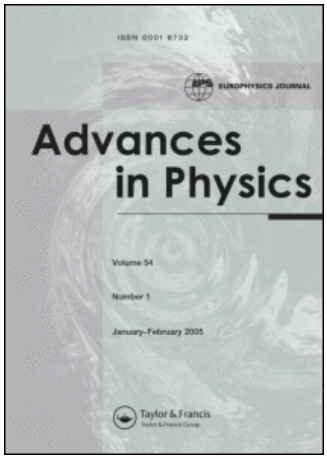

Advances in Physics
Publication details, including instructions for authors and subscription information:
http://www.informaworld.com/smpp/title~content=t713736250

Origins of scale invariance in growth processes

Joachim Krug [ab]
[a] Institut für Festkörperforschung, Forschungszentrum Jülich, Jülich, Germany
[b] Fachbereich Physik, Universität-Gesamthochschule Essen, Essen, Germany

Online Publication Date: 01 April 1997
To cite this Article: Krug, Joachim (1997) 'Origins of scale invariance in growth processes', Advances in Physics, 46:2, 139 - 282
To link to this article: DOI: 10.1080/00018739700101498
URL: http://dx.doi.org/10.1080/00018739700101498

ADVANCES IN PHYSICS, 1997, VOL. 46, NO. 2, 139–282

Origins of scale invariance in growth processes

By JOACHIM KRUG†
Institut für Festkörperforschung, Forschungszentrum Jülich,
D-52425 Jülich, Germany

[Accepted 16 January 1996]

Abstract

This review describes recent progress in the understanding of the emergence of scale invariance in far-from-equilibrium growth. The first section is devoted to 'solvable' needle models which illustrate the relationship between long-range competition mediated, for example, through shadowing or a Laplacian field, and scale invariance. The following three sections, which comprise the bulk of the article, develop the theory of kinetic surface roughening in a comprehensive manner. The two large classes of kinetic roughening processes, characterized by non-conserved (Kardar–Parisi–Zhang) and conserved (ideal molecular beam epitaxy (MBE)) surface relaxation, respectively, are treated separately. For the former case, which has been extensively reviewed elsewhere, the focus is on recent developments. For the case of ideal MBE we give a systematic derivation of the various universality classes in terms of microscopic processes, and compare the predictions of continuum theory to computer simulations and experiments.

Contents

†Present and permanent address: Fachbereich Physik, Universität-Gesamthochschule Essen, D-45117 Essen, Germany.

Haben Sie schon gesehn in was für Figuren die Schwämme auf dem Boden wachsen? Wer das lesen könnt. Georg Büchner, Woyzeck, 8. Szene.

1. Introduction

The study of growth processes has always constituted, explicitly or implicitly, an integral part of solid state physics and materials science. Indeed, most properties of real materials depend crucially on the presence of imperfections—bulk vacancies, dislocations, surface and interface roughness—that are remnants of the non-equilibrium conditions under which the material has formed. Over the centuries the art and science of crystal growth has progessed to ever more closely approximate the ideal of a perfect, crystalline solid, as evidenced impressively by modern techniques such as molecular beam epitaxy (MBE), which allow for the engineering of solid state devices at the level of individual atomic planes. Nevertheless, the success of this and other techniques depends crucially on the ability to control the disordering effects of the non-equilibrium growth conditions, and to assess, at least empirically, the relationship between the growth conditions and the resulting structure.

Apart from its eminent technological significance, the growth of solids is of considerable fundamental interest, since it may provide us with important clues to the way in which complex structures form in Nature, through the agglomeration of simple, microscopic processes operating in a highly disordered, noisy environment. This aspect was dramatically brought to the attention of the theoretical physics community in 1981, with the invention of the diffusion-limited aggregation (DLA) model by Witten and Sander [1], which has since been found to describe a wide variety of naturally occurring patterns [2, 3]. To add to the excitement, it was found that the structures generated by DLA and related models typically show spatial *scale invariance*, thus requiring for their quantitative characterization the notions of fractal geometry pioneered by Mandelbrot [4]. Mandelbrot has presented a vast amount of empirical evidence in support of his thesis that fractal structures occur quite commonly in Nature, as the outcome of many complex physical, geological, biological and even social processes. As has been remarked by Kadanoff [5] and others, Mandelbrot's observation raises a fundamental scientific problem insofar as not many *mechanisms* are known that could account for the genericity of scale invariant behaviour.

The problem was posed in more pointed form in 1987 by Bak, Tang and Wiesenfeld [6], who suggested the concept of *self-organized criticality* (SOC) as a framework within which to formulate general principles that are responsible for scale invariance in nature. The term is motivated by viewing the ubiquity of scale invariant behaviour against the background of equilibrium statistical mechanics, where scale invariance is associated, since the advent of the renormalization group, with critical point phenomena. Given that in nature no experimenters are available to tune systems to their critical points, the argument goes that natural systems can show scale invariance only if they tune themselves, as it were, through some kind of self-organization mechanism. While this line of reasoning is appealing and has stimulated a tremendous amount of work on extended non-equilibrium systems, it should be kept in mind that the association of scale invariance with critical point behaviour has its roots in a somewhat arbitrary historical development, in which equilibrium critical phenomena happened to provide the first example of non-trivial scale invariance that could be understood on a fundamental level. There is no guarantee

that the analogy with critical phenomena will serve as a reliable guide when venturing into the vast unknown territory of scale invariance far from equilibrium.

With hindsight, it appears rather unlikely that principles of the generality originally envisioned by Bak and co-workers [6] will be found at the origin of all, or even a significant fraction of, instances where scale invariance is encountered in natural processes. Consequently, workers in the field now tend to reserve the term SOC to describe a more specific class of mechanisms which produce scale invariance through a separation of time scales between driving and relaxation (as, for example, in earthquakes; see [7]). Nevertheless, growth processes such as DLA (and other, less spectacular examples which will form the main part of this review) come quite close to fulfilling the requirements for a robust, ubiquitous mechanism for scale-invariant behaviour: non-equilibrium growth processes are involved in the formation of virtually any natural structure; they can be classified according to some broad characteristics such as the presence of a Laplacian field (as in DLA), the presence of a well defined growth interface with approximately local dynamics (in kinetic roughening phenomena, see below), symmetries, conservation laws, etc., and for many such classes it is possible to formulate simple models and theories that can be used to extract quantitative, sometimes universal information about the scale-invariant structures that form.

This article describes some recent progress in our understanding of how scale-invariant structures emerge through far-from-equilibrium growth processes. Since exhaustive reviews [2, 3, 8–12] and concise summaries [13–17] of various aspects of the subject are available, the emphasis here will be on a comprehensive and systematic development of a few key concepts. Simplicity is favoured over generality; priority is given to elementary arguments based on scaling ideas and dimensional analysis, which provide the maximum yield in terms of intuitive insights. No attempt has been made to remove the unavoidable bias introduced by the author's interests and contributions into the selection and weighting of topics. It is hoped that this shortcoming is partly compensated by the extensive bibliography.

1.1. *Outline*

It is evident already from a superficial look at a growth process like DLA that the *competition* between different parts of the growing structure plays a central role in developing long-ranged spatial correlations and scale invariance. Of course, it is an altogether different matter to turn this qualitative insight into a quantitative theory. Section 2 is devoted to a restricted class of *needle models for competitive growth* which allow a detailed analysis of the relation between competition and scale invariance. Competition mediated by a Laplacian field (as in DLA) as well as through geometric shadowing will be considered, and special attention will be paid to the role of fluctuations and the extent of universality of the resulting scaling properties. Sections 2.1 and 2.2 mainly summarize results that have been presented in detail elsewhere, while the discussion of the shadowing instability (section 2.3) and Laplacian needle growth (section 2.4) considerably extends the brief published accounts.

The main part of the article—sections 3, 4 and 5—deals with growth processes that can be reduced to the motion of a well-defined interface with approximately local dynamics. This explicitly excludes diffusion-limited growth, but includes many technologically relevant vapour deposition techniques. In this case scale-invariant behaviour appears in the form of *kinetically induced surface roughness* [8, 10–15]. The

underlying mechanism is the interaction of microscopic fluctuations with the slow dynamics of the long-wavelength interface degrees of freedom.

The basic concepts are introduced in section 3, in a (hopefully!) pedagogical manner. The starting point is that of macroscopic interface equations of motion, derived from thermodynamic and kinetic considerations in the spirit of the classic work of Mullins [18]. Special attention is paid to terms in the equations which originate from the non-equilibrium character of the process. Two types of terms are generally encountered—*kinematic* terms (such as the celebrated Kardar–Parisi–Zhang (KPZ) nonlinearity [19]) that appear simply because the interface is moving, and *dynamic* terms that reflect changes in the interface relaxation processes due to the non-equilibrium conditions. Terms of the latter type play an important role in the description of crystal growth from atomic beams [20].

Given a macroscopic interface equation of motion, a continuum theory of kinetic roughening is obtained by adding appropriate noise terms that describe the (equilibrium or non-equilibrium) fluctuations in the problem. In section 3, this will be carried out at the level of *linear* fluctuation theory. While mathematically undemanding, the linear theory already contains most key features of kinetic roughening phenomena; moreover, as will be explained in section 3.4, physically relevant situations exist in which the linear theory is exact.

In sections 4 and 5, the discussion is specialized to two broad classes of kinetic roughening phenomena, which can be distinguished according to whether or not the surface relaxation processes conserve the volume of the growing structure. The generic description for *non-conserved* dynamics is provided by the Kardar–Parisi–Zhang equation introduced in 1986 [19]. In view of the extensive accounts that have appeared during the last few years [8, 10–12, 14], only the most important properties of the equation—tilt invariance, the fluctuation–dissipation theorem, and the mapping to directed polymers in random media—will be presented in section 4. The remainder of the section describes some recent developments which have not been summarized previously, notably the topics of amplitude universality, finite size effects, chaotic interfaces and inhomogeneous growth.

Conserved growth equations apply to MBE-type vapour deposition processes, where desorption of material from the surface, as well as the formation of bulk defects can be neglected. They represent a distinct class of kinetic roughening phenomena, which has been the focus of much activity over the last five years. Section 5 attempts to provide a unified picture of the current understanding of these processes. The central goal will be to identify the microscopic mechanisms underlying the relevant dynamic non-equilibrium terms in the large scale description; most of the material presented here has not been published previously. Since one of the main motivations for these studies has been to more closely approximate the conditions under which epitaxial growth is actually conducted in the laboratory, section 5 also contains a preliminary assessment of pertinent experiments. A remarkable recent development in this area is the discovery of generically *unstable growth*, a non-stochastic disordering mechanism which gives rise to surfaces that are rough but not scale invariant (see sections 5.3 and 5.6.2).

The sections are written such as to be reasonably self-contained. Each main section contains a few introductory paragraphs that place it into the general context. In particular, section 2 is largely independent of the rest of the article. While section 3 is a prerequisite for the discussions in sections 4 and 5, readers who have some

familiarity with kinetic roughening phenomena should be able to turn directly to the last two sections.

2. Competitive growth

In this section a sequence of models is introduced, in which one-dimensional (1D) structures ('needles') grow from linear or planar substrates and interact through some kind of screening or shadowing mechanism. We shall investigate in detail how the competition gives rise to a scale-invariant power law distribution of needle heights

$$N(h) \sim h^{-\gamma}, \tag{2.1}$$

and, correspondingly, a density profile

$$n(h) = \int_h^\infty \mathrm{d}h\, N(h) \sim h^{-(\gamma-1)}, \tag{2.2}$$

both relations being understood to hold for the frozen, stationary structure which evolves after a long time; in some cases the power laws are modified by logarithmic corrections. The models are discussed in the order of increasing complexity of the competition mechanism, which ranges from unidirectional geometric shadowing to Laplacian (that is, electrostatic) screening.

While the models are mainly motivated by their simplicity and should not be expected to precisely describe any specific system, physical situations are conceivable in which the competing structures are, to a good approximation, linear, and insights gained from the study of needle models could prove useful. Examples are patterns of linear cracks driven into a solid by thermal shock [21, 22], arrays of dendritic side branches [23, 24] and polymer brushes [25].

2.1. *Ballistic deposition at oblique incidence*

Ballistic deposition is a simple model for the growth of amorphous thin films at low temperatures [26]. In this model, particles are released at random positions above the surface and move towards the deposit along straight line ('ballistic') trajectories which form a fixed angle θ with the substrate normal. Corresponding to the assumption of low temperature and, hence, negligible atomic mobility, the particles stick permanently at the point of first contact with the deposit. It has long been recognized [27] that the structures grown by this simple rule attain a characteristic *columnar* morphology when the deposition angle θ is increased towards the limit of grazing incidence, $\theta \to 90°$ (figure 1). The deposit breaks up into columns which grow more or less independently of each other and interact only through geometric shadowing. The columns are needle-shaped in the case of growth from a 1D (linear) substrate, and have a sheet-like structure when grown from a plane [28, 29]. Much experimental interest has focused on the growth angle of the columns, which is distinct from the angle of deposition [27]. In fact this angle is related to the angular dependence of the deposit density [30], and can be computed in a mean-field approximation [31].

A closer look at figure 1 suggests the idealization depicted in figure 2: the columns are replaced by needles which grow independently by the accretion of flux at their tips. In this view, the competition is seen to be *noise driven*: while the average growth rate is the same for all needles, the shot noise in the particle flux makes it possible for some needles to temporarily grow ahead of their neighbours. Once a needle has been

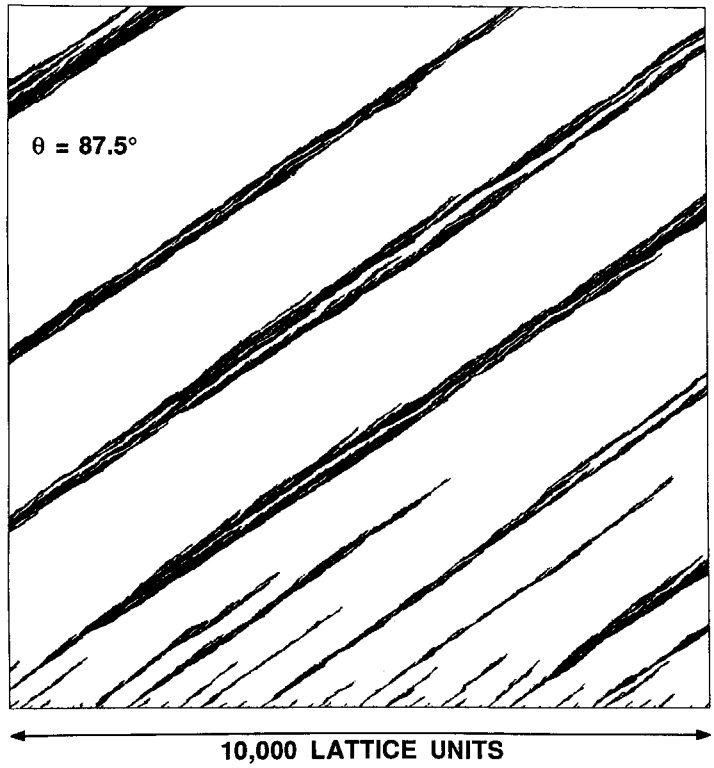

Figure 1. Lattice simulation of ballistic deposition onto a 1D substrate. Particles enter from the right, following trajectories which form an angle of 87·5° with respect to the surface normal. In this particular model the columns (black) grow at an angle of about 52° relative to the normal. The picture shows part of a larger system. (Courtesy of Paul Meakin.)

completely shaded, it is forever excluded from further growth: the competition mechanism is *exclusive* in the sense that needles are either completely unaffected by the presence of others (the *active* state), or else completely shaded.

These qualitative considerations can be turned into precise predictions by exploiting the mapping [32] to coalescing random walks indicated in figure 2. The positions of the active needle tips are projected onto a line perpendicular to the substrate, and are interpreted as the positions of point particles. Owing to the growth of the needles, the particles have an (unessential) constant upward drift, superimposed by independent random walks. The shading of one needle by another corresponds to the coalescence of the walkers. The crucial advantage of this mapping, then, is that the *non-local* geometric shadowing interaction between needles is turned into a *local* contact interaction among random walkers.

An elementary property of coalescing random walks is that their average distance increases with time t as $\sqrt{t}$. This is simply a consequence of the fact that, apart from the contact interactions, the walkers are independent: after a time t, a *free* walker has explored a region of size $\sqrt{t}$; in the presence of other walkers, it can survive up to time t only if it has depleted a region of that size around it. Similarly, in the needle model, the height fluctuations of an active needle grow with time t or, equivalently,

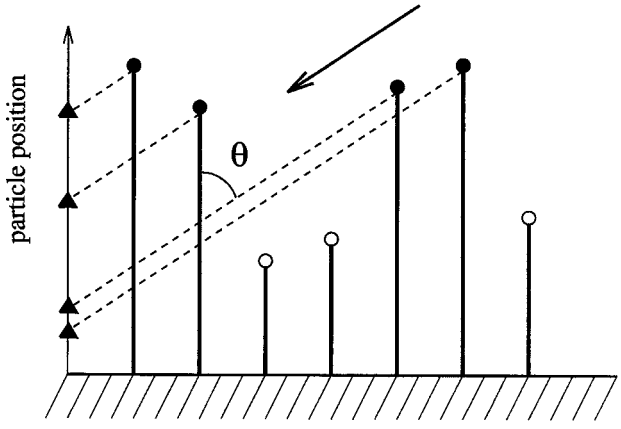

Figure 2. Schematic of the needle model for oblique incidence ballistic deposition. Active (shaded) needles are identified by full (open) tips. The arrow shows the direction of the beam incident at an angle θ. The broken lines indicate the mapping of the active tip positions onto coalescing particles which are represented by triangles.

with height h as $\delta h \sim \sqrt{h}$. Through the geometric shadowing mechanism this vertical length scale is translated into a horizontal *shadowing length* $\xi(h) \sim \delta h$ over which a surviving needle of height h is expected to have shaded other needles. The density at height h can then be estimated as $n(h) \sim 1/\xi(h) \sim h^{-1/2}$, so $\gamma = 3/2$ in equation (2.1).

More precisely, the mapping to coalescing random walks yields the following expression for the asymptotic fraction of surviving needles [32, 33],

$$\rho(t) \approx \cot\theta/(\pi t)^{1/2}. \tag{2.3}$$

Since shaded needles stop growing entirely, only those which are active at time t contribute to the density profile for $h \geq h_a(t)$, where $h_a(t)$ denotes the average height of active needles. We therefore have the identity

$$\rho(t) = n(h_a(t)), \tag{2.4}$$

and, since $h_a(t) = t$ in the present case (unit deposition rate),

$$N(h) = -\frac{dn}{dh} \approx \frac{\cot\theta}{2\sqrt{\pi}} \frac{1}{h^{3/2}}. \tag{2.5}$$

Equation (2.4) expresses a particularly simple relation between the dynamics of competition—as described by the survivor density ρ—and the scaling of the frozen structure; the relation is a consequence of the exclusive nature of shadowing in the present model, and can only be approximately generalized to other situations. At some finite time t the height distribution is a superposition of the distribution of shaded needles, which follows equation (2.5) up to $h \approx h_a(t)$, and a Gaussian of width $\sim\sqrt{t}$ and total weight $\rho(t)$, centred around $h_a(t)$, which contains the active part of the population; of course in a finite system eventually a state is reached in which only a single needle is growing [32].

Within the idealized needle model, the value $\gamma = 3/2$ is evidently *universal*, i.e. it is independent of deposition angle, growth rate, etc. [33]. The needle model also seems to give an accurate description of several versions of the full ballistic deposition problem, provided θ is chosen sufficiently large to ensure the formation

of well separated columns [31, 32]. In the full problem it is more natural to consider the distribution of column masses s, rather than heights h. The two are related as follows [32]. The shape of individual columns is characterized by exponents, $\nu_\parallel$, $\nu_\perp$, which describe how their height h and width w scale with mass, $h \sim s^{\nu_\parallel}$ and $w \sim s^{\nu_\perp}$. The mass distribution is therefore given by

$$N(s) = \frac{\mathrm{d}h}{\mathrm{d}s} N(h) \sim s^{-\tau}, \tag{2.6}$$

with $\tau = 1 + \nu_\parallel(\gamma - 1)$. For processes like ballistic deposition, where both the individual columns and the deposit as a whole are compact, we also have the general relation [34] $\nu_\parallel = 2 - \tau$. Together these relations imply

$$\tau = 2 - 1/\gamma, \tag{2.7}$$

so $\tau = 4/3$ in the present case.

In conclusion, unidirectional geometric shadowing in conjunction with deposition flux shot noise is an example of competitive growth which gives rise to scale-invariant structures, equation (2.1), with robust, universal scaling exponents. To a certain extent these ideas also apply to deposition onto a plane, where the coalescing objects are lines rather than point particles [28, 29].

2.2. *Noisy versus deterministic competition*

2.2.1. *Nagatani's forest formation model*

Nagatani [35] proposed a modification of the needle model described above, in which the growth rate v_i of an active needle depends on its height h_i as $v_i \sim h_i^\alpha$. One particular realization of this idea is a model [33] in which all active needles are chosen for growth with equal probability, but the height of the chosen needle is incremented by an amount proportional to h_i^α. The scaling approach of the preceding section is directly applicable here. The height fluctuation of a surviving needle increases with height as $\delta h \sim h^{(1+\alpha)/2}$; estimating $n(h) \sim 1/\xi(h) \sim 1/\delta h$, one obtains the height distribution exponent

$$\gamma = \frac{3 + \alpha}{2}, \tag{2.8}$$

in good agreement with simulations [33].

A conceptually interesting feature of the Nagatani model is the possibility, for $\alpha > 0$, of purely *deterministic* competition. Let us consider the following deterministic growth model [33]. On each site i of the integer lattice we define a real positive height variable $h_i(t)$. Each height grows independently, according to

$$\frac{\mathrm{d}h_i}{\mathrm{d}t} = h_i^\alpha, \tag{2.9}$$

as long as the needle is not shaded, i.e. as long as the condition

$$h_i > h_j - (j - i)\cot\theta \tag{2.10}$$

is fulfilled for all $j > i$ (figure 2); shaded needles stop growing entirely. The initial values $h_i(0)$ are drawn at random from some distribution $P(h)$.

For $\alpha > 0$ the initial height fluctuations are amplified by the growth process, and needles of large initial heights are able to shade those which are less fortunate. Due to the simplicity of equations (2.9) and (2.10) it is possible to write down an explicit expression [33] for the fraction of surviving needles in terms of $P(h)$, for general α.

Here we sketch the special case $\alpha = 1$, in which the active needles grow exponentially, $h_i(t) = h_i(0) \exp t$. From (2.10) the surviving fraction can be written as

$$\rho(t) = \int_0^\infty \mathrm{d}h\, P(h) \prod_{i=1}^{\infty} \int_0^{h+i/l} \mathrm{d}h'\, P(h'), \tag{2.11}$$

where $l = \exp(t) \tan\theta$.

Consider first a uniform distribution, $P(h) = 1$ for $0 < h < 1$. In this case the product in equation (2.11) only extends to $i_{\max} = l(1-h)$. We replace the product by the exponential of a sum and approximate the sum by an integral. A change of variables then yields

$$\rho \approx \int_0^1 \mathrm{d}h \exp\left[-l(1-h) - l(h+1/l)\ln(h+1/l) + 1\right] \approx \left(\frac{\pi}{2l}\right)^{1/2}; \tag{2.12}$$

in the last step a saddle point integration was performed. Not surprisingly, the form of the integrand in (2.12) shows that the survival probability is dominated, for large l, by the needles with the largest initial heights, around $h = 1 - 1/l$. Since the average height of active needles grows as $h_a(t) = (1/2)\exp t = (l/2)\cot\theta$, we can use equation (2.4) to conclude that

$$N(h) \approx [(\pi \cot\theta)^{1/2}/4] h^{-3/2}, \tag{2.13}$$

and thus $\gamma = 3/2$ in equation (2.1).

It is instructive to repeat this calculation for an unbounded initial distribution, such as $P(h) = \exp(-h)$. Proceeding as before we obtain, in analogy with (2.12), the expression

$$\rho \approx \int_0^\infty \mathrm{d}h \exp\left[-h - l\exp(-h)\right]. \tag{2.14}$$

Here the integral is dominated by contributions around $h \sim \ln l$, and the saddle point integration results in $\rho \approx (\pi/2)^{1/2}(el)^{-1}$. With $h_a(t) = \exp t = l\cot\theta$, we obtain, from equation (2.4),

$$N(h) \approx \left(\frac{\pi}{2}\right)^{1/2} \frac{\cot\theta}{e} h^{-2}, \tag{2.15}$$

so in contrast to (2.13), here the height distribution exponent is $\gamma = 2$.

The important lesson to be learned is that, in deterministic competition processes, the properties of the emerging scale-invariant structure depend not only on the dynamical rule (encoded, for example, in the exponent α in (2.9)), but also on the statistics of the random initial conditions; in that sense, there is less robustness (or universality) than in noisy processes. The reason can be traced to the fact that, in contrast to the noisy model discussed in section 2.1, the survivors in the deterministic case are not *typical*; instead, they are recruited from the needles of largest initial height [33]. Consequently, the statistics of the active needle population at some given time t, which determines the further evolution of the structure, is related to the *extremal statistics* [36] of the initial height distribution $P(h)$, that is, the probability distribution of the *largest* initial height among $l(t)$ independent samples. The sensitivity of deterministic growth processes to the statistical properties of initial conditions has been noted before in various contexts [8, 37, 38], and will be a recurrent theme throughout section 2.

2.2.2. *Self-thinning in plant populations*

Competition for sunlight is believed to play an important role in the dynamics of plant populations. Through a process referred to as *self-thinning*, larger plants cause increased mortality among smaller ones by depriving them of light. Empirically, this process is observed to proceed according to a universal scaling law relating the mean weight of survivors m to their number density per unit area ρ as [39]

$$m \sim \rho^{-3/2}. \tag{2.16}$$

If we plausibly assume that plant weight is related to plant height as $m \sim h^3$, we see that this implies the lateral distance between plants, $\xi = \rho^{-1/2}$, increasing in proportion to h. In the traditional explanation of (2.16), ξ is identified with the crown diameter which, on dimensional grounds, is also assumed to scale as $m^{1/3}$, and therefore $\xi \sim h$. The weakness of this argument lies in the complicated allometry of real plants, i.e. in the fact that different linear size measures such as stem diameter, crown diameter, or height, empirically scale with different powers of plant weight [40].

It is therefore of some interest to attempt a *dynamical* explanation based on simple screening models of the kind discussed in the previous section. Following Nagatani [35], we consider a 1D geometry, as in figure 2, with sunlight streaming in from the right at a fixed angle θ. We further assume that shadowing is exclusive, i.e. fully shaded plants die instantaneously while those which still receive some light grow as if there were no shading at all.

As a first step in the modelling procedure, the growth dynamics of individual (non-interacting) plants has to be ascertained. There is empirical evidence [41] that the increase in plant height can be characterized by a (possibly time-dependent) relative growth rate r, such that

$$\frac{\mathrm{d}h_i}{\mathrm{d}t} = r(t)h_i. \tag{2.17}$$

The essential point is that the growth rate is proportional to the height; the time dependence of $r(t)$ can be eliminated through a redefinition of time, which reduces equation (2.17) to the deterministic Nagatani model, equation (2.9), with $\alpha = 1$.

Next it has to be decided whether the competition process is noise-driven, i.e. due to random fluctuations of the growth rate r, or whether it is primarily deterministic and merely expresses the exponential amplification of randomness in the initial conditions (that is, the sizes of seedlings). In the first case the stochastic version of Nagatani's model described briefly in the previous section (model II of Meakin and Krug [33]) would provide an appropriate starting point. With $\alpha = 1$, equation (2.8) gives $\gamma = 2$, which implies that the lateral distance between survivors scales as $\xi = 1/n \sim h$, in agreement with the empirical law (2.16). If, on the other hand, the competition were mainly deterministic, the initial distribution of seedling heights would have to be known. Heuristically, one expects the distribution to be unbounded but rapidly decaying, such as a Gaussian or exponential distribution. For such distributions the calculation sketched in the previous section shows that, again, $\xi \sim h$, possibly with logarithmic corrections [33]. Thus, in this particular case, noisy and deterministic competition leads to similar results.

The relative success of these simple, 1D models should not be overinterpreted; for example, the relation $\xi \sim h$ is equivalent to the empirical rule (2.16) only if the conventional, and questionable [40], allometric relation $m \sim h^3$ is used. However,

they do show that the shadowing length ξ need not be related, as is traditionally the case, to the allometry of individual plants (indeed, in the model no lateral length scale is associated with individual needles), but rather can emerge from the competitive *interaction* between individuals.

2.3. *The shadow instability*

In the ballistic deposition model described in section 2.1, the deposition flux is assumed to be collimated and unidirectional. While this is a reasonable approximation in some situations, other growth processes such as sputter deposition are characterized by particle trajectories approaching the surface from a wide range of directions. It was first pointed out by Karunasiri, Bruinsma and Rudnick (KBR) [42] that this leads to a deterministic *shadow instability* in that valleys receive less flux than hills and are therefore left behind. Subsequent studies [43–48] have explored various aspects of the instability.

2.3.1. *The grass model*

A needle model for the shadow instability is illustrated in figure 3. We focus on the simplest nontrivial case, neglecting both roughening through shot noise and smoothening by surface relaxation processes. The growth rate of the ith needle is given by [46]

$$\frac{\mathrm{d}h_i}{\mathrm{d}t} = V(\theta_i), \tag{2.18}$$

where the *exposure angle* θ_i, $0 \leq \theta_i \leq \pi$, describes the range of directions in which straight lines can be drawn from the tip of needle i without intersecting any of the other needles (figure 3), and V is a monotonically increasing function with $V(0) = 0$. As in section 2.2, the initial values $h_i(0)$ are drawn independently from a distribution $P(h)$.

Some insight into the competition process is gained from the distribution $P_t(\theta)$ of exposure angles at time t (figure 4). As the growth progresses, the distribution becomes increasingly bimodal. The peak close to $\theta = 0$ contains needles which are essentially excluded from further growth, while the (diminishing) peak close to $\theta = \pi$ contains those which have not yet been subject to shadowing; only a small fraction of needles resides between the peaks. The structure of the distribution allows us to

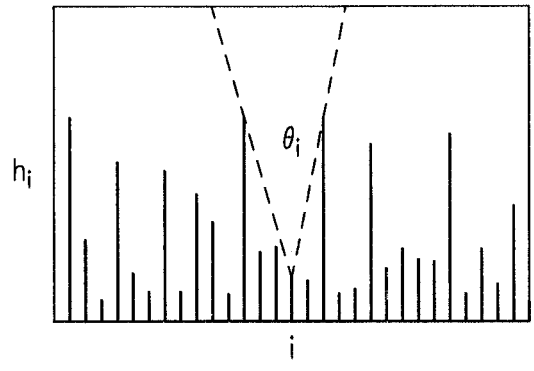

Figure 3. The grass model for the shadow instability.

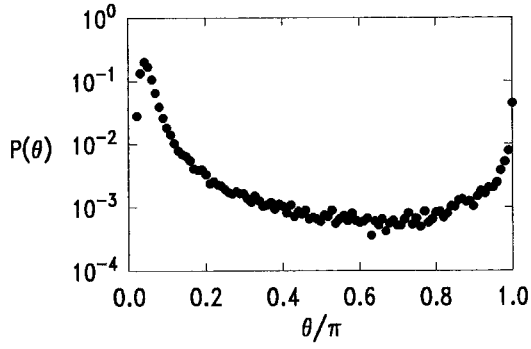

Figure 4. Distribution of exposure angles at time $t = 20$, from simulations using $V(\theta) = \theta$. The data constitute an average over 100 runs for a system of 500 needles [46].

extend the distinction between active and shaded needles, developed in the unidirectional case, to the present, more involved situation in which no needle ever entirely ceases to grow. We *define* a surviving (*active*) needle through the condition $\theta_i(t) > \theta_{\text{th}}$, for some arbitrary threshold angle θ_{th}, say, $\theta_{\text{th}} = \pi/2$. The surviving fraction $\rho(t)$ can then be written as

$$\rho(t) = \int_{\theta_{\text{th}}}^{\pi} \mathrm{d}\theta \, P_t(\theta). \tag{2.19}$$

While the simple identity (2.4) between the surviving fraction and the density profile does not hold here, a similar, approximate relation can be derived as follows. Note first that averaging the equations of motion (2.18) over initial conditions yields

$$\int_0^{\pi} \mathrm{d}\theta \, P_t(\theta) V(\theta) = \frac{\mathrm{d}}{\mathrm{d}t} \langle h \rangle = \frac{\mathrm{d}}{\mathrm{d}t} \int_0^{\infty} \mathrm{d}h \, h N_t(h), \tag{2.20}$$

where a time index has been added to the height distribution $N(h)$ to express the fact that we are considering the transient behaviour. Using the definition (2.2) of the density profile and performing a partial integration, the right hand side of equation (2.20) can be written as

$$\frac{\mathrm{d}}{\mathrm{d}t} \langle h \rangle = \frac{\mathrm{d}}{\mathrm{d}t} \int_0^{V(\pi)t} \mathrm{d}h \, n_t(h) = V(\pi) n_t(V(\pi)t) + \int_0^{V(\pi)t} \mathrm{d}h \frac{\partial n_t}{\partial t}, \tag{2.21}$$

introducing explicitly the maximal height $V(\pi)t$. On the other hand, from its definition (2.19) the surviving fraction can be bounded by

$$\rho(t) \leq \int_{\theta_{\text{th}}}^{\pi} \mathrm{d}\theta \, P_t(\theta)[V(\theta)/V(\theta_{\text{th}})] \leq V(\theta_{\text{th}})^{-1} \int_0^{\pi} \mathrm{d}\theta \, P_t(\theta) V(\theta) \tag{2.22}$$

(recall that $V(\theta)$ is monotonic!). Inserting equations (2.20) and (2.21) we see that $\rho(t)$ is bounded by $[V(\pi)/V(\theta_{\text{th}})] n(V(\pi)t)$ *provided* the term arising from the explicit time dependence of n_t in equation (2.21) can be neglected; as we shall see below, this is not always true. We will nevertheless assume a relation of the form

$$\rho(t) \sim n(h_{\text{a}}(t)), \tag{2.23}$$

with $h_{\text{a}}(t) \approx V(\pi)t$ the typical height of active needles, to relate the dynamics of competition to the frozen structure.

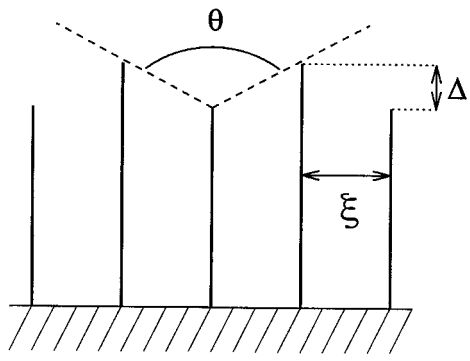

Figure 5. Periodic needle array used in the analysis of the shadowing model.

The analysis [46] focuses on the transfer of the needle population from the 'active' to the 'shaded' peak in figure 4. We consider a late stage in the process, when the typical distance between active needles is $\xi \gg 1$. For the sake of simplicity we use a *periodic* array of active needles (figure 5), with spacing ξ and alternating heights $h_1 = h_{\max} = V(\pi)t$ and $h_2 = h_1 - \Delta$, with $\Delta \ll \xi$; any effect from the shaded needles will be disregarded. In the course of time the shorter of the active needles increasingly lag behind the longer ones and eventually join the shaded majority. For a quantitative description one introduces an exponent ν to characterize the behaviour of $V(\theta)$ close to $\theta = \pi$, $V(\pi) - V(\theta) \sim (\pi - \theta)^\nu$ for $\theta \to \pi$. Elementary geometry then yields

$$\frac{\mathrm{d}\Delta}{\mathrm{d}t} = V(\pi) - V(\theta) \sim (\pi - \theta)^\nu \sim \left(\frac{\Delta}{\xi}\right)^\nu. \tag{2.24}$$

The solution of this equation is

$$\Delta(t) = [\Delta(0)^{1-\nu} + (1-\nu)t/\xi^\nu]^{1/(1-\nu)} \tag{2.25}$$

for $\nu \neq 1$ and $\Delta(t) = \Delta(0)\exp(t/\xi)$ for $\nu = 1$. As a measure for the time scale of shadowing we introduce t^* through $\Delta(t^*) = \xi$; in our simplified situation, the exposure angle of the shorter needles has decreased to $\theta(t^*) = \theta_{\mathrm{th}} = \pi/2$ at time t^*. From equation (2.25) we obtain

$$t^* = \frac{\xi}{1-\nu}\left\{1 - \left[\frac{\Delta(0)}{\xi}\right]^{1-\nu}\right\} \tag{2.26}$$

for $\nu \neq 1$, and

$$t^* = \xi \ln[\xi/\Delta(0)] \tag{2.27}$$

for $\nu = 1$. In the relevant limit $\Delta(0)/\xi \ll 1$, equation (2.26) behaves as $t^* \sim \xi$ for $\nu < 1$, and $t^* \sim \xi^\nu/\Delta(0)^{\nu-1}$ for $\nu > 1$.

The origin of scale invariance in this class of competitive growth processes lies in the fact that the shadowing time t^* increases with ξ: further shadowing is slowed down as active needles become scarce. This is analogous to the coarsening of a 1D phase separating system, where the interaction between domain walls, providing the thermodynamic driving force for coarsening, decreases (exponentially) with increasing domain size; Langer's treatment of spinodal decomposition [49] is in fact similar to the present approach in that it is based upon an estimate of the lifetime t^* of

metastable periodic order parameter profiles, which decay via the disappearance of every second domain.

The analogy with coarsening gives an important clue on how to proceed. Since, in the simplified periodic configuration analysed here, the active needle spacing doubles when the shorter needles are shaded, we may interpret $1/t^*$ as *the growth rate of the needle spacing* ξ, and write

$$\frac{\mathrm{d}\xi}{\mathrm{d}t} \sim \frac{\xi}{t^*(\xi)}. \tag{2.28}$$

In evaluating this relation we are faced with the problem that t^* depends, for $\nu \geq 1$, on the initial height difference $\Delta(0)$ as well as on the needle spacing. In the deterministic process considered here, $\Delta(0)$ generally acquires a ξ dependence due to the fact that the active needles which survive up to a time t are those with the largest initial height in a region of size $\xi(t)$ (see section 2.2). The estimate of $\Delta(0)$ for a given distribution of initial values is an exercise in extremal statistics [46, 33, 36]. The result is a relation of the type

$$t^*(\xi) \sim \xi^z, \tag{2.29}$$

where the *dynamic exponent* $z > 1$ depends, for $\nu > 1$, both on ν and on the initial distribution; for example, for uniform, bounded initial distributions, $z = 2\nu - 1$, while for unbounded, rapidly decaying distributions, $z = \nu$ [46]. This is another instance of the lack of robust universality in deterministic growth processes alluded to previously. For $\nu = 1$ we always have $t^* \sim \xi \ln \xi$ and the initial distribution merely affects the prefactor.

Integrating equation (2.28) we obtain the *coarsening law*

$$\xi(t) \sim t^p, \tag{2.30}$$

where p takes the universal value $p = 1$ for $\nu < 1$ and $p = 1/z$ for $\nu > 1$. In the borderline case $\nu = 1$, equation (2.30) is replaced by

$$\xi(t) \sim t/\ln t. \tag{2.31}$$

The density of survivors is $\rho(t) \sim 1/\xi(t)$ and, using equation (2.23), we have

$$\gamma = 1 + p. \tag{2.32}$$

In particular, we obtain the universal result $\gamma = 2$ for $\nu \leq 1$, with a logarithmic correction

$$N(h) \sim \frac{\ln h}{h^2} \tag{2.33}$$

for $\nu = 1$. These predictions are in excellent agreement with simulations carried out for a range of values of ν, $1/2 \leq \nu \leq 5$, and a variety of initial distributions [46].

2.3.2. *Shaded needles*

Two examples of numerically determined height distributions are shown in figure 6. The graphs nicely illustrate the decomposition into a time-independent ('frozen') power law part and a peak at $h \approx h_a(t)$ which contains the active needles. However, figure 6 (*b*) indicates that this is not the whole story: a second peak is seen to develop and to move towards increasing height at a sublinear rate. This peak is associated with the dynamics of the *shaded* needles.

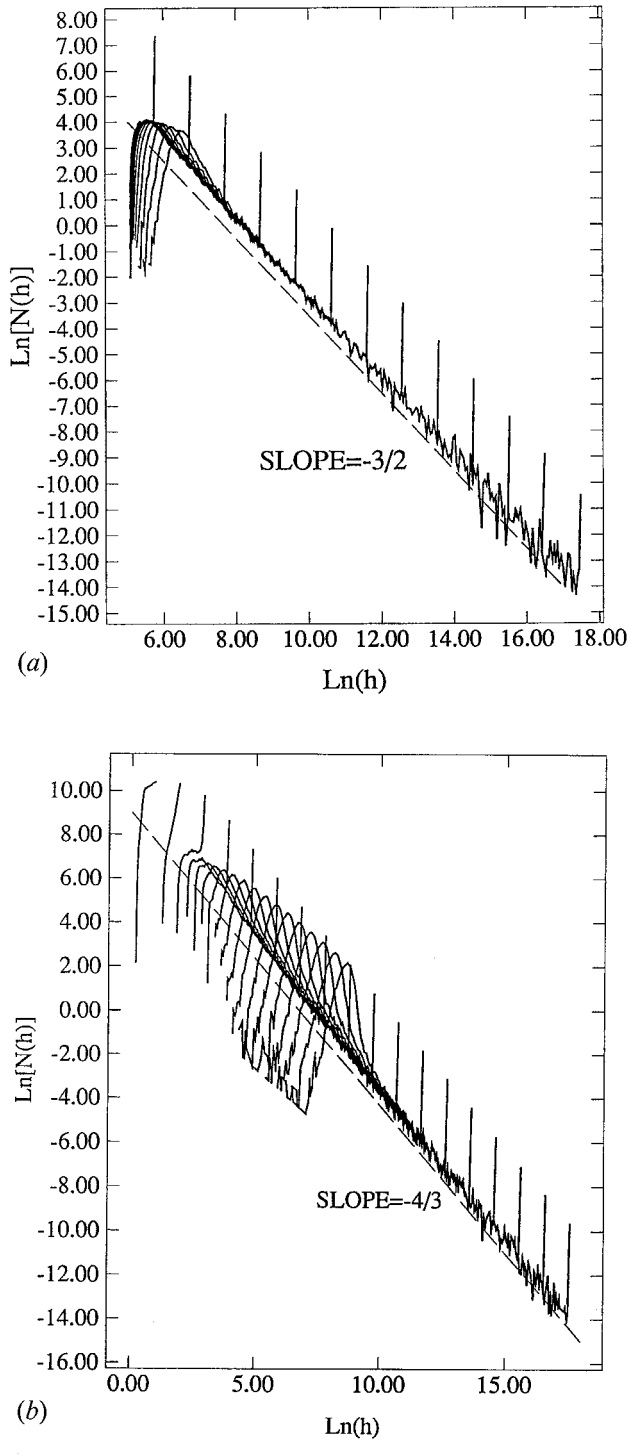

Figure 6. Height distributions of the needle model for shadowing, with growth rate function (*a*) $V(\theta) = \pi^{3/2} - (\pi - \theta)^{3/2}$ and (*b*) $V(\theta) = (1 - \cos\theta)^{3/8}$. In both cases the initial heights were drawn from a uniform distribution. The broken lines indicate the theoretical predictions for the height distribution exponent γ.

Suppose that the growth rate behaves as $V(\theta) \sim \theta^{\eta}$ for $\theta \to 0$. We need to estimate the typical exposure angle θ_s characteristic of the shaded needles. An upper bound on θ_s is obtained by taking into account only the shadowing due to the highest, active needles; their spacing being ξ, we have $\theta_s \leq \xi/h_a(t) \sim \xi/t$, and hence the typical height $h_s(t)$ of the shaded needles evolves as

$$dh_s/dt = V(\theta_s) \leq (\xi/t)^{\eta} \sim t^{-\eta(1-p)}. \tag{2.34}$$

The height of the shaded needles remains bounded for all times if $\eta > 1/(1-p)$; in general, however, we may only conclude that $h_s \sim t^{\mu}$ with

$$\mu \leq 1 - \eta(1-p) \leq 1. \tag{2.35}$$

Numerically, it appears [46] that this bound overestimates the value of μ, in particular in the case $p = 1$ where the bound becomes trivial; this implies that considerable shadowing must also go on *within* the population of shaded needles. Nevertheless, in most cases μ is found to be positive, e.g. $\mu \approx 0{\cdot}3$ when $V(\theta) = \theta$. Consequently, the $t \to \infty$ limit of the height distribution $N(h)$ is trivial for any fixed h, since for sufficiently long times *all* needles have grown beyond height h. Instead, the scaling behaviour (2.1) is encountered in the scaling range $h_s(t) < h < h_a(t)$, as is clearly seen in figure 6(*b*). In other words, the typical form of the density profile is

$$n_t(h) \begin{cases} = 1, & 0 \leq h \leq h_s(t) \sim t^{\mu}, \\ \sim h^{-p}, & h_s(t) \leq h \leq h_a(t) \sim t, \\ = 0, & h > h_a(t). \end{cases} \tag{2.36}$$

Note that there is a sharp drop in $n(h)$ at $h \sim h_s$, corresponding to the peak seen in $N(h)$ (figure 6(*b*)).

To delineate the limits of consistency of our approach, we now use the approximate form (2.36) of the density profile to evaluate the right hand side of equation (2.21). We find two contributions to the averaged growth rate, one of the order $dh_s(t)/dt \sim t^{\mu-1}$ from the shaded needles and one of the order t^{-p} from the active ones. The fundamental assumption of our approach has been that the dynamics is *dominated* by the active needles. This requires $\mu < 1 - p$; using the bound (2.35), a *sufficient* condition is

$$\eta > p/(1-p). \tag{2.37}$$

One can also derive this condition by evaluating the left hand side of equation (2.20) with the following simple Ansatz for the exposure angle distribution $P_t(\theta)$:

$$P_t(\theta) = [1 - \rho(t)]\delta[\theta - \theta_s(t)] + \rho(t)\delta(\theta - \pi). \tag{2.38}$$

Again, this gives rise to two competing contributions to the average growth rate, and with the bound $\theta_s \leq \xi/t$ the peak at $\theta = \pi$ is found to dominate if (2.37) is fulfilled. Surely, the condition (2.37) is too restrictive to be useful; for example, it is only marginally satisfied in the case depicted in figure 6(*a*) ($p = 1/2$ and $\eta = 1$), although in this case the shaded needles are seen to play no significant role.

2.3.3. *The effect of noise*

Consider adding random forces $f_i(t)$ on the right hand side of equation (2.18). The shadowing dynamical equation (2.24) then becomes

$$\frac{d\Delta}{dt} = \left(\frac{\Delta}{\xi}\right)^{\nu} + f(t), \tag{2.39}$$

where we take f to be Gaussian with zero mean and covariance

$$\langle f(t)f(t')\rangle = D\delta(t - t'). \tag{2.40}$$

The solution of this equation is straightforward in the linear case $\nu = 1$ (compare with section 3.2.2). In a situation where initially all active needles have the same height, $\Delta(0) = 0$, the height difference grows according to

$$\langle \Delta(t)^2 \rangle = \frac{D\xi}{2}[\exp(2t/\xi) - 1], \tag{2.41}$$

and the shadowing time, obtained by equating equation (2.41) to ξ^2, is

$$t^*(\xi) = (\xi/2)\ln(1 + 2\xi/D). \tag{2.42}$$

For large ξ this is of the form (2.27), with an effective initial height difference $\Delta(0)_{\text{eff}} \sim D$.

The comparison indicates how equation (2.39) may be approximately solved for arbitrary value of ν. Equation (2.41) describes two distinct regimes. For $t \ll \xi/2$, the process is noise dominated and $\langle \Delta(t)^2 \rangle \approx Dt$, while for $t \gg \xi/2$ the deterministic term in equation (2.39) takes over. It is plausible that the succession of a noise-dominated early time regime and a late time regime dominated by deterministic shadowing should be a general feature of equation (2.39). We can therefore match the early time behaviour, $\Delta(t) = (Dt)^{1/2}$, to the deterministic solution (2.25), requiring continuity of Δ and $d\Delta/dt$ at the crossover time t_c; such an approach was first suggested by Rossi [50] in the context of Laplacian needle growth (see section 2.4). The two conditions serve to fix t_c, as well as the initial condition $\Delta(0) = \Delta(0)_{\text{eff}}$ in equation (2.25), thereby selecting a particular trajectory from the one-parameter family of deterministic solutions. The result is

$$t_c = (1/2)(D/2)^{\frac{1-\nu}{1+\nu}}\xi^{\frac{2\nu}{1+\nu}} \tag{2.43}$$

and

$$\Delta(0)_{\text{eff}} = [(1+\nu)/2]^{1/(1-\nu)}(D/2)^{1/(1+\nu)}\xi^{\nu/(1+\nu)}. \tag{2.44}$$

The first important observation is that $\Delta(0)_{\text{eff}}/\xi \to 0$ for $\xi \to \infty$, for any value of ν. This implies that the prediction $p = 1$ in the universal regime $\nu < 1$ is unaffected by the noise, since $t^*(\xi) = \xi/(1-\nu)$ for large ξ, as before (equation (2.26)). On the other hand, for $\nu > 1$, insertion of equation (2.44) into equation (2.26) yields the shadowing time

$$t^* = \frac{\nu+1}{\nu-1}t_c \sim \xi^{\frac{2\nu}{1+\nu}}, \tag{2.45}$$

for large ξ. The coarsening exponent is

$$p = \frac{1+\nu}{2\nu} < 1. \tag{2.46}$$

Somewhat remarkably, the shadowing time in equation (2.45) is of the same order (though always greater than) the crossover time t_c from the noise-dominated regime, which might raise doubts concerning the consistency of the approach. Nevertheless, Rossi [50] found good agreement with equation (2.46) from an exact enumeration analysis of a discrete version of equation (2.39).

2.3.4. *Beyond the needle model*

We conclude this section by commenting on numerical work on the shadowing instability that includes fluctuations (due to the shot noise in the deposition flux) and surface tension effects. These studies have considered either discretized continuum equations, or lattice models in which particles are deposited ballistically from a range of directions. The most general continuum equation is of the form

$$\frac{\partial}{\partial t}h(x, t) = \sigma\nabla^2 h - \kappa\nabla^4 h + \frac{\lambda}{2}(\nabla h)^2 + \theta[h(x, t)] + f(x, t), \tag{2.47}$$

where $h(x, t)$ is the continuous version of the height variables $h_i(t)$, and the exposure angle θ is defined as before, in figure 3, as a functional of the instantaneous surface configuration; it is assumed that the vertical local growth rate is proportional to the exposure angle, with a factor of proportionality (the deposition flux) that has been set to unity. The coefficients $\sigma, \kappa > 0$ are related to the surface tension; the σ term describes surface relaxation due to evaporation–condensation processes, while the κ term captures smoothening through surface diffusion (see section 3). The $(\nabla h)^2$ nonlinearity was first proposed in the celebrated work of Kardar, Parisi and Zhang (KPZ) [19], and will be thoroughly discussed in section 4. Finally, $f(x, t)$ is a Gaussian random force with short-range correlations in space and time, and variance D (see equations (2.40) and (3.16)). The needle model discussed in the bulk of this section corresponds to the simplest case where $\sigma = \kappa = \lambda = D = 0$, and the linear appearance of θ in equation (2.47) implies that one is dealing with the 'borderline' situation $\nu = 1$.

A serious deficiency of equation (2.47) lies in the fact that all coupling terms appearing in the equation are the result of a small gradient expansion (see section 3), which is clearly inappropriate in view of the large modulations caused by the shadow instability. A more satisfactory continuum description, in which the local normal growth rate is proportional to the normal projection of the incident flux, integrated over the exposure angle, was proposed by Bales and Zangwill [44]. The surface morphology generated by this model is quite different from that obtained with needle models and continuum equations of the type (2.47), which assume a single-valued height function at all times; in fact, the surface develops a structure of domed columns, separated by deep narrow grooves that occasionally close, due to the formation of overhangs, and leave chains of vacancies in the bulk. However, because of the high computational cost associated with the Bales–Zangwill model, it has not been possible so far to quantitatively study its scaling and coarsening properties.

In their original paper [42] on the shadow instability, KBR studied equation (2.47) with $\sigma = \lambda = D = 0$, i.e. the deterministic problem with surface diffusion relaxation. For small values of κ, $\kappa \leq 10^{-4}$, they found a power law density profile with an exponent $p = \gamma - 1$ *increasing* from $p \approx 1$ for $\kappa = 0$ to $p \approx 1{\cdot}5$ for $\kappa = 10^{-4}$; for larger values of κ an abrupt transition, from compact growth with a flat interface to a spiky morphology, is observed at a critical height $h^* \sim \kappa^{1/3}$, but the spikes do not appear to have a power law height distribution. The result $p > 1$ is very surprising in view of our interpretation of p as a *coarsening* exponent, as in equation (2.30); indeed, $p > 1$ would correspond to superlinear coarsening, and it is hard to see how such a behaviour could arise from a local coupling as in equation (2.47) (it is *not* due to the shadowing interaction because then it should appear also in the needle model). It is possible that KBR in fact observed the steep transition region between the constant plateau and the power law decay in the density profile (2.36), which may

give rise to large, spurious values of p; another possibility is that the coupling by the κ term enhances the growth of the shaded background of needles to such an extent that, at least for larger values of κ, the power law regime disappears altogether. Clearly this case requires further investigation.

Yao, Roland and Guo [45] considered equation (2.47) with $\kappa = 0$, $\sigma > 0$ and $\lambda \neq 0$. They found linear coarsening, $p = 1$, both in the presence and absence of noise. Apart from the logarithmic correction in (2.31), which may have been too weak to detect, this result agrees with our analysis of the needle model. On the other hand, a subsequent study of the case $\lambda = 0$, $\sigma > 0$, reported by Yao and Guo [47], resulted in a smaller coarsening exponent $p \approx 0{\cdot}7$. The main contribution of Yao and Guo [47] was an extension of equation (2.47), with $\lambda = 0$ and $\sigma > 0$, to two-dimensional (2D) surfaces, where the coarsening was found to progress surprisingly slowly, with $p \approx 0{\cdot}33$.

Lattice models for the shadow instability were introduced by Roland and Guo [45, 51] and by Tang and Liang [48]. The model of Roland and Guo is subject to the solid-on-solid (SOS) constraint, i.e. overhangs and bulk vacancies are not allowed to form; surface sites are selected for deposition by launching particles towards the surface along randomly directed ballistic trajectories, but the success of the deposition attempt is decided by energetic considerations, thereby bringing surface tension and temperature into play. In contrast, the model of Tang and Liang is very close in spirit to standard ballistic deposition (section 2.1), i.e. particles stick permanently at the site of first impact, and the deposit is highly defective. In both models the maximal exposure angle $\theta_{\max}$ is treated as a control parameter, and both models show evidence of a phase transition from a 'flat' phase at small $\theta_{\max}$, in which the surface roughens as predicted by KPZ theory (see section 4), to a grooved, columnar phase dominated by shadowing at large $\theta_{\max}$. However, the scaling in the grooved phase is quite different in the two models. While Tang and Liang [48] find a column mass distribution exponent $\tau \approx 1{\cdot}47$, consistent, via the relation (2.7), with the needle model prediction $\gamma = 2$, Roland and Guo [45, 51] report a coarsening exponent $p \approx 0{\cdot}56$. These results suggest that the Tang–Liang model might be appropriately described by the continuum equation (2.47) with $\sigma > 0$ and $\lambda \neq 0$, while the Roland–Guo model corresponds, roughly, to the case $\lambda = 0$. It is obvious, however, that we are still far from a coherent picture of the various approaches to modelling the shadow instability, let alone an understanding of universality classes of possible asymptotic behaviours.

2.4. *Laplacian needles*

Diffusion-limited needle growth was considered independently by Meakin [52] and Rossi [50, 53] as a simplification of the notoriously difficult DLA problem. In this model, needles grow perpendicular to a d-dimensional substrate plane by the accretion of individual random walkers. The walkers are released, one by one, from randomly chosen lateral positions at the height of the highest needle (figure 7). Growth occurs only if the walker hits the tip of a needle. In the original version [50, 52, 53] of the model, walkers that hit the side of a needle are reflected. Here we shall also discuss a version [55] referred to as *model A*, in which walkers are *absorbed* at the sides of needles, this boundary condition being, as will be argued below, somewhat more faithful to DLA; the original version with *reflecting* boundary conditions then constitutes *model R*. A typical configuration generated by model R is shown in figure 8. Since the positional probability distribution of the random walker satisfies the

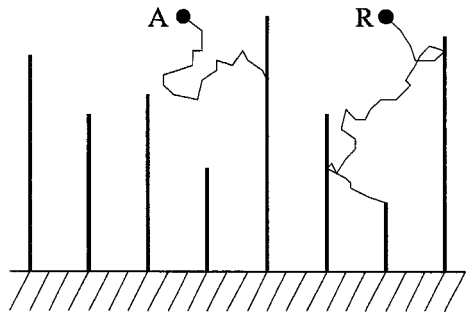

Figure 7. Illustration of the two versions of Laplacian needle growth. In model A, the random walker is absorbed at the sides of the needles, while in model R the walker is reflected.

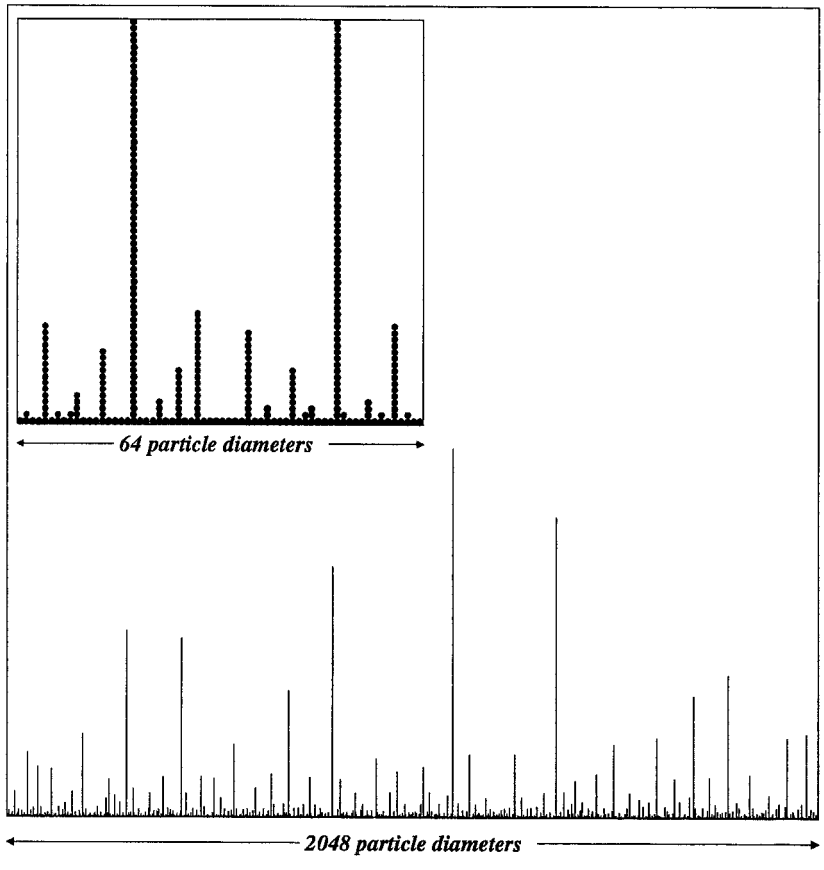

Figure 8. Needle forest generated in a 2D off-lattice simulation of Laplacian growth, with reflecting boundary conditions at the sides of the needles. The forest consists of 20 000 particles. The inset shows a magnification of the lower left corner. (Courtesy of Thomas Rage.)

Laplace equation, with appropriate (absorbing or reflecting) boundary conditions at the sides of the needles, this model is a simple example of *Laplacian growth* [2, 3].

Rossi [50] proposed to analyse the problem within a two-absorber approximation, which is closely analogous to the approach applied to the shadow instability in section 2.3. He considered the initial stage of screening for a configuration of two needles in the plane (i.e. growth occurring from a line, $d = 1$) with lateral spacing ξ and heights h_1 and $h_2 = h_1 - \Delta$, with $\Delta/\xi \ll 1$, and supplemented with periodic boundary conditions (see figure 5). The quantity of interest is the probability $\mathscr{P}(\xi, \Delta)$ that the next walker to be launched onto this configuration is absorbed by the tallest needle h_1. Rossi observes that, in the continuum limit where ξ and Δ are large compared to the lattice spacing (or particle size), the scale invariance of the Laplace equation implies that $\mathscr{P}$ should depend only on the ratio Δ/ξ and, since $\mathscr{P}(\xi, 0) = 1/2$, one expects an expansion of the form

$$\mathscr{P}(\xi, \Delta) \approx \frac{1}{2}\left[1 + C\left(\frac{\Delta}{\xi}\right)^{\nu}\right] \tag{2.48}$$

for $\Delta/\xi \ll 1$. The rate at which the height difference Δ increases due to screening is proportional to $2\mathscr{P} - 1$, and hence Δ satisfies an equation of the form (2.24), or rather, since the process is manifestly noisy, its stochastic counterpart (2.39). The analysis of section 2.3 can then be taken over, and a prediction for the height distribution exponent γ (equivalently, the coarsening exponent p) follows in terms of the (unknown) exponent ν in equation (2.48). For example, under the plausible assumption that a walker launched at a random lateral position and height h_1 will invariably be absorbed at the needle tip that is closer to its starting point, one has

$$\mathscr{P} = 1/2 + \Delta^2/2\xi^2, \tag{2.49}$$

so $\nu = 2$ and equation (2.46) would predict that $p = 3/4$, which is close to (but smaller than) the early numerical estimate [50, 52] $p \approx 0{\cdot}83$. It is interesting to note that the value $p = 0{\cdot}78 \pm 0{\cdot}02$ was obtained numerically in a model of 'shortest-path' aggregation, for which equation (2.49) is exact [54].

Krug, Kassner, Meakin and Family [55] extended Rossi's analysis in two directions. First, they pointed out that, for model A in $d = 1$, the probability $\mathscr{P}(\xi, \Delta)$ can be computed using the conformal mapping technique. The calculation, which will be sketched shortly, shows that in fact $\nu = 1$, and therefore the density profile is found (from equations (2.2) and (2.33)) to decay as

$$n(h) \sim \frac{\ln h}{h} \tag{2.50}$$

(see figure 9); while the conformal mapping calculation applies only to model A, scaling arguments and numerical simulations [55] indicate that equation (2.50) holds for model R as well. Second, the breakdown of the two-absorber picture in high dimensions—more precisely, above an upper critical dimension d_c—was predicted. This breakdown is expected to occur because, in high dimensionalities, the needle deposit becomes increasingly transparent to the random walkers and the screening capacity of an individual needle becomes small. For $d \geq d_c$, screening is a *collective* effect involving many needles. This regime can be described by a continuum theory of mean field type [56, 57], which will be discussed in section 2.4.3. Presently we focus on $d = 1$, which is below d_c both for model R and A.

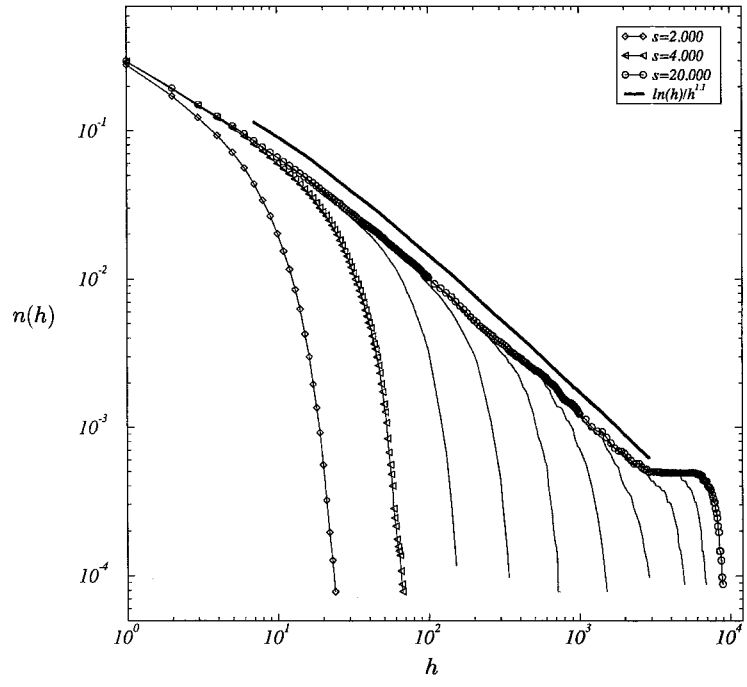

Figure 9. Density profiles obtained by averaging 50 independent off-lattice simulations of model A, in $d = 1$, for a system size of $L = 2048$ particle diameters. The figure shows a series of curves obtained at different stages of growth. At the latest stage, when 20 000 particles (per run) have been deposited, the plateau in the density indicates that only a single needle remains. The bold curve represents the best fit of the form $n(h) \sim \ln h/h^{-(\tilde{\gamma}-1)}$, with $\tilde{\gamma} = 2{\cdot}1$, which is only slightly better than the predicted decay law (2.50) with $\tilde{\gamma} = 2$. (Courtesy of Thomas Rage.)

2.4.1. *Screening efficiency*

Before taking a closer look at the conformal mapping approach, we should issue one word of caution. Even in the regime $d < d_c$, in which screening is dominated by individual needles, it is far from clear that the two-absorber approximation captures the essence of the full problem. The tacit assumption of the approximation is that the screening interaction between the dominant, tallest needles can be isolated from the influence of the background of shorter needles that have been screened previously. In the shadowing model of section 2.3 this assumption was, to some extent, justified by the observation that the needle population naturally decomposes into a group of 'shaded' and a group of 'active' individuals, as evidenced by the two peaks in the exposure angle distribution (figure 4). In the Laplacian case there is no evidence that the distribution of growth probabilities has a similar, bimodal structure.

An impression of the dynamic significance of the background of 'screened' needles is gained by comparing the time evolution of the height distribution $N_t(h)$, as shown for model R, for example in figure 2 of [52], with the corresponding behaviour in the shadowing model (figure 6 (*a*)). While in the latter case a clear distinction between the frozen bulk of the deposit, and a small subpopulation of active needles, is seen to evolve, in the Laplacian model growth appears to occur simultaneously at all levels (all values of h), indicating that a considerable flux of

random walkers penetrates the deposit far below the height of the tallest, 'active' needles. Model A seems to be better behaved in this respect—the time evolution of the density profile shown in figure 9 indicates that the bulk of the deposit is essentially frozen once several particles per site have been deposited.

For a preliminary assessment of screening effects in the two versions of the Laplacian needle model, we consider the penetration of a random walker into a periodic needle array in $d = 1$ lateral dimensions. Let the needle spacing be ξ, and denote by $P_\xi(r)$ the probability that a walker released at the height of the needle tips penetrates at least a distance r into the deposit before being absorbed. For model A, we can invoke the well-known electrostatic analogy [58], which replaces the needles with grounded conductors and relates the density of random walkers to the electrostatic potential, to conclude that the penetration probability (and therefore the growth rate of a screened needle) decays exponentially, as

$$P_\xi(r) \sim \exp(-\pi r/\xi), \quad \text{(model A)}. \tag{2.51}$$

For model R, absorption can occur only when the walker returns to the plane $r = 0$ (the height of the needle tips). We can analyse the vertical motion using standard results for (discrete) 1D random walks in the presence of a single weak absorber at the origin. The tail of $P_\xi(r)$ is dominated by walkers that return to the origin many times. Asymptotically for long walks the lateral positions of the walker at subsequent returns are uncorrelated, hence the absorption probability per return is $p_a \approx 1/\xi$ ($p_a \sim 1/\xi^d$ in d lateral dimensions). The probability for a walk of length t to return exactly n times is [59] $2^{n-t}(t-n)!/[(t/2)!(t/2-n)!]$, and consequently the survival probability in the presence of an absorber of strength p_a can be estimated as

$$\begin{aligned}\psi(t) &= \sum_{n=0}^{t/2} (1-p_a)^n 2^{n-t} \frac{(t-n)!}{(t/2)!(t/2-n)!} \\ &\approx (2/\pi)^{1/2} t^{-1/2} \int_0^\infty \mathrm{d}n\, (1-p_a)^n \exp(-n^2/2t) \approx (2/\pi)^{1/2} t^{-1/2} p_a^{-1}.\end{aligned} \tag{2.52}$$

Since the maximal vertical displacement of a walk of length t is $r \sim t^{1/2}$, we can rewrite this as

$$P_\xi(r) \sim \xi/r, \quad \text{(model R)} \tag{2.53}$$

in $d = 1$, and $P_\xi(r) \sim \xi^d/r$ in general.

We see that the screening capacity of a periodic array of needles is dramatically different in the two models. In particular, only model A features exponentially small growth probabilities in deep fjords, which presumably is an important property of DLA. This is why we expect the needle model A to be more closely related to the full DLA problem.

Using (2.51) together with the predicted density profile (2.50), we can also give a rough estimate of the growth probabilities in the screened bulk of the model A needle forest. Let us assume, in the spirit of the two-absorber approach, that we can identify a set of 'active' needles of reasonably uniform height $h_a(t)$ and spacing $\xi(h_a) = 1/n(h_a) \approx c h_a/\ln h_a$, with some constant c. Suppose now that we want to probe the growth probability at some height $h = \alpha h_a$, $0 < \alpha < 1$. Under the (admittedly questionable) hypothesis that the screening is dominated by active needles at any height h, we can estimate the growth probability $P_G(h)$ from equation (2.51), with $r = h_a - h$. The result is of the form

$$P_G(h) \sim h_a^{-\pi(1-\alpha)/c}. \tag{2.54}$$

The growth probability decays as a power law with the 'deposit thickness' h_a, but with a *height-dependent exponent*. In DLA, the dependence of the smallest growth probability on the cluster size has been a hotly debated issue for some time, and functional relations ranging from stretched exponentials to power laws have been proposed [60, 61]. Here, we have a simple but nontrivial prediction, which should be accessible to numerical verification.

For a comparison with the shadowing model we may identify $P_\xi(r)$ with the growth rate $V(\theta)$, and ξ/r (or, in d dimensions, ξ^d/r) with the exposure angle θ. Our considerations then show that model A corresponds to a shadowing model with $V(\theta) \sim \exp(-1/\theta)$ for $\theta \to 0$ ($\eta = \infty$ in the notation of section 2.3.2), while model R corresponds to the standard case $V(\theta) \sim \theta$, $\theta \to 0$ ($\eta = 1$). We have seen in section 2.3.2 that the two-absorber approximation—equivalently, in the shadowing model, the sharp distinction between active and shaded needles—becomes more accurate for large values of η (see, for example, equation (2.37)). Thus, it is no surprise that the assumption of a frozen background of shaded needles is more closely realized for model A, as displayed in figure 9, than for model R.

2.4.2. *Conformal mappings*

The analytic transformation [62]

$$z(\zeta) = -\frac{\xi}{\pi k}\left[\frac{\zeta^2}{2} + (1-k)\zeta - k\,\mathrm{Log}\,\zeta - k + \frac{1}{2}\right], \tag{2.55}$$

$z, \zeta \in \mathbb{C}$, maps the real axis of the ζ plane onto a pair of semi-infinite needles that lie parallel to the real axis of the z plane (figure 10). To see this, we evaluate equation (2.55) for real ζ, noting that $\mathrm{Log}\,\zeta = \ln\zeta$ for $\zeta > 0$ and $\mathrm{Log}\,\zeta = \ln|\zeta| + \mathrm{i}\pi$ for $\zeta < 0$. With $z = x + \mathrm{i}y$ it follows that $y = \mathrm{Im}\,\zeta = 0$ for $\zeta > 0$ and $y = \xi$ for $\zeta < 0$. Thus, the positive real axis maps onto a needle that lies on the real axis of the z plane, and the negative real axis maps onto a needle that runs parallel to the real axis, at a distance $y = \xi$. The real part $x(\zeta)$ has two maxima, at $\zeta = -1$ and $\zeta = k$, where $x(-1) = 0$ and

$$\Delta \equiv x(k) = \frac{\xi}{\pi}\left(\frac{k}{2} + \ln k - \frac{1}{2k}\right), \tag{2.56}$$

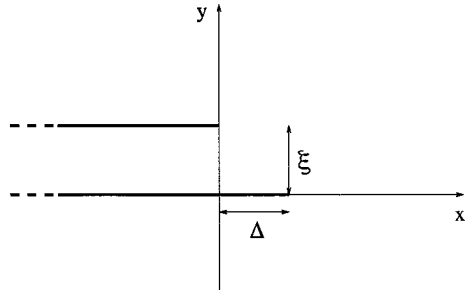

Figure 10. Sketch of the complex z plane. The bold lines indicate the image of the real axis of the ζ plane under the mapping (2.55).

respectively. The maxima correspond to the needle tips, and the parameter k determines the height difference Δ or, rather, the ratio Δ/ξ. In the relevant limit $\Delta/\xi \ll 1$, equation (2.56) can be inverted as

$$k \approx 1 + (\pi/2)\Delta/\xi. \tag{2.57}$$

To compute the electrostatic potential close to the tips, we expand equation (2.55) to second order around $\zeta = -1$ and $\zeta = k$, obtaining

$$\begin{aligned} z(\zeta) &\approx \mathrm{i}\xi - \frac{\xi}{2\pi k}(1+k)(\zeta+1)^2, \qquad \zeta \to -1, \\ z(\zeta) &\approx \Delta - \frac{\xi}{2\pi k^2}(1+k)(\zeta-k)^2, \quad \zeta \to k. \end{aligned} \tag{2.58}$$

In the ζ plane, the electrostatic potential is simply $\phi = \mathrm{Im}\,\zeta$. Setting $\zeta = \zeta_0 + \mathrm{i}\phi$ in (2.58), with $\zeta_0 = -1$ and k, respectively, and solving for ϕ we find

$$\begin{aligned} \phi(x, y=\xi) &\approx \left[\left(\frac{2\pi k}{1+k}\right)\frac{x}{\xi}\right]^{1/2}, \qquad x \to 0, \\ \phi(x, y=0) &\approx \left[\left(\frac{2\pi k^2}{1+k}\right)\frac{x-\Delta}{\xi}\right]^{1/2}, \quad x \to \Delta. \end{aligned} \tag{2.59}$$

The behaviour of the potential near the tips gives rise to the familiar square root divergence of the electric field. Here we are interested in the *ratio* of the fields at the two tips, which equals the ratio of the fluxes of random walkers onto the two needles. From equation (2.59) we have the simple result

$$E_1/E_2 = \sqrt{k}, \tag{2.60}$$

with E_1 (E_2) denoting the field at the taller (shorter) needle, and hence the fundamental quantity $\mathscr{P}(\Delta, \xi)$ of the two-absorber approximation is given by

$$\mathscr{P}(\Delta, \xi) = \frac{E_1}{E_1 + E_2} = \frac{\sqrt{k}}{1+\sqrt{k}} \approx \frac{1}{2}\left(1 + \frac{\pi\Delta}{8\xi}\right), \tag{2.61}$$

which confirms the expansion (2.48) and proves that $\nu = 1$, at least for this particular configuration of absorbers.

It is also of interest to consider variants of model A in which all walkers that are absorbed on the sides of the needles contribute to the growth [24]. In that case the electrostatic quantity that determines $\mathscr{P}(\Delta, \xi)$ is the normal electric field—that is, the flux of random walkers—*integrated* over the sides of the needles. For the two-needle configuration considered here, it only makes sense to integrate over the inner sides of the needles, since the outer sides are not subject to screening. It is immediately clear from the definition of the mapping that the ratio of the integrated fluxes is simply k, so

$$\mathscr{P}(\Delta, \xi) = \frac{k}{1+k} \approx \frac{1}{2}\left(1 + \frac{\pi\Delta}{4\xi}\right), \tag{2.62}$$

and $\nu = 1$ as before.

While the mapping (2.55) has the virtue of being simple to analyse, the collective screening effects of the full needle forest are more faithfully represented by a *periodic* needle array, with spacing ξ and alternating heights h_1 and $h_2 = h_1 - \Delta$ (see figure 5). A conformal mapping that allows one to compute the electrostatic potential around such an array was presented and analysed in [55]. The results are equivalent to those

derived here: $\mathscr{P}(\Delta, \xi)$ behaves as in (2.48), with $\nu = 1$, and $C = \pi/4$ when only the flux onto the needle tips is considered, and $C = 1$ in the case of the integrated flux.

2.4.3. *High dimensionality behaviour and mean field theory*

We now generalize the discussion of a single random walker penetrating into a periodic needle array to d-dimensional substrates. Our objective is to estimate the distance R_a that the walker is able to venture into the forest before being absorbed, in terms of the needle spacing ξ. We have already seen that $R_a \sim \xi$ for both models in $d = 1$ (equations (2.51) and (2.53)). Moreover, the estimate of the penetration probability $P_\xi(r) \sim \xi^d/r$ for the d-dimensional model R, derived after equation (2.53), allows us to determine R_a from (say) $P_\xi(R_a) = 1/2$, and hence

$$R_a \sim \xi^d, \quad (\text{model R}). \tag{2.63}$$

For model A we employ an opacity argument [55]. In the $d + 1$-dimensional space, the sites visited by a random walk of length t form a cloud of radius $R \sim t^{1/2}$ and density $\rho_w \sim t/R^{d+1} \sim R^{1-d}$ (figure 11). When this cloud is placed inside the needle forest, the number of absorbing sites N_a within the cloud is $N_a \sim R(R/\xi)^d$. In order to have at least one absorption event we require $\rho_w N_a \approx 1$, or $R \sim R_a$ with

$$R_a \sim \xi^{d/2}, \quad (\text{model A}, \ d > 1). \tag{2.64}$$

These estimates immediately provide us with bounds on the height distribution exponent γ. Note first that a density profile $n(h) \sim h^{-(\gamma-1)}$ implies that the spacing between needles increases with h as $\xi \sim h^p$ with

$$p = (\gamma - 1)/d \tag{2.65}$$

(this is the d-dimensional version of equation (2.32)). The absorption length for a needle forest of height h therefore scales as $R_a \sim h^{\gamma-1}$ for model R, and as $R_a \sim h^{(\gamma-1)/2}$ for model A. Consistency clearly requires that $R_a \leq h$, otherwise the walkers would be able to reach the substrate and fill up the deposit until the inequality is restored. We conclude

$$\begin{aligned} &\gamma \leq 2, \quad (\text{model R}), \\ &\gamma \leq 3, \quad (\text{model A}). \end{aligned} \tag{2.66}$$

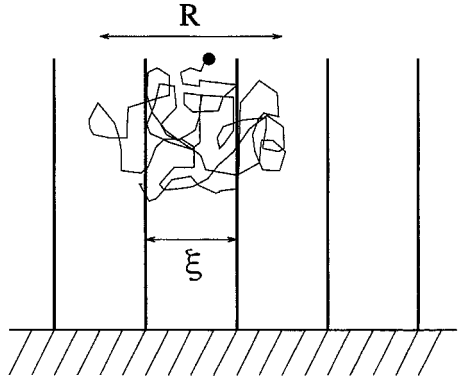

Figure 11. A 'ghost' walker released into a periodic needle array.

Next, we observe that the estimates (2.63) and (2.64) imply a qualitative change in the screening behaviour at an *upper critical dimensionality* $d_c = 2$ for model R, and $d_c = 3$ for model A, in the sense that $R_a \gg \xi$ for $d \geq d_c$. In this high dimensionality regime the random walker effectively averages over many needles before being absorbed, and the two-absorber approximation is clearly inappropriate. Instead, one may attempt a continuum description, in which the lateral structure is ignored and the needle forest is represented by a continuous density function $n(h, t)$. Likewise, the density of walkers is given by a function $u(h, t)$, and the two are coupled through the equations of motion

$$\frac{\partial n}{\partial t} = \sigma_R \rho_{tip} u = -\sigma_R \frac{\partial n}{\partial h} u, \tag{2.67}$$

$$\frac{\partial u}{\partial t} = \frac{\partial^2 u}{\partial h^2} - \left(\sigma_A n - \sigma_R \frac{\partial n}{\partial h}\right) u. \tag{2.68}$$

Equation (2.67) describes the growth by accretion of walkers at the needle tips, and we have used the fact that the tip density is $\rho_{tip} = -\partial n/\partial h$ [53]; σ_R is an absorption coefficient. Equation (2.68) is a balance equation for the walker density. The absorption term has two parts, one describing the absorption at the sides of needles, which occurs only in model A (model R has $\sigma_A = 0$), and the other accounting for the loss of walkers due to needle growth (this part is the negative of the right hand side of equation (2.67)). These 'mean field' equations, with $\sigma_A = 0$, were first written down by Cates [56], and further analysed by Kassner [57].

To extract the essence of these equations, we make a scaling ansatz for the needle density as

$$n(h, t) = h^{-(\gamma-1)} f(h/t^{\kappa}). \tag{2.69}$$

Inserting this into equation (2.67), we find that the walker density must be of the form

$$u(h, t) = t^{-(1-\kappa)} g(h/t^{\kappa}). \tag{2.70}$$

The exponent γ can now be determined by inserting equations (2.69) and (2.70) into equation (2.68) and balancing the diffusion and the absorption terms on the right hand side. With $\sigma_A = 0$, this results in [56, 57]

$$\gamma_{MF} = 2, \quad \text{(model R)}. \tag{2.71}$$

Clearly if $\sigma_A > 0$, the absorption on the sides of the needles dominates that at the tips, and the $\partial n/\partial h$ term on the right hand side of equation (2.68) can be neglected. Therefore

$$\gamma_{MF} = 3, \quad \text{(model A)}. \tag{2.72}$$

The mean field exponents saturate the bounds (2.66), as was already noted by Cates [56] for model R.

To fix the dynamic exponent κ we need to invoke the left hand side of equation (2.68). Not surprisingly, one obtains $\kappa = 1/2$, corresponding to the *diffusive* advancement of the deposit thickness, $h_a(t) \sim t^{1/2}$. Of course, these values for γ and κ provide only *necessary* conditions for scaling solutions of the form (2.69) and (2.70); to actually establish their existence, it must be shown that the resulting equations for the scaling functions f and g admit solutions with physically reasonable behaviour. Kassner's detailed analysis [57] shows that all scaling solutions have the property that the walker density u vanishes for $h \to \infty$. Indeed, Cates [56] had

noted that the scaling forms (2.69) and (2.70) do not admit constant flux boundary conditions, $\partial u/\partial h = \text{const.}$ for $h \to \infty$; such a boundary condition requires that the scaling variable h/t^{κ} be replaced by $h/\exp(\lambda t)$, i.e. the deposit thickness grows exponentially with time, as is obvious from mass balance considerations.

In summary, we have arrived at the following picture for Laplacian needle growth from d-dimensional substrates. In *low dimensionalities*, $d < d_c$, screening is dominated by individual needles and a two-absorber approximation in the spirit of Rossi [50, 53] should be applicable. For model A in $d = 1$, the two-absorber approach was put on a firm basis using the conformal mapping technique; thus we showed that $\nu = 1$ in equation (2.48), and hence the density profile behaves as equation (2.50). There is considerable numerical, and some analytic evidence [55], that these results extend to model R in $d = 1$. In *high dimensionalities*, $d \geq d_c$, we expect the mean field equations (2.67) and (2.68) to provide a reasonable description. This is confirmed by simulations of Rossi [50], who found that $\gamma = \gamma_{MF} = 2$ for model R, both in $d = 2$ and $d = 3$. For model A, $d_c = 3$, so the case $d = 2$ (growth from a plane) should still be in the low dimensionality regime covered by the two-absorber approach. It has been conjectured [55] that $\nu = 2$ in this case, which would imply, according to equation (2.46), a coarsening exponent $p = 3/4$ and hence, from equation (2.65), $\gamma = 5/2$. This prediction, as well as the prediction $\gamma = \gamma_{MF} = 3$ for model A in $d \geq 3$, still has to be verified by numerical simulations. Here, we merely remark an interesting consequence if indeed $\gamma > 2$ in $d \geq 1$: the fact that the average needle height remains bounded (the density profile (2.2) being integrable) even if an infinite amount of mass is added to the deposit; almost all the mass is absorbed on the sides of the needles where it does not contribute to the growth. This scenario is not possible for model R, where all absorbed walkers eventually contribute to the mass of the deposit, as is reflected in the bound (2.66) as well as in the mean field exponent (2.71) which corresponds to a (marginally) non-integrable density profile.

These results do not easily carry over to the full DLA problem [24, 63]. The two problems are fundamentally different in that the needle models possess, due to the effective transparency of needle forests in high dimensionalities, an upper critical dimension, while DLA does not [58]. On the other hand, the two-absorber approach with its emphasis on the binary competition between branches of comparable height (or mass) provides an appealing picture of the elementary screening process, which should be applicable to DLA as well. We may note in this context that Halsey and Leibig [64] and Halsey [65] have recently presented a quantitative, predictive theory of DLA built precisely on an analysis of the elementary process of binary branch competition.

3. Fundamentals of kinetic roughening

Kinetic roughening phenomena are encountered whenever an interface is set into motion in the presence of fluctuations, be it of thermal, kinetic, or chaotic origin, or due to quenched disorder. The earliest theoretical investigations of surface roughness in growth processes [66–68] were concerned with the Eden model [69], originally proposed to describe the shape of cell colonies, and [70] with the ballistic deposition model introduced in the previous section. Following the progress in understanding the *universal* aspects of these processes which was achieved through the seminal work of Kardar, Parisi and Zhang (KPZ) [19] in 1986, a wide variety of more or less exotic instances of kinetic roughening have been suggested and experimentally investigated.

Vicsek, Cserzö and Horváth [71], realizing the original intent of Eden's work, studied the roughening edge of a growing bacterial colony; several groups investigated the roughening of a stable two-fluid interface in a porous medium [72–74]; and Zhang, Zhang, Alstrom and Levinsen [75] considered the roughening edge of a sheet of paper as it is consumed by fire [76]. Curiously, while all of these experiments were motivated by the KPZ theory, none of them was able to quantitatively confirm its predictions. The discrepancy between theory and experiment has spurred considerable theoretical activity involving modifications of the KPZ theory through the introduction of, for example, correlated [77], non-Gaussian [78–80] and quenched noise [81–84]; a review of these developments has been given by Halpin-Healy and Zhang [11] and by Tang [14].

Here, we shall adopt a somewhat conservative point of view, and introduce the basic concepts of kinetic roughening within the 'classic' context of a moving interface separating two isotropic thermodynamic phases. The reader with some background in statistical mechanics may visualize, for concreteness, an Ising model below its critical temperature, with an interface separating domains of positive and negative magnetization, and subject to an external magnetic field that favours one of the phases, thereby setting the interface into motion. (Strictly speaking, the permanence of a well-defined interface in such a situation requires a careful tuning of temperature and magnetic field to avoid bulk nucleation of the favoured phase [85].) We are going to derive effective, nonlinear equations of motion for the interface, appropriate for different types of interfacial relaxation mechanisms, and then proceed to analyse the roughening process within the *linear* approximation. While not always quantitatively correct, the linear theory already contains the essential ingredients of kinetic roughening phenomena, and provides us with a firm foundation for explorations into the realm of nonlinear theories. As a first step towards a nonlinear theory, the effect of nonlinearities on large scales is estimated using power counting arguments. Retaining only nonlinear terms which are *relevant* in this sense, one arrives, for a particular but broad class of conditions to be specified below, at the KPZ equation, some aspects of which will be treated in section 4.

3.1. *Interface equations of motion*

Consider an interface oriented on average parallel to a d-dimensional 'substrate' hyperplane in $(d+1)$-dimensional space. On a somewhat coarse-grained level we may describe the interface position by a height function $x_{d+1} = h(\mathbf{x}, t)$, where $\mathbf{x} = (x_1, \ldots, x_d)$ is the substrate coordinate. In the presence of an external field $\mu_0 > 0$, which favours the phase occupying the half space $x_{d+1} < h$ over the phase in $x_{d+1} > h$ (figure 12), the free energy of the system can be written as

$$\mathscr{F}[h(\mathbf{x}, t)] = \sigma \int \mathrm{d}^d\mathbf{x}\, [1 + (\nabla h)^2]^{1/2} - \mu_0 \int \mathrm{d}^d\mathbf{x}\, h, \tag{3.1}$$

where the interfacial tension σ is assumed, for simplicity, to be independent of orientation. The interfacial free energy in equation (3.1) corresponds to the 'drumhead' model [86] which neglects the intrinsic interface width (expected to be of the order of the bulk correlation length).

The driving force for morphological changes is the interface chemical potential

$$\mu = \delta\mathscr{F}/\delta h. \tag{3.2}$$

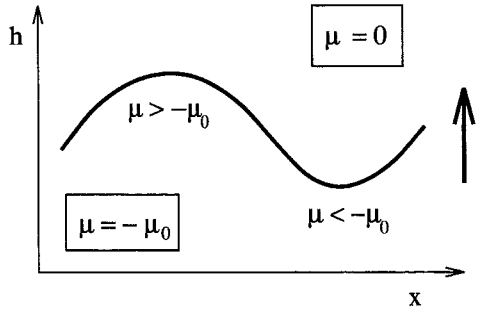

Figure 12. Interface between a favoured ($\mu = -\mu_0 < 0$) and an unstable ($\mu = 0$) phase. The chemical potential is increased (reduced) at local maxima (minima). The arrow indicates the direction of interface motion.

A conventional relaxation ansatz for the dynamics then yields the normal interface velocity as

$$v_n = -\Gamma \frac{\delta \mathscr{F}}{\delta h} = -\Gamma \mu, \tag{3.3}$$

where $\Gamma > 0$ is the interface mobility [87]; to arrive at an equation of motion for $h(\mathbf{x}, t)$ we merely note that, from an obvious geometric construction,

$$\partial h/\partial t = v_n[1 + (\nabla h)^2]^{1/2}. \tag{3.4}$$

In the interest of keeping the notation transparent, we give explicit expressions only for the case $d = 1$, where $h(x, t)$ is a curve. Performing the functional derivative of equation (3.1) we arrive at

$$\mu = -\frac{\sigma \nabla^2 h}{[1 + (\nabla h)^2]^{3/2}} - \mu_0, \tag{3.5}$$

where the term multiplying the interfacial tension σ is the local *curvature* (see figure 12). Thus the full equation of motion reads

$$\frac{\partial h}{\partial t} = \Gamma[1 + (\nabla h)^2]^{1/2}\left\{\mu_0 + \frac{\sigma \nabla^2 h}{[1 + (\nabla h)^2]^{3/2}}\right\}. \tag{3.6}$$

It is interesting to note that, besides the trivial flat solution $h = \Gamma \mu_0 t$, equation (3.6) admits (semi-)circular 'droplet' solutions of the form

$$h(x, t) = [R^2(t) - x^2]^{1/2}, \quad x^2 \leq R^2, \tag{3.7}$$

where the radius $R(t)$ satisfies

$$\mathrm{d}R/\mathrm{d}t = \Gamma(\mu_0 - \sigma/R). \tag{3.8}$$

From this we infer the existence of a critical droplet radius $R_c = \sigma/\mu_0$ such that droplets with $R > R_c$ grow while those with $R < R_c$ shrink under surface tension; $R = R_c$ is an unstable equilibrium. Equation (3.8) (and, indeed, equation (3.6)) is an expression of the familiar Gibbs–Thomson relation which states that a larger thermodynamic driving force is required to move a curved interface.

Let us now specifically apply these considerations to a solid growing from a vapour phase. The Gibbs–Thomson effect is then microscopically realized through

an increased (decreased) evaporation rate at negatively (positively) curved portions of the surface. It turns out, however, that many technologically relevant vapour deposition processes are operated under conditions of negligible evaporation [20, 88]. In such cases the 'evaporation–condensation'-dynamical ansatz (3.3) is inappropriate and has to be replaced by an equation describing relaxation through mass transport *along* the surface [18]. To arrive at such a description, first note that the quantity defined in equation (3.2) may be interpreted, in the present situation, as the *chemical potential of adatoms*; indeed, $\delta\mathscr{F}/\delta h$ is precisely the change in surface free energy associated with removing or adding a small amount of mass to the surface. When desorption is kinetically suppressed, chemical potential differences that arise due to modulations of the surface profile (as in figure 12) relax through surface diffusion currents, viz the migration of adatoms in the direction of chemical potential gradients. Thus, the normal velocity of the surface is given by

$$v_n = -\partial J/\partial s, \tag{3.9}$$

where J is (in the 1D situation considered here) the mass current along the arc length

$$s = \int \mathrm{d}x\, [1 + (\nabla h)^2]^{1/2}. \tag{3.10}$$

As the current is driven by chemical potential gradients, we have

$$J = -\Gamma_a \frac{\partial \mu}{\partial s} = -\frac{\Gamma_a}{[1 + (\nabla h)^2]^{1/2}} \frac{\partial \mu}{\partial x}, \tag{3.11}$$

with an *adatom mobility* $\Gamma_a > 0$. Putting everything together, we arrive at the equation

$$\frac{\partial h}{\partial t} = -\frac{\partial}{\partial x} \frac{\Gamma_a}{[1 + (\nabla h)^2]^{1/2}} \frac{\partial}{\partial x} \frac{\sigma \nabla^2 h}{[1 + (\nabla h)^2]^{3/2}}. \tag{3.12}$$

The explicit form of the 2D generalization of this equation has been derived in several recent papers [89–91].

The reader will have noticed at this point that the external field μ_0, introduced in equation (3.1) to set the surface into motion, has effectively disappeared from the description; in fact the surface governed by equation (3.12) does not move. We can of course cure this deficiency by adding a constant deposition flux F to the right hand side of equation (3.12), however, this implies only a trivial change that can be undone by going to a frame moving at a speed F. The physical reason behind this surprising result is clear: within the framework of the classical theory, as expressed in equations (3.9) and (3.11), the surface diffusion processes, being sensitive only to spatial gradients in the chemical potential μ, are not affected by an overall constant shift μ_0. It is also clear that this is unlikely to be the whole truth. A more careful consideration of the microscopic kinetics reveals that the mass transport on the surface can be rather drastically altered by the presence of a deposition flux F. On the level of effective interface equations of motion this implies the appearance of additional *dynamic* non-equilibrium terms in equation (3.12), the coefficients of which are proportional to F. We postpone to section 5 the detailed discussion of the microscopic origins of these terms, and present here only the main results.

As was first suggested by Villain [20], two types of terms are expected to be present generically. The first set of terms arises because under non-equilibrium conditions the local chemical potential (or, rather, its appropriate non-equilibrium

generalization, see section 5.4) acquires a dependence on the local surface *orientation*. In equilibrium it is clear from the definition (3.2) of μ as a functional derivative, and from the fact that the free energy $\mathcal{F}$ should be invariant under vertical translations $h \to h + \text{const.}$, that the leading dependence of μ is on the local *curvature*. From symmetry considerations one expects the non-equilibrium contribution to be an even function of ∇h, and thus to admit an expansion

$$\mu_{\text{NE}} = \lambda_2(\nabla h)^2 + \lambda_4(\nabla h)^4 + \cdots. \tag{3.13}$$

The second type of non-equilibrium effects leads to a contribution to the current J in equation (3.9) which, rather than being proportional to the gradient of some (equilibrium or non-equilibrium) chemical potential, is itself a function of the local surface orientation [92]. General symmetry arguments and detailed calculations, to be presented in section 5.2, show that the non-equilibrium current is an odd function of ∇h, such that, in a gradient expansion.

$$J_{\text{NE}} = -[\nu_1 + \nu_3(\nabla h)^2 + \cdots]\nabla h. \tag{3.14}$$

Here the leading term $\nu_1 \nabla h$ is of special importance in that it changes the character of the equation of motion already on the level of the linearization around the flat state, which will be the focus of the next section. In particular, if $\nu_1 < 0$ ('uphill' current) the surface can be *destabilized* by (non-equilibrium) surface diffusion (see section 5.3).

Including the non-equilibrium contributions (3.13) and (3.14), through equations (3.9) and (3.11), in the interface equation of motion leads to a problem of rather formidable complexity. Schematically, the final result reads as

$$\frac{\partial h}{\partial t} = \frac{\partial}{\partial x} \frac{\Gamma_{\text{a}}}{[1 + (\nabla h)^2]^{1/2}} \frac{\partial}{\partial x}(\mu + \mu_{\text{NE}}) - \frac{\partial}{\partial x} J_{\text{NE}} + F, \tag{3.15}$$

and it should be remembered that $\mu_{\text{NE}}, J_{\text{NE}} = \mathcal{O}(F)$. Equation (3.15) provides the most general macroscopic description of growth under conditions of volume-conserving surface relaxation. Correspondingly, equation (3.6) is the general equation of motion for *non-conserved* interface dynamics.

3.2. *Linearized fluctuation theory*

The theory of kinetic roughening is concerned with the question of how microscopic fluctuations, which are present in virtually any interface displacement process, are transformed, through effective interface equations of the kind derived in the previous section, into large-scale behaviour with universal properties. This transformation becomes transparent and easily tractable when the equations of motion are linearized about the flat solution $h(\mathbf{x}, t) = v_0 t$. One may hope that the linearization is appropriate when the interface is flat on average, or when one considers length scales on which macroscopic modulations of the interface orientation are negligible. We shall see later that this hope is not quite warranted, due to the possibility of *relevant* nonlinearities which dominate the large scale properties of an interface even in the absence of macroscopic modulations; however, in order to appreciate the role of nonlinearities we first need to acquire a thorough understanding of the linear fluctuation theory.

3.2.1. *Langevin equations*

Fluctuations are commonly modelled by adding a stochastic noise term $\eta(\mathbf{x}, t)$ to the right hand side of the interface equation of motion. The noise is assumed to be Gaussian and uncorrelated, with zero mean and covariance

$$\langle \eta(\mathbf{x}, t)\eta(\mathbf{x}', t')\rangle = D\delta^d(\mathbf{x} - \mathbf{x}')\delta(t - t'). \tag{3.16}$$

Here and in the following the angular brackets imply an average over noise histories. Since we aim at a theory that is as general as possible, we will not, at this point, specify the physical origin of the noise. In processes that operate at or close to equilibrium, the fluctuations are mainly of a thermal nature; far from equilibrium additional sources of noise appear, such as shot noise in deposition processes or the frozen disorder in interface displacements in porous media (in the latter case the fluctuations can be modelled by a time-dependent noise term only if the displacement is sufficiently rapid [93]).

However, one remark is in order, regarding the different roles of the noise in the two classes of processes described by equations (3.6) and (3.15), respectively. In the case of nonconserved dynamics (equation (3.6)), as exemplified by a moving Ising interface, the noise term $\eta(\mathbf{x}, t)$ is present even in equilibrium, when $\mu_0 = 0$; the coefficient D in equation (3.16) is then proportional to the temperature T. In contrast, with mass conserving surface diffusion dynamics (equation (3.15)), the deposition flux is the sole source of noise that can change the total amount of mass on the surface; the *thermal* fluctuations which arise due to the particulate nature of the surface transport, and which survive in equilibrium, when $F = 0$, conserve the volume of the solid. Mathematically, this is expressed through a *conserved* noise term η_c which can be written as the divergence of a stochastic current, $\eta_c(\mathbf{x}, t) = -\nabla\cdot\mathbf{j}_s(\mathbf{x}, t)$, and hence has a covariance of the form

$$\langle \eta_c(\mathbf{x}, t)\eta_c(\mathbf{x}', t')\rangle = -D_c\nabla^2\delta^d(\mathbf{x} - \mathbf{x}')\delta(t - t'), \tag{3.17}$$

with $D_c \sim T$, whereas the coefficient of the non-conserved noise term D is proportional to the flux F. In growth processes where surface relaxation occurs mainly through surface diffusion, the noise itself is a non-equilibrium effect; we shall see that this implies very pronounced fluctuations in these systems. The 'mismatch' between nonconserved noise and conserved relaxation dynamics provides a general mechanism for power laws and generic scale invariance also in systems that do not possess the translational symmetry of interfaces [94, 95]. It is intuitively plausible that a nonconserved noise term, when present, dominates the conserved noise η_c on large length and time scales, and that the latter can therefore be neglected; a more precise argument will be given below.

We now linearize the equations of motion (3.6) and (3.15) around a flat, uniformly moving front $h_0(t) = v_0 t$, with $v_0 = \Gamma\mu_0$ for equation (3.6) and $v_0 = F$ for equation (3.15). Adding the noise term one has, in the moving frame,

$$\frac{\partial h}{\partial t} = -(-\nu\nabla^2)^m h + \eta. \tag{3.18}$$

The case $m = 1$ includes the linearization of equation (3.6), where $\nu = \Gamma\sigma$, as well as that of equation (3.15) in the presence of a stabilizing non-equilibrium current (3.14), such that $\nu = \nu_1 > 0$ (the linearization is clearly useless in the unstable case $\nu_1 < 0$, which will be treated in section 5.3); the fourth order derivative $\nabla^4 h$ that arises from the linearization of the equilibrium equation (3.12) can then be neglected. This leads

to an important general conclusion: A non-equilibrium current, provided it is directed downhill so that $\nu_1 > 0$, may effectively mimic evaporation–condensation dynamics (in the sense that $m = 1$ in equation (3.18)) even if evaporation is kinetically suppressed. If, on the other hand, J_{NE} is absent or negligible, the linearization of equation (3.15) results in equation (3.18) with $m = 2$ and $\nu = \Gamma_a \sigma$. Note that while the explicit forms of the full nonlinear equations were given in equations (3.6) and (3.15) only for $d = 1$, the linearization (3.18) holds in arbitrary dimensionality.

Equation (3.18) with $m = 1$ has been employed to describe the equilibrium dynamics of interfaces, for example in the contexts of thermal roughening and wetting [96, 97]. In the kinetic roughening literature it is commonly referred to as the Edwards–Wilkinson equation. Edwards and Wilkinson [98] were the first to derive this equation for a nonequilibrium situation, specifically, as a description of the sedimentation of granular particles. In that case the relaxation term $\nu\nabla^2 h$ arises from the expansion (3.14) of a nonequilibrium mass current driven downhill by gravity, and the coefficient ν_1 is proportional to the particle flux. While gravity obviously plays no role on the atomic level, microscopic mechanisms associated, for example, with the transient kinetic energy of the deposited atoms [99] exist which can give rise to downhill currents in vapour deposition processes.

Equation (3.18) with $m = 2$ was first written down and discussed by Golubović and Bruinsma [100] and by Wolf and Villain [101]; since its deterministic form ($\eta = 0$) originates in the work of Mullins [18], we refer to it as the (noisy) *Mullins equation*.

3.2.2. *General solution*

To solve equation (3.18) we introduce the Fourier decomposition

$$\begin{aligned} h(\mathbf{x}, t) &= \sum_{\mathbf{q}} h_{\mathbf{q}}(t) \exp(i\mathbf{q}\cdot\mathbf{x}), \\ \eta(\mathbf{x}, t) &= \sum_{\mathbf{q}} \eta_{\mathbf{q}}(t) \exp(i\mathbf{q}\cdot\mathbf{x}), \end{aligned} \tag{3.19}$$

where the sums run over the allowed reciprocal vectors of a lattice of linear size L, periodic boundary conditions and a lattice constant a. From equation (3.16) we find the covariance of the Gaussian noise components

$$\langle \eta_{\mathbf{q}}(t)\eta_{\mathbf{q}'}(t')\rangle = L^{-d} D \delta_{\mathbf{q}+\mathbf{q}'}\delta(t - t'), \tag{3.20}$$

while for the conserved noise defined by equation (3.17) one has

$$\langle \eta_{c\mathbf{q}}(t)\eta_{c\mathbf{q}'}(t')\rangle = L^{-d} D_c \mathbf{q}^2 \delta_{\mathbf{q}+\mathbf{q}'}\delta(t - t'). \tag{3.21}$$

This shows why η_c can be neglected on large scales (small q), if a non-conserved noise source is present. The Fourier components of h evolve independently according to

$$\frac{\partial}{\partial t} h_{\mathbf{q}} = -\nu |\mathbf{q}|^z h_{\mathbf{q}} + \eta_{\mathbf{q}}, \tag{3.22}$$

where we have set $z = 2m$. Odd values of z can appear when the relaxation dynamics is *nonlocal*, for example $z = 1$ applies to diffusion-limited erosion [102] or relaxation through plastic flow [16, 18], and $z = 3$ describes a surface relaxing to equilibrium through volume diffusion [18]. Since there is no difficulty in solving equation (3.22) for general z, we can treat all these cases on the same footing.

According to equation (3.22), each mode behaves as a randomly perturbed harmonic oscillator with restoring force $\nu|\mathbf{q}|^z$. The general solution is

$$h_{\mathbf{q}}(t) = \exp(-\nu|\mathbf{q}|^z t)\, h_{\mathbf{q}}(0) + \int_0^t \mathrm{d}\tau \exp[-\nu|\mathbf{q}|^z(t-\tau)]\, \eta_{\mathbf{q}}(\tau). \tag{3.23}$$

Here we will mostly be concerned with the *transient* roughening of an initially flat interface, so we set $h_{\mathbf{q}}(0) = 0$ for all $\mathbf{q}$. Growth on rough substrates will be treated in section 3.2.5. Multiplying equation (3.23) with $h_{\mathbf{q}'}(t)$ and averaging over the noise according to equation (3.20), we obtain

$$\langle h_{\mathbf{q}}(t) h_{\mathbf{q}'}(t)\rangle = S(q, t)\delta_{\mathbf{q}+\mathbf{q}'}, \tag{3.24}$$

with $q = |\mathbf{q}|$ and

$$S(q, t) = L^{-d}\frac{D}{2\nu q^z}[1 - \exp(-2\nu q^z t)]. \tag{3.25}$$

Since $h_{\mathbf{q}}(t)$ derives from the Gaussian random variable $\eta_{\mathbf{q}}(t)$ through a linear transformation, the height modes themselves are Gaussian and higher-order correlation functions are simply related to the covariance (3.24); thus equation (3.25) completely specifies the statistics of interfacial fluctuations. Two features of equation (3.25) are noteworthy. First, the relaxation time of a mode with wavenumber q is proportional to q^z, i.e. long wavelength modes relax slowly. Second, the prefactor in equation (3.25) diverges for $q \to 0$, thus giving large statistical weight to long wavelength modes. Together these two observations bring out the central mechanism of kinetic roughening; note also that both effects are more pronounced the larger the value of z.

To proceed, we translate equation (3.25) into more conventional measures of interface roughness. Of particular interest are the interface width W, defined through

$$W^2 = \langle[h - \bar{h}(t)]^2\rangle = \sum_{\mathbf{q}\neq\mathbf{0}} S(q, t), \tag{3.26}$$

and the (second order) height difference correlation function

$$G_2 = \langle(h(\mathbf{x}+\mathbf{r}, t) - h(\mathbf{x}, t))^2\rangle = 2\sum_{\mathbf{q}} S(q, t)(1 - \cos\mathbf{q}\cdot\mathbf{r}). \tag{3.27}$$

In equation (3.26) the instantaneous spatial average $\bar{h}(t) = h_{\mathbf{q}=\mathbf{0}}(t)$ has been subtracted; since the noise operates also at $\mathbf{q} = \mathbf{0}$, $\bar{h}(t)$ performs a random walk with diffusion constant D/L^d.

For a first estimate of the width we approximate the sum in equation (3.26) by an integral and obtain, up to factors of order unity,

$$W^2 \sim \frac{D}{\nu}\int_{2\pi/L}^{\pi/a} \mathrm{d}q\, q^{d-1-z}[1 - \exp(-2\nu q^z t)]. \tag{3.28}$$

The integral is governed by the interplay of *three length scales*: the lattice constant a, the substrate size L, and the *dynamical correlation length*

$$\xi(t) \equiv (2\nu t)^{1/z}. \tag{3.29}$$

The lattice constant is irrelevant, in the sense that the integral converges for $a \to 0$, below the upper characteristic dimensionality

$$d_c^{(1)} = z. \tag{3.30}$$

For $d > d_c^{(1)}$, we may let $L, t \to \infty$ to obtain a finite limiting interface width $W^2 \approx (D/\nu)a^{z-d}$. This implies that the noise is able to *roughen* the interface, in the sense of a proliferation of long wavelength fluctuations leading to a divergent width for $L, t \to \infty$, only in sufficiently low dimensionalities.

In the rough regime $d < d_c^{(1)}$, the power law prefactor of the integrand in equation (3.28) implies a divergence at small q which is limited by the smaller of the lengths L and ξ. We may let $a \to 0$ and summarize the dependence on the remaining two length scales in the scaling form [68, 70]

$$W^2(L, t) \sim L^{2\zeta} f(\xi(t)/L), \tag{3.31}$$

with the *roughness exponent*

$$\zeta = (z - d)/2 > 0, \tag{3.32}$$

and the scaling function

$$f(x) = \frac{D}{\nu} \int_{2\pi}^{\infty} \mathrm{d}y\, y^{d-1-z} \{1 - \exp[-(xy)^z]\}. \tag{3.33}$$

The scaling form (3.31) brings out the significance of the correlation length ξ: the width saturates, that is, it becomes time-independent, when $\xi \sim L$, at a time of the order of

$$t_c \approx L^z/\nu. \tag{3.34}$$

This time scale marks the transition from the transient to the *stationary* regime where the memory of the flat initial condition is lost. At early times when $\xi \ll L$, expanding equation (3.33) shows that the width increases as

$$W^2 \sim (D/\nu)\xi^{2\zeta} \sim t^{2\zeta/z}. \tag{3.35}$$

In the borderline dimensionality $d = d_c^{(1)}$, all three length scales have to be taken into account, and one finds

$$W^2 \sim \begin{cases} (D/\nu) \ln(\nu t/a), & \xi \ll L, \\ (D/\nu) \ln(L/a), & \xi \gg L. \end{cases} \tag{3.36}$$

For future reference we record some exact expressions for 1D interfaces, $d = 1$, in the rough regime, i.e. for $z > 1$. Consider first the stationary limit, $t \to \infty$. With $a \to 0$ the sum (3.26) can be written as

$$\lim_{t\to\infty} W^2(L, t) = (2\pi)^{-z} \zeta_R(z)(D/\nu)L^{2\zeta}, \tag{3.37}$$

where

$$\zeta_R(z) \equiv \sum_{k=1}^{\infty} \frac{1}{k^z} \tag{3.38}$$

denotes the Riemann zeta function; for even integer values of z, $\zeta_R(z) = 2^{z-1}\pi^z B_{z/2}/z!$ with the Bernoulli numbers B_m, and equation (3.37) simplifies to

$$\lim_{t\to\infty} W^2(L, t) = \frac{B_{z/2}}{z!} \frac{D}{2\nu} L^{2\zeta}. \tag{3.39}$$

Of primary interest are the cases $z = 2$, where $B_1/2! = 1/12$, and $z = 4$ with $B_2/4! = 1/720$. In these cases the full distribution of W^2 can also be computed [103–105].

To evaluate the width in the transient case, $\xi \ll L$, we let $L \to \infty$ as well as $a \to 0$ at fixed t. The sum (3.26) then converges to an integral, which yields, after some simple manipulations,

$$\lim_{L\to\infty} W^2(L, t) = \frac{1}{2\pi}\frac{D}{\nu}\frac{\Gamma(1/z)}{z-1}(2\nu t)^{2\zeta/z}, \tag{3.40}$$

with Γ denoting the gamma function. From equations (3.37) and (3.40) we can derive a more precise estimate of the crossover time t_c introduced in equation (3.34). Matching the two expressions we conclude that the crossover from the transient to the stationary regime occurs when the ratio of the correlation length (3.29) to the system size is

$$\frac{\xi}{L} = \frac{1}{2\pi}\left[\frac{(z-1)\zeta_R(z)}{\Gamma(1/z)}\right]^{1/(z-1)}. \tag{3.41}$$

The numerical value of the right hand side is $\sqrt{\pi/12} \approx 0{\cdot}148$ for $z = 2$, and $\approx 0{\cdot}153$ for $z = 4$.

3.2.3. *Anomalous scaling*

In the height difference correlation function (3.27) the distance r between the two substrate points introduces a further length scale. For some special cases in $d = 1$ the series for the stationary, $t \to \infty$, correlation function can be summed exactly. For $z = 2$ one obtains

$$G_2(r, L) = (D/2\nu)r(1 - r/L), \tag{3.42}$$

and for $z = 4$

$$G_2(r, L) = (D/24\nu)Lr^2(1 - r/L)^2. \tag{3.43}$$

Comparing the two expressions we notice that equation (3.42) has a finite limit $G_2(r) = (D/2\nu)r$ for $L \to \infty$, while equation (3.43) does not.

To appreciate the origin of the different behaviours, we turn to the general case and approximate equation (3.27) as

$$G_2 \sim \frac{D}{\nu}\int_{2\pi/L}^{\pi/a} \mathrm{d}q_\parallel\,(1 - \cos q_\parallel r)\int_{2\pi/L}^{\pi/a} \mathrm{d}q_\perp\, q_\perp^{d-2} q^{-z}[1 - \exp(-2\nu q^z t)], \tag{3.44}$$

where $q_\parallel$ and $q_\perp$ denote the components of $\mathbf{q}$ parallel and perpendicular to $\mathbf{r}$, and $q = (q_\parallel^2 + q_\perp^2)^{1/2}$. We focus on the rough case, $d < d_c^{(1)}$, where the limit $a \to 0$ can be performed, and also let $L \to \infty$, since we expect the roles of L and ξ to be interchangeable. Then equation (3.44) reduces to

$$G_2 \sim \frac{D}{\nu}\int_0^\infty \mathrm{d}q_\parallel\, q_\parallel^{d-1-z}(1 - \cos q_\parallel r)F(q_\parallel \xi), \tag{3.45}$$

where $F(s) \sim s^{z-d+1}$ for $s \to 0$ and $F(s \to \infty) = \text{const}$. For $r \gg \xi$ the cosine term in the integrand can be dropped and G_2 saturates at a value of the order $\xi^{z-d} = \xi^{2\zeta}$, as would be expected on the basis of the identity

$$\lim_{r\to\infty}\lim_{L\to\infty} G_2 = 2W^2. \tag{3.46}$$

To extract the behaviour for small r, $r \ll \xi$, one might attempt a series expansion of $1 - \cos q_\parallel r$. The coefficient of the leading r^2 term is finite, and of order ξ^{z-d-2}, only if

$$d < d_c^{(2)} = z - 2. \tag{3.47}$$

Otherwise G_2 is nonanalytic for $r \to 0$, $G_2 \sim r^{z-d} = r^{2\zeta}$, with a prefactor of order D/ν.

The dimensionality $d_c^{(2)}$ thus separates two regimes of qualitatively different behaviour for G_2. For $d > d_c^{(2)}$, *conventional* scaling holds in the sense that G_2 satisfies a scaling form analogous to that of the width (3.31):

$$G_2(r, t) = r^{2\zeta} g[r/\xi(t)]. \tag{3.48}$$

However, for $d < d_c^{(2)}$, the $r^{2\zeta}$ singularity of G_2 is 'hidden' by the regular r^2 term, which dominates it for small r, and equation (3.48) is replaced by the *anomalous* scaling form [106–108]

$$G_2(r, t) = \xi^{2\alpha} r^{2\tilde{\zeta}} \tilde{g}(r/\xi(t)), \tag{3.49}$$

featuring a different r dependence and an additional power of ξ. Both scaling functions tend to constants of order D/ν for small arguments, $r \ll \xi$, and decay as $g(s) \sim s^{-2\zeta}$, $\tilde{g}(s) \sim s^{-2\tilde{\zeta}}$ for large arguments. The anomalous scaling exponents in equation (3.49) take the values

$$\alpha = \zeta - 1, \quad \tilde{\zeta} = 1. \tag{3.50}$$

In the borderline case, $d = d_c^{(2)}$, $\alpha = 0$, the short distance behaviour becomes [106] $G_2 \sim r^2 \ln(\xi/r)$, $r \ll \xi$. In general, we observe that because of equation (3.46), consistency between equations (3.49) and (3.35) requires

$$\alpha + \tilde{\zeta} = \zeta. \tag{3.51}$$

In the stationary limit $\xi \gg L$, analogous scaling forms hold with ξ replaced by L (see equations (3.42) and (3.43)).

Comparing equations (3.32) and (3.47) we recognize that the dimensionality $d_c^{(2)}$ is characterized by

$$\zeta(d_c^{(2)}) = 1. \tag{3.52}$$

The value $\zeta = 1$ of the roughness exponent is special because it signals, in a certain sense, that the assumption of a well-defined average orientation of the interface (parallel to the substrate plane) becomes inconsistent: the orientational fluctuations at scale L estimated, for example, as $W(L, \infty)/L$, decrease with L only if $\zeta < 1$ [100]. The conclusions that can be drawn, if it is found that $\zeta = 1$ for a particular dimensionality, depend on the physical context. For equilibrium interfaces $\zeta = 1$ is commonly associated with the breakdown of two-phase coexistence at the lower critical dimensionality of the *bulk* system [109]; for example, for the pure Ising model $\zeta = (2 - d)/2 = 1$ in bulk dimension $d + 1 = 1$, while for the Ising model with random fields [110] the Imry–Ma expression $\zeta = (4 - d)/3$ shows that the disorder shifts the (bulk) lower critical dimensionality to $d + 1 = 2$. Fluid membranes governed by bending elasticity rather than surface tension have $\zeta = (4 - d)/2$, and hence $\zeta = 1$ in the physical dimension $d = 2$; this reflects the tendency of membranes to *crumple* on scales larger than the (possibly astronomical) persistence length [111].

In the present context the anomalous scaling regime described by equation (3.49) appears only in the case of surface diffusion dynamics without nonequilibrium currents, where $z = 4$ so $\zeta \geq 1$ in dimensionalities $d \leq 2$. Physically, the anomalous behaviour is a consequence of the 'mismatch' between mass conserving relaxation

dynamics and non-conserving shot noise previously alluded to. Relaxation through surface diffusion is insufficient to counteract the disordering influence of the shot noise even locally; thus *local* roughness measures such as the slope fluctuation $\langle(\nabla h)^2\rangle$ become enslaved by the long wavelength modes and diverge with increasing correlation length (or system size) as $\langle(\nabla h)^2\rangle \sim \xi^{2\alpha}$ with $\alpha > 0$ (cf. equation (3.49)). While nonlinearities are expected to significantly alter this picture, there is numerical evidence [107, 108, 112] that the anomalous scaling form (3.49) (possibly with nonuniversal values of the exponents α and $\tilde{\zeta}$) is generic for deposition processes with conserved surface relaxation in low dimensionalities. Moreover, two recent experiments on the Si(111) surface have reported a logarithmic divergence of the slope fluctuations, consistent with the marginal case $z = 4$, $\zeta = 1$ [113, 114]. We will return to this issue in section 5.5.2.

3.2.4. *Long distance asymptotics of height correlations*

We have seen above that the roughness exponent ζ characterizes the (possibly hidden) short-distance singularity of the height-difference correlation function. It is clearly legitimate to enquire also about the asymptotics in the opposite limit $r \gg \xi$. Surprisingly, this question has been addressed only very recently [115]. It is not merely of academic interest, since the interpretation of scattering data from rough surfaces typically requires a model for the full height correlations, including the regimes $r \approx \xi$ and $r \gg \xi$ [16, 17, 116–118] (see section 5.6).

The problem is posed most naturally in terms of the height–height correlation function

$$C(r, t) = \langle h(\mathbf{x} + \mathbf{r}, t)h(\mathbf{x}, t)\rangle = W^2 - \tfrac{1}{2}G_2(r, t), \tag{3.53}$$

which decays to zero for $r \gg \xi$. Since $C(0, t) = W^2$, we can write

$$C(r, t) = W^2\mathscr{C}(r/\xi(t)), \tag{3.54}$$

with $\mathscr{C}(s \to 0) = 1 - \mathcal{O}(s^{2\zeta})$ in the case of conventional scaling, and $\mathscr{C}(s \to 0) = 1 - \mathcal{O}(s^{2\tilde{\zeta}})$ in the anomalous case. The large-distance asymptotics of $\mathscr{C}$ has been computed for the linear theories with $z = 2$ and $z = 4$, in dimensionalities $d = 1$ and 2 [115]. The results indicate that the decay is generally of the form

$$\mathscr{C}(s) \sim s^{-\gamma} \exp(-cs^{\delta}), \tag{3.55}$$

with $\gamma > 0$ and $\delta = z/(z - 1)$. The coefficient c is real for the Edwards–Wilkinson equation ($z = 2$), but complex for $z = 4$; in the latter case the correlations decay in a damped oscillatory manner, analogous to the spatial oscillations that occur in the macroscopic shape evolution governed by surface diffusion [18].

A closed expression for $C(r, t)$ can be derived in the case $z = 1$, $d = 1$, which describes diffusion-limited erosion in $1 + 1$ dimensions [102] (see also section 3.4). One obtains

$$C(r, t) = \frac{D}{2\nu}\ln(1 + \xi^2/r^2) \approx \frac{D}{2\nu}\frac{\xi^2}{r^2}, \tag{3.56}$$

for $r \gg \xi$. The power law decay reflects the nonlocality of the interface dynamics or, equivalently, the fact that $S(q, t)$ in equation (3.25) is nonanalytic at $q = 0$. Conversely, whenever the dynamics is local (i.e. for even integer values of z) one expects an exponential-like decay as in equation (3.55).

3.2.5. *Growth on rough substrates*

In most applications of thin film growth the substrate possesses some residual roughness. Within the linear theory this is easily incorporated by choosing the initial conditions in equation (3.23) from a suitable statistical ensemble. Let us assume for concreteness that the substrate is rough with roughness exponent $\zeta_0 > 0$ and correlation length ξ_0. The initial correlations are then of the form

$$\langle h_{\mathbf{q}}(0) h_{\mathbf{q}'}(0) \rangle = \delta_{\mathbf{q}+\mathbf{q}'} q^{-(d+2\zeta_0)} g_0(q\xi_0), \tag{3.57}$$

with $g_0(s \to 0) \sim s^{d+2\zeta_0}$ and $g_0(s \to \infty) = \text{const}$. Using the general solution (3.23) in the evaluation of the surface width (3.26), one obtains the decomposition

$$W^2 = W_0^2 + W_{\text{flat}}^2, \tag{3.58}$$

where W_{flat} is the growth-induced roughness from flat initial conditions discussed previously in this section, and W_0 is the width of the initially rough interface which evolves deterministically under the *noiseless* dynamics, equation (3.18) with $\eta = 0$. Since the deterministic equation is relaxational, W_0 decreases with time, as the rough initial features are covered up by the growing film. The detailed analysis shows that [115]

$$W_0(t) \approx \begin{cases} W_0(0), & \xi \ll \xi_0, \\ W_0(0)[\xi_0/\xi(t)]^{d/2}, & \xi \gg \xi_0, \end{cases} \tag{3.59}$$

where $\xi(t)$ is the usual correlation length of the growth process. The fact that the total width (3.58) is the sum of a decreasing (W_0^2) and an increasing (W_{flat}^2) part implies the possibility of nonmonotonic time evolution, as has been experimentally observed [119, 120].

3.3. *Relevant nonlinearities*

To what extent can the linearized fluctuation theory be trusted when it comes to describing real interfaces? The short answer is that the *qualitative* behaviour derived above is expected to remain valid. That is, *any* kinetic roughening process entails a dynamic correlation length

$$\xi \sim t^{1/z} \tag{3.60}$$

which enters the scaling forms (3.31), (3.48) and, possibly (3.49), for the width and the height-difference correlation function, but the values of the *dynamic exponent* z and the roughness exponent ζ, as well as the detailed shapes of the scaling functions may differ from the expressions of the linear theory; in particular, the height fluctuations may become non-Gaussian, involving, in extreme cases [112], separate roughness exponents for different moments of h.

The 'stability' of the large scale behaviour of the linear theory against the inclusion of nonlinear terms can be probed by a simple technique referred to as *power counting*, which we illustrate here for the leading growth-induced kinematic nonlinearity of the nonconserved interface equation (3.6). Expanding the square root in front of the curly bracket and adding the noise we have, in a frame moving at velocity $v_0 = \Gamma\mu_0$,

$$\frac{\partial h}{\partial t} = \nu \nabla^2 h + \frac{\lambda}{2}(\nabla h)^2 + \eta, \tag{3.61}$$

where we have set $\lambda = \Gamma\mu_0 = v_0$. We now perform a rescaling transformation

$$\tilde{h}(\mathbf{x}, t) = b^{-\zeta} h(b\mathbf{x}, b^z t), \tag{3.62}$$

with a scaling factor $b > 1$. The transformation of the noise is dictated by the invariance of the covariance (3.16); this yields

$$\tilde{\eta}(\mathbf{x}, t) = b^{(d+z)/2} \eta(b\mathbf{x}, b^z t). \tag{3.63}$$

Inserting equations (3.62) and (3.63) into equation (3.61) we find that $\tilde{h}$ satisfies equation (3.61) with the rescaled coefficients

$$\tilde{\nu} = b^{z-2}\nu, \quad \tilde{D} = b^{z-d-2\zeta} D, \quad \tilde{\lambda} = b^{z+\zeta-2}\lambda. \tag{3.64}$$

It is easily checked that equation (3.62) constitutes, for $b > 1$, a *coarse graining* operation. Thus equation (3.64) provides, for $b \to \infty$, a measure of the relative importance of the various terms in equation (3.61) on large scales. In order to evaluate the large-scale effects of the nonlinear term we now set ζ and z in equation (3.64) equal to the values $\zeta = (2 - d)/2$ and $z = 2$, characteristic of the linear theory. Not surprisingly, the coefficients ν and D that appear already in the linear equation then remain invariant; however, the coefficient λ of the nonlinearity *increases*, for $d < 2$, as b^{ζ}. We conclude that this term is *relevant* and presumably alters the scaling behaviour of the linear theory. The same kind of analysis applied to higher-order terms appearing in the gradient expansion of equation (3.6), such as $[(\nabla h)^2]^2$ and $(\nabla h)^2 \nabla^2 h$, shows that these are *irrelevant*, that is, their coefficients *decrease* under rescaling. Thus the nonlinear equation (3.61), which was first derived by Kardar, Parisi and Zhang [19] in 1986, gives a complete description of the large-scale properties of interfaces moving locally in the direction of the driving force, as in equation (3.3). Some properties of this equation will be discussed in section 4.

In the case of conserved surface relaxation, as described by equation (3.15), the situation is much more complicated. First, since the linear theory (without non-equilibrium currents) shows anomalous scaling with $\zeta \geq 1$ for $d \leq 2$, *all* nonlinearities that arise from expanding the geometric factors in equation (3.12) are relevant [89, 90] in dimensions $d \leq 2$. Similarly, the terms $\lambda_{2m}(\nabla h)^{2m}$ in the expansion (3.13) of the non-equilibrium chemical potential are relevant for $d < 4m/(2m - 1)$; in $d = 2$ *all* these terms are relevant. Existing renormalization-group treatments of the nonlinearities [90, 121, 122] have taken into account only the lowest-order terms; however, it is not clear that such a procedure can be justified for infinite sequences of relevant terms (see sections 5.4.3 and 5.5.2).

On the other hand, matters simplify drastically in the presence of a stabilizing (downhill) non-equilibrium current, equation (3.14) with $\nu_1 > 0$. As already mentioned, the linear theory is then given by the Edwards–Wilkinson equation (3.18) with $m = 1$, and power counting shows that all conceivable nonlinearities (which are consistent with the conserved nature of the dynamics) are irrelevant [121, 122]. Thus in this instance the linear theory provides the *exact* description of the large-scale properties. Below in section 3.4 we explore some further examples of microscopic models for which the linear theory becomes exact.

Golubović and Bruinsma [100] have investigated the effect of adding the KPZ nonlinearity $(\lambda/2)(\nabla h)^2$ to the fourth-order surface diffusion equation (3.18) with $m = 2$. In that case power counting shows that the nonlinearity is relevant below 8 interface dimensions. It should, however, be clear from the derivation in section 3.1

that the Golubović–Bruinsma equation

$$\partial h/\partial t = -\nu\nabla^4 h + (\lambda/2)(\nabla h)^2 + \eta \tag{3.65}$$

does not constitute a consistent description of interface dynamics: since the KPZ term does not conserve volume, it should always be accompanied by an evaporation–condensation term proportional to $\nabla^2 h$. Indeed, the renormalization group analysis of Golubović and Bruinsma does demonstrate the generation of such a term on large length scales, but its sign turns out to be *negative* (i.e. destabilizing) to leading order in $\epsilon = 8 - d$. In view of recent work on the related, deterministic Kuramoto–Sivashinsky equation, to be described in section 4.4.1, it seems unlikely that this result has any consequences in physical dimensionalities.

The reader should not be left with the impression that power counting always gives fully reliable answers. There are, at least, two kinds of situations where it may fail. The first case is the appearance of a *strong coupling* regime in which a nonlinear term with a *small* (in some dimensionless sense) coefficient is irrelevant, as predicted by power counting, but the same term becomes relevant when the coefficient exceeds some critical value. So far this scenario has been found to apply only to the KPZ equation and some of its variants (see section 4), but our understanding of the phenomenon is insufficient at present to be able to decide how commonly it occurs in the context of general, nonlinear interface models.

A second case in which linear analysis, including power counting, gives misleading results is growth with conserved relaxation on a 1D vicinal surface stabilized by step edge barriers (see section 5.2.1). These barriers give rise to a nonequilibrium current $J_{\mathrm{NE}}(\nabla h)$ which, when expanded around the average orientation of the vicinal surface, is of the form (3.14) with $\nu_1 > 0$. Thus, following the above line of reasoning, such a surface should be exactly described by the linear (Edwards–Wilkinson) theory. Simulations of a microscopic model [123] reveal, however, that the state in which the linear theory applies is *metastable*: at long times, fluctuations nucleate large local deviations from the average orientation which bring the surface into a regime where $\nu_1 < 0$, eventually leading to a global instability not anticipated by the linear analysis.

3.4. *Microscopic realizations of the linear theory*

The large-scale behaviour of a given microscopic model conforms exactly to the linear theory if (i) all nonlinearities permitted by the physics of the problem turn out to be irrelevant, or (ii) if the model possesses additional (possibly artificial) symmetries that suppress relevant nonlinearities.

An example of the first kind is provided by the process of diffusion-limited erosion (DLE), which was studied numerically by Meakin and Deutch [124] and analytically by Krug and Meakin [102]. DLE is the time-reversed process of DLA. As in DLA, individual diffusing particles are launched far away to wander towards the interface; however, instead of accreting to the growing deposit, upon contact they annihilate with a deposit particle, thus eroding the surface. The model applies to diverse processes such as electrolytic polishing and stable fluid invasion in the regime of high capillary numbers [102]. The reversal of the interface motion with respect to the gradient of the diffusion field implies that the destabilizing effect of the latter, as expressed in the conventional stability analysis for solidification fronts [125], is

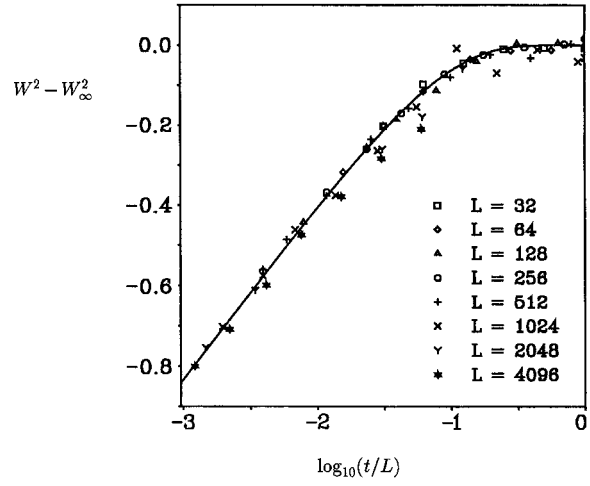

Figure 13. Simulation results (symbols) compared to the theoretical scaling function (3.66) (full curve) for the surface width in diffusion-limited erosion on the square lattice. The numerical data were averaged over a number of independent runs ranging from 4000 for $L = 32$ to 20 for $L = 4096$ [102].

turned into a rather efficient *stabilizing* force, since local protrusions are preferentially eroded.

Krug and Meakin [102] showed that the appropriate linear fluctuation theory for this problem is given by equation (3.22) with $z = 1$, and the coefficient ν equal to the average interface velocity v; this makes it plain that the relaxation term is of purely nonequilibrium origin. Moreover, all nonlinearities are found to be irrelevant by power counting. The agreement with the linear theory is illustrated in figure 13, where simulation data for $d = 1$ (the marginal dimensionality $d_c^{(1)}$ for this model) are compared to the analytic expression for the interface width. For $z = 1$, $d = 1$, the series (3.26) defining W^2 can in fact be summed exactly, with the result

$$W^2 = \frac{D}{2\pi\nu}\{\ln(L/a) + \ln[1 - \exp(-4\pi\nu t/L)]\}. \tag{3.66}$$

In the figure, the non-universal short range cut-off a has been removed by subtracting the stationary limit of the width; also, the interface velocity $\nu = 1$ by definition of the time scale, so that the noise strength $D \approx 1{\cdot}2$ remains as the only fit parameter.

A class of microscopic models tailored to represent the linear continuum theory was recently introduced by Kim and Das Sarma [126], building on earlier work by Family [127]. The models are solid-on-solid (SOS) models [128] in which the position of the surface is specified by an integer-valued height variable $h_{\mathbf{x}}$ defined on the d-dimensional substrate lattice. Deposition occurs by randomly choosing a lattice site $\mathbf{x}_0$; however, rather than simply increasing the height at $\mathbf{x}_0$ (which would lead to a trivial model) the depositing particle is allowed to relax in a local neighbourhood, typically including $\mathbf{x}_0$ and its nearest neighbours. The relaxation is governed by a function $K_{\mathbf{x}}$ of the heights and their discrete derivatives, which is assigned to each lattice site and can be viewed as a representation of the local surface chemical

potential. The final deposition site is the one in the neighbourhood that has the smallest value of K prior to deposition; if the minimum is not unique, a random choice is made.

In the model of Family [127], the 'chemical potential' K is simply the height itself, $K_{\mathbf{x}} = h_{\mathbf{x}}$. The model may therefore be regarded as a lattice version of the sedimentation process envisioned by Edwards and Wilkinson [98], in which granular particles settle in local surface minima under the influence of gravity. As was pointed out by Krug [129], in the context of sedimentation the assumption of a regular lattice is too strong a simplification: the fact that real sediments are disordered provides a mechanism for the generation of the quadratic KPZ nonlinearity, which invalidates the predictions of the linear theory on large scales (see section 5). On the other hand, a regular lattice appears naturally if one intends to describe epitaxial growth with conserved surface relaxation. In that case the post-deposition relaxation in Family's model could arise from the transient kinetic energy of the depositing particles, which allows them to 'funnel' downhill before being incorporated into the lattice [99]. In the continuum language this causes a downhill current with a stabilizing linear coefficient $\nu_1 > 0$ in equation (3.14) which, as we have repeatedly argued, supersedes all allowed nonlinearities (the metastability scenario sketched at the end of the previous section cannot alter this conclusion, since the current in Family's model is a monotonic function of inclination, so that $\nu_1 > 0$ for all surface orientations). Thus, this model (including variants with longer-ranged, gravity-driven relaxation [130]) is an exact realization of the Edwards–Wilkinson equation, as was confirmed by numerical work in one [127] and two [131] dimensions.

For the *curvature model* defined by $K_{\mathbf{x}} = -(\nabla^2 h)_{\mathbf{x}}$ (the right hand side denoting the lattice Laplacian) the corresponding argument [112] requires somewhat greater care. Here, the crucial observation is that, since the dynamics can be formulated solely in terms of the local curvatures, the model is invariant under arbitrary tilts, $h_{\mathbf{x}} \to h_{\mathbf{x}} + \mathbf{u}\cdot\mathbf{x}$. Consequently, any nonlinear contributions to the coarse-grained surface chemical potential have to be powers of second and higher derivatives of h, which are all irrelevant by power counting. Related symmetries are discussed in section 5.2.2.

Of course, the extra symmetry of the curvature model is due to the somewhat artificial relaxation rule—if the local curvature is replaced, for example by the coordination number of the deposited atom, as a more realistic representation of the actual atomic kinetics [101, 132, 133], the tilt invariance is lost and the scaling properties of the model become considerably more complex [107, 108, 112]. Such models are described in section 5.1.1.

Since we expect the large-scale behaviour of the curvature model to be governed by the linear, noisy Mullins equation (equation (3.18) with $m = 2$), we may utilize the exact expressions derived in section 3.2.2 both to ascertain our expectation, and to determine the coefficient ν in the continuum equation. The noise strength D is fixed from the outset: in the whole class of models introduced by Kim and Das Sarma [126], particles are deposited *at random* and relax only locally, within a region of a few lattice spacings; therefore, the coarse-grained noise has Poisson (shot noise) statistics and $D = 1$ in units where time is counted in deposited monolayers. In figure 14 we show simulation data for the width and the mean-squared step height $\langle(\nabla h)^2\rangle \equiv \langle(h_{x+1} - h_x)^2\rangle$ for a large ($L = 10^5$) 1D system (the precise relaxation rule implemented here is described in [112]). The predictions of the linear continuum theory for the infinite system can be written as

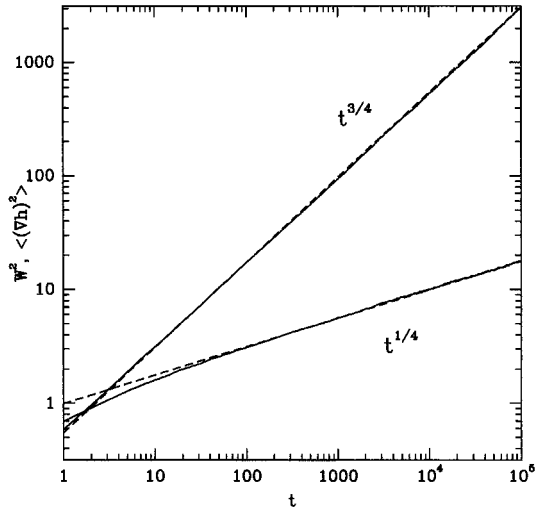

Figure 14. Simulation results for the surface width W^2 and the local height gradient $\langle(\nabla h)^2\rangle$ of the curvature model [112]. The broken lines are power law fits with the predicted exponents.

$$\lim_{t\to\infty} W^2/t^{3/4} = (D/\nu)(2\nu)^{3/4}\Gamma(1/4)/6\pi,$$
$$\lim_{t\to\infty} \langle(\nabla h)^2\rangle/t^{1/4} = (D/\nu)(2\nu)^{1/4}\Gamma(3/4)/2\pi. \tag{3.67}$$

From the fits indicated in the figure we estimate $\nu \approx 0{\cdot}140$ and $D/\nu \approx 7{\cdot}0$, in accordance with the argument that $D = 1$ for this general class of models. The example illustrates how numerical measurements of correlation functions, such as the interface width, can be used to extract the model-dependent parameters that enter the large-scale continuum theory. This procedure will recur in the nonlinear context in sections 4.2 and 5.4.2.

4. Aspects of Kardar–Parisi–Zhang theory

The Kardar–Parisi–Zhang equation [19]

$$\frac{\partial h}{\partial t} = \nu\nabla^2 h + \frac{\lambda}{2}(\nabla h)^2 + \eta \tag{4.1}$$

is the most thoroughly studied continuum theory of kinetic roughening. While the derivation in section 3 was based on the macroscopic equation (3.6) for an interface that moves locally normal to itself, it should be recognized that equation (4.1) is a valid description of large-scale interface fluctuations under much more general conditions. The KPZ equation applies whenever the macroscopic interface equation of motion has the form

$$\frac{\partial h}{\partial t} = v(\nabla h) + \text{curvature corrections}, \tag{4.2}$$

with an *inclination-dependent growth rate* $v(\nabla h)$ that is a nonlinear function of the local orientation; in the isotropic case of equation (3.6), $v(\nabla h) = \Gamma\mu_0[1 + (\nabla h)^2]^{1/2}$.

The characteristic quadratic nonlinearity of equation (4.1) then results from a gradient expansion of v [8, 129, 134]:

$$v(\nabla h) \approx v(\mathbf{0}) + \sum_{i=1}^{d} \partial_i v(\mathbf{0}) \frac{\partial h}{\partial x_i} + \frac{1}{2} \sum_{i=1}^{d} \lambda_i \left(\frac{\partial h}{\partial x_i} \right)^2 + \cdots . \tag{4.3}$$

Here, the substrate plane coordinates have been chosen such that the matrix of second derivatives $\partial_{ij}^2 v(\mathbf{0})$ is diagonal with eigenvalues λ_i. To arrive at the usual form $(\lambda/2)(\nabla h)^2$ of the nonlinearity one has to transform further to a tilted, co-moving frame in which the constant and linear terms in equation (4.3) vanish, and to assume in-plane isotropy so that $\lambda_i \equiv \lambda$ for all i. This is achieved trivially by a spatial rescaling if all λ_i have the same sign; otherwise novel physics can arise, as will be discussed shortly. The curvature corrections in equation (4.2) involve second and higher derivatives of h, such as the Gibbs–Thomson term in equation (3.6). In the presence of a non-trivial inclination-dependent growth rate these terms do not affect the evolution of macroscopic shapes, since they become arbitrarily small under a coarse-graining operation that rescales h and $\mathbf{x}$ coordinates in the same manner (this should not be confused with the coarse-graining of fluctuations in section 3.3; there, h and $\mathbf{x}$ are treated differently when $\zeta \neq 1$).

Equation (4.2) is useful in clarifying what kind of physical growth processes would be expected *not* to fall into the KPZ universality class. First, the dynamics of h is assumed to be local. This rules out all situations in which the interface motion couples to some nontrivial bulk dynamics, such as the diffusion-limited erosion process described in section 3.4, the competitive growth models of section 2 and the classical continuum theories of solidification [125]. Second, growth with volume-conserving surface relaxation is not covered by the KPZ theory, since in that case the growth rate is controlled entirely by the external deposition flux, $v = F$, and is therefore independent of inclination [129]. We may remark in this context that the orientation independence of the growth rate is a well-established experimental feature in the molecular beam epitaxy (MBE) of silicon [88], lending support to the application of the conserved growth equation (3.15) to this system (a detailed discussion is found in section 5). Finally, the KPZ theory assumes that the fluctuations in the growth process can be reasonably modelled by a noise term that is a random function of $\mathbf{x}$ and t. This assumption fails for interface motion in a random medium close to the depinning threshold, where the *quenched* nature of the fluctuations, i.e. their dependence on the interface position h, becomes essential [81, 84, 82, 93].

For practical purposes, the mechanisms neglected in the KPZ equation typically define some crossover length scales which limit the applicability of the theory. For example, while desorption may well be negligible in most MBE processes, it is never entirely absent and should in principle lead to a reappearance of KPZ behaviour on sufficiently large length scales; defect formation would have the same effect (see section 5). Similarly, an interface moving through a random medium should be describable by the KPZ theory on scales that much exceed the correlation length associated with the depinning transition. Thus, the fact that in many cases the physics on relevant length scales is governed by effects not included in the KPZ equation should not obscure the status of this equation as the *generic* description of the *asymptotic* fluctuation behaviour of a broad class of interface displacement processes—though it must be said that non-KPZ physics seems to dominate all

experimental situations considered so far, to the extent that no clean experimental confirmation of KPZ behaviour has yet emerged (see section 5.6.1).

Strong coupling. From a theoretical perspective, the most intriguing feature of the KPZ equation is the occurrence of a nonequilibrium phase transition for dimensionalities $d > 2$, from a weak coupling phase for small λ where the nonlinearity is irrelevant (as expected on the basis of power counting, see section 3.3), to a strong coupling phase characterized by nontrivial scaling exponents not accessible to perturbative methods. The physical case $d = 2$ is at the lower critical dimensionality of the transition, which has important implications for the length and time scales required to observe the asymptotic behaviour [135]. Most of the work published in the five years following the seminal paper [19] of Kardar, Parisi and Zhang attempted to elucidate the nature of the transition, and to obtain accurate numerical estimates of the strong coupling scaling exponents. These efforts have been reviewed elsewhere [8]; for a representative sample of current numerical work see [136–138].

Recent analytic approaches have yielded promising but not quite conclusive results. Two-loop renormalization group (RG) calculations have been presented by Sun and Plischke [139] and by Frey and Täuber [140]. Whereas Sun and Plischke claim to identify the strong coupling fixed point in $d = 2$ and derive estimates for the scaling exponents, the analysis of Frey and Täuber indicates a scenario that is similar to the earlier one-loop results [19, 77]—only the critical fixed point governing the phase transition is accessible in an expansion around $d = 2$ dimensions, but the strong coupling regime remains elusive. For a discussion of the discrepancy between the two groups see [141, 142]. Lässig [143] has shown that certain features of the phase transition predicted by the two-loop analysis [140] are exact to all orders, and an appealing physical interpretation of the transition has been proposed by Newman and Kallabis [144].

The non-perturbative nature of the strong coupling regime suggests that a self-consistent mode-coupling approach [145] may be more appropriate than perturbative RG schemes. Mode-coupling equations have been written down before in related contexts [146–149], but only recently have approximate solutions been attempted [150–152] in order to extract the dimensionality dependence of the strong coupling exponents. Moore and co-workers [153] have found an *analytic* solution of the mode-coupling equations for $d > 4$, which indicates that $d = 4$ may play the role of an upper critical dimensionality, in the sense that the dynamic scaling exponent in the strong coupling phase takes on its weak coupling value $z = 2$ for $d \geq 4$. Such a scenario was suggested earlier by Halpin-Healy on the basis of a functional RG calculation [154, 155], and has received recent support from other approaches [142–144, 156]. On the other hand, a numerical solution of the mode coupling equations [157] yields $z < 2$ for all dimensions, in line with the available simulation data [136].

A third analytic approach that holds considerable promise with regard to an improved understanding of the strong coupling regime is the study of anisotropic generalizations of the KPZ equation. Building upon the observation of Villain [20] that growth on vicinal crystal surfaces (in the presence of desorption) may display a regime in which the two coefficients λ_1, λ_2 in equation (4.3) have different signs, Wolf [158] showed that in such a situation the nonlinearities are in fact (marginally) *irrelevant*, i.e. the strong coupling regime disappears and the surface is described by the linear theory (up to logarithmic corrections). Subsequently, Fisher and Grinstein [159] and Hwa [160] considered, in the contexts of electrical transport in insulators

and driven flux line liquids, respectively, higher-dimensional anisotropic variants of the KPZ equation. Depending on the number of non-zero coefficients λ_i in equation (4.3) and on their relative signs, strong coupling behaviour may or may not be present. Therefore, the anisotropic equation can be used to systematically interpolate [160] between the (isotropic) KPZ equation and the problem of driven diffusive systems (DDS) [147], which corresponds, roughly speaking, to a situation where only one of the λ_i is nonzero. The DDS problem does not possess a strong coupling regime and is therefore amenable to standard perturbative analysis [161].

Outline of section. In the remainder of this section we shall be concerned almost exclusively with the 1D KPZ equation. The 1D problem is special due to the validity of a fluctuation–dissipation theorem which fixes the values of the scaling exponents (section 4.1). This allows one to pose more refined questions regarding scaling functions, universal amplitudes and the probability distribution of height fluctuations (sections 4.2 and 4.3). Section 4.4 briefly reviews recent work on interface displacement processes in which the fluctuations are of *chaotic* origin, while section 4.5 introduces the well-known 'directed polymer' representation of the KPZ equation. Finally, section 4.6 addresses the problem of KPZ-type growth in the presence of defects or open boundaries, which break the translational symmetry in the substrate x direction. In such situations the nontrivial *dynamic* scaling properties of the KPZ equation reappear in the *spatial* domain in the form of power law height profiles and correlations [162], which in some cases can be computed exactly [163–166]. Moreover, morphological phase transitions can be induced by the defects, which have a particularly appealing interpretation in the directed polymer representation.

4.1. *Exact invariants*

The 1D KPZ equation has two important invariance properties, the first of which applies in arbitrary dimensionalities d. To derive it, consider the *tilt transformation*

$$h'(\mathbf{x}, t) = h(\mathbf{x} - \mathbf{u}_0 t, t) - \frac{1}{\lambda}\mathbf{u}_0 \cdot \mathbf{x} + \frac{1}{2\lambda}\mathbf{u}_0^2 t, \tag{4.4}$$

parameterized by some d-dimensional vector $\mathbf{u}_0$. It is easily checked that h' satisfies the same KPZ equation (4.1) as h, with a shifted noise term

$$\eta'(\mathbf{x}, t) = \eta(\mathbf{x} - \mathbf{u}_0 t, t). \tag{4.5}$$

Provided the temporal correlations of η are sufficiently short ranged, the shift does not affect the statistical properties of the noise [77], and we may conclude that the statistics of the height fluctuations are invariant under the transformation (4.4). In the literature this property is often referred to as *Galilean invariance*, since it was first discussed by Forster, Nelson and Stephen [167] in the context of randomly stirred fluids governed by the noisy Burgers equation

$$\frac{\partial \mathbf{u}}{\partial t} + \mathbf{u} \cdot \nabla \mathbf{u} = \nu \nabla^2 \mathbf{u} - \lambda \nabla \eta, \tag{4.6}$$

which follows from equation (4.1) with the identification $\mathbf{u} = -\lambda \nabla h$; the tilt transformation (4.4) is precisely a Galilean transformation for the fluid velocity $\mathbf{u}$. In the context of interface motion the tilt invariance appears as a residue of the full rotational symmetry of the isotropic equation (3.6).

The significance of the tilt invariance lies in the fact that the transformation (4.4) contains explicitly the coefficient λ. Thus, if the invariance is to be preserved under coarse graining, it is clear that the rescaling operation (3.62) should not change the value of λ. From the last of equations (3.64) we read off that this enforces the exponent identity [26, 77, 148]

$$\zeta + z = 2 \tag{4.7}$$

between the roughness exponent and the dynamic exponent.

In order to determine the values of ζ and z individually, we would require a second identity derived from some invariant combination of the coefficients ν, D and λ. No such invariant is known for $d > 1$; in the 1D case the appropriate combination is the ratio D/ν. In fact a much stronger statement holds [8, 167, 168]. The Gaussian stationary probability distribution of the ($z = 2$) linear theory,

$$\mathscr{P}[h] \sim \exp\left[-\frac{\nu}{D}\int \mathrm{d}x\,(\nabla h)^2\right], \tag{4.8}$$

is also the stationary solution of the full Fokker–Planck equation that corresponds to the nonlinear KPZ equation. This can be seen by computing the contribution introduced by the KPZ nonlinearity on the right hand side of the Fokker–Planck equation

$$\frac{\delta}{\delta h}\int \mathrm{d}x \frac{\lambda}{2}(\nabla h)^2 \mathscr{P}[h] = \left[\int \mathrm{d}x\,\lambda(\nabla h)^2 \frac{\nu}{D}\nabla^2 h\right]\mathscr{P}[h], \tag{4.9}$$

which vanishes by partial integration (assuming periodic boundary conditions in x). Similar results can be proved for certain microscopic realizations of the KPZ equation [8].

The remarkable conclusion is that *all* stationary correlations of the nonlinear KPZ equation in one dimension are given *exactly* by the linear theory. Specifically, for the transient roughening of an initially flat interface considered in section 3.2, we know that the two-point function $S(q, t)$ defined by equation (3.24) satisfies

$$\lim_{t\to\infty} S(q, t) = L^{-1}\frac{D}{2\nu q^2}. \tag{4.10}$$

Corresponding relations for higher order correlations follow immediately from the Gaussian nature of the probability density (4.8). A particular consequence is that the roughness exponent $\zeta = 1/2$ as in the linear case, and the dynamic exponent $z = 3/2$ from the scaling relation (4.7). It is much harder to demonstrate directly that $z = 3/2$. For a particular microscopic model this has been achieved by Gwa and Spohn [169]; extensions of their work can be found in [170–172].

We now exploit the invariance of λ and D/ν to determine the full scaling form of $S(q, t)$. First, we derive an expression for the dynamic correlation length $\xi(t)$ using only dimensional arguments. From the KPZ equation (4.1), the dimensions of λ and D/ν are given by

$$[\lambda] = [x]^2/[h][t], \quad [D/\nu] = [h]^2/[x]. \tag{4.11}$$

The task is to construct a lateral length scale (of dimension $[x]$) from the invariant quantities λ, D/ν, and the time t. The only solution is

$$\xi(t) = [(D/2\nu)^{1/2}|\lambda|t]^{2/3}, \tag{4.12}$$

where a factor of 2 has been inserted for later convenience. Together with the

asymptotic constraint (4.10) it follows that S can be written as

$$S(q, t) = L^{-1} \frac{D}{2\nu q^2} g(q\xi(t)), \tag{4.13}$$

where, in analogy with the expressions (3.25) and (3.29) derived in the linear case, g is now expected to be a *universal* function with the limiting behaviours

$$g(0) = 0, \quad \lim_{s\to\infty} g(s) = 1. \tag{4.14}$$

In the linear theory, equation (4.13) holds with $g(s) = 1 - \exp(-s^2)$. The scaling function for the KPZ equation is not known explicitly. A closely related function describing the temporal correlations in the stationary state has been studied analytically [147, 149, 161] and numerically [173] by several groups. In the next section we show how the scaling function can be characterized through dimensionless amplitudes of statistical observables such as the interface width.

4.2. *Universal amplitudes*

Using the scaling form (4.13) we can proceed to compute real space correlation functions from the general formulae (3.26) and (3.27). Since all stationary ($t \to \infty$) correlations are identical to those of the linear theory, the focus is on *transient* quantities, i.e. we take the limit $L \to \infty$ at fixed t. For the width this yields the expression [174]

$$W^2 = c_2[(D/2\nu)^2|\lambda|t]^{2/3}, \tag{4.15}$$

with a dimensionless prefactor c_2 that is expressed in terms of the universal scaling function g as

$$c_2 = \frac{1}{\pi}\int_0^\infty \frac{\mathrm{d}s}{s^2} g(s). \tag{4.16}$$

Similar expressions can be written for higher-order correlation functions and higher moments of the height fluctuation distribution. Of particular interest are quantities that reveal the deviation of the distribution from a Gaussian, such as the skewness

$$\mathcal{S} = \frac{\langle (h - \langle h\rangle)^3\rangle}{\langle (h - \langle h\rangle)^2\rangle^{3/2}}, \tag{4.17}$$

and the kurtosis

$$\mathcal{Q} = \frac{\langle (h - \langle h\rangle)^4\rangle}{\langle (h - \langle h\rangle)^2\rangle^2} - 3. \tag{4.18}$$

The skewness is a measure of the asymmetry of the fluctuation distribution, to be expected because the growth direction breaks the $h \to -h$ symmetry, while $\mathcal{Q}$ gauges the weight contained in the tails of the distrubution relative to a Gaussian; for a Gaussian $\mathcal{S} = \mathcal{Q} = 0$. Simulations of a variety of microscopic models belonging to the KPZ universality class indicate [174, 175] that the skewness in the transient regime converges to a universal value $|\mathcal{S}| = 0{\cdot}28 \pm 0{\cdot}04$, and the sign of $\mathcal{S}$ is equal to the sign of λ in equation (4.1); the value of $\mathcal{Q}$ is in the range $\mathcal{Q} \approx 0{\cdot}12$–$0{\cdot}16$. The theoretical significance of these results is discussed by Friedberg and Yu [176].

A few remarks are in order regarding the numerical procedure [173, 174, 177] employed to extract universal amplitudes like c_2, $\mathcal{S}$ and $\mathcal{Q}$ from simulations of microscopic models. Two steps are involved. First, the transient behaviour of the quantity of interest (e.g. the width) is measured, executing care that the asymptotic

($W^2 \sim t^{2/3}$) regime is well established in the time range used to determine the prefactor. Then, in order to arrive at *dimensionless* coefficients such as c_2, the dimensionful invariants D/ν and λ have to be computed for the particular model at hand. In a few cases this can be done analytically [173, 174]; however, in general one has to resort to simulations. The ratio D/ν figures prominently in the correlation functions of the linear theory, and can therefore be obtained from numerically determined *stationary* quantities, using exact relations like equation (3.39). The coefficient λ is most easily estimated from a direct measurement of the tilt dependence of the growth rate [134], as defined in equation (4.3); for this purpose a macroscopic tilt $u = \langle \nabla h \rangle$ is imposed through *helical* boundary conditions, $h(x + L) = h(x) + uL$ (for an example see figure 17).

The knowledge of the universal amplitude c_2 can be exploited to estimate the crossover time t_c at which the interface width saturates in a finite system, i.e. the nonlinear analogue of equation (3.41). To this end we match the transient expression (4.15) to the stationary result (3.39) (with $z = 2$), and obtain

$$\xi(t_c)/L = (12c_2)^{-1} \approx 0{\cdot}21, \tag{4.19}$$

with the numerical estimate [174] $c_2 \approx 0{\cdot}40$. Similar considerations apply to the crossover from an intermediate, Edwards–Wilkinson (EW) scaling regime in cases where the value of the nonlinearity in equation (4.1) is small (in a dimensionless sense) compared to the linear term $\nu\nabla^2 h$. Matching the KPZ asymptotics (4.15) to the exact expression (3.40) for the transient regime of the $z = 2$ linear (EW) equation, the crossover is found to occur at a time

$$t_c^{\mathrm{EW}\to\mathrm{KPZ}} = 32\pi^{-3} c_2^{-6} \nu^5 D^{-2} |\lambda|^{-4} \approx 252 \nu^5 D^{-2} |\lambda|^{-4}. \tag{4.20}$$

This relation has been particularly useful in identifying the asymptotic behaviour in models of *chaotic* interfaces, to be described in section 4.4.

4.3. *Finite size effects*

An interesting feature of the nonlinear term in the KPZ equation is the coupling that it induces between the spatially averaged, centre of mass motion of the interface

$$\bar{h}(t) = h_{q=0}(t) = L^{-1} \int_0^L \mathrm{d}x\, h(x, t), \tag{4.21}$$

and the internal fluctuation modes. This is illustrated by writing the instantaneous global interface velocity as

$$v(t) \equiv \frac{\mathrm{d}\bar{h}}{\mathrm{d}t} = \frac{\lambda}{2} \sum_{q \neq 0} q^2 |h_q(t)|^2 + \eta_{q=0}(t). \tag{4.22}$$

Several important conclusions can be drawn from this expression. First, averaging over both sides and taking $t \to \infty$ we find, using equation (4.10), that the right hand side is a sum over $N - 1$ identical terms $L^{-1}(D/2\nu)$, where $N = L/a$ is the total number of modes (the $q = 0$ mode does not contribute). It follows that the stationary average growth rate has a universal finite size correction [178]

$$\Delta v = \langle v(L) \rangle - \langle v(\infty) \rangle = -\frac{D\lambda}{4\nu L}. \tag{4.23}$$

The average growth rate itself, $\langle v(\infty)\rangle = D\lambda/4\nu a$, depends on the lattice cut-off a and is therefore nonuniversal. Similarly, in the transient regime one finds a correction proportional to $t^{-2/3}$. The non-dimensional coefficient in equation (4.23) is altered when the periodic boundary conditions are replaced by open ones [179].

Second, the coupling to the internal modes induces [180] *long-ranged temporal correlations* in the growth rate, on time scales smaller than the correlation time $t_c \sim L^{3/2}$. This effect is displayed in the centre of mass dispersion

$$W_c^2 = \langle (\bar{h} - \langle \bar{h} \rangle)^2 \rangle, \tag{4.24}$$

obtained by twice integrating the velocity correlation function $\langle v(t)v(s)\rangle$. In one dimension, this quantity behaves as

$$W_c^2 \sim \begin{cases} L^{-1}t^{4/3}, & t \ll L^{3/2}, \\ L^{-1/2}t, & t \gg L^{3/2}, \end{cases} \tag{4.25}$$

i.e. the dispersion is *superdiffusive* in the transient regime, leading to a $1/f$-type divergence in the velocity power spectrum [147, 159, 180, 181]. In the stationary regime ordinary diffusion is recovered, however, with a prefactor that is enhanced relative to the $1/L$ dependence of the linear theory (see below).

Equation (4.25) highlights the necessity of carefully distinguishing between the ensemble average $\langle h\rangle$ and the spatial average $\bar{h}$ in a finite system. The height fluctuation relative to the *ensemble* average

$$\tilde{W}^2 \equiv \langle (h - \langle h \rangle)^2 \rangle \tag{4.26}$$

is *dominated* by the centre of mass dispersion for $t > t_c$, where $W_c^2 \gg W^2$, and $\tilde{W}$ can be equated to the conventional definition (3.26) of the width W only for $t \ll t_c$; of course in simulations $\tilde{W}$ is of little relevance, since the ensemble average $\langle h\rangle$ is generally not known.

These considerations apply also at the level of the linear theory; however, there they are comparatively trivial since the centre of mass motion only couples to the $q = 0$ mode of the noise, so that $W_c^2 = Dt/L^d$ for all times. Incidentally, this remains true in nonlinear theories with conserved relaxation—indeed, the requirement of volume conservation in all relaxation processes implies precisely that these processes do not couple to the average height. In RG language this leads to the nonrenormalization of the noise strength D and the concomitant exponent identity [95, 101, 121, 122, 180]

$$z = d + 2\zeta, \tag{4.27}$$

as can be read off from the scaling transformation (3.64).

It is instructive to rederive the second part of equation (4.25) from a scaling argument. Dimensionally, W_c^2 is no different from the width W^2, hence one should be able to write a scaling form analogous to equation (3.31):

$$W_c^2 = \frac{D}{2\nu} L f_c(\xi/L). \tag{4.28}$$

To inform the shape of the scaling function f_c, we note that for times large compared to the correlation time, i.e. for $\xi \gg L$, the interface velocity becomes uncorrelated and one expects that $W_c^2 \sim t$. Since the KPZ correlation length behaves as $\xi \sim t^{2/3}$,

this requires that $f_c(s) = c_0 s^{3/2}$ for large arguments, and using the expression (4.12) we obtain

$$W_c^2 = c_0 (D/2\nu)^{3/2} |\lambda| L^{-1/2} t \quad (t \gg L^{3/2}), \tag{4.29}$$

which determines also the prefactor in equation (4.25) up to the universal constant c_0.

Remarkably, the amplitude c_0 is known analytically by virtue of a recent exact solution of a specific model due to Derrida, Evans and Mukamel (DEM) [182]. These authors were concerned with the tracer diffusion of particles in a 1D lattice gas with hard core repulsion—the asymmetric simple exclusion process (ASEP). The equivalence between the ASEP and a simple growth model, the single step model, has been known for some time [8, 26]. Any configuration of lattice gas occupation numbers $\epsilon_i = 0, 1$ can be mapped onto a solid-on-solid interface through the identification $h_{i+1} - h_i = 1 - 2\epsilon_i = \pm 1$, the integer height variables h_i specifying the interface position. In the ASEP particles jump to the right to vacant nearest neighbour sites; each jump increases the local height as $h_i \to h_i + 2$. Thus, h_i measures (twice) the *time-integrated particle current* through bond i. DEM computed the time-integrated displacement Y_t of a tagged particle, and showed that, for long times,

$$\langle Y_t^2 \rangle - \langle Y_t \rangle^2 = \Delta t, \tag{4.30}$$

with a diffusion constant

$$\Delta = \frac{\sqrt{\pi}}{2} \frac{(1-\rho)^{3/2}}{\rho^{1/2}} \frac{1}{L^{1/2}}, \tag{4.31}$$

where $0 < \rho < 1$ denotes the particle density. Equation (4.31) represents the leading behaviour in $1/L$ when the stationary limit $t \to \infty$ is performed first, followed by the limit $L \to \infty$ at fixed density ρ.

To establish the connection with equation (4.29), note first that since the particle current is equal to the product of density and velocity, the time-integrated current is ρY_t and $h = 2\rho Y_t$. Equations (4.30) and (4.31) therefore translate into

$$\tilde{W}^2 = \langle (h - \langle h \rangle)^2 \rangle = 2\sqrt{\pi} [\rho(1-\rho)]^{3/2} t / L^{1/2}, \tag{4.32}$$

which is also equal to W_c^2 in the stationary ($t \gg L^{3/2}$) regime considered here. Next we remark that the stationary correlations of the ASEP (with periodic boundary conditions!) are trivial: for $L \to \infty$ every site is occupied independently with probability ρ (for an explicit proof see [26, 181]). Consequently it is an easy matter to show that the dimensionful invariants of the equivalent growth model are [174]

$$\lambda = -1, \quad D/2\nu = 4\rho(1-\rho). \tag{4.33}$$

Thus equation (4.32) conforms exactly to the scaling prediction (4.29), and allows us to identify the dimensionless prefactor as

$$c_0 = \sqrt{\pi}/4. \tag{4.34}$$

The universality of this number is illustrated by simulation results for the centre-of-mass dispersion of a different growth model, the restricted solid-on-solid model of Kim and Kosterlitz [183] (figure 15). For this model the quantities D/ν and λ are known only numerically [174].

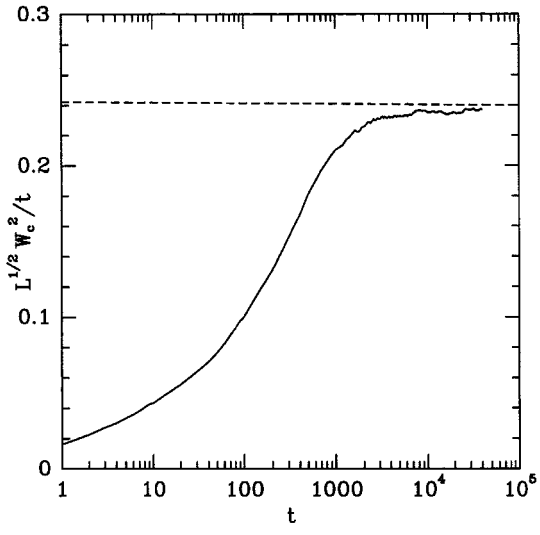

Figure 15. Centre of mass fluctuation W_c^2 of the interface in the restricted solid-on-solid growth model of Kim and Kosterlitz [183], scaled by system size ($L = 100$) and time according to the scaling form (4.29). The data represent an average over 10^4 independent runs, extending over 4×10^4 deposition attempts per site. The broken line is the prediction for the prefactor obtained from equation (4.29) with the universal amplitude (4.34) and the dimensionful parameters, $D/2\nu = 0{\cdot}81$ and $\lambda = -0{\cdot}75$, which were determined numerically in [174].

4.4. *Chaotic interfaces*

4.4.1. *The Kuramoto–Sivashinsky equation*

A number of recent studies have been devoted to purely deterministic models of interface motion where the fluctuations, rather than being induced externally by thermal or kinetic noise, are generated by some local *chaotic* dynamics. The prime representative for this class of systems is the Kuramoto–Sivashinsky (KS) equation

$$\partial h/\partial t + \nabla^2 h + \nabla^4 h - (\nabla h)^2 = 0, \tag{4.35}$$

which appears as an asymptotic local approximation to various moving boundary value problems, such as laminar flame propagation [184], solidification at large undercooling [185], and terrace edge evolution during step flow growth [186, 187] (see also section 5.2.1). Similar equations have been derived in plasma physics [188] and in the context of chemical turbulence [146, 189].

The units in equation (4.35) have been chosen such that all coefficients are equal to unity. Usually the 1D equation is considered, with periodic boundary conditions on an interval of length L. The trivial solution $h = \text{const.}$ is linearly unstable when $L > 2\pi$. For large L, almost all initial conditions evolve to a state of *spatio-temporal chaos*, which can be viewed as a collection of cell-like structures that split and merge in a random fashion. The cell size is set by the wavelength $l_0 = \sqrt{2}(2\pi)$ with the largest growth rate $1/\tau_0 = 1/4$ under the linearized dynamics.

In the present context, the fundamental question is to what extent the large scale dynamics of this 'turbulent' state, coarse grained beyond the typical cell size l_0, can be described by a *stochastic* theory of kinetic roughening. Yakhot [190] was the first to suggest, on the basis of a renormalization group coarse graining procedure, that

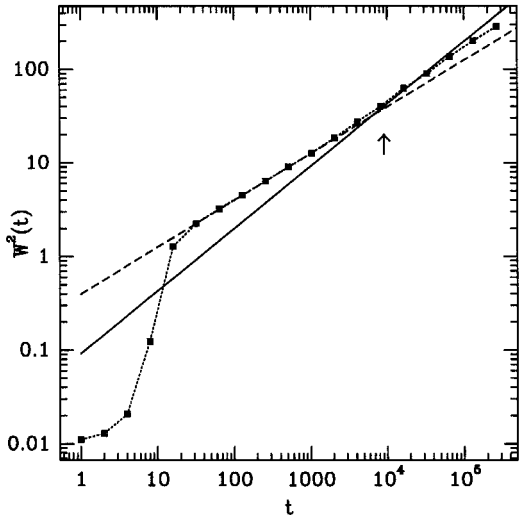

Figure 16. Width of a 1D Kuramoto–Sivashinsky interface of length $L = 65\,536$. The squares show numerical data obtained by averaging over 70 independent runs. The broken line is a fit to the early time Edwards–Wilkinson behaviour, $W^2 = 0{\cdot}397t^{1/2}$. The full line represents the asymptotic KPZ behaviour, $W^2 = 0{\cdot}092t^{2/3}$, with the prefactor calculated from equation (4.15) using the numerical estimates of $D/2\nu$ and λ. The arrow indicates the crossover time $t_c^{\mathrm{EW}\to\mathrm{KPZ}} \approx 7000$ predicted from equation (4.20). The last few data points are already affected by finite size effects—the saturation time determined by equation (4.19) is about 3×10^5 for this system size [193].

the appropriate large-scale theory is the KPZ equation (at the time known as the noisy Burgers equation [167]). Yakhot's conjecture is very plausible intuitively; it only requires that (i) the stabilizing effect of the nonlinearity in equation (4.35) can be described in terms of a positive, effective interfacial tension $\nu > 0$ on large scales, and (ii) the random cell interaction events are sufficiently uncorrelated to give rise to a white noise forcing. However, a formal proof by conventional renormalization group methods is difficult because the cell size l_0 interferes with the RG flow [191].

A careful numerical test of the conjecture was performed by Zaleski [192], who found it exceedingly difficult to access the asymptotic KPZ regime. A subsequent quantitative crossover analysis [193], utilizing the amplitude relations derived in section 4.2, estimated that the asymptotic behaviour sets in only on length scales $L > 2500$ and time scales $t > 7000$ (figure 16). Similar crossover scales were observed in the stationary regime [194]. Somewhat paradoxically, the crossover time (4.20) is large because of the large value of the effective interface tension ν, which starts out being *negative* on the 'microscopic' (=sub cell size) level. Assuming that ν is generated by the cell dynamics, a rough estimate involving the characteristic cell scales is $\nu = l_0^2/\tau_0 = 19{\cdot}7$. Numerically, one finds $\nu = 10{\cdot}5 \pm 0{\cdot}6$ [193]. An analytic approach to estimating ν, as well as the other effective parameters in the large-scale stochastic evolution equation, was presented by Chow and Hwa [195].

The intuitive picture suggests that a KPZ-type large-scale description should apply also in higher dimensions. Recent numerical work in two dimensions [196, 197] has not succeeded in unambiguously confirming this hypothesis, and the issue remains controversial [198–201]. It is unclear at present whether the problem is only

one of computational resources, or whether the 2D equation is different from the 1D case in some more fundamental way. Qualitatively novel behaviour certainly occurs if the differential operators in equation (4.35) are made anisotropic; indeed, under suitable conditions the stabilization mechanism breaks down completely, so that no large-scale stochastic description exists [202].

We briefly comment on the relationship between the KS equation (4.35), and the Golubović–Bruinsma equation (3.65), which may be viewed as the $\nu_0 \to 0$ limit of the generalized KPZ equation [191]

$$\partial h/\partial t = \nu_0 \nabla^2 h - \nabla^4 h + (\nabla h)^2 + \eta. \tag{4.36}$$

The work summarized in this section has shown that an interface governed by equation (4.36) with zero external noise strength $D = 0$, and a *negative* bare interface tension $\nu_0 < 0$, can be described on large scales by an equation with a non-zero intrinsic noise strength $D_{\text{intr}} > 0$ and a *positive* effective tension $\nu > 0$. It appears plausible that the properties of the chaotic state of equation (4.35) should not be qualitatively altered by the addition of an external noise source. Moreover, if the nonlinearity in equation (4.36) is capable of generating a positive interface tension out of a negative bare value $\nu_0 < 0$, this should remain true in the limit $\nu_0 \to 0^-$. Thus, one is lead to conclude that a positive interface tension would be generated also in the case of equation (3.65), in contradiction to the $\epsilon = 8 - d$ expansion of Golubović and Bruinsma [100].

The argument is somewhat less firm than it seems, because it presupposes that the limit $\nu_0 \to 0$ in equation (4.36) (which takes equation (4.36) to equation (3.65)) commutes with the limit $D \to 0$ (which takes equation (4.36) to equation (4.35)). To gain some insight into this issue, consider equation (4.36) with $D = 0$ and $\nu_0 < 0$. This reduces to the parameter-free equation (4.35) through the transformation

$$\tilde{h}(x, t) = |\nu_0|^{-1} h(|\nu_0|^{-1/2} x, |\nu_0|^{-2} t). \tag{4.37}$$

Using this transformation together with the results obtained for equation (4.35) in [193], it is an easy matter to show that the effective large-scale interface tension of the deterministic version of equation (4.36) vanishes as $\nu \sim -\nu_0$, and the intrinsic noise strength vanishes as $D_{\text{intr}} \sim |\nu_0|^{7/2}$ when $\nu_0 \to 0$. If the limit $\nu_0 \to 0$ is performed at fixed external noise strength $D > 0$, one therefore enters a regime where the external noise dominates over that generated by the chaotic fluctuations, and which may behave differently from the deterministic equation (4.35). The transition between the two regimes was studied numerically by Karma and Misbah [187], who found a smooth crossover with no singular features.

4.4.2. *Related models*

It should be emphasized that, since equation (4.35) contains no control parameters apart from the system size L, the large crossover scale in one (and possibly also two) dimensions is an *intrinsic* property of the equation. This lack of versatility was one of the motivations that led Bohr and co-workers [203, 204] to introduce lattices of *coupled circle maps* as a new class of chaotic interface models. These models are defined in terms of real, unbounded height variables $h_t(i)$ that live in discrete time and on a discrete space (the integer lattice, for the present discussion). In the absence of coupling, each variable is updated according to a rule

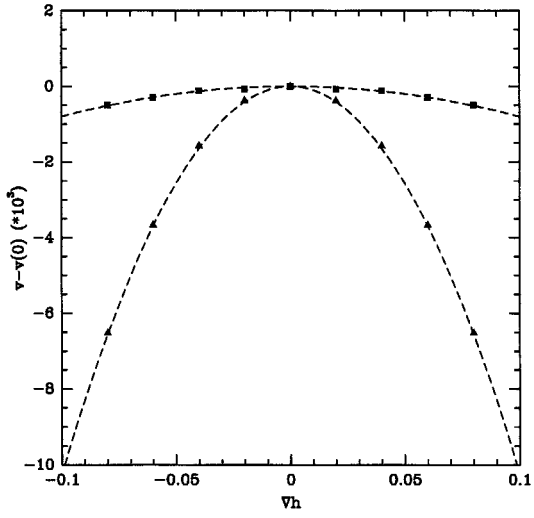

Figure 17. Inclination dependence of the interface velocity v for coupled circle maps with diffusive (squares) and totalistic (triangles) coupling. The local updating rule (4.38) was the logistic map with $R = 4$ in both cases. The data were obtained from simulations of systems of size $L = 1000$, with a duration of 10^6 time steps per data point. The broken curves indicate parabolic fits.

that is a combination of a constant shift (to break the $h \to -h$ symmetry) and a nonlinear map on the unit interval acting on the fractional part of h:

$$h \to F(h) = h + f(h - [h]). \tag{4.38}$$

A typical choice is the logistic map, $f(x) = Rx(1 - x)$. Two kinds of coupling schemes have been considered [203, 204]: a *diffusive* coupling defined by

$$h_{t+1}(i) = F(h_t(i)) + \epsilon[h_t(i + 1) + h_t(i - 1) - 2h_t(i)], \tag{4.39}$$

and a *totalistic* coupling

$$h_{t+1}(i) = F([h_t(i + 1) + h_t(i) + h_t(i - 1)]/3). \tag{4.40}$$

It turns out [204] that the magnitude of the KPZ nonlinearity in the large scale dynamics, and therefore the observability of KPZ scaling, depends crucially on the choice of coupling. This is illustrated in figure 17, which shows the variation of the average interface velocity $v = \langle h_{t+1}(i) - h_t(i) \rangle$ with inclination $\nabla h = \langle h_t(i + 1) - h_t(i) \rangle$, for the two coupling schemes (4.39) (with $\epsilon = 0{\cdot}2$) and (4.40). From the indicated parabolic fits one estimates that $\lambda \approx -0{\cdot}16$ for the diffusive coupling, and $\lambda \approx -2{\cdot}0$ in the totalistic model. According to equation (4.20), this implies that the crossover times to asymptotic KPZ behaviour differ by a factor of $2{\cdot}4 \times 10^4$! Indeed, while clean KPZ scaling was observed in simulations of the totalistic rule, with the diffusive coupling only the pre-asymptotic EW regime could be accessed [204].

Clearly, the coupled map models differ from the KS equation (4.35) in several, possibly important, respects. Here, the chaotic fluctuations arise (for appropriate choices of f) simply from the local updating rule (4.38); there is no analogue of the unstable spatial coupling in equation (4.35), nor of the resulting cellular structure. Also, the coupled map models have only discrete translational symmetry in i and h;

moreover, in two dimensions the continuous *rotational* symmetry of equation (4.35) is lost. Nevertheless, the great variability that can be achieved by different choices of local maps and different coupling schemes makes them promising objects for explorative studies of spatio-temporal chaos.

The goal of constructing models of spatio-temporal chaos which are similar to the Kuramoto–Sivashinsky equation but afford a greater flexibility was also a major motivation in the recent work of Rost and Krug [205], who proposed a particle model for the KS cell dynamics. The crucial idea in the construction is to let the particle positions evolve according to the laws of classical mechanics, which automatically ensures Galilean invariance of the velocity field. The merging and splitting of cells is represented through the coalescence and creation of particles; the rules for these events are constrained by the requirement that the particle velocities should correspond to the gradient of an interface height profile with *local* dynamics at all times. Numerical simulations of the model show KPZ behaviour on relatively short length and time scales. Single particle trajectories wander superdiffusively, analogous to 'tracer' particles in the KS equation [206] (cf. the discussion of tracer diffusion in the ASEP in section 4.3).

4.5. *Directed polymers in random media*

The directed polymer representation [19, 77] of the KPZ equation provides a link between the *non-equilibrium* dynamics of interfaces and the *equilibrium* statistical mechanics of flexible lines in a quenched random environment. The conceptual basis of the mapping between the two problems is quite simple. The d-dimensional substrate space of the interface is enlarged into a $(d+1)$-dimensional space by treating the time direction as an additional coordinate. Thereby each noise history $\eta(\mathbf{x}, t)$ can be viewed as a realization of a quenched random potential in $d+1$ dimensions. The time evolution of the interface is then encoded by an ensemble of 'infection paths', to be specified shortly, which are directed along the t axis. The statistical weight of each path can be written as a Boltzmann factor with an energy that comprises an elastic term and a random contribution due to the disorder potential. Thus, the paths can be identified with conformations of physical objects such as flux lines, directed polymers or (in $d = 1$) *equilibrium* interfaces.

Mathematically, the mapping is achieved through the Cole–Hopf transformation, which was discovered some forty years ago as a means to exactly linearize the (deterministic, 1D) Burgers equation [207]. Here, we shall proceed in the converse direction—we first state the directed polymer problem, and then show how it leads to the KPZ equation. Throughout this section we will be working with a general number of transverse dimensions d, and return to specific applications to $d = 1$ in section 4.6.

Consider then a directed line that runs through the random potential η, connecting the origin $(\mathbf{0}, 0)$ to some endpoint $(\mathbf{x}, t)$ (figure 18). The total energy of the line can be written as

$$\mathscr{H}[\mathbf{y}(s)] = \int_0^t \mathrm{d}s \left\{ \frac{\gamma}{2} \left(\frac{\mathrm{d}\mathbf{y}}{\mathrm{d}s} \right)^2 + \eta(\mathbf{y}(s), s) \right\}, \tag{4.41}$$

with a line tension $\gamma > 0$. The restricted partition function of all conformations that run from $(\mathbf{0}, 0)$ to $(\mathbf{x}, t)$ takes the form of a path integral:

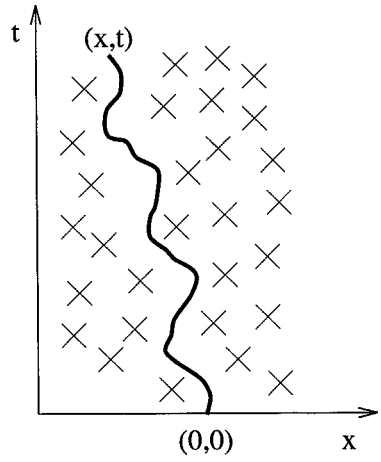

Figure 18. Directed line in a random potential, represented by the crosses.

$$\mathscr{Z}(\mathbf{x}, t) = \int_{(\mathbf{0},0)}^{(\mathbf{x},t)} \mathbf{D}\mathbf{y}[\cdot] \exp\{-\mathscr{H}[\mathbf{y}]/k_B T\}. \tag{4.42}$$

By standard techniques [208] this is brought into the differential form of a diffusion equation:

$$\frac{\partial \mathscr{Z}}{\partial t} = \frac{k_B T}{2\gamma} \nabla^2 \mathscr{Z} - \frac{1}{k_B T} \eta \mathscr{Z}. \tag{4.43}$$

In the last step we introduce the restricted free energy

$$\mathscr{F}(\mathbf{x}, t) = -k_B T \ln \mathscr{Z}(\mathbf{x}, t), \tag{4.44}$$

which satisfies, according to equation (4.43), the KPZ equation

$$\frac{\partial \mathscr{F}}{\partial t} = \frac{k_B T}{2\gamma} \nabla^2 \mathscr{F} - \frac{1}{2\gamma} (\nabla \mathscr{F})^2 + \eta, \tag{4.45}$$

with coefficients $\nu = k_B T/2\gamma$ and $\lambda = -1/\gamma$. The equivalence between equations (4.42) and (4.45) was first observed by Huse, Henley and Fisher [168].

Several remarks are in order. First, since equation (4.45) is written for $\mathscr{F}$ rather than for $\mathscr{Z}$, the *thermal* average is already implicitly performed when describing the directed polymer by the KPZ equation, whereas the conventional noise average in the interface dynamics corresponds to a subsequent *disorder* average. The succession of the two averages implies that we are dealing with a case of *quenched* disorder. Second, it should be noted that the natural initial condition for $\mathscr{F}$ is different from the flat initial state commonly considered in the interface context: from the definition of the path integral (4.42) we have $\mathscr{Z}(\mathbf{x}, 0) = \delta^d(\mathbf{x})$, corresponding to a deep narrow groove in the 'interface' $\mathscr{F}(\mathbf{x}, t)$. Third, it is clear from the derivation that the mapping always leads to the *isotropic* KPZ equation; different signs of the λ_i in equation (4.3) cannot be accommodated [158]. This hints at some fundamental differences between the isotropic and anisotropic equations, which still wait to be elucidated.

Readers who feel uneasy about the formal manipulations of the continuum path integral (4.42) will be reassured to learn that the mapping can be formulated and explicitly carried out also on the level of microscopic, stochastic lattice growth

models [8, 179, 209–211]. In these cases the resulting directed polymer problem typically resides as *zero temperature*, so that the thermal average is replaced by the selection of a single, optimal ground state path. This is nonessential as long as the finite (low) temperature behaviour and the behaviour at $T = 0$ fall into the same universality class, which is true for the standard directed polymer (see below) but fails, for example, in the presence of columnar disorder [212] (see section 4.6.3).

We now summarize the main correspondences induced by the mapping (details can be found in the cited literature). The rough interface configuration $h(\mathbf{x}, t)$ translates into the rugged free energy landscape felt by a polymer of length t. The interface velocity equals the free energy per unit length $f = \partial \mathscr{F}/\partial t$. This immediately provides us with an appealing interpretation of the finite size correction to the stationary interface velocity derived in section 4.3: identifying the coefficients from equation (4.45) we see that equation (4.23) expresses the increase in the free energy per unit length

$$\Delta f = \frac{D}{2k_B TL} \tag{4.46}$$

due to the *confinement* of the polymer to a cylinder of circumference L. The effect is analogous to the increase in free energy incurred by a thermally excited line (in the absence of disorder) confined to a region of lateral extent L, due to the loss of configurational *entropy* [213]. The corresponding expression

$$\Delta f_{\text{thermal}} \sim \frac{(k_B T)^2}{\gamma L^2} \tag{4.47}$$

is easily derived [179] from equation (4.45) with $\eta = 0$ and appropriate boundary conditions. Besides the different L dependences of equations (4.46) and (4.47), which show that the disorder always dominates the behaviour on scales larger than $L_c = (k_B T)^3/\gamma D$, it is interesting to note the opposite roles played by temperature in the two cases, as well as the fact that equation (4.46), in contrast to equation (4.47), is independent of the line tension γ.

Somewhat less obviously, the dynamic correlation length $\xi(t) \sim t^{1/z}$ turns out to be proportional to the *transverse displacement* of the polymer

$$\delta x(t) = \langle [\mathbf{x}(t)]^2 \rangle^{1/2} \sim \xi(t) \sim t^{1/z}, \tag{4.48}$$

where square (angular) brackets indicate thermal (disorder) averages. The displacement is superdiffusive when $z < 2$, due to the random potential which encourages large transverse fluctuations; diffusive behaviour, $z = 2$, is characteristic of the entropic wandering of a thermally excited line.

The directed polymer representation has been instrumental in developing an intuitive understanding of the weak coupling/strong coupling phase transition of the KPZ equation in dimensions $d > 2$. In the directed polymer context the transition appears as a thermal phase transition between a disorder-dominated, glassy low temperature phase (strong coupling) and a high temperature phase in which the polymer is essentially unobstructed by the disorder (weak coupling). Rigorous proofs for the existence of the transition, and bounds on the transition temperature have been obtained [8, 214].

Another issue that deserves more than summary treatment is the interpretation of the tilt (or Galilean) invariance of the KPZ equation in the directed polymer language. We have argued in section 4.1 that, as a consequence of the invariance

of the equation under the tilt transformation (4.4), the coefficient λ of the nonlinearity is not renormalized. From equation (4.45) we see that this implies the non-renormalization of the polymer line tension γ. Indeed, by applying the tilt invariance argument on the level of the partition function (4.42) it can be shown [215] that the *average* elastic response of the polymer is completely unaffected by the disorder, in the sense that the average free energy profile for a polymer of length t, fixed at the origin, is

$$\langle \mathscr{F}(\mathbf{x}, t) - \mathscr{F}(\mathbf{0}, t) \rangle = \frac{\gamma \mathbf{x}^2}{2t}. \tag{4.49}$$

Since the transverse displacement of the endpoint from $\mathbf{0}$ to $\mathbf{x}$ stretches the polymer, to leading order, by the amount $\mathbf{x}^2/2t$, equation (4.49) is simply a manifestation of Hookes law with the line tension γ of the *pure* system. This is a highly non-trivial result, which has its roots in the statistical translational invariance of the disorder potential, i.e. the fact that η' and η in equation (4.5) have the same correlation functions; statistical translational invariance, when regarded as a symmetry property, has powerful consequences for a large class of disordered systems [216]. The simplicity of the *average* free energy (4.49) notwithstanding, the *actual* response of a polymer in a single realization of randomness is dominated by rare, large fluctuations drawn from a non-trivial power law distribution [217].

While the line tension remains unrenormalized, the temperature T does not—from equation (4.45) we see that $T \sim \nu$, and hence, according to the scaling transformation (3.64), temperature is driven to zero under renormalization, provided $z < 2$; the low temperature (strong coupling) phase of the directed polymer is governed by a zero-temperature fixed point [154]. This is the reason for the equivalence of zero and finite temperature scaling properties alluded to previously. The equivalence may break down if the translational invariance of the disorder potential is broken, as is the case in the situations discussed in the following section.

4.6. *Inhomogeneous growth*

In this section we shall concern ourselves with situations where the translational invariance parallel to the interface (in the substrate plane) is broken due to the presence of an external, position-dependent contribution to the local growth rate. There is no principal difficulty in studying this problem in general dimensionalities; however, since almost all studies so far have addressed the 1D case, we will specialize to $d = 1$ from the outset. Consider then the following generalization of the KPZ equation:

$$\frac{\partial h}{\partial t} = \nu \nabla^2 h + \frac{\lambda}{2}(\nabla h)^2 + \eta(x, t) + V(x). \tag{4.50}$$

We will discuss two types of growth rate inhomogeneities $V(x)$. In the first case (the *single defect* case), $V(x)$ is localized in a small spatial region and can be modelled, in the continuum limit, by a δ-function:

$$V(x) = V_0 \delta(x - x_0). \tag{4.51}$$

Here, x_0 may be located either in the bulk [218–221], or at the boundary of the system; the latter possibility is realized in the dynamics of an interface of finite lateral extent L in which growth rate inhomogeneities arise at $x = 0$ and $x = L$ due to some set of 'free' boundary conditions [162, 179]. Here the main interest is in *morphological phase transitions* that may occur, by a mechanism to be explained shortly, as the

strength V_0 of the inhomogeneity is varied. In the second case (*many defects*), $V(x)$ is a random function with short-ranged correlations. Not surprisingly, as will be shown in section 4.6.3, this turns out to severely modify the roughness of the interface. Finally, in section 4.6.4 we consider a different type of boundary effect, which occurs in stationary non-equilibrium interfaces *anchored* at one end [222].

4.6.1. *Morphological transitions*

The basic mechanism whereby a growth rate inhomogeneity of the type (4.51) can change the large-scale morphology of the interface is easily accounted for [218] (figure 19). Consider an interface with a growth rate that is a symmetric function of inclination, $v(\nabla h) = v(0) + (\lambda/2)(\nabla h)^2$, and suppose for concreteness that $\lambda > 0$. This implies that the interface can *increase* its growth rate by assuming a nonzero tilt. Consequently, a macroscopic hill can form in response to a sufficiently large, positive growth rate inhomogeneity $V_0 > 0$: since the sides of the hill are tilted by some amount $\pm u$ relative to the reference line, the hill grows faster than the planar interface and thus allows the system to accommodate the external bias. This is not possible if the growth rate is *reduced* at x_0, i.e. if $V_0 < 0$, since the planar interface already propagates as slowly as possible and cannot slow down by tilting; a defect with $V_0 < 0$ does not affect the large-scale morphology. Clearly the roles of positive ($V_0 > 0$) and negative ($V_0 < 0$) inhomogeneities are reversed if $\lambda < 0$.

It is natural to regard the magnitude of the induced tilt u as an order parameter of the transition, and to write

$$u \sim |V_0 - V_0^c|^\beta, \quad V_0 \to V_0^c \tag{4.52}$$

to define an order parameter exponent β (note that possibly $V_0^c = 0$). The transition is associated with a diverging correlation length, which can be identified as follows.

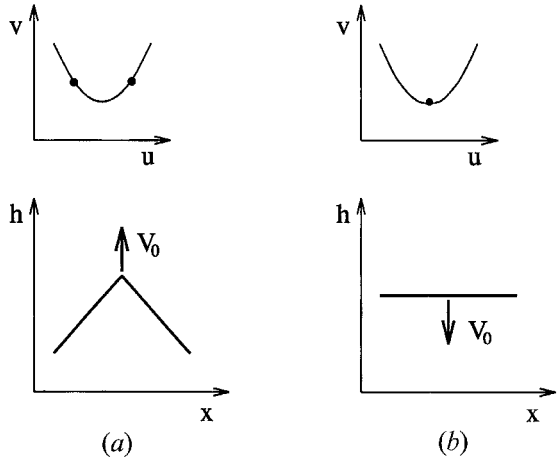

Figure 19. Illustration of the mechanism for tilting transitions induced by a localized growth rate inhomogeneity. The growth rate v is assumed to be an increasing function of inclination u. (*a*) If $V_0 > 0$, the interface can increase its growth rate by forming a macroscopic hill; the slopes of the hillsides are indicated by dots in the v–u graph. (*b*) If $V_0 < 0$, no transition occurs because the flat interface is already moving as slowly as possible.

In the tilted state, we consider the interface fluctuations about the average profile $h_0(x, t) = ux + v(u)t$, i.e. setting $h(x, t) = h_0(x, t) + \hat{h}(x, t)$ one has

$$\frac{\partial \hat{h}}{\partial t} = \nu \nabla^2 \hat{h} + \lambda u \nabla \hat{h} + \frac{\lambda}{2}(\nabla \hat{h})^2 + \eta(x, t) + V(x). \tag{4.53}$$

The essential feature is the linear term $\lambda u \nabla \hat{h}$ induced by the tilt. This term describes a drift of fluctuations with velocity $c = -\lambda u$. In contrast to the translationally invariant situation discussed subsequent to equation (4.3), here the drift term cannot be eliminated by going to a suitably chosen moving frame, since such a transformation would not be compatible with the inhomogeneity $V(x)$. Instead, the drift is expected to play an essential role in the dynamics [162] (for a related situation see section 4.6.4). In view of the dimensional arguments employed in section 4.1, the primary effect of the additional term is that it provides us with a third dimensionful coefficient, the drift velocity c, that can be used together with the invariants λ and D/ν to construct a *time-independent* length scale

$$l(u) = \lambda^2 (D/\nu)|c|^{-2} = (D/\nu)|u|^{-2}, \tag{4.54}$$

which diverges upon approaching the transition. Introducing the correlation length exponent ψ through

$$l \sim |V_0 - V_0^c|^{-\psi}, \tag{4.55}$$

it follows that $\psi = 2\beta$.

It is informative to contrast the quadratic divergence of equation (4.54) with the corresponding behaviour in a 'mean field' approximation [218, 162] to equation (4.50), in which the noise term $\eta(x, t)$ is neglected. In the absence of noise the invariant quantities of the equation are λ, the drift velocity c and the coefficient ν of the Laplacian term. Since the dimension of ν is $[\nu] = [x]^2/[t]$, a length scale can be constructed from ν and c,

$$l_{\mathrm{MF}}(u) = \nu/|c| = (\nu/|\lambda|)|u|^{-1}, \tag{4.56}$$

which diverges *linearly* in $1/|u|$. This indicates that the presence of noise changes the universal features of the transition. To clarify these issues we now turn to the interpretation of inhomogeneous growth in the directed polymer representation.

4.6.2. *Delocalization and unbinding*

To arrive, via the mapping described in section 4.5, at the generalized KPZ equation (4.50), we have to start from the energy expression

$$\mathscr{H}[\mathbf{y}(s)] = \int_0^t \mathrm{d}s \left\{ \frac{\gamma}{2} \left(\frac{\mathrm{d}\mathbf{y}}{\mathrm{d}s} \right)^2 + \eta(\mathbf{y}(s), s) + V(y(s)) \right\}, \tag{4.57}$$

which contains an additional potential term V acting on the polymer. Since V is independent of the 'time' coordinate t, a localized inhomogeneity (4.51) corresponds to a defect line that traverses the random energy landscape parallel to the t axis (figure 18). Noting that $\lambda < 0$ in the KPZ equation (4.45) for the polymer free energy, it becomes evident why a phase transition can be expected to occur for $V_0 < 0$. The defect potential being *attractive*, it competes with the roughening tendency of the bulk disorder η and may, if sufficiently strong, *bind* the transverse position of the polymer close to x_0; in the bound phase the restricted free energy

$\mathscr{F}(x, t)$ increases linearly with the distance from the defect, corresponding to a macroscopically tilted interface. Thus the morphological transitions induced by the growth rate inhomogeneity re-emerge in the guise of unbinding or delocalization transitions of a kind that has been much studied in the context of thermal and disorder-induced fluctuations of equilibrium interfaces [213].

At this point it becomes important to distinguish between the two possible locations of the defect position x_0 in the bulk or at the boundary of the system, respectively. When the defect resides in the bulk, the defect potential $V(x)$ is symmetric in $x - x_0$. This property is inherited by the positional probability distribution of the polymer. Consequently, the average position will be equal to x_0 irrespective of whether the polymer is bound to the defect or not; in order to observe the transition, the width (second moment) of the probability distribution has to be monitored. Following Forgacs, Lipowsky and Nieuwenhuizen [213] this case will be referred to as a *delocalization* transition. In contrast, if the defect is located at the boundary of the system ($x_0 = 0$, say), the polymer is subject to an additional 'hard wall' potential which arises from the constraint that $y(s) \geq 0$ for all paths (this corresponds [179] to a free boundary condition for the interface). Therefore the *total* defect potential has a repulsive hard core and an attractive short-range part of strength V_0. In this case the liberation of the polymer from the defect will result in a divergence of the *average* distance from the boundary, a phenomenon known as [213] *unbinding*. In both cases the 'liberation' of the polymer from the defect is expressed in the divergence of the correlation length l, which measures the typical distance of the polymer from the defect; for this reason the exponent ψ in equation (4.55) is occasionally referred to as the liberation exponent.

To appreciate why the two situations may lead to qualitatively different behaviours, it is useful to first consider the 'mean field' version of the problem in which $\eta = 0$ in equations (4.50) and (4.57). Note that this simplification has a very natural interpretation in the directed polymer language. In the absence of disorder, equation (4.57) reduces to the energy of a *thermally* excited line (or 1D interface) subject to an external potential, a class of problems much studied in diverse contexts ranging from wetting phenomena [213] to the adhesion and unbinding of fluid membranes [111].

In the thermal case the study of the delocalization or unbinding of a line reduces to an exercise in elementary quantum mechanics. Taking the limit $t \to \infty$, the diffusion equation (4.43) for the restricted partition function $\mathscr{Z}(x, t)$ (derived from the Hamiltonian (4.57)) becomes a stationary Schrödinger equation

$$\left[-\frac{(k_B T)^2}{2\gamma} \nabla^2 + V \right] \mathscr{Z} = f_0 \mathscr{Z}, \tag{4.58}$$

where f_0 denotes the free energy per unit length. The transition is associated with the disappearance of the last bound state of the Schrödinger problem and the concomitant vanishing of the eigenvalue f_0. Outside the range of V such a bound state decays exponentially on a scale $l = k_B T/(-2\gamma f_0)^{1/2}$, hence the order parameter $u = \partial \mathscr{F}/\partial x$ is $u = k_B T/l$ in accordance with equation (4.56) (note that from equation (4.45) we have $\nu/|\lambda| = k_B T/2$). From the well-known fact that a symmetric, attractive potential always possesses at least one bound state in one dimension, we conclude that the delocalization transition occurs at zero potential strength, $V_0^c = 0$, while the threshold for unbinding is expected to be non-zero.

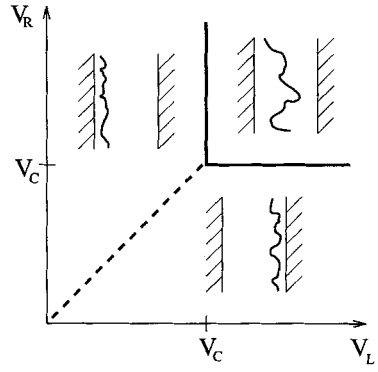

Figure 20. Phase diagram for a directed polymer confined by two attractive walls, as obtained from the exact solution of the ASEP with open boundary conditions [179]. V_L and V_R denote the (negative) contact potentials at the left and right walls. The full bold lines indicate continuous unbinding transitions, while the broken bold line represents a first-order transition between two bound phases.

Specifically, if the potential is modelled by a square well of width a and depth $-V_0$, one obtains

$$l = \frac{k_B T}{u} = \frac{(k_B T)^2}{\gamma a}(V_0^c - V_0)^{-1}, \tag{4.59}$$

with $V_0^c = 0$ for delocalization and $V_0^c = -(k_B T)^2(\pi/2a)^2/2\gamma < 0$ for unbinding. Comparing with equation (4.52) we see that the order parameter exponent $\beta = 1$ in the thermal case, both for delocalization and unbinding.

Delocalization and unbinding transitions in the presence of quenched bulk disorder constitute a highly nontrivial class of problems that has been intensely studied in the years following the pioneering work of Kardar [223]. It was pointed out only very recently [179] that the particular problem of zero-temperature disorder-induced unbinding affords an *exact* solution in one transverse dimension, $d = 1$. The solution is obtained in a somewhat indirect fashion, through a sequence of mappings that take a zero temperature, discrete directed polymer problem to a growth model (the single step model briefly discussed at the end of section 4.3) and further to a version of the asymmetric simple exclusion model (ASEP, see section 4.3) with open boundaries originally introduced by Krug [162]. The ASEP, in turn, was solved exactly by Derrida, Evans, Hakim and Pasquier [163] and independently by Schütz and Domany [164].

The main features of the unbinding transition that emerge from the exact solution are as follows (see also figure 20). The transition occurs at a finite value of the binding potential, and the order parameter exponent in equation (4.52) is $\beta = 1$ as in the thermal case (in fact the entire phase diagram of the model is reproduced *exactly* by the mean-field/thermal approximation, for reasons that are not completely understood). The relation (4.54) would then suggest that the liberation exponent ψ defined by equation (4.55) should take the value $\psi = 2$, different from the thermal result $\psi = 1$ (see equation (4.59)). This was already predicted by Kardar [223], and is explicitly confirmed by the exact solution [179].

While early numerical studies [223–225] suggested that disorder-induced delocalization may be rather similar to unbinding, recent analytic and numerical work

[226–229] seems to converge (some controversy remains, however; see [230]) on the view that the two problems are in fact fundamentally different. First, as in the thermal case, delocalization occurs at zero potential strength, $V_0^c = 0$. Second, and more importantly, the values of the exponents β and ψ are formally infinite, in the sense that the power law divergence (4.55) is replaced by an essential singularity

$$l \sim \exp(-C/V_0), \tag{4.60}$$

with $C > 0$, for $V_0 < 0$; the relation (4.54) is nevertheless satisfied [228]. Needless to say, the direct numerical verification of equation (4.60) is exceedingly difficult [226, 227].

4.6.3. *Many defects*

Much of the recent work on the disorder-induced delocalization of directed polymers has been motivated by the application to flux lines in dirty high-temperature superconductors [231, 227]. There, the localizing potential is provided by a *columnar defect* which may either be present in the material in the form of a screw dislocation, or may be deliberately created by ion irradiation, with the intent of increasing the critical current through enhanced pinning. Localization at the defect is counteracted by thermal fluctuations (i.e. entropy) as well as by bulk disorder that appears in the form of *point defects* such as oxygen vacancies.

In this context it is very natural to consider the behaviour of a flux line in an array of *many* columnar defects with randomly distributed pinning strengths. Within the continuum theory defined by equation (4.57), this can be modelled by choosing the potential V as a Gaussian random variable with zero mean and short ranged correlations:

$$\langle V(x)V(x')\rangle = V_0^2\delta(x - x'). \tag{4.61}$$

In terms of interfaces described by the inhomogeneous KPZ equation (4.50), this corresponds to a growth rate with a time-independent, spatially random component (not to be confused with the quenched, h-dependent noise that appears in the study of interface displacement in random media [81–84]). Physically, such disorder could represent [232], for example, a random array of screw dislocations which locally enhance the growth rate [233]. It also arises in the context of *phase-disordered interfaces*, where the h variable is subjected to a periodic potential with quenched random phase shifts between different points in the lateral x direction [234, 235]. In the following discussion we will however use the directed polymer language, which provides the most natural framework for analytic arguments.

As it stands, the KPZ equation (4.50) with random inhomogeneities poses a rather formidable problem, the directed polymer being subject to the conflicting influences of point disorder, columnar defects and thermal fluctuations. The problem without point disorder ($\eta = 0$) has a rich history [212, 236], with applications ranging from the conformation of (undirected!) Gaussian polymers in random media [237, 238] to the evolution of biological species [239]; the full problem ($\eta \neq 0$) has also been studied in the context of driven diffusion with disorder [240]. Here, we shall focus on two special cases, (i) the purely columnar problem ($\eta = 0$) at *finite* temperature, and (ii) the zero temperature problem in the presence of both columnar and point disorder. We will argue that the thermal fluctuations and the point disorder play very similar roles in counteracting the localizing tendency of the

columnar defects in the two cases, and can in fact be treated on the same footing [241].

To avoid some subtleties associated with the continuum formulation of the problem, we envision, for the purposes of the present discussion, a suitable discretization. For example, in the case of directed paths on the square lattice with the transverse displacement restricted to at most one lattice spacing per time step, the discrete version of the diffusion equation (4.43) for the restricted partition function reads [212, 241]

$$Z(x, t+1) = \exp\{-[\eta(x, t) + V(x)]/k_B T\}[Z(x, t) + Z(x-1, t) + Z(x+1, t)]. \tag{4.62}$$

In the zero-temperature limit this reduces to a recursion for the ground state energies $E(x, t) = -\lim_{T\to 0} k_B T \ln Z(x, t)$.

The competition between the localizing defect and the delocalizing influence of thermal or point disorder fluctuations has already been emphasized as the driving force behind delocalization and unbinding transitions. In the presence of a random array of columnar defects, this competition extends to all scales, thereby dramatically enhancing the transverse wandering of the polymer. To see this, we first need to identify the 'optimal' disorder regions to which the polymer is attracted. In the presence of either point disorder or thermal fluctuations, the (free) energy cost per unit length required to localize the polymer in a region of transverse extent l is of order $l^{-\tau}$, where (for $d = 1$ transverse dimension) $\tau = 1$ for point disorder, and $\tau = 2$ in the thermal case (see equations (4.46) and (4.47)). Due to the confinement energy, the polymer is primarily attracted to *wide* regions in which all columnar defect energies are lower than average; naturally, such regions are rare, and to reach them large transverse fluctuations are necessary.

For a quantitative estimate consider, for example, a binary distribution of columnar defect energies, $V = -V_0$ with probability p and $V = 0$ with probability $1-p$. The probability for finding l subsequent attractive defects (which have $V = -V_0$) is then p^l, and the (free) energy per unit length for a polymer residing in such a region can be estimated as $-V_0 + \epsilon$, with $\epsilon \sim 1/l^{\tau}$. This translates into a 'density of states'

$$\rho(\epsilon) \sim p^l \sim \exp\left(-\frac{|\ln p|}{\epsilon^{1/\tau}}\right), \tag{4.63}$$

and a similar form is obtained for continuous, bounded disorder distributions. A standard variable range hopping argument [212, 241] applied to equation (4.63) then shows that the transverse displacement increases as

$$\delta x(t) \sim \frac{t}{(\ln t)^{1+\tau}}, \tag{4.64}$$

in reasonable agreement with simulations [212, 241] (see figure 21). In d transverse dimensions the exponent of the logarithmic factor in equation (4.64) is $1 + \tau/d$. The result $\delta x \sim t/(\ln t)^3$ for the thermal case in one dimension has been rigorously confirmed by Sznitman [242].

In case (ii), point and columnar defects at zero temperature, the result (4.64) has the surprising, and somewhat counterintuitive, feature that the displacement due to the combined effect of both types of defects is larger than that produced by any of the two types alone: the pure point problem has the standard KPZ behaviour

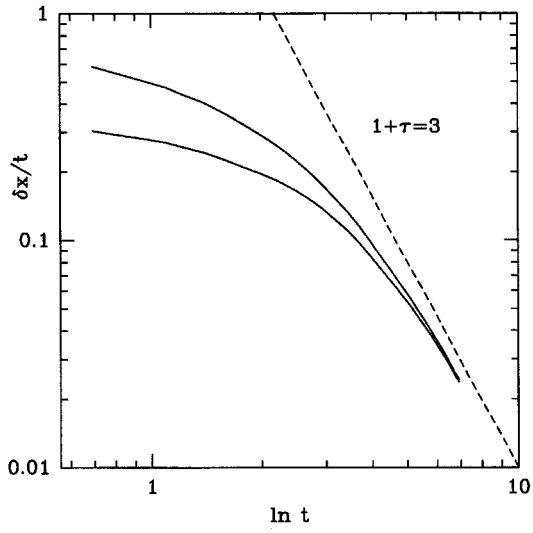

Figure 21. Measures of the transverse wandering of a finite temperature directed polymer in $1+1$ dimensions, subject to binary columnar disorder, but no point disorder ($\eta = 0$ in equation (4.62)). The upper and the lower curves show $\langle [x(t)^2] \rangle^{1/2}$ and $\langle [x(t)]^2 \rangle^{1/2}$, respectively, divided by the path length t. The broken line indicates the prediction (4.64) for the logarithmic prefactor, with $\tau = 2$ in the entropic case. The data were obtained by averaging over 10^4 realizations of disorder [212].

$\delta x \sim t^{1/z} = t^{2/3}$, while purely columnar defects at zero temperature, with a uniform distribution of defect energies, lead to a wandering as $\delta x \sim t^{1/2}$ [212, 238].

The behaviour of the transverse wandering as a function of temperature and the ratio D/V_0^2 of point to columnar disorder is summarized in figure 22. In the bulk of the diagram, where $T > 0$ and $D > 0$, one expects asymptotically the point disorder to dominate over thermal fluctuations, as the confinement length $l \to \infty$ (compare to section 4.3). It should be noted that the point $T = 0$, $D = 0$ is nonuniversal, in the sense that the scaling depends on the shape of the columnar disorder probability distribution [212, 238]. The rest of the diagram is universal for all distributions of finite support. For *rapidly* decaying, unbounded distributions (e.g. Gaussian or exponential) the wandering is still subballistic, $\delta x \sim t/(\ln t)^{\mu}$, but the value of μ differs from that in equation (4.64) [212]. The effect of *slowly* decaying (power law) distributions of columnar disorder has so far been studied only in the absence of both thermal fluctuations and point disorder, where it typically leads to ballistic wandering, $\delta x \sim t$, and non-extensive behaviour of the ground state energy [212, 238].

Returning to the kinetic roughening of interfaces described by the KPZ equation (4.50) with random inhomogeneities, the main interest is in the temporal behaviour of the interface width W, rather than the correlation length ξ. Since typical interface configurations show a hill-and-valley morphology with a lateral peak-to-peak distance ξ, one has simply

$$W \sim \xi \sim t/(\ln t)^{1+\tau}. \tag{4.65}$$

This has been confirmed in simulations of phase-disordered solid-on-solid models [234, 235].

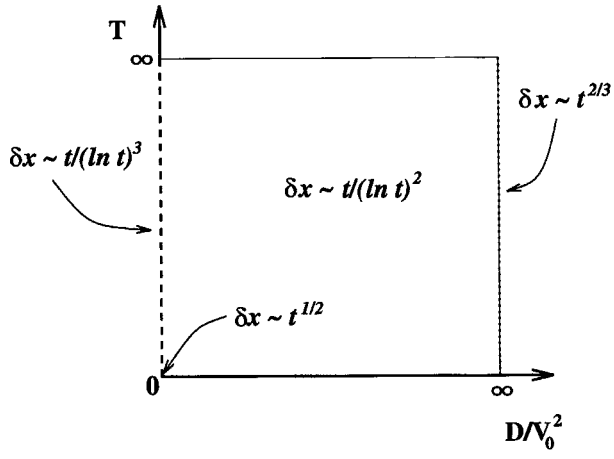

Figure 22. Phase diagram for the $1+1$ dimensional directed polymer subject to point disorder, columnar disorder and thermal fluctuations. In the bulk of the diagram the transverse wandering behaves as $\delta x \sim t/(\ln t)^2$. Differing behaviours are observed only at $D/V_0^2 = 0$ (pure columnar disorder) and $D/V_0^2 = \infty$ (pure point disorder). In the former case the point $T = 0$ is special.

4.6.4. *Anchored interfaces*

Here we describe a type of boundary effect that occurs for certain *stationary* non-equilibrium interfaces. Consider an interface displacement process characterized by a growth velocity $v(\nabla h)$ that changes sign at some orientation $u_c > 0$, $v(u_c) = 0$. Let the height variable $h(x, t)$ be defined on the half-axis $x > 0$, with an 'anchoring' boundary condition

$$h(0, t) = 0 \tag{4.66}$$

at all times. If in addition

$$c \equiv v'(u_c) < 0, \tag{4.67}$$

then the interface will be driven to a stationary, non-moving state with average position $\langle h(x, t)\rangle = u_c x$. Such interfaces arise as domain walls in Toom's cellular automaton, a nonequilibrium 2D Ising model [222, 243]. Another rather natural realization is the surface of a $(1+1)$-dimensional sandpile, which is kept in steady state by the balance between a continuous deposition flux and the outflow at the anchored boundary [244] (figure 23); in that case u_c defines the angle of repose.

The fluctuations $\hat{h}(x, t) = h(x, t) - u_c x$ around the average profile are described by the KPZ-type equation

$$\frac{\partial \hat{h}}{\partial t} = \nu \nabla^2 \hat{h} + c \nabla \hat{h} + \frac{\lambda}{2}(\nabla \hat{h})^2 + \frac{\lambda'}{6}(\nabla \hat{h})^3 + \cdots + \eta, \tag{4.68}$$

where $\lambda = v''(u_c)$ and $\lambda' = v'''(u_c)$, supplemented with the boundary condition (4.66). As in section 4.6.1, the lack of translational invariance implies that the drift term $c\nabla h$ cannot be removed by a tilt transformation. Owing to the stability condition (4.67), the drift transports fluctuations in the positive x direction, away from the anchoring point. This provides a mechanism for translating *temporal* into *spatial* fluctuations.

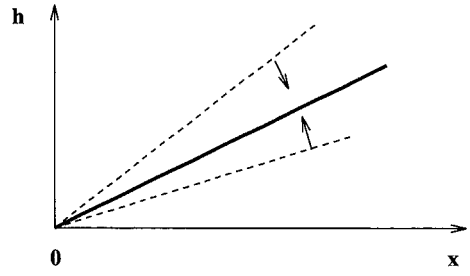

Figure 23. Schematic of an anchored interface, such as the surface of a semi-infinite sandpile. The stationary profile (bold line) is stable against upward or downward tilting (broken lines).

Let us estimate the stationary fluctuation amplitude at some point $x > 0$. At $x = 0$ the fluctuations are completely suppressed due to equation (4.66). At $x > 0$ they have travelled a time $t \approx x/c$, during which they have grown according to the KPZ dynamics (4.68). Thus their magnitude is of order $t^{1/3} \sim x^{1/3}$ or, more precisely, using equation (4.15) we expect [222]

$$\langle [h(x, t) - \langle h(x, t) \rangle]^2 \rangle \approx [(D/2\nu)^2 |\lambda x/c|]^{2/3}, \tag{4.69}$$

provided $\lambda \neq 0$ in the expansion (4.68). If for symmetry reasons $\lambda = 0$, then the fluctuations are governed by the cubic term in equation (4.68), which is marginally irrelevant in $d = 1$ (compare to section 3.3). In this case the right hand side of equation (4.69) is of the order of $[x(\ln x)^{1/2}]^{1/2}$ [245, 246]. These predictions have been confirmed by simulations of Toom interfaces [222] and sandpile models [244]; for sandpiles with two open boundaries additional effects occur due to the interaction between the two anchored interfaces [247].

5. The role of surface diffusion

Despite the challenging unresolved problems posed by the KPZ theory, over the last few years the attention of the kinetic roughening community has turned increasingly towards a class of surface growth processes that are *not* described by the KPZ equation. The shift of focus is motivated mainly by a critical reassessment [20] of the physical relevance of the KPZ nonlinearity in *deposition* processes, which would appear to provide the most natural realization of kinetic roughening phenomena.

We have emphasized in section 4 that the origin of the (kinematic) KPZ nonlinearity lies in a nontrivial inclination dependence of the growth rate v, measured in the vertical (h) direction (see equation (4.3)). However, as was first pointed out by Krug [129], in the most simplistic model of crystal growth from the vapour (the Wilson–Frenkel model; see [128] and [88]), in which every atom impinging on the surface is immediately incorporated into a perfect crystal lattice, the growth rate is manifestly *independent* of inclination. In suitable units it can be written as

$$v = F/\rho, \tag{5.1}$$

where F denotes the deposition flux and ρ is the deposit density (equivalently, $1/\rho$ is the atomic volume); in the situation just described, both are independent of surface

orientation. In the framework of the derivation of the isotropic continuum equation (3.6) in section 3.1, this result may be regarded as a consequence of crystalline anisotropy, which enforces an orientation dependence of the normal surface velocity v_n that precisely cancels the geometric factor $[1+(\nabla h)^2]^{1/2}$ in equation (3.4).

Equation (5.1) is useful in identifying the mechanisms by which the simplistic Wilson–Frenkel picture fails in real deposition processes. At *low temperatures*, the mobility on the surface is insufficient for every deposited atom to reach a lattice site before the arrival of other atoms, and a finite concentration of vacancies and other defects results. This implies a shift in the deposit density which, as is well known for the extreme case of ballistic deposition [31] (see also section 2.1), is a function of the surface inclination relative to the deposition beam. On an inclined surface one has a higher concentration of steps, at which overhangs and, eventually, overgrown vacancies can form; consequently the density ρ decreases, and, according to equation (5.1), the growth rate increases with the tilt [129].

At *high temperatures* there is a non-negligible probability for a deposited atom to redesorb from the surface; the sticking coefficient is less than unity. As the desorption probability depends on the local bonding environment, the desorption flux varies with the step density, and hence with surface inclination. To account for desorption, the total deposition flux in equation (5.1) should be replaced by a net flux $F - F_{\mathrm{desorp}}(\nabla h)$, which, again, induces an inclination dependence in v. This mechanism is also evident in the celebrated Burton–Cabrera–Frank (BCF) expression for the growth rate of a vicinal surface [88, 233] (see also section 5.2.1):

$$v_{\mathrm{BCF}} = 2F[(D_s\tau)^{1/2}/l]\tanh[l/2(D_s\tau)^{1/2}]. \tag{5.2}$$

Here, $l = |\nabla h|^{-1}$ is the step distance, D_s is the surface diffusion coefficient, and τ is the inverse desorption rate. In the limit $\tau \to \infty$ (no desorption) equation (5.2) reduces to equation (5.1), $v_{\mathrm{BCF}} \to F$.

In the context of simple stochastic growth models, the 'desorption' mechanism may be viewed as being responsible for the inclination dependence of the growth rate for the class of restricted solid-on-solid (RSOS) models introduced by Meakin *et al.* [26], Kim and Kosterlitz [183] and others [136, 248]. In these models deposition attempts are accepted only if certain conditions on the local height configuration are met; obviously this can be interpreted in terms of a zero sticking coefficient, or immediate redesorption, for some local environments.

The conclusion is that vapour desposition processes *do* fall into the KPZ universality class; however, the two underlying mechanisms apply mainly at either high or low temperatures. It turns out that technologically relevant deposition methods—in particular molecular beam epitaxy (MBE)—are often operated in the temperature window where *both* mechanisms, desorption as well as defect formation, can be neglected. This is perhaps not entirely surprising, since the practitioner would attempt to optimize the process towards growing perfect crystals (no defects) at maximal yield (no desorption). Empirically, the absence of the two mechanisms is demonstrated directly by the observed independence of the growth rate on miscut angle (that is, inclination), for example in the MBE of silicon [88].

Given the widespread interest in MBE applications, and availability of MBE growth chambers as well as sophisticated experimental techniques for the characterization of the growing surface, it is obviously desirable to bring the concepts of

kinetic roughening to bear upon the MBE process. This has prompted a large amount of theoretical work devoted to the limiting case, termed *ideal MBE* by Lai and Das Sarma [121], of deposition in the complete absence of both desorption and defect formation. The fundamental interest in this class of processes arises from the hope of finding new, non-trivial universality classes— distinct from the KPZ class which is excluded by construction. As we shall see in this section, the removal of the dominant KPZ term opens up a Pandora's box of possible behaviours. Moreover, the assignment of a universality class (represented by a specific large-scale equation of motion) to a given microscopic model turns out to be a rather subtle problem, with seemingly minor details playing a decisive role in a way unprecedented by the experience with KPZ-type models.

Ideal MBE. In the absence of desorption all relaxation processes on the surface conserve the mass of the growing film. The assumption of perfect crystalline structure transforms mass conservation into volume (or height) conservation. Thus, apart from the deposition flux, which is by definition uncorrelated with the surface configuration, ideal MBE is a *conservative* growth process that can be described by a driven continuity equation

$$\frac{\partial h}{\partial t} + \nabla \cdot \mathbf{J} = F, \tag{5.3}$$

where F includes the average deposition flux as well as shot noise fluctuations. Clearly, the question of universality classes reduces to a classification of the possible forms for the surface diffusion current $\mathbf{J}$.

We remarked already in section 3.1 that, in addition to the classical equilibrium surface diffusion current, two types of non-equilibrium contributions generically occur. Here, we re-emphasize that these contributions are fundamentally different from the KPZ nonlinearity, in the following sense. The KPZ term is obtained from a purely kinematic relation, equation (3.4), and arises physically simply because the interface is moving on average. In contrast, for the MBE equation (5.3) the mean motion is irrelevant, because it *does not couple to the surface fluctuations* (compare to section 4.3). Instead, the non-equilibrium contributions to the current $\mathbf{J}$ are of *dynamical* origin, reflecting the perturbation of the surface diffusion processes imposed by the external deposition flux. Consequently, the microscopic interpretation of these contributions requires considerable insight into the behaviour of adatoms on the surface.

The purpose of this section is to review our present theoretical understanding of non-equilibrium effects in ideal MBE. The two types of non-equilibrium contributions—inclination-dependent currents and inclination-dependent chemical potentials—are discussed separately in sections 5.2 and 5.4. A central theme is provided by the idea that the main effect of the deposition flux is to *remove the constraints* imposed on equilibrium surface diffusion by the requirement of detailed balance in microscopic processes [249]. This view is supported by the fact that closely analogous non-equilibrium effects arise if a surface is driven out of equilibrium by some mechanism other than growth, provided detailed balance is broken [92, 250, 251]. A separate section 5.3 is devoted to the surface instabilities which arise generically as a consequence of growth-induced currents. In section 5.5 the emerging picture is summarized, and the experimental situation is evaluated in section 5.6. To set the stage, we begin in section 5.1 with a survey of microscopic models.

5.1. *A survey of models for molecular beam epitaxy*

5.1.1. *Limited mobility models*

The first example of a growth model that conforms to the 'ideal MBE' restrictions of no desorption and no defect formation was proposed by Family in 1986 [127]; we have described the model in section 3.4. Although the title of Family's paper features the term 'surface diffusion', the basic assumption of the model—that the motion of adatoms is biased in the direction of decreasing absolute height–is hardly realistic in the context of MBE (unless one assumes that the adatom dynamics is completely dominated by transient mobility and downward funnelling effects, which may well be true on metal surfaces at low temperatures [99, 252, 253]). Recognizing this weakness, Wolf and Villain [101] and Das Sarma and Tamborenea [132] independently proposed variants of Family's model in which the preferred incorporation sites for the adatom are determined by the local bonding environment; roughly speaking, the function $K_{\mathbf{x}}$ introduced in section 3.4, which the mobile adatom seeks to minimize, is identified with the negative coordination number.

In fact the two models introduced by Wolf and Villain [101] and by Das Sarma and Tamborenea [132] differ slightly in their microscopic rules. For later reference, we make the effort to precisely define *three* versions of these models, the first two of which (DT1 and DT2) are probably close to the model actually simulated by Das Sarma and Tamborenea, while the third (WV) is the model proposed by Wolf and Villain. Bizarre as it may seem at this point, we will argue in section 5.2.3 that all three models belong to different universality classes asymptotically—a striking example of the sensitive dependence on microscopic details alluded to above.

To keep matters simple, we restrict the discussion to 1D surfaces, and allow the freshly deposited atom to search for an incorporation site only among the nearest neighbours of the deposition site. As in section 3.4, the surface configuration is described by a set of integer height variables h_i defined on the 1D substrate lattice $i = 1, \ldots, L$ (with periodic boundary conditions, say). The bonding environment at each site i is characterized by the lateral coordination number k_i (that is, the number of lateral nearest neighbour bonds) that *an additional atom would have if it were deposited at i*:

$$k_i = \begin{cases} 0, & h_i \geq h_{i+1} \text{ and } h_i \geq h_{i-1}, \\ 1, & h_{i-1} \leq h_i < h_{i+1} \text{ or } h_{i-1} > h_i \geq h_{i+1}, \\ 2, & h_i < h_{i-1} \text{ and } h_i < h_{i+1} \end{cases} \tag{5.4}$$

(see figure 24). In one deposition step, a site i is chosen at random and the coordination numbers (k_{i-1}, k_i, k_{i+1}) are examined.

In the *DT models*, sites with $k_i = 1$ or 2 are permanent traps; the freshly deposited atom is moved to one of the neighbouring sites $i \pm 1$ only if $k_i = 0$ *and* $k_{i-1} > 0$ or $k_{i+1} > 0$. The atom is moved to the right if $(k_{i-1}, k_{i+1}) = (0, 1)$ or $(0, 2)$, and to the left if $(k_{i-1}, k_{i+1}) = (1, 0)$ or $(2, 0)$. In a symmetric environment, $(k_{i-1}, k_{i+1}) = (1, 1)$ or $(2, 2)$, a random choice is made to move the atom left or right with equal probability. The two versions DT1 and DT2 differ in their treatment of the cases $(k_{i-1}, k_{i+1}) = (1, 2)$ and $(2, 1)$. Rule DT1 treats them as symmetric configurations, i.e. one of the two neighbouring sites is chosen at random, while DT2 always moves the atom to the site with the largest value of k_i, i.e. to the right for $(k_{i-1}, k_{i+1}) = (1, 2)$ and to the left for $(k_{i-1}, k_{i+1}) = (2, 1)$.

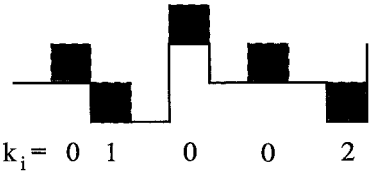

Figure 24. Illustration of the lateral coordination number defined in equation (5.4). The shaded squares are virtual atoms about to be deposited onto the (bold) surface.

The *WV rule* coincides with DT2 when $k_i = 0$; however, in addition atoms deposited on sites where $k_i = 1$ are allowed to move, if they can increase the coordination number. The atom is moved to the right if $(k_i, k_{i+1}) = (1, 2)$ and to the left if $(k_{i-1}, k_i) = (2, 1)$; the symmetric case $(k_{i-1}, k_i, k_{i+1}) = (2, 1, 2)$ cannot occur.

It is worthwhile to point out that in all three models (DT1, DT2 and WV) the height of the incorporation site is always less or equal to that of the deposition site, i.e. there are no 'uphill' jumps (this is no longer true if next nearest neighbour jumps are included). Naively, one might expect this asymmetry to give rise to a 'downhill' non-equilibrium current, as discussed in section 3, and consequently place all models in the Edwards–Wilkinson universality class (see section 3.2). We will show in section 5.2.2 why this simple-minded reasoning fails.

The work of Wolf and Villain [101] and Das Sarma and Tamborenea [132] was of great importance because it numerically demonstrated, for the first time, the possibility of scaling behaviour in vapour deposition processes that is distinct from the familiar Edwards–Wilkinson and KPZ universality classes. A confusing variety of related models have been subsequently proposed, with rules that are not always easy to decipher from the published description [121, 133, 254–259].

An interesting variant was introduced recently by Kim, Park and Kim [260]. This model is a *restricted* solid-on-solid (RSOS) model in which a strict constraint on the absolute magnitude of nearest-neighbour height differences is enforced at all times. Since it is required, under the rules of ideal MBE, that every deposited atom be incorporated somewhere on the surface, such a constraint can be maintained only if the region around the deposition site in which the atom searches for an eligible incorporation site is unlimited. In the implementation of Kim *et al.* [260] the search is conducted in shells of ever increasing radius around the deposition site.

The common feature of all these models (and the rationale for subsuming them under the 'limited mobility' heading) is that only freshly deposited atoms are regarded as mobile; once the preferred incorporation site has been chosen, according to some rule, in the neighbourhood of the deposition site, the deposited atom is placed there permanently. If, as is commonly done, the potential incorporation region is restricted to the nearest neighbours of the deposition site, the adatom mobility is very limited indeed, and the model strongly overemphasizes the disordering influence of the shot noise in the atomic beam. Consequently, the surface morphology is extremely rough (figure 25). In a certain sense the limited mobility models do not allow for any true surface relaxation, since there is *no dynamics when the beam is turned off*. The crucial improvement afforded by the collective diffusion models, to be described next, addresses precisely this problem.

These remarks make it clear that the limited mobility models have the status of toy models, rather than providing a (semi-)realistic description of MBE. We should

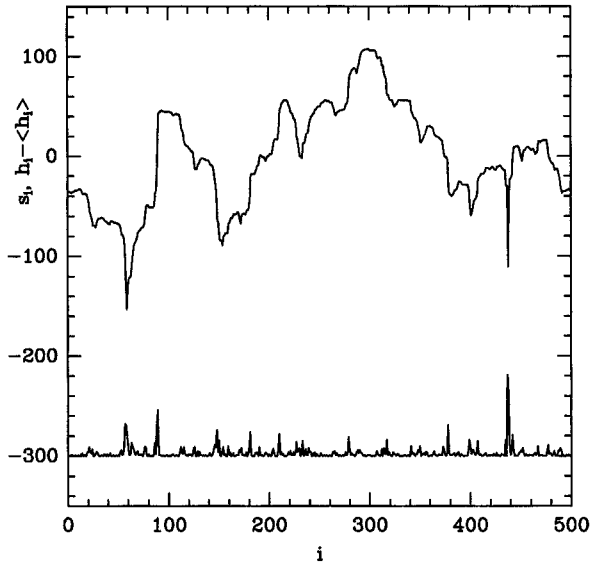

Figure 25. Surface configuration $h_i - \langle h \rangle$ (upper curve) and local step size $s_i = |h_{i+1} - h_i|$ (lower curve shows $s_i - 300$) generated by the DT1 rule. A total of 10^5 monolayers were deposited on a substrate of $L = 500$ lattice sites [112].

mention, however, that a realistic interpretation of these models does exist, in terms of a coarse-grained algorithm for island nucleation and growth, when the growth rule is supplemented by a noise-reduction algorithm [261]. Moreover, limited mobility models have been found to rather closely mimic the behaviour of more realistic models, at least for limited time regimes, provided the diffusion and deposition rates of the latter are chosen appropriately [262–264].

5.1.2. *Collective diffusion models*

An important number for characterizing epitaxial growth is the ratio of the surface diffusion constant D_s to the deposition flux F. To arrive at a properly nondimensional quantity, we express the flux in terms of the monolayer completion time τ_{ML} and the diffusion constant through the atomic hopping rate R, as

$$F = (a^d \tau_{ML})^{-1}, \quad D_s = a^2 R, \tag{5.5}$$

where a is the lattice constant, and d is the substrate dimension. The relevant number is then $R\tau_{ML}$. Note that D_s refers to the *tracer* diffusion of a single adatom on a perfect, flat surface without steps or islands; the *collective* diffusion constant, which determines the adatom mobility in the macroscopic theory, equation (3.11), can be significantly reduced relative to D_s [265].

For an order of magnitude estimate, consider a metal at room temperature (300 K) and a growth rate of one monolayer per minute. The conventional Arrhenius ansatz for the hopping rate reads

$$R = \omega_0 \exp(-E_S/k_B T), \tag{5.6}$$

with a vibrational attempt frequency $\omega_0 \approx 2k_B T/h = 3{\cdot}64 \times 10^{13}\ s^{-1}$ (here h denotes Planck's constant). Using a typical value of $E_S \approx 0{\cdot}5$ eV for the surface diffusion activation barrier, yields $R\tau_{ML} \approx 3 \times 10^6$. Thus, growth under MBE conditions must

be viewed as a competition between two opposing processes—disordering through deposition and smoothening through diffusion—that occur on *widely separated time scales*. The models described in this section are designed to deal with this situation, at least in principle (in practice computational resources limit the values of $R\tau_{\mathrm{ML}}$ that can actually be achieved [261]). Accordingly, their dynamics consists of two sets of rules—a deposition rule and a diffusion rule—that can be applied at widely different rates.

5.1.2.1. *Arrhenius dynamics.* The most popular model in this class is the Arrhenius model first introduced by Gilmer and Bennema [266] in 1972, and extensively used by Vvedensky and co-workers several years prior to the advent of ideal MBE in the kinetic roughening community [267–269] (see also [270] and references therein). These studies were concerned mainly with reproducing experimentally observed features of the early stages of growth, such as the characteristic oscillations in the reflection high-energy electron diffraction (RHEED) signal (see section 5.4.4).

The surface is modelled in the conventional solid-on-solid (SOS) fashion [128], its position being specified by a set of integer height variables $h_{\mathbf{x}}$ above the substrate ($\mathbf{x}$) lattice. Deposition occurs, at a rate F, by selecting a site $\mathbf{x}$ at random and letting $h_{\mathbf{x}} \rightarrow h_{\mathbf{x}} + 1$; more involved deposition schemes, in which the kinetic energy of the depositing atom allows it to search, in the spirit of the limited mobility models, for a highly coordinated site in the neighbourhood of the deposition site, have also been implemented [269, 272].

The modelling of the diffusion step adheres to the Arrhenius form (5.6) for the hopping rate with, however, an activation barrier that depends on the local bonding environment. The barrier is assumed to be of the form

$$E = E_{\mathrm{S}} + nE_{\mathrm{N}}, \tag{5.7}$$

where E_{S} is the barrier on a flat surface used in equation (5.6), and E_{N} is a bonding contribution multiplying the number n of in-plane (lateral) nearest neighbour bonds of the adatom that attempt to jump. It is important to point out that the lateral coordination number n is different from the coordination numbers k_i introduced in section 5.1.1, since it refers to an atom that is actually present on the surface, rather than to a 'virtual' atom about to be deposited. For clarity we give here the definition of n for a 1D surface, in analogy with equation (5.4):

$$n_i = \begin{cases} 0, & h_i > h_{i+1} \text{ and } h_i > h_{i-1}, \\ 1, & h_{i-1} < h_i \leq h_{i+1} \text{ or } h_{i-1} \geq h_i > h_{i+1}, \\ 2, & h_i \leq h_{i-1} \text{ and } h_i \leq h_{i+1} \end{cases} \tag{5.8}$$

(see figure 26). Since jumps of isolated adatoms ($n = 0$) constitute the fastest process in the problem, they define the time scale and are accepted with unit probability (note that this implies a considerable speed-up, by a factor of $\exp(E_{\mathrm{S}}/k_{\mathrm{B}}T)$, compared to a molecular dynamics simulation that operates at the attempt frequency ω_0 in equation (5.6)). Jumps of more highly coordinated atoms ($n > 0$) are executed with probability $\exp(-nE_{\mathrm{N}}/k_{\mathrm{B}}T)$. It should be emphasized that, within the SOS model, the topmost atom above *each* substrate site is a potentially mobile adatom; even fully coordinated surface atoms, which have $n = 2d$ on a d-dimensional surface, can move, albeit at a very small rate.

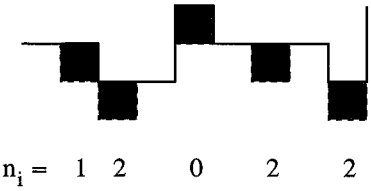

Figure 26. Definition of the coordination numbers (5.8). The surface configuration is identical to that in figure 24, but here the relevant environments are those of (shaded) surface atoms that attempt to hop.

When a jump occurs, the atom is removed ($h_{\mathbf{x}} \to h_{\mathbf{x}} - 1$) and placed at a *randomly* chosen nearest neighbour site **y** ($h_{\mathbf{y}} \to h_{\mathbf{y}} + 1$). At least in this basic, most commonly used version of the model, the jump rate is independent of the bonding environment at the final site; variants which abandon this simplifying (and, as we shall see, crucial) assumption have been considered recently [271–274]. Of particular interest are attempts to incorporate realistic barrier energies, obtained from semi-empirical potential calculations, into Arrhenius-type models [275]. A noteworthy feature of the *equilibrium* ($F = 0$) dynamics of the basic Arrhenius model is a simple relation between the collective diffusion coefficient and the tracer surface diffusion coefficient on a flat surface, namely, their ratio is $\exp(-dE_{\mathrm{N}}/k_{\mathrm{B}}T)$ for a d-dimensional surface [276].

5.1.2.2. *Detailed balance.* It was first suggested by Siegert and Plischke [89, 277] (see also [278]) that, as a minimal criterion in the choice of surface diffusion rules in MBE models, one should require the surface to relax into a reasonable thermodynamic equilibrium state when the beam is turned off. This would ensure that the observed non-equilibrium effects are really associated with the external particle flux, rather than being artifacts of the surface diffusion dynamics. A sufficient condition is that the jump rates satisfy detailed balance with respect to some short-ranged energy function $\mathscr{H}$. Explicitly, denoting by $R_{\mathbf{xy}}$ the jump rate from site **x** to a nearest-neighbour site **y**, the condition reads

$$R_{\mathbf{xy}}(H)/R_{\mathbf{yx}}(H^{\mathbf{xy}}) = \exp\{-[\mathscr{H}(H^{\mathbf{xy}}) - \mathscr{H}(H)]/k_{\mathrm{B}}T\}, \tag{5.9}$$

where H is a shorthand notation for a height configuration $\{h_{\mathbf{x}}\}$ and $H^{\mathbf{xy}}$ is the configuration obtained from H by moving an atom from **x** to **y**; for clarity, the dependence of the jump rates on the configuration has been indicated also.

Simple energy expressions for a solid-on-solid surface are the Hamiltonians

$$\mathscr{H}_q = K_q \sum_{\langle \mathbf{xy} \rangle} |h_{\mathbf{x}} - h_{\mathbf{y}}|^q, \tag{5.10}$$

the sum running over nearest-neighbour pairs. The case $q = 1$ is known as the standard SOS model, and $q = 2$ is the discrete Gaussian model [279]. It is easily checked that the basic Arrhenius rules for surface diffusion satisfy detailed balance with respect to the standard SOS model ($q = 1$), provided the bonding contribution to the activation barrier is set to $E_{\mathrm{N}} = 2K_1$ [276].

Of course, the requirement of detailed balance is fulfilled by a large variety of jump rates. Siegert and Plischke [89, 277] chose the 'Metropolis' function

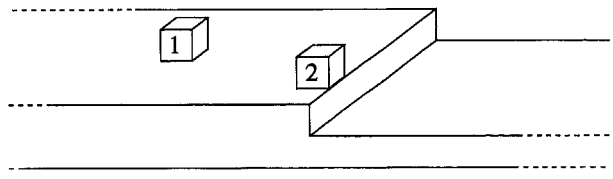

Figure 27. The excess step edge energy (5.12) is the enegy difference between atom 2 and atom 1.

$$R_{xy} = (1 + \exp\{[\mathscr{H}(H^{xy}) - \mathscr{H}(H)]/k_B T\})^{-1}, \tag{5.11}$$

and studied the effect of varying the power q in equation (5.10), with rather remarkable results (see section 5.2.2). One motivation for considering different values of q comes from the observation [280] that the Hamiltonian (5.10) mimics, for $q > 1$, the effect of *step edge barriers* (also referred to as *Schwoebel barriers* [281, 282]) which are known to exist on certain metal surfaces. Field-ion microscopy studies [283–285] show that atoms diffusing on a terrace can be reflected when attempting to jump down from the terrace edge. This is interpreted in terms of an increased energy barrier for inter-layer diffusion, due to the reduced bonding experienced by the atom at an edge position (the energy landscape is illustrated in figure 30).

To see that the Hamiltonian (5.10) incorporates this effect, consider adding an isolated adatom ($n = 0$) to a perfectly flat terrace (figure 27). From equation (5.10) the excess energy associated with the atom is $2dK_q$ in d dimensions. Now imagine moving the atom to the cliff edge of a straight, monatomic step. At such an edge site the energy of the atom is $(2d - 1)K_q + (2^q - 1)K_q$, since one of the neighbouring sites is now *two* lattice units lower, rather than one. Thus, the energy at a step edge is increased by an amount

$$\Delta\mathscr{H} = (2^q - 2)K_q > 0 \tag{5.12}$$

for $q > 1$. If the jump rates are sensitive to the energy at the final site (this is true, e.g. for the rates (5.11)), then a diffusing atom approaching a step from above is likely to be reflected, rather than being incorporated at the step. This effect is one of the main microscopic mechanisms that give rise to a nonequilibrium surface diffusion current [20] and will be discussed in detail in section 5.2.1.

In our opinion, the requirement of detailed balance for surface diffusion processes is a useful guiding principle that should be abandoned only if compelling reasons exist to do so; as we shall see below, matters are sufficiently complicated even without artifacts arising from ill-chosen diffusion dynamics. Nevertheless, a number of investigations of collective diffusion models of MBE have been carried out in which surface diffusion is governed by energetic considerations, but detailed balance is *not* (or only approximately) fulfilled. For example, in some studies of the Arrhenius model the slowest processes, involving the motion of atoms with $n = 2$ in $d = 1$, are completely suppressed for numerical convenience [132, 133]; this clearly violates detailed balance, though the effects may be small at low temperatures. Phillips and Chrzan [280] proposed a model of crystal growth (in the presence of desorption) in which surface diffusion is governed by the Gaussian Hamiltonian, $q = 2$, but the system is updated *in parallel*, in violation of detailed balance [278]. Finally, in some recent papers [257, 286], Arrhenius-type dynamics is supplemented

with an additional rule that prevents atoms from jumping up, a further source for possibly artificial, non-detailed balance behaviour.

5.1.3. *Beyond the solid-on-solid approximation*

All models described so far are of the SOS type, wherein the crystal is viewed as an array of columns of heights h_x above the substrate lattice. The SOS restriction is quite natural in the context of ideal MBE, since it prevents, by construction, the formation of bulk defects. Nevertheless, it has been criticized as becoming unphysical in the presence of high surface steps [287, 288]. Indeed, since atoms move laterally, from the top of one column to another, irrespective of the height difference involved, the *vertical* motion is effectively instantaneous, as the time required for diffusion does not depend on the distance *along* the surface. This is hardly a problem for collective diffusion on 2D surfaces, especially for realistically large value of $R\tau_{\mathrm{ML}}$, since high steps are exceedingly rare in that case; but the criticism is clearly relevant in one dimension, where fluctuation effects can create large local height gradients, especially in the limited mobility models. Furthermore, it is of some interest to understand the crossover from ideal MBE to (presumably) KPZ scaling once overhangs are allowed to form through 'vertical' diffusion.

Deposition models which include both surface diffusion and defect formation have long been considered in the optical thin film community [289] as well as in the detailed microscopic modelling of semiconductor MBE [290, 291]; however, in these works the emphasis was not on obtaining information about the statistical properties of the surface. The interplay between bulk defects and surface roughening was addressed by Pellegrini and Jullien [292], who investigated a model which combines Family's downward diffusion rule [127] (see section 3.4) with standard ballistic deposition [26], in an attempt to elucidate the strong coupling phase transition of the KPZ equation. Because of the significant computational demands, models which treat surface diffusion in a realistic and isotropic manner have been introduced only recently.

Yan [287] studied two models on the square lattice ($d = 1$) which are essentially isotropic variants of the limited mobility models of section 5.1.1. Deposition occurs either in the manner of ballistic deposition (sticking at the first empty site with an occupied nearest neighbour; see section 2.1), or as in the SOS models (deposition onto the topmost atom in a lattice column). The freshly deposited atom then performs a number of random walk steps along the arclength of the surface, vertically or horizontally. The atom is trapped permanently at sites with two or more nearest neighbours, or else it stops walking when the number of steps has reached a prescribed threshold L_{RW}. For both kinds of deposition rules a rather gradual crossover from an early time regime, possibly described by the noisy Mullins equation (see section 3.2), to KPZ-type scaling was observed, and it was confirmed that the deposit acquires a finite density of defects $1 - \rho$ which approaches zero upon increasing L_{RW}.

The model of Kessler, Levine and Sander [288] is closer in spirit to the collective diffusion models of section 5.1.2, in the sense that any atom that is not fully coordinated may move, even if it was not recently deposited. A move occurs if a more highly coordinated site can be found within a box of length and height $2L_{\mathrm{D}} + 1$, where the 'diffusion length' L_{D} is to be roughly identified with $\sqrt{L_{\mathrm{RW}}}$ in Yan's model. The model was studied on the square lattice, with a 'ballistic' deposition rule (see above). In this case the crossover from an early time regime,

apparently characterized by Edwards–Wilkinson scaling (see section 3.2), to the KPZ regime is observed to be rather violent, with a rapid intermediate increase of the width attributed to the sudden proliferation of bulk defects.

A similar scenario was found by Das Sarma, Lanczycki, Ghaisas and Kim [293] in simulations on both 2D and 3D lattices ($d = 1$ and 2) with the 'ballistic' deposition rule. These authors employed an Arrhenius-type collective diffusion model in which the activation barrier is proportional to the *total* number of (horizontal and vertical) nearest neighbours of the atom. If the hopping attempt is accepted, the atom is moved to a randomly chosen nearest- or next-nearest-neighbour site, provided the landing site is at the surface, i.e. it possesses at least one occupied nearest neighbour. It should be noted that this rule includes the possibility of the deposit becoming disconnected—for example, if part of the deposit is connected to the rest only through a single, doubly coordinated atom which hops away; auxiliary rules have to be introduced to suppress such moves. The simulations show an early time 'epitaxial' regime consistent with Edwards–Wilkinson scaling ($W \sim t^{1/4}$ in $d = 1$ and $W \sim \mathcal{O}(\log t)$ in $d = 2$), followed by a rapid increase of the width and a final power-law regime, which is clearly resolved (and consistent with KPZ behaviour) only at low temperatures, in $d = 1$. The crossover time (or thickness) at which epitaxial growth breaks down shows the expected, activated temperature dependence. By monitoring the deposit density, Das Sarma *et al.* verified that the crossover is associated with the onset of bulk defect formation. The defect density is rather small in the square lattice simulations, about 1% at 700 K, but the 3D cubic lattice deposits turn out to be extremely porous, with a saturation defect density of about 2/3 which, moreover, appears to be temperature independent.

Schimschak and Krug [262] recently carried out a detailed study of the defect-induced crossover to KPZ scaling in which both the pre-asymptotic 'epitaxial' regime, and the KPZ regime were clearly resolved, and the available information about the universal KPZ amplitudes was exploited. The model was defined on the square lattice, and the rules were chosen as a compromise between realism and tractability. First, to avoid defect formation already in the deposition stage, an SOS deposition rule was used in which particles slide down lattice columns until they reach the topmost occupied site (cf. [287]); physically this can be viewed as a consequence of downward funnelling [99]. Second, a collective diffusion rule in the spirit of Das Sarma *et al.* [293] was employed, with diffusion limited, however, to singly coordinated atoms, in order to ensure the connectivity of the deposit; in this sense the model is the low temperature limit of that of Das Sarma *et al.* [293]. Diffusion proceeds along the arclength of the surface, and hops to nearest- and next-nearest-neighbour sites (from the point of view of the square lattice) occur at equal probability; the inclusion of step edge barriers which suppress 'around the corner' jumps to next-nearest-neighbour sites is straightforward.

The control parameter in the model is the ratio $R\tau_{\mathrm{ML}}$ of the hopping rate to the deposition rate. A typical deposit grown at $R\tau_{\mathrm{ML}} = 200$ is shown in figure 28. The most striking feature is the appearance of vertical void chains that seem to originate from deep narrow grooves in the surface; at least in this regime of rather high-quality epitaxial growth (the deposit density is about 0·98), the bulk defects are seen to be *induced by surface fluctuations*. The surface grooves themselves are reminiscent of structures found in the 1D limited mobility models (compare to figure 25). Indeed, the analysis of spatial and temporal correlation functions reveals that the surface

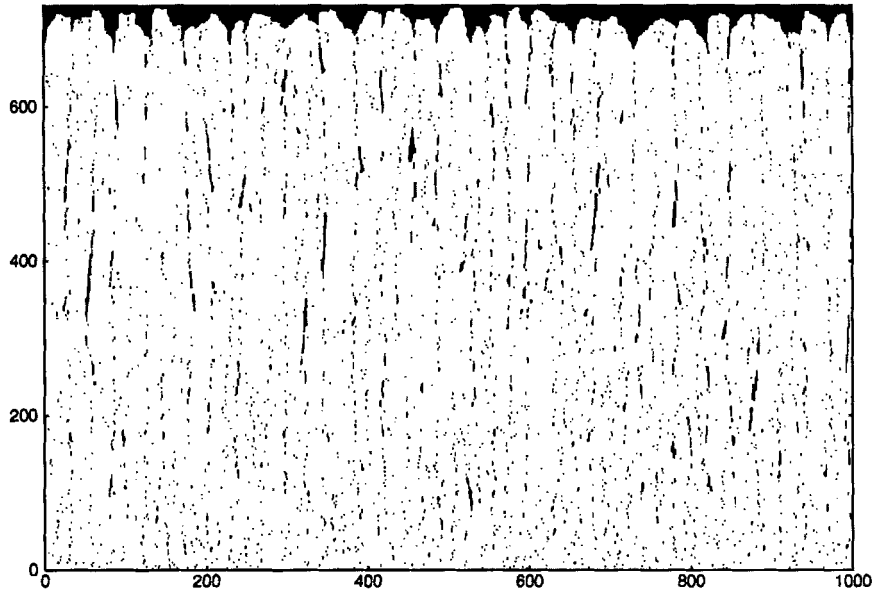

Figure 28. Two-dimensional deposit grown with a rule that allows for the formation of defects through isotropic surface diffusion [262].

fluctuations on short length and time scales (up to about 50 lattice spacings and 1000 monolayers) are virtually identical to those found in the limited mobility models of Wolf and Villain [101] and Das Sarma and Tamborenea [132], *including* the anomalous scaling of the height difference correlation function [107, 108, 112] (see also sections 3.2.3 and 5.5.2).

The crossover to KPZ scaling that occurs on larger scales is illustrated in figure 29. While the scaling range available for determining the asymptotic exponents is quite limited, KPZ universality can be unambiguously identified by including the prefactors into the analysis. As was described in section 4.2, the relevant numbers are D/ν, which can be extracted, via equation (3.39), from the stationary surface width shown in the inset of figure 29, and λ, which is obtained from a measurement of the tilt dependence of the deposit density (compare to equations (4.3) and (5.1)). The prediction for the KPZ asymptotics resulting from equation (4.15) is plotted in figure 29; it is interesting to note that, in contrast to the crossover from Edwards–Wilkinson scaling (figure 16), here the asymptote is approached from below.

5.2. *Non-equilibrium surface currents*

As was noted in the preliminary discussion of non-equilibrium effects in section 3.1, the central importance of the non-equilibrium surface current (3.14) lies in the fact that it changes the surface dynamics already on the level of the *linearized* equation of motion, and hence ultimately decides the stability of the surface. Possible mechanisms for generating an 'Edwards–Wilkinson' (EW) term $\nu\nabla^2 h$ under MBE conditions were discussed by Wolf and Villain [101] in their pioneering paper; numerical evidence for the presence of such a term was reported by Kessler *et al.* [288] and by Kessler and Orr [294], but its origin remained unclear. The thoughtful study of Villain [20] focused attention on the role of step edge barriers (termed

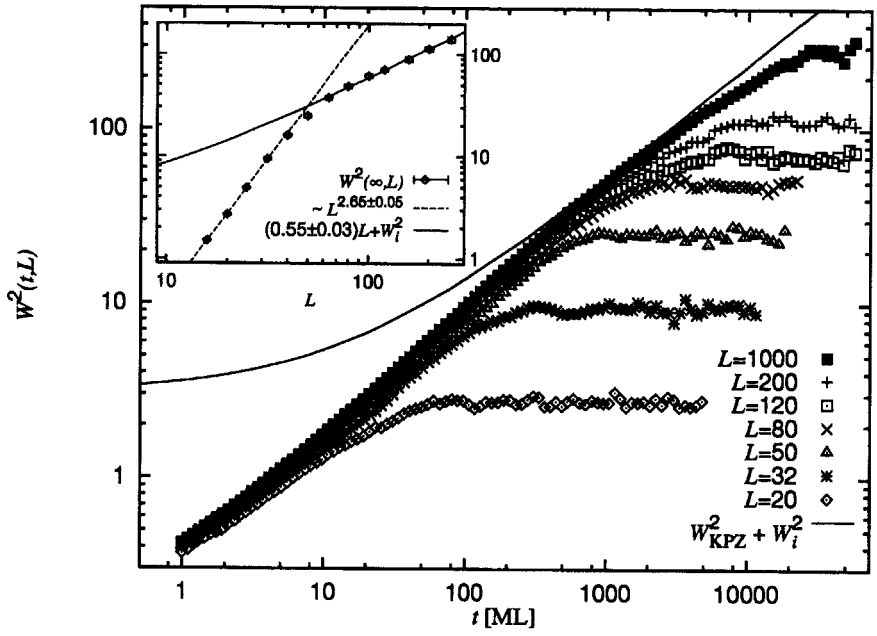

Figure 29. Surface width W as a function of the number of monolayers t for system sizes $L = 20 - 1000$. The ratio of hopping rate to deposition rate is $R_{\mathrm{ML}} = 200$. The full curve is the KPZ prediction (4.15), evaluated with the numerically determined KPZ parameters $D/2\nu = 6{\cdot}6 \pm 0{\cdot}4$ and $\lambda = 0{\cdot}0314 \pm 0{\cdot}0006$, and corrected for the intrinsic width W_i. The inset shows the stationary ($t \to \infty$) width as a function of system size. The broken line corresponds to a roughness exponent $\zeta \approx 1{\cdot}3$; the slope of the full line has been used to determine $D/2\nu$ according to equation (3.39) [262].

'diffusion bias' by Villain) in producing an EW term with a coefficient that could be either stabilizing ($\nu > 0$) or destabilizing ($\nu < 0$); unknowingly Villain rediscovered the results of Schwoebel [281, 282], who had investigated the effects of step edge barriers in the framework of a step dynamical model (see section 5.2.1).

Subsequently, Krug, Plischke and Siegert [92] offered a somewhat different point of view by proposing that inclination-dependent surface currents with an expansion (3.14) should be regarded as a *generic* consequence of the non-equilibrium conditions of MBE growth. The core of the argument can be phrased as follows: On a vicinal surface the in-plane direction of the miscut induces an asymmetry in the statistics of local bonding environments; for example, the density of up steps differs from that of down steps. Generically, an adatom moving on the surface will be influenced by the asymmetry, and consequently acquire a systematic drift along the direction of the miscut, *unless* some constraint is present which prevents the asymmetric bonding environments from being reflected in the hopping rates. In equilibrium, such a constraint is always present in the form of detailed balance. However, once detailed balance is broken by the presence of a deposition flux, or some other external influence, the drift of the particles adds up to a systematic mass current directed either 'uphill' or 'downhill'. The step edge barrier arguments of Schwoebel and Villain focus on one particular set of bonding environments; however, it is clear that many other configurations potentially play a role in determining the overall current. This implies, in particular, that non-equilibrium surface currents can appear also on

surfaces where the simplest kind of step edge barrier [283, 284] is absent or undetectably weak.

An analogy may be useful in clarifying the spirit of this argument. There has been much recent interest in the Brownian motion of particles in 1D, periodic, 'ratchet'-like potentials ([295] and references therein). According to a famous remark of Feynman, the left–right asymmetry of the potential is unable to induce a drift in the particle motion *provided* the stochastic dynamics satisfies the fluctuation–dissipation relation of thermal equilibrium. On the other hand, fluctuations that are of non-equilibrium origin, modelled, for example, by a 'coloured' noise term in the Langevin equation, do generically produce a systematic motion of the particle, even if the fluctuations themselves are symmetric [296, 297]. While the magnitude of the induced current is of the order of the correlation time of the noise, as would be expected, the *sign* of the drift results from an interplay between the shape of the potential and the detailed noise statistics, in a way not easily accessible to intuitive reasoning. It is our contention that the non-equilibrium surface currents in MBE growth can be viewed as a similar, though more complex phenomenon. Indeed, rather than dealing with a single particle in an external potential, we are confronted with the *collective* diffusion of adatoms on a surface whose structure is determined by the moving atoms themselves [276].

Krug *et al.* [92] corroborated their hypothesis by numerically measuring the surface current as a function of misorientation, for MBE models of the 'collective diffusion' and the 'limited mobility' varieties, as well as for models of nonequilibrium surface diffusion *without* growth, in which detailed balance is broken by a suitable choice of hopping rates [250]. Here, we focus on the (rather limited) *analytic* understanding of these effects. Three types of analytic results have been obtained so far. First, in section 5.2.1 the growth-induced surface current is calculated for the classic step dynamical model of crystal growth at vicinal orientations [88, 233]. This model is intermediate between continuum theories (as introduced in section 3.1) and atomistic models, in the sense that certain microscopic structures (steps) are retained, but deposition and surface diffusion are described in terms of a continuous adatom density. While the neglect of fluctuation and nucleation effects leads to some artificial features, the results are useful for the order-of-magnitude comparison with experiments that will be attempted in section 5.3. Second, for some of the models described in section 5.1, hidden symmetries can be identified that force the non-equilibrium current to be zero, despite the absence of detailed balance in the conventional sense; these 'negative' results are summarized in section 5.2.2. Third, in section 5.2.3 an approximate, microscopic calculation of the current is presented for the 1D limited mobility models introduced in section 5.1.1. In these models only a few local configurations contribute to the current, the statistical weights of which can be reasonably estimated.

5.2.1. *Burton–Cabrera–Frank theory with step edge barriers*

The classic BCF theory [233] (here we follow the presentation of Ghez and Iyer [88]) considers a vicinal surface consisting of perfectly straight steps at a fixed spacing l. The (effectively 1D) geometry, and the basic processes are indicated in figure 30. Particles impinge on the surface at a flux F, diffuse on the terraces with a diffusion constant D_s, and incorporate into the crystal at the steps; the presence of step edge barriers is modelled through the rates $r_\pm$ at which atoms coming from the

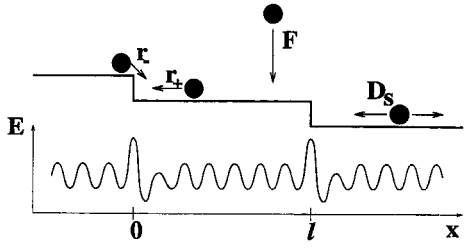

Figure 30. Schematic of a vicinal surface according to Burton, Cabrera and Frank [233]. The underlying adatom energy landscape is also indicated.

lower (r_+) and the upper (r_-) terrace are incorporated; the conventional behaviour corresponds to $r_+ > r_-$ [281, 282]. As usual in ideal MBE, desorption is neglected.

We adopt the quasistatic approximation, assuming that the adatom population on the terrace equilibrates on a time scale that is fast compared to the step motion; the consistency of this approximation will be addressed shortly. The adatom density $n(x)$ on the terrace (more precisely, the deviation of the density from its equilibrium value) then satisfies, in steady state, the stationary diffusion equation ($n'(x) = \mathrm{d}n/\mathrm{d}x$, $n''(x) = \mathrm{d}^2n/\mathrm{d}x^2$)

$$D_s n'' + F = 0, \tag{5.13}$$

with the incorporation boundary conditions [88]

$$D_s n'(0) = r_+ n(0), \quad D_s n'(l) = -r_- n(l). \tag{5.14}$$

The resulting parabolic density profile is easily written down. For later reference we note that the density scale is

$$n_0 = Fl^2/D_s, \tag{5.15}$$

as could be guessed from dimensional considerations.

Here we are mainly interested in the surface current, which is obtained by averaging the local diffusion current $j = -D_s n'$ over the terrace. This yields

$$J = (D_s/l)[n(0) - n(l)] = J_\infty \left(\frac{l_- - l_+}{l + l_- + l_+} \right), \tag{5.16}$$

where the length scales

$$l_\pm = D_s/r_\pm \tag{5.17}$$

have been introduced, and

$$J_\infty = -\tfrac{1}{2} Fl \tag{5.18}$$

refers to the maximal current that results when mass transport between layers is completely inhibited, $r_- = 0$; equation (5.18) was previously derived by Villain [20]. Under normal conditions ($r_+ > r_-$) the current is negative because particles preferentially attach at the left, in the *uphill* direction (figure 30).

For an estimate of the length scales $l_\pm$ we write, in analogy to equation (5.6),

$$r_\pm = \omega_0 a \exp(-E_\pm/k_B T), \tag{5.19}$$

with $E_\pm$ denoting the energy barriers that have to be overcome to attach to the step (compare to figure 30). Together with the expressions (5.5) and (5.6) for D_s, this implies

$$l_\pm = a \exp(\Delta E_\pm / k_B T), \tag{5.20}$$

where $\Delta E_\pm = E_\pm - E_S$. Since attachment from below the step is usually expected to be facilitated (this need not be true in the presence of surfactants; see [298]), $\Delta E_+ < 0$; consequently l_+ is at most of the order of the lattice constant, and can be neglected relative to l and l_- in equation (5.16). In contrast, l_- can be significantly larger than a; for example, using the experimental estimate $\Delta E_- \approx 0{\cdot}2$ eV for tungsten [284], one obtains $l_-/a \approx 2300$ at room temperature. The meaning of the incorporation length l_- is clarified by considering the probability p_+ (p_-) that a deposited atom will be incorporated at the upward (downward) step. Since the total flux impinging onto the terrace is Fl, we have (neglecting l_+)

$$p_+ = \frac{D_s n'(0)}{Fl} \approx \frac{1/2 + l_-/l}{1 + l_-/l}, \quad p_- = 1 - p_+. \tag{5.21}$$

Hence incorporation becomes symmetric, $p_+ \approx p_-$, for terraces much wider than l_-. In the same approximation ($l_+ \to 0$),

$$J \approx J_\infty (1 + l/l_-)^{-1}, \tag{5.22}$$

illustrating the reduction of the current relative to J_∞ due to the finite interlayer transport.

5.2.1.1. *Island nucleation.* In figure 31 the current (5.22) is plotted as a function of the surface inclination $\nabla h = -a/l$. The current is discontinuous at the high

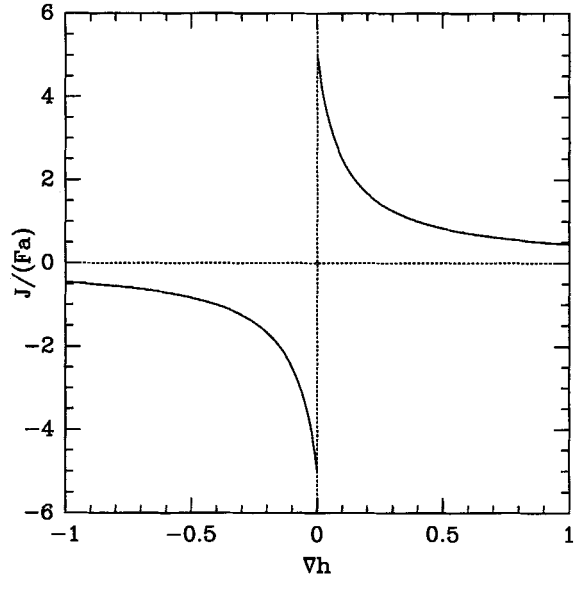

Figure 31. Growth-induced current (5.22) computed from the BCF theory without nucleation. The incorporation length is $l_-/a = 10$.

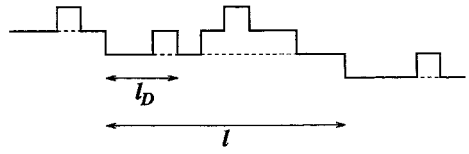

Figure 32. Schematic of a vicinal surface in the nucleation dominated regime, $l > l_D$. The broken line indicates the original surface prior to growth.

symmetry orientation $\nabla h = 0$, because equation (5.22) has a finite limit $-Fl_-/2$ for $l \to \infty$. This is of course an artifact of not allowing for the nucleation of islands on the terraces, a process that becomes important when the terrace width l exceeds the *diffusion length* l_D which characterizes the typical island size on the singular ($\nabla h = 0$) surface. Rate equation arguments [299] show that l_D is typically given by a relation of the form

$$l_D \sim (D_s/F)^\gamma, \tag{5.23}$$

where the exponent γ depends on the size of the smallest stable island, the fractal dimensionality of islands, etc. In the simplest case of stable dimers and compact islands, one finds $\gamma = 1/(2d+2)$ for a d-dimensional surface.

Heuristically, the effect of island nucleation can be treated as follows [20, 300]. When $l \gg l_D$, the surface morphology more closely resembles figure 32 than figure 30. Rather than a well-ordered step train, one has to consider a disordered array of steps of both signs, with a small fraction l_D/l of excess (down) steps representing the overall vicinality of the surface. Only the excess steps contribute to the current, and the contribution of each is given by equation (5.22) evaluated at $l = l_D$. Thus the current vanishes for $l \to \infty$, as required by symmetry. Specifically, $J \approx \nu_1(a/l) = -\nu_1 \nabla h$ as in equation (3.14), with a coefficient

$$\nu_1 \approx \begin{cases} -Fl_D^2/a, & l_- \gg l_D, \\ -F(l_D l_-)/a, & l_- \ll l_D. \end{cases} \tag{5.24}$$

Myers-Beaghton and Vvedensky [301, 302] have proposed to include island nucleation in the BCF theory through a quadratic pair-formation term in the balance equation (5.13). In the following we show that this extended BCF theory, supplemented with the boundary conditions (5.14), reproduces the behaviour of the current expected on heuristic grounds. At high adatom densities, where nucleation becomes significant, one may also expect the steps to move sufficiently fast to invalidate the quasi-static approximation [88]. Thus, the stationarity condition replacing (5.13) reads, in a frame moving with the step velocity c [301],

$$D_s n'' + cn' + F = ma^2 Fn + r_2 D_s n^2. \tag{5.25}$$

The first loss term on the right hand side accounts for events in which an atom is deposited next to an adatom (m is the number of nearest-neighbour sites of the adatom and ma^2 is the corresponding capture area), while the second term describes loss of adatoms due to dimer formation, which occurs with probability r_2. In the absence of desorption the step velocity is $c = l/\tau_{ML} = a^2 Fl$ by mass balance (compare to equation (5.5)).

The significance of the various terms in equation (5.25) can be assessed by going over to scaled quantities, $n(x) = n_0 \rho(x/l)$, with the BCF density scale (5.15). This results in

$$\rho'' + (l/l_0)^2 \rho' + 1 = m(l/l_0)^2 \rho + (l/l_D)^4 \rho^2, \tag{5.26}$$

where the length scales

$$l_0 = (D_s/Fa^2)^{1/2} = (D_s \tau_{ML})^{1/2}, \quad l_D = (D_s/Fr_2)^{1/4} \tag{5.27}$$

have been introduced. The length l_0 is the distance covered by a freely diffusing adatom during the monolayer completion time, while l_D can be identified with the diffusion length introduced above. The value $\gamma = 1/4$ for the exponent in equation (5.23) results because the dominant nucleation effect has been assumed to be the formation of dimers; in fact it is much more likely that an adatom is captured by a pre-existing island, which would give $\gamma = 1/6$ [304]. This effect could be included by writing a separate equation for the island density [301–303].

For the purpose of the present discussion, the main point is that $l_D \ll l_0$ for $R\tau_{ML} \gg 1$. Thus, as l is increased away from the step flow regime (where island nucleation is negligible), the first appreciable correction is due to the pairwise nucleation term, and both the convection term cn' and the deposition term ma^2Fn in equation (5.25) can be neglected. Keeping the relevant terms, we rewrite equation (5.25) as

$$n'' = -F/D_s + r_2 n^2 = -V'(n) \tag{5.28}$$

to emphasize the analogy with a Newtonian particle of unit mass, moving in a cubic potential $V(n) = (F/D_s)n - (r_2/3)n^3$. This analogy is very useful in extracting the behaviour of the density profile in the limit $l \to \infty$. Since l is the total travel time of the particle, for $l \to \infty$ it has to spend most of its time close to the unstable equilibrium position $n_1 > 0$ where $V'(n_1) = 0$. Thus, the adatom density on the terrace approaches, for $l \to \infty$, the value

$$n_1 = (F/D_s r_2)^{1/2} = Fl_D^2/D_s, \tag{5.29}$$

which is, not surprisingly, of the same form as equation (5.15). The boundary values $n(0)$ and $n(l)$ that determine the current (5.16) can now be obtained from the law of energy conservation for the particle problem (5.28), which states that the quantity

$$E(x) = [n'(x)]^2/2 + V(n(x)) \tag{5.30}$$

is independent of x. Indeed, since the particle is almost at rest (the density profile is almost constant) close to n_1, for $l \to \infty$ the energy converges to $E = V(n_1)$. Using the boundary conditions (5.14), the boundary densities are then given by two uncoupled cubic equations:

$$[n(0)/l_+]^2/2 + V(n(0)) = [n(l)/l_-]^2/2 + V(n(l)) = V(n_1). \tag{5.31}$$

We now specialize to the case where attachment to the step from below is rapid, so that $l_+ = 0$ and $n(0) = 0$ is ensured. The current (5.16) is then simply $J = -(D_s/l)n(l)$. Writing $n(l) = \mu n_1$, the dimensionless coefficient μ satisfies

$$(l_D/l_-)^2 \mu^2/2 + \mu - \mu^3/3 - 2/3 = 0, \tag{5.32}$$

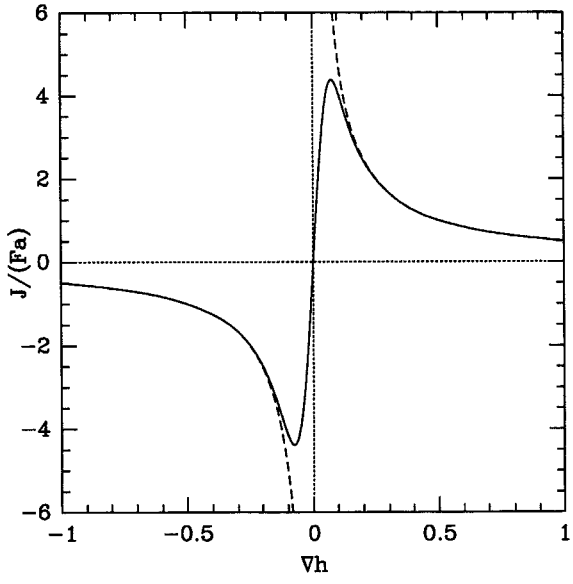

Figure 33. Growth-induced current in the presence of island nucleation, for $l_- = \infty$ and $l_D/a = 10$. The full curve shows the lower bound (5.34), and the broken curve shows the current (5.18) obtained in the absence of nucleation.

which implies that $\mu \approx 1$ for $l_D \ll l_-$, and $\mu \approx (2/\sqrt{3})l_-/l_D$ for $l_D \gg l_-$. As expected, the current vanishes linearly in $\nabla h = -a/l$, and the coefficient is given by

$$\nu_1 = \begin{cases} -Fl_D^2/a, & l_- \gg l_D, \\ -(2/\sqrt{3})F(l_D l_-)/a, & l_- \ll l_D, \end{cases} \tag{5.33}$$

in accordance with equation (5.24).

To obtain the full inclination dependence of the current, one would require the solution of the mechanical problem (5.28) for arbitrary l, which is not available in closed form. For the case of perfect step edge barriers ($r_- = 0$, $r_+ = \infty$), the lower bound

$$J \geq J_b = 2J_\infty (l_D/l)^4 \{[1 + (l/l_D)^4]^{1/2} - 1\} \tag{5.34}$$

can be derived, which reproduces the exact asymptotics for $l \ll l_D$ and $l \gg l_D$; an upper bound is given in [123]. The expression (5.34) is shown in figure 33, together with the current (5.18) obtained in the absence of nucleation. A similar, heuristic interpolation formula was proposed by Johnson *et al.* [274].

5.2.1.2. *Stability and metastability.* Irrespective of its derivation, the bound (5.34) is representative of the generic form of the inclination-dependent surface current induced by step edge barriers, and can be used to discuss the stability of the growing surface. We consider the physical dimensionality $d = 2$, and assume in-plane isotropy. The non-equilibrium contribution to the surface current **J** in equation (5.3) can then be written as [92]

$$\mathbf{J}_{NE} = \phi(|\nabla h|^2)\nabla h, \tag{5.35}$$

where the function ϕ corresponding to (5.34) is

$$\phi(u^2) = F(l_D^2/a)\{[ul_D/a)^4 + 1]^{1/2} - (ul_D/a)^2\}. \tag{5.36}$$

The important (and generic) features of (5.36) are that $\phi \approx -\nu_1$ for $u \ll a/l_D$ and $\phi \approx Fa/2u^2$ for $u \gg a/l_D$.

We now insert (5.35) into (5.3) and expand the equation of motion about a growing surface uniformly tilted in the x direction:

$$h(x, y, t) = ux + Ft + \epsilon(x, y, t). \tag{5.37}$$

We disregard for the moment the fourth-order derivatives due to the equilibrium part of the current, since they do not affect the stability with respect to long wavelength fluctuations (see section 5.3.2). This results in

$$\frac{\partial \epsilon}{\partial t} = \nu_{\parallel} \frac{\partial^2 \epsilon}{\partial x^2} + \nu_{\perp} \frac{\partial^2 \epsilon}{\partial y^2}, \tag{5.38}$$

with

$$\begin{aligned} \nu_{\parallel} &= -[\phi(u^2) + 2u^2 \phi'(u^2)], \\ \nu_{\perp} &= -\phi(u^2). \end{aligned} \tag{5.39}$$

The stability coefficient in the tilt direction can be written in terms of the BCF current function $J(l)$ as

$$\nu_{\parallel} = -(l^2/a)\, \mathrm{d}J/\mathrm{d}l, \tag{5.40}$$

which changes sign at $l \approx l_D$. Thus, as was pointed out by Schwoebel and Shipsey [281, 282] and others [305, 306], the step edge barriers *stabilize* the surface in the step flow regime, $l < l_D$, but the same effect acts to *destabilize* it once island nucleation becomes appreciable for $l > l_D$ [20]. However, even in the step flow regime the surface is not completely stable, because the transverse coefficient $\nu_{\perp} < 0$ for all u [307].

The transverse instability is related to the meandering instability of terrace edges discussed by Bales and Zangwill [308] (see also [186, 187]). In the context of the present continuum theory, a terrace edge is simply a height contour line in the x–y plane. In the regime of step flow growth treated by Bales and Zangwill, the surface is stable in the tilt direction, $\nu_{\parallel} > 0$. It is then reasonable to consider perturbations that vary only in the transverse direction, $\epsilon = \epsilon(y, t)$ in equation (5.37). Defining the position of the $h = Ft$ contour line by the relation $x = \chi(y, t)$, we see from equation (5.37) that $\chi = -\epsilon/u$ and χ evolves according to

$$\frac{\partial \chi}{\partial t} = \nu_{\perp} \frac{\partial^2 \chi}{\partial y^2}. \tag{5.41}$$

For a quantitative comparison with [308], consider the case of absolute step edge barriers ($r_- = 0$, $r_+ = \infty$), where $\nu_{\perp} = (l/a)J_{\infty}$. The growth rate for a transverse modulation of wavenumber q is then equal to $(1/2)(Fl^2/a)q^2$, which coincides with the appropriate limit (no desorption, $ql \ll 1$) of the expression derived by Bales and Zangwill [308].

The converse scenario of transverse stability ($\nu_{\perp} > 0$) and longitudinal instability ($\nu_{\parallel} < 0$) is possible if adatoms preferentially approach the step from *above* ('reverse' Schwoebel effect). Due to the strongly anisotropic surface diffusion rates on the

dimer-reconstructed terraces, this case is approximately realized on vicinal Si(001) [309].

We conclude that truly stable growth requires that (i) the current is a decreasing function of inclination, so that $\nu_{\parallel} > 0$, and (ii) the current is in the downhill direction, $\phi \leq 0$, to ensure that $\nu_{\perp} > 0$ also. Within the BCF theory the latter condition can be met only by assuming 'reversed' step edge barriers with $r_+ < r_-$ (this may be possible in the presence of surfactants [298]), while the former requires the surface to be in the nucleation-dominated regime, $l > l_D$. On the other hand, the BCF theory is expected to apply only to orientations vicinal to a high symmetry direction, and it is quite conceivable that a more refined treatment will reveal additional features of the current, such as zeros related to other crystallographic symmetries [92] or 'hot atom' effects [99, 273, 300], which favour stable growth.

Since the transverse destabilization is absent for 1D surfaces, one may hope that the stable step-flow regime envisioned by Schwoebel may be realizable at least in 1D stochastic growth models. This conclusion appears to be invalidated by the second important feature, apart from the transverse step fluctuations, that is left out by the BCF theory, namely the shot noise in the deposition flux. Krug and Schimschak [123] have carried out simulations of a 1D SOS model that incorporate the basic processes of the extended BCF theory described above—deposition at rate F, diffusion of singly bonded adatoms, and the formation of immobile islands when two adatoms meet (a related model, however, without shot noise, has been studied by Elkinani and Villain [310]). The step edge barriers are assumed to be absolute ($r_- = 0$) so that mass transport between layers is completely inhibited. For the singular orientation, $\nabla h = 0$, this is well known to give rise to a Poisson distribution of layer coverages, and a width that increases diffusively,

$$W^2 = Ft, \tag{5.42}$$

with no saturation even on a finite substrate [311]. On vicinal surfaces, for large values of $R\tau_{\mathrm{ML}}$ (typically $R\tau_{\mathrm{ML}} = 5 \times 10^5$), step flow behaviour is observed that conforms to the predictions of BCF theory for the current (equation (5.18)), as well as for the fluctuations, described by the Edwards–Wilkinson equation with $\nu = \nu_{\parallel} > 0$ (see section 3.2). However, the step flow regime is *metastable* and terminates at a transition time t_c (measured in units of τ_{ML}) that scales as

$$t_c \sim u^2 (R\tau_{\mathrm{ML}})^{3/4} \tag{5.43}$$

with the surface inclination u and the diffusion rate. The transition proceeds through the nucleation of a large fluctuation in the local orientation that brings the surface into the regime where $\nu_{\parallel} < 0$ (figure 34). For times $t \gg t_c$ the surface configurations resemble the strongly disordered morphology obtained on a flat substrate ($u = 0$), and the width asymptotically approaches the maximal 'Poisson' randomness given by equation (5.42). It is interesting to note that W^2 increases *faster* than linearly with t, as $W^2 \sim t^2$, in the transition region (figure 35). Step flow growth is stable only in the limiting case $R\tau_{\mathrm{ML}} = \infty$, which can be solved exactly [123].

5.2.2. *Symmetry arguments*

In this section we return to the microscopic level, and begin by formulating a precise microscopic definition of the nonequilibrium surface current for SOS models.

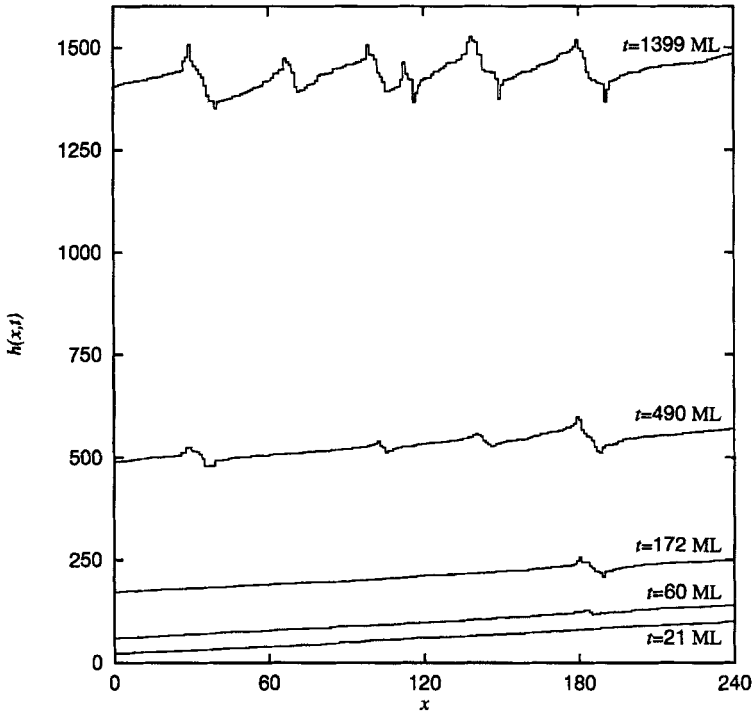

Figure 34. Evolution of a 1D vicinal surface ($l/a = 3$) in the presence of absolute step edge barriers. The ratio of hopping to deposition rate is $R\tau_{\mathrm{ML}} = 5 \times 10^5$. Note the nucleation of an unstable region after 60 monolayers, and the development of an approximately periodic pattern at late times [123].

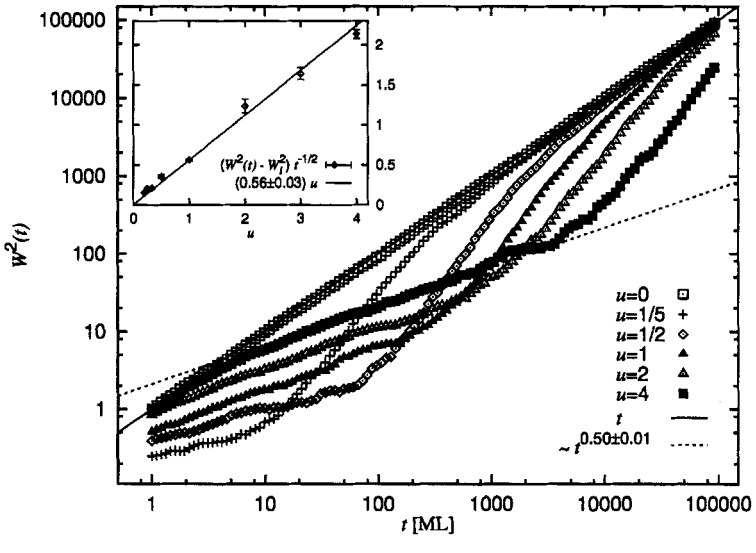

Figure 35. Time evolution of the surface width for various values of $u = -a/l$, at $R\tau_{\mathrm{ML}} = 5 \times 10^5$. Initially $W^2 \sim t^{1/2}$ with a prefactor that is correctly predicted by the EW equation (inset). After the nucleation of unstable regions (figure 34) W^2 increases faster than linearly in order to catch up with the Poisson behaviour (5.42) [123].

To unburden the notation we focus on a 1D surface described by discrete height variables h_i, $i = 1, \ldots, L$. The average heights then evolve according to

$$\frac{\mathrm{d}}{\mathrm{d}t}\langle h_i \rangle + \langle J_i - J_{i-1} \rangle = F, \tag{5.44}$$

the discrete analogue of equation (5.3), where the current is given in terms of the jump rates R_{ij} between neighbouring sites, $j = i \pm 1$, as

$$J_i = R_{ii+1} - R_{i+1i}. \tag{5.45}$$

The inclination-dependent current of the macroscopic description is obtained by averaging equation (5.45) with respect to the stationary probability distribution of height configurations of *fixed average tilt* $u = \langle h_{i+1} - h_i \rangle$, imposed, for example, through helical boundary conditions

$$h_{i+L} = h_i + uL. \tag{5.46}$$

Thus we would like to evaluate the expectation

$$J(u) = \langle R_{ii+1} - R_{i+1i} \rangle_u. \tag{5.47}$$

Numerically, this is done simply by keeping track of the cumulative number of jumps executed to the right and to the left [92]. Note that the vertical displacements of the atoms—whether their *actual* height is increased or decreased by a jump—plays no role in determining the current (this is of course not true in non-SOS models with isotropic diffusion [262]). Therefore, in the following we shall use the terms 'uphill' and 'downhill' motion to imply moves in the direction of increasing or decreasing *average* height, respectively. If $u > 0$ in equation (5.46), uphill jumps are directed to the right, downhill jumps to the left.

The analytic computation of equation (5.47) is difficult because the stationary distribution of the growth process is not known. However, in some cases either the jump rates or the stationary state itself possess a symmetry that forces J to vanish identically. This is obviously true if the rates satisfy detailed balance. It is also true for the Arrhenius growth model introduced in section 5.1.2. There, the key point is that the jump rates depend only on the bonding environment at the initial site, $R_{ii+1} = \exp(-n_i E_N / k_B T)$, where n_i denotes the number of lateral neighbours at site i. Thus

$$J = \langle \exp(-n_i E_N / k_B T) \rangle_u - \langle \exp(-n_{i+1} E_N / k_B T) \rangle_u = 0, \tag{5.48}$$

by translational invariance. Physically, the current vanishes because the jump rates do not couple to the asymmetry of the local environment.

A somewhat different argument applies to the discrete Gaussian model, defined by equation (5.10) with $q = 2$, equipped with random deposition and the Metropolis-type jump rates (5.11). These rates depend on the initial *and* final position of the atom, and therefore the motion does couple to the asymmetry of local environments. Instead, in this case the stationary state at fixed tilt u turns out to be *independent* of u; since the current vanishes by symmetry at $u = 0$, it then has to vanish identically for all u. The tilt invariance follows from writing the energy difference involved in a jump as [312] (the notation is explained in section 5.1.2)

$$\begin{aligned} K_2^{-1}[\mathscr{H}(H^{ii+1}) - \mathscr{H}(H)] &= 6 - 2(h_{i+2} + h_i - 2h_{i+1}) + 2(h_{i+1} + h_{i-1} - 2h_i) \\ &= 6 - 2[(\nabla^2 h)_{i+1} - (\nabla^2 h)_i]. \end{aligned} \tag{5.49}$$

The dynamics depends only on differences in the discrete local curvature, and is therefore invariant† under global tilts, $h_i \to h_i + ui$. In this sense, the discrete Gaussian 'collective diffusion' model is similar to the 'limited mobility' curvature model introduced in section 3.4, and the conclusion drawn for this model applies here also: As a consequence of the tilt invariance there are *no relevant nonlinearities*, and the large-scale properties of the surface should be given exactly by the linear noisy Mullins equation. While the original simulations of Siegert and Plischke [89] seemed to indicate a different behaviour, more recent numerical results are in accord with this prediction [312].

Two comments are in order. First, we recall having argued, in section 5.1.2, that the discrete Gaussian model has a sizable step edge barrier [280] (see equation (5.12)); nevertheless, we have shown here that the nonequilibrium surface current vanishes identically. Thus, the presence of step edge barriers is not sufficient to produce a nonzero net current, because their effect can be cancelled by other, less conspicuous local configurations. Second, the fact that the step edge barrier energy (5.12) is an increasing function of q, vanishing at $q = 1$, leads to a plausible conjecture regarding the q dependence of the current: since $J = 0$ at $q = 2$, we expect a net current in the uphill (downhill) direction for $q > 2$ ($q < 2$). This conclusion is corroborated by a detailed analysis of how the jump rates in various local environments change as q is moved away from $q = 2$ [314]. It is further confirmed by the direct measurement of the current for $q = 1$ and $q = 4$ [92], as well as by the resulting behaviour of the surface, which shows clean Edwards–Wilkinson scaling for $q = 1$ [277], and unstable growth for $q = 4$ [89, 312].

The symmetry arguments for the Arrhenius and the Gaussian models apply in arbitrary surface dimensionalities. In contrast, our last example, the version DT1 of the limited mobility rules described in section 5.1.1, can be simply analysed only in $d = 1$. For the present discussion, the important property of the rule is that it does not distinguish between incorporation sites with one ($k_i = 1$) and two ($k_i = 2$) lateral nearest neighbours (the coordination numbers k_i are defined in (5.4)). The behaviour of adatoms on the surface can therefore be predicted on the basis of a *two-state* variable $\tilde{k}_i = \min [k_i, 1] = 0, 1$ assigned to each site i. The local environments that contribute to the current are $(\tilde{k}_{i-1}, \tilde{k}_i, \tilde{k}_{i+1}) = (0, 0, 1)$ and $(1, 0, 0)$, where the atom is thought to be deposited at i and incorporates at $i + 1$ or $i - 1$, respectively.

For a fixed height configuration $H = \{h_i\}$ subject to helical boundary conditions (5.46), we now consider the spatially and temporally averaged surface current $\bar{J}$ defined by depositing many 'test' atoms onto each site i, and recording where they incorporate. Clearly,

$$\bar{J}(H) = L^{-1}[N_{001}(H) - N_{100}(H)], \tag{5.50}$$

where N_{lmn} is the number of local environments $(\tilde{k}_{i-1}, \tilde{k}_i, \tilde{k}_{i+1}) = (l, m, n)$ in the configuration H. The crucial observation is that $N_{001} = N_{100}$ for *any* string of 0's and 1's with periodic boundary conditions, both numbers being equal to the number of clusters of at least two consecutive 0's (figure 36). Thus, $\bar{J}(H) = 0$ for any configuration, and the ensemble average over H vanishes also. The proof is easily

†Strictly speaking, the argument only implies invariance for *integer* values of the tilt. Indeed, careful simulations of the discrete Gaussian model [313] reveal a non-zero current that is a *periodic* function of the tilt, with unit period; however, its amplitude ($\approx 2 \times 10^{-7}$) is so small as to make it negligible for all practical purposes.

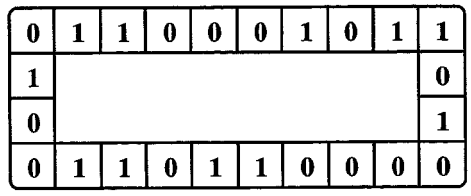

Figure 36. In a random sequence of 0's and 1's on a ring, the number of triples (001) is equal to the number of triples (100).

extended to versions of the rule where the atoms are allowed to search in a larger neighbourhood for a favourable incorporation site, as long as the property of having only two possible values for the effective coordination number $\tilde{k}_i$ is preserved. The remaining two rules defined in section 5.1.1, DT2 and WV, do not have this property and hence give rise to a non-zero current, which is approximately computed in the next section.

5.2.3. *Approximate microscopic theory*

Having established that the surface current vanishes identically for rule DT1, we may conclude that the current for the more elaborate rules DT2 and WV must be due solely to configurations in which these rules differ from DT1. For DT2, these are the asymmetric configurations $(k_{i-1}, k_i, k_{i+1}) = (1, 0, 2)$ and $(2, 0, 1)$, which bias the deposited particles to the right and to the left, respectively. We may therefore write

$$J_{\mathrm{DT2}} = \mathrm{Prob}\,(1, 0, 2) - \mathrm{Prob}\,(2, 0, 1). \tag{5.51}$$

For the Wolf–Villain (WV) rule, an additional contribution comes from the motion of particles deposited onto a site with $k_i = 1$ that has a neighbour for which $k_j = 2$. Thus

$$J_{\mathrm{WV}} = J_{\mathrm{DT2}} + \mathrm{Prob}\,(1, 2) - \mathrm{Prob}\,(2, 1). \tag{5.52}$$

In order to evaluate the probabilities occurring in equations (5.51) and (5.52), we now make two rather drastic approximations. First, we assume that the local height differences (also referred to as *step heights*) $\sigma_i = h_{i+1} - h_i$ at different sites are *statistically independent*. The probabilities in (5.51) and (5.52) can then be expressed as products of the three numbers p_+, p_- and p_0 defined by

$$p_+ = \mathrm{Prob}\,\{\sigma_i > 0\}, \quad p_- = \mathrm{Prob}\,\{\sigma_i < 0\}, \quad p_0 = \mathrm{Prob}\,\{\sigma_i = 0\}. \tag{5.53}$$

The height configurations contributing to Prob (1, 0, 2) and Prob (1, 2) are illustrated in figure 37. We conclude that

$$\mathrm{Prob}\,(1, 0, 2) = (p_0 + p_+)p_+^2 p_- + p_0 p_-^2 p_+, \quad \mathrm{Prob}\,(1, 2) = p_-^2 p_+, \tag{5.54}$$

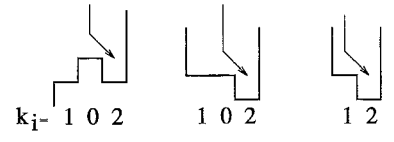

Figure 37. Height configurations contributing to the current in the limited mobility rules DT2 and WV.

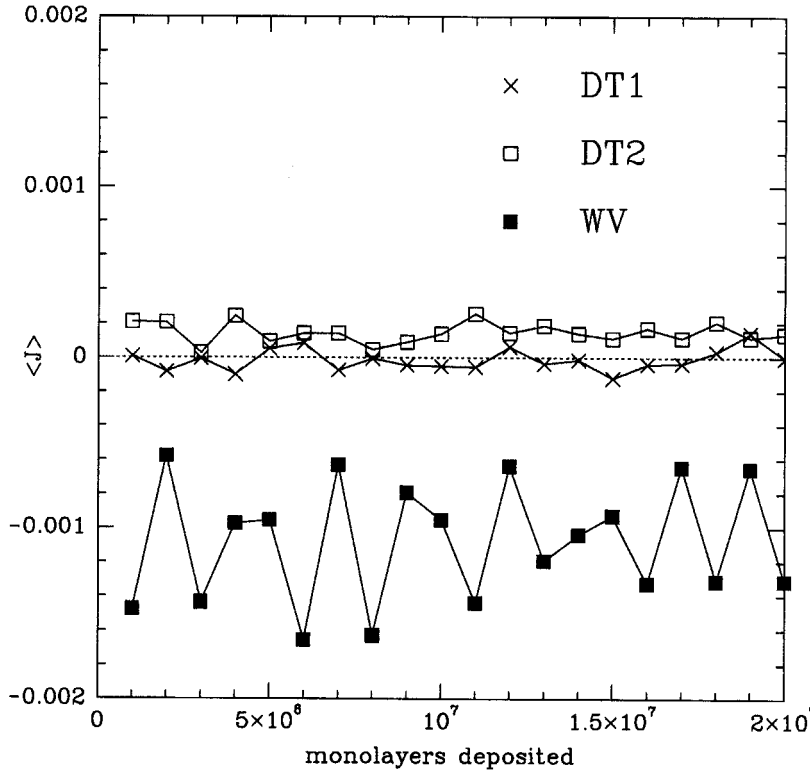

Figure 38. Simulation results for the growth-induced current, at surface inclinattion $\nabla h = 1$, obtained using the three limited mobility rules described in section 5.1.1. Each data point represents an average over 10^6 monolayers deposited onto a substrate of size $L = 100$.

and therefore

$$\begin{aligned} J_{\mathrm{DT2}} &= p_+ p_- (p_+^2 - p_-^2), \\ J_{\mathrm{WV}} &= J_{\mathrm{DT2}} + p_+ p_- (p_- - p_+) = -p_+ p_- p_0 (p_+ - p_-). \end{aligned} \tag{5.55}$$

If the surface is flat on average, $p_+ = p_-$ by symmetry and the currents vanish. A positive average surface inclination increases p_+ relative to p_-. Thus, a first conclusion from the expressions (5.55) is that the current is directed *uphill* for the DT2 model, $J_{\mathrm{DT2}}(u > 0) > 0$, while $J_{\mathrm{WV}}(u > 0) < 0$. The two rules belong to different universality classes, in the sense of different signs for the coefficient ν_1 in the expansion (3.14). This is confirmed by the direct numerical measurement of the currents (figure 38). Note, however, that J_{DT2} is extremely small and barely distinguishable from the noise. The fact that $\nu_1 < 0$ for this model therefore does not lead to any observable consequences on accessible time and length scales.

The inclination dependence of the currents can be obtained by making a second assumption regarding the probability distribution of the step heights σ_i. For convenience, we choose an exponential distribution

$$P(\sigma) = \frac{1}{Z} \exp(-K|\sigma| + m\sigma), \tag{5.56}$$

where the 'slope chemical potential' m controls the average inclination through the relation

$$u = \langle \sigma \rangle = \frac{\sinh m}{\cosh K - \cosh m}. \tag{5.57}$$

The coupling K controls the spread of the distribution, which can be characterized, for $u = m = 0$, by the variance

$$\langle \sigma^2 \rangle = (\cosh K - 1)^{-1}, \tag{5.58}$$

and $Z(K, m)$ is a normalization constant. Equation (5.56) would be exact if the surface were in equilibrium, governed by the Hamiltonian (5.10) with $q = 1$. The actual height difference distribution for the 1D limited mobility models is much broader, and better described by a stretched exponential [112]. In view of the uncontrolled approximations inherent in the present approach, however, the form (5.56) is quite sufficient for our purposes. The generalization to other choices for $P(\sigma)$ is straightforward.

Using equation (5.56), the probabilities $p_{\pm}, p_0$ and thus the currents are easily evaluated. In the following we discuss only the Wolf–Villain rule. In figure 39 the calculated current is compared to the results of direct simulations. Since the current tends to strongly decrease with increasing system size (see below), we have chosen

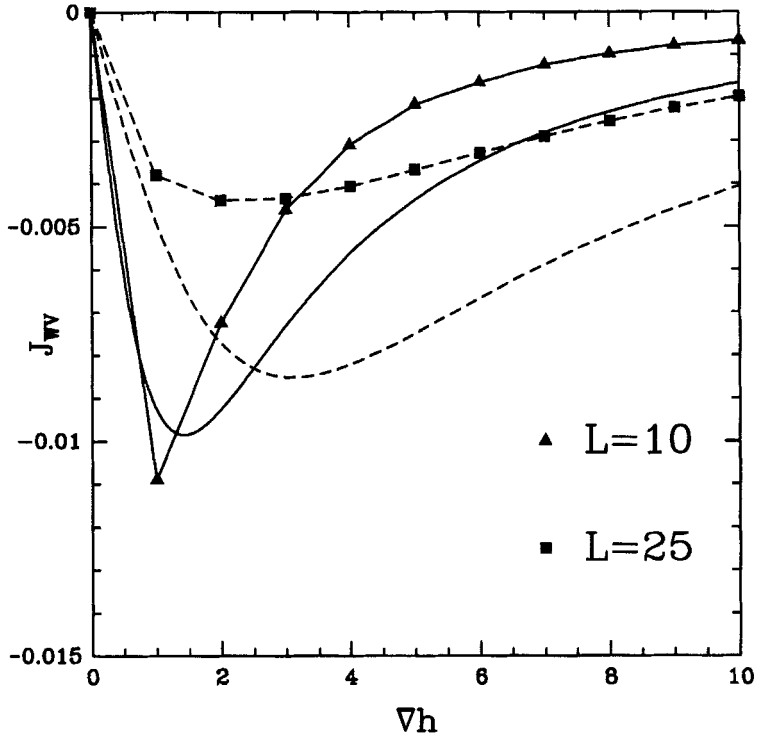

Figure 39. The inclination-dependent current in the 1D Wolf–Villain model. The symbols show simulation results for two different system sizes, obtained by averaging over 10^8 monolayers per data point. The full and broken curves without symbols show the corresponding analytic approximation.

small systems for the simulations, $L = 10$ and $L = 25$, and averaged over 10^8 monolayers for each value of the inclination. For comparison with the simulations, the parameter K in the exponential distribution (5.56) was chosen such that the variance (5.58) matches that of the numerically determined step height distribution; for $L = 10$ this gives $K = 0{\cdot}797$ (in this case $\langle\sigma^2\rangle \approx 2{\cdot}986$), and for $L = 25$ we chose $K = 0{\cdot}361$ (corresponding to $\langle\sigma^2\rangle \approx 15{\cdot}21$). It can be seen that the approximate theory reproduces the overall inclination dependence rather well, but the magnitude of the current is significantly overestimated, especially at larger tilts.

It is of particular interest to understand how the shape of the current–inclination curve changes as the step height distribution $P(\sigma)$ broadens, for example by decreasing K in equation (5.56). Qualitatively, figure 39 shows that the minimum in $J(u)$ shifts to larger slopes, such that the absolute magnitude of the current decreases with decreasing K for slopes smaller than the minimum, but increases for large slopes. On a more quantitative level, one obtains the following simple expressions for the derivative at zero slope,

$$\nu_1 = -J'_{\mathrm{WV}}(0) = \frac{\exp(-2K)[1-\exp(-K)]^2}{[1+\exp(-K)]^4}, \tag{5.59}$$

and for the asymptotics for $u \to \infty$ at fixed K,

$$J_{\mathrm{WV}}(u) \approx -\frac{\exp(-K)}{2\sinh K}\frac{1}{u^2}, \quad u \to \infty. \tag{5.60}$$

Thus, ν_1 vanishes as $\nu_1 \sim K^2/16$ for $K \to 0$, while the prefactor in (5.60) diverges for small K. In figure 40, equation (5.59) is plotted as a function of the variance (5.58). Somewhat surprisingly, the asymptotic $1/u^2$ behaviour predicted by (5.60) seems to

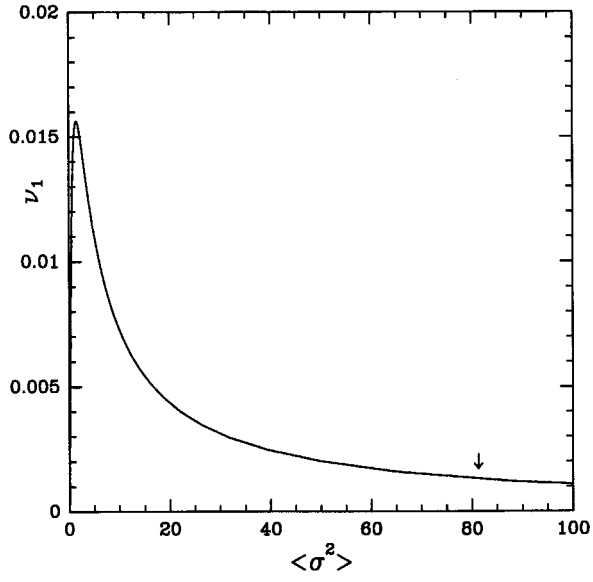

Figure 40. The expression (5.59) for the (negative) derivative of J_{WV} at zero tilt, as a function of the variance of the step height distribution. The arrow indicates the value at which $\langle\sigma^2\rangle$ saturates for large system sizes and long times.

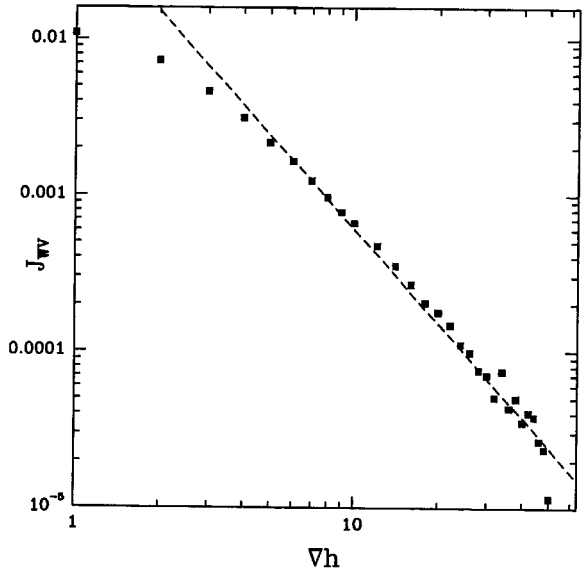

Figure 41. Inclination-dependent current in the 1D Wolf–Villain model, for a small system ($L = 10$) and large slopes. Each data point corresponds to an average over 10^8 monolayers. The broken line indicates the $|\nabla h|^{-2}$ decay predicted by the approximate theory.

be confirmed by simulations of the WV model (figure 41). Note that this asymptotics is distinct from that obtained using simple step-edge barrier arguments, which always lead to a decay of the current as $1/u$ (see section 5.2.1).

These considerations can be used to discuss the strong size dependence of the current in the Wolf–Villain model observed by Krug *et al.* [92]. Recent numerical work [107, 108, 112] has revealed that the 1D limited mobility models are generally characterized by a stationary step size distribution $P(\sigma)$ that broadens with increasing system size L; more precisely, the moments appear to satisfy scaling laws of the form [112]

$$\langle \sigma^q \rangle^{1/q} \sim L^{\alpha_q}, \tag{5.61}$$

with non-trivial, q-dependent exponents α_q. We have encountered a simple form of this 'anomalous' scaling behaviour in our investigation of the noisy Mullins equation in section 3.2; in that case $P(\sigma)$ is a Gaussian of width $\sim L^{1/2}$ in one dimension. From our approximate theory we conclude that such broadening will result in a decrease of the current with increasing system size. This is not hard to understand: if the step height distribution is very broad, the excess steps introduced by an external tilt will have little effect, and thus the current will be small.

For the Wolf–Villain model, Schroeder *et al.* [107] found that the broadening of $P(\sigma)$ ceases when the system size exceeds $L \approx 250$, at which point the variance has reached a value of $\langle \sigma^2 \rangle \approx 80$. From equation (5.58) we see that this corresponds to a value of $K \approx 0{\cdot}158$ and, using equation (5.59), $\nu_1 \approx 0{\cdot}001\,32$ (see figure 40). In comparison, in the direct numerical measurements reported by Krug *et al.* [92] the current was found to become size independent at $L \approx 320$, where $J(u = 1) \approx -0{\cdot}0008$. Thus, the approximate theory appears to provide a reasonable description

of the relation between the statistics of step heights and the resulting non-equilibrium current. It does not, however, explain why the step height distribution broadens according to equation (5.61) in the first place (see also section 5.5.2). We may note in this context that the broadening appears to continue indefinitely for the DT1 rule [112], which allows no current by symmetry (section 5.2.2), indicating that the saturation of $P(\sigma)$ observed for the WV rule is indeed due to the fact that J_{WV} is non-zero.

5.3. *Unstable growth: theory versus experiment*

Perhaps the most remarkable corollary of the ubiquity of growth-induced surface currents is the conclusion that ideal MBE growth is *generically unstable*, in the sense that destabilizing 'uphill' currents occur as frequently as stabilizing 'downhill' currents. Among the models discussed in the preceding sections we have encountered examples of both kinds—the Metropolis model (5.11) with Hamiltonian (5.10) is stable when $q = 1$ but unstable when $q = 4$, and similarly the limited mobility model WV is stable, while DT2 is (asymptotically) unstable. In fact, if we adopt the common view that non-equilibrium currents arise on real surfaces mainly due to repulsive step edge barriers, unstable growth on singular surfaces should be the rule rather than the exception. It is therefore gratifying that several recent MBE experiments have obtained surface morphologies that are indicative of a growth instability of the kind anticipated by theory. In this section we relate these experiments to the theoretical concepts that have been developed so far. We will restrict attention to singular surfaces; systematic studies of unstable growth on vicinal surfaces have only just been initiated [315, 316].

5.3.1. *Experimental phenomenology*

The experimentally observed morphologies can be broadly grouped into two categories.

(i) The 'Poisson/wedding cake morphology' is typical of metal homoepitaxy at low temperatures, where interlayer transport is strongly inhibited. In this case the instability emerges already during the growth of the first few layers. The lateral scale is set by the island spacing l_D of the submonolayer regime (see equation (5.23)); subsequent layers then form islands on top of islands, giving rise to an array of (American) wedding cakes. The actual shape of the features also mimics the shapes of submonolayer islands and is strongly dependent on the amount of edge diffusion; compare for example the STM images for Pt(111) [317] and Ag(111) [318].

For a quantitative description of this regime one may assume, as a first approximation, that interlayer transport is completely suppressed (figure 42). This yields several definite predictions. First, the layer coverages have a Poisson distribution [311], as has been verified for Cu(111) [319] and Pt(111) [317]. Second, the variance of the surface height is proportional to the total coverage $\theta = Ft/a$ (equation (5.42)), in agreement with LEED measurements on Ag(111) [320] and Fe(110) [321]. Third, since the lateral spacing of features remains fixed at l_D (see figure 42), while their vertical size (peak-to-valley height difference) increases as $a\sqrt{\theta}$, one expects the slopes of the wedding cakes to steepen as $(a/l_D)\sqrt{\theta}$ [123], or, equivalently, the terrace width on the hillsides to decrease as

$$l(t) \sim l_D/\sqrt{\theta}. \tag{5.62}$$

This agrees with measurements on Ag(111) at 130 K [320], though at higher temperatures a decay as $l \sim 1/\theta$ was reported for the same surface [322]. Equation

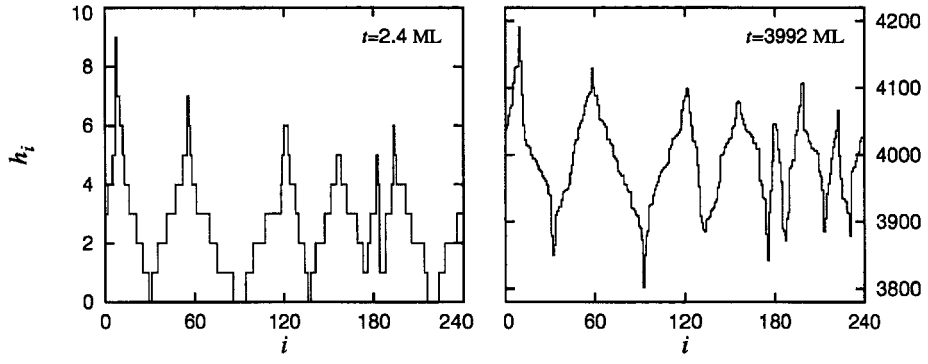

Figure 42. Wedding cakes in $d = 1$. The figure was generated using the model described in section 5.2.1, which incorporates diffusion of singly bonded adatoms, deposition, and complete suppression of interlayer transport. The ratio of diffusion to deposition rate was $D_s/F = 5 \times 10^5$. The left panel corresponds to a coverage $\theta = 2{\cdot}4$, the right panel to $\theta = 3992$. Note that the lateral extent and positions of the mountains in the high coverage regime correspond exactly to the first monolayer islands in the left panel; there is no coarsening [123].

(5.62) may need to be modified in the low coverage regime, where part of the substrate is still uncovered.

(ii) On semiconductor surfaces, as well as for some metals at elevated temperatures, the growth instability takes a different form which we will refer to as the 'mound morphology' [323]. The distinguishing feature of this growth mode is that it appears only after the deposition of many layers, that the initial size of features (mounds) much exceeds the submonolayer island spacing l_D, and that the feature size, rather than remaining fixed, increases with time, implying a *coarsening* of the morphology.

Mound formation has been reported for GaAs(001) [274, 324, 325, 326], InP(100) [327, 328], Ge(001) [329, 330], Si(100) [316], Fe(001) [331, 332] and, possibly, Si(111) [333]. The theoretical predictions for this growth mode are much less clear cut than in the Poisson case, and will be summarized in the following two sections. At this point, we merely remark that the distinction between wedding cakes and mounds is probably not exclusive; for example, the experiments of Ernst *et al.* on Cu(100) [334, 335] (see also [319]) seem to represent an intermediate case. Moreover, it seems likely that in many cases the Poisson growth mode constitutes an early time regime which crosses over to mounding [332] once the terrace width (5.62) becomes small enough to allow for interlayer transport despite strong barriers, though the transition between the two regimes has not been investigated in detail. Nevertheless, the distinction between the two limiting cases is a useful first step towards a quantitative understanding of unstable growth.

5.3.2. *Strong and weak barriers*

Obviously, the two types of morphologies described above correspond to situations with 'strong' (wedding cakes) and 'weak' (mounds) step edge barriers, respectively. To make this notion more precise, we resort to the linearization of the general conserved growth equation (3.15), which reads

$$\partial h/\partial t = \nu_1 \nabla^2 h - \kappa \nabla^4 h + F. \tag{5.63}$$

The coefficient ν_1 was computed in section 5.2.1, and can be written as $\nu_1 \approx -F\tilde{l}_D^2/a$, where

$$\tilde{l}_D = \min [l_D, (l_D l_-)^{1/2}] \tag{5.64}$$

defines an effective diffusion length. The fourth-order derivative describes relaxation through surface diffusion and $\kappa = \Gamma_a \sigma$ is the product of adatom mobility and surface tension. We first note that κ and F can be combined into a 'capillarity' length

$$l_\kappa = (a\kappa/F)^{1/4}, \tag{5.65}$$

which gauges the importance of diffusional smoothening versus deposition [123]. For semiconductors a typical value of κ appears to be 1 μm^4 per hour [336], which yields $l_\kappa \approx 1300$ Å at a deposition rate of 1 ML s^{-1}.

Since $\nu_1 < 0$, equation (5.63) possesses a band of unstable wavelengths. The fastest growing mode corresponds to a wavelength

$$\lambda^* = 2\pi(-2\kappa/\nu_1)^{1/2} \approx \sqrt{2}\, 2\pi\, l_\kappa^2/\tilde{l}_D, \tag{5.66}$$

and the corresponding time scale τ^*, expressed in terms of coverage, is

$$\theta^* = F\tau^*/a \approx 4(l_\kappa/\tilde{l}_D)^4. \tag{5.67}$$

Equations (5.66) and (5.67) can be combined to give the relation

$$\lambda^* = \pi(2\theta^*)^{1/2}\tilde{l}_D. \tag{5.68}$$

Clearly values of $\theta^* < 1$ are nonsensical: the instability cannot manifest itself unless several layers are deposited. We therefore conclude that for $l_\kappa < \tilde{l}_D$ wedding cakes form during the deposition of the first few layers, so that effectively $\theta^* \approx 1$ and $\lambda^* \approx l_D$; this regime cannot be expected to be well described by continuum theory. Correspondingly, $l_\kappa \gg \tilde{l}_D$ is identified as the mounding regime, and equation (5.68) connects two of its characteristic features: the fact that the instability develops only after the deposition of many layers ($\theta^* \gg 1$) at a lateral wavelength that much exceeds the diffusion length ($\lambda^* \gg \tilde{l}_D$).

It should be emphasized that the microscopic barrier strength enters the ratio $l_\kappa/\tilde{l}_D$ in two distinct ways. First, as was shown in section 5.2.1, it determines whether $\tilde{l}_D \approx l_D$ or $\tilde{l}_D \approx (l_D l_-)^{1/2}$. Second, it affects the value of κ through the adatom mobility Γ_a, which is a *macroscopic* quantity averaged over all possible environments of the adatom [276]. Step edge barriers may constitute the rate limiting process for macroscopic mass transport along the surface; in particular $\Gamma_a \approx 0$ if interlayer exchange is strongly suppressed.

The relation (5.68) can be used to estimate $\tilde{l}_D$ from observational data. For example in the experiment of Orme *et al.* [325] mounds were observed to form after the deposition of 270 bilayers, at a spacing of 0·25 μm. Using equation (5.68) this yields $\tilde{l}_D \approx 34$ Å, considerably smaller than the diffusion length $l_D \approx 165$ Å estimated in a separate experiment under identical conditions [337]. We conclude that this system is in the weak carrier regime, in the sense of section 5.2.1, where $\tilde{l}_D = (l_D l_-)^{1/2}$, and obtain $l_- \approx 7$ Å. This can be converted into an estimate of the step edge barrier energy ΔE_- by invoking the relation (5.20). With $a \approx 2{\cdot}8$ Å, the bilayer thickness, and $T = 555$°C, we obtain $\Delta E_- \approx 0{\cdot}06$ eV, a very small number compared to the energy barrier $E_S \approx 1{\cdot}3$ eV for surface diffusion on GaAs(001) [338]. Direct experimental information on the magnitude of ΔE_- is not available. Šmilauer and Vvedensky [339] obtained $\Delta E_- \approx 0{\cdot}175$ eV by fitting the results of an

Arrhenius-type computer simulation (see section 5.1.2) to RHEED data monitoring the thermal smoothening of MBE grown vicinal surfaces.

The discrepancy between the two estimates should be no surprise. On the one hand, Šmilauer and Vvedensky [340] have recently shown in the framework of Arrhenius model simulations that the approach based on equation (5.68) tends to underestimate the size of the barrier; on the other hand, the approach of [339] seems likely to yield a value that is too large [341]. Thus one may hope that the two estimates at least provide bounds on the true barrier energy.

In view of its importance for the growth morphology, it is clearly desirable to obtain reliable experimental estimates of step-edge barrier energies. While the method outlined above may prove useful in the mounding regime, an approach adapted to the case of strong barriers has recently been proposed by Meyer *et al.* [342] and by Šmilauer and Harris [343]. The central idea is to estimate the first layer coverage at which second layer nucleation sets in on top of islands. For Ag(111) and Pt(111) the authors estimate barrier energies of the order of $\Delta E_{-} \approx 0{\cdot}15$–$0{\cdot}2$ eV, while for Fe(001) Šmilauer and Harris report a much smaller value, around 0·05 eV. Bartelt and Evans [344] obtain a similar estimate $\Delta E_{-} \approx 0{\cdot}045 \pm 0{\cdot}005$ eV by fitting their Monte Carlo simulations to STM data for the early time surface morphology [345]. This provides some rationalization for the fact that Fe(001) is the only metal surface on which mounds rather than wedding cakes have been clearly observed so far [331, 332].

Semiempirical potentials have also been used extensively to compute step edge barriers on a metal surface [346]. It is worth pointing out, however, that the application of these results to a growth situation is far from straightforward, since the relevant *effective* step crossing barriers in growth constitute an average over many different local configurations, involving rough step edges and possible 'exotic' collective diffusion mechanisms [347].

5.3.3. *Coarsening and slope selection*

Experimental studies of the coarsening stage of the mound morphology [325, 326, 329–332, 334] pose two key questions to be addressed by theory. First, how is the characteristic slope at the sides of the mounds selected, and is it constant or time dependent? Second, what determines the dynamic exponent z in the coarsening law (see also section 2.3.1)

$$\xi(t) \sim t^{1/z}, \tag{5.69}$$

according to which the typical lateral extent of mounds ξ grows as a function of time or film thickness? On both issues, a variety of behaviours are observed experimentally. For metal surfaces (Fe(001) [331, 332] and Cu(100) [334]) a time-independent 'magic slope' appears to be selected, which is often identified with specific crystallographic orientations [331, 334]. On semiconductor surfaces the mounds are typically very shallow†, with slopes that seem to remain constant in the case of GaAs [325, 326] but show a strong thickness dependence for Ge(001) [329]. Three experimental estimates of the coarsening exponent $1/z$ are available at this time. For Fe on Fe(001) one observes $1/z \approx 0{\cdot}16 \pm 0{\cdot}04$ at room temperature [332], while for Fe on

†However, the formation of pyramids with crystallographic faces has been reported for Si(111) [333].

Mg(001) at 400–450 K a value of $1/z \approx 0{\cdot}25$ was reported; the third estimate, obtained for Ge(001) at 427 K, is $1/z \approx 0{\cdot}42 \pm 0{\cdot}04$ [330].

Rather than invoking the full nonlinear conserved interface equation (3.15), we will use a simplified model wherein both the non-equilibrium chemical potential μ_{NE} and the geometric nonlinearities are neglected. While the former approximation is motivated by convenience only, the latter can be justified by noting that the relevant slopes in the mounding problem are of the order of $a/l_{\mathrm{D}} \ll 1$ (compare to section 5.2.1). We further leave out the noise terms, since we are dealing with a deterministic instability. The equation of interest is therefore

$$\partial h/\partial t = -\kappa(\nabla^2)^2 h - \nabla \cdot \mathbf{J}_{\mathrm{NE}}(\nabla h) + F. \tag{5.70}$$

Assuming moreover an isotropic current function of the form (5.35), equation (5.70) can be rewritten as an equation of motion for the height gradient $\mathbf{u} = \nabla h$:

$$\frac{\partial \mathbf{u}}{\partial t} = -\kappa(\nabla^2)^2 \mathbf{u} + \nabla\left(\nabla \cdot \frac{\partial \mathscr{V}}{\partial \mathbf{u}}\right). \tag{5.71}$$

Here, the potential $\mathscr{V}(\mathbf{u})$ is given by

$$\mathscr{V}(\mathbf{u}) = -(1/2)\int_0^{\mathbf{u}^2} \mathrm{d}s\, \phi(s), \tag{5.72}$$

and the function ϕ was defined in equation (5.35). The form (5.71) emphasizes the analogy with the equation of motion for a conserved vector order parameter, 'model B' of phase ordering dynamics [348],

$$\frac{\partial \mathbf{u}}{\partial t} = -\kappa(\nabla^2)^2 \mathbf{u} + (\nabla \cdot \nabla)\frac{\partial \mathscr{V}}{\partial \mathbf{u}}, \tag{5.73}$$

where one typically chooses $\mathscr{V}(\mathbf{u}) = (1 - \mathbf{u}^2)^2$. The only difference between equations (5.71) and (5.73) lies in the order of the differential operators in front of the second term on the right hand side. This is clearly irrelevant in $d = 1$ but crucial in the physical dimensionality $d = 2$, since it ensures that $\mathbf{u}$ remains a gradient field (with $\nabla \times \mathbf{u} = 0$) at all times.

The analogy between unstable growth and phase ordering was first pointed out by Golubović and Karunasiri [349] for the 1D case. It is useful in particular for clarifying the issue of slope selection. In the thermodynamic context, the system will clearly seek to locally establish values of $\mathbf{u}$ which correspond to minima of $\mathscr{V}$, i.e. to (stable) zeros of the non-equilibrium current $\mathbf{J}_{\mathrm{NE}}$ [92, 300, 307]. Microscopically, the origin of such zeros is not well understood. Krug *et al.* [92] pointed out that stable zeros must appear simply because $\mathbf{J}_{\mathrm{NE}}$ is forced to vanish at all high-symmetry orientations, but this cannot explain the rather shallow slopes that seem to be selected in many experiments. Therefore, kinetic mechanisms such as knock-out processes or downward funnelling [99, 273] may have to be invoked [307].

Whatever their precise origin, it is a simple matter to include selected 'magic slopes' in the continuum equation (5.70) through a suitable choice of $\mathbf{J}_{\mathrm{NE}}$. The resulting equation was solved numerically by Siegert and Plischke [300], who found a coarsening exponent $z \approx 4$ irrespective of the detailed functional form of $\mathbf{J}_{\mathrm{NE}}$; in particular, the coarsening behaviour is affected neither by including in-plane anisotropy, nor by using a function $\mathbf{J}_{\mathrm{NE}}$ which cannot be derived from a potential $\mathscr{V}(\mathbf{u})$ [307]. On the other hand, Stroscio *et al.* [332] reported an exponent $1/z = 0{\cdot}18 \pm 0{\cdot}02$, close to $1/6$, from simulations in which the first, linear term in

equation (5.70) is replaced by a sixth-order derivative $(\nabla^2)^3 h$, and a non-equilibrium chemical potential term $\nabla^2(\nabla h)^2$ is added on the right hand side. It is interesting to note that the observed values of z, $z \approx 4$ and $z \approx 6$, correspond to the result of naive dimensional analysis of equation (5.70) involving only the linear relaxation terms $(\nabla^2)^2 h$ and $(\nabla^2)^3 h$, respectively. In the theory of phase ordering kinetics such dimensional reasoning is known to fail if a second length scale, other than the domain size ξ, exists in the problem; for example, the thickness of domain walls or the core size of topological defects [348]. It is not clear at present whether this complication arises also in the context of equation (5.70). The approximate agreement with the predictions of naive dimensional analysis was also noted by Liu and Metiu [350] in simulations of closely related equations describing the faceting of *thermodynamically* unstable crystal surfaces.

Let us next consider the case when $\mathbf{J}_{\mathrm{NE}}$ does not vanish anywhere except at the singular orientation $\mathbf{u} = 0$. Then no slope selection is possible, but rather the mound morphology steepens indefinitely; in the thermodynamic analogy, the system can gain unlimited free energy by further increasing the value of the order parameter. This constitutes a novel type of phase ordering phenomenon which is not merely of academic interest—coarsening accompanied by steepening has been observed experimentally on Ge(001) [329] as well as in growth simulations (see below). Moreover, we have seen above in section 5.2 that simple models (such as the generalized BCF theory and microscopic SOS models [92]) typically produce current functions without magic slopes.

The relationship between coarsening and steepening is easily evaluated in one dimension. We assume that for large ξ the mound shape approaches the stationary solution of equation (5.70) with wavelength ξ [49, 351]. In one dimension, the stationarity condition takes the form of Newton's equation for a particle moving in the potential $-\mathscr{V}(u)$, $\kappa u'' = \mathscr{V}'(u(x))$ [352]. In the case of interest here $-\mathscr{V}$ is a potential well with a single minimum at $u = 0$. The stationary solutions of wavelength ξ correspond to 'trapped' periodic trajectories with period ξ. Using energy conservation, the relationship between the wavelength and the maximal slope $u_{\max}$ (that is, the turning point of the particle trajectory) can be written as

$$\xi = 4\sqrt{\kappa} \int_0^{u_{\max}} \mathrm{d}u \, \{2[\mathscr{V}(u) - \mathscr{V}(u_{\max})]\}^{-1/2}. \tag{5.74}$$

For example, if the current decays to zero as

$$J_{\mathrm{NE}}(u) \sim u^{-\gamma}, \quad u \to \infty, \tag{5.75}$$

evaluation of equation (5.74) yields

$$u_{\max} \sim \xi^{2/(1+\gamma)}. \tag{5.76}$$

Together with equation (5.69) this predicts how the morphology steepens as a function of time.

A detailed study of the BCF case $\gamma = 1$ has been performed by Hunt, Orme, Williams, Orr and Sander [351], who estimate a coarsening exponent $1/z \approx 0{\cdot}22$. Another case of interest is $\gamma = 0$, corresponding to a finite limiting current for $u \to \infty$. This behaviour was found numerically for the $q = 4$ Metropolis model [92]. With $\gamma = 0$, (5.76) predicts that $u_{\max} \sim \xi^2$, which is reasonably close to the result $u_{\max} \sim \xi^{2{\cdot}6}$ obtained in simulations of the model [89, 312]. However, the agreement

may well be fortuitous, since the anisotropies in the surface tension and the adatom mobility probably have significant effects at the large slopes involved [276].

The simultaneous coarsening and steepening of the surface pattern can lead to a rather rapid temporal increase of the modulation *amplitude*. Combining equations (5.69) and (5.76), the surface width $W \sim u_{\max}\xi$ is seen to grow as

$$W \sim t^{(3+\gamma)/z(1+\gamma)}. \tag{5.77}$$

Depending on the values of z and γ, the exponent in (5.77) may well exceed 1/2, the value describing the most rapid *stochastic* roughening of a surface through purely random deposition, with no relaxation whatsoever; for example, Siegert and Plischke [312] found $W \sim t^{0.61}$ in simulations of the 1D $q = 4$ Metropolis model (see section 5.1.2), where $z \approx 6$ and $u_{\max} \simeq \xi^{2.6}$ (see above).

This effect has been made responsible for the rapid roughening behaviour observed in the epitaxial growth of Si(001) [353] and other materials (see section 5.6.3). It is, however, worth pointing out that a rather general bound on the temporal increase of the surface width can be derived directly from the equation of motion (5.70) [354]. Multiplying both sides by h, integrating over space and performing a few partial integrations, one obtains

$$\begin{aligned} \partial W^2/\partial t &= (\partial/\partial t)L^{-d}\int \mathrm{d}^d\mathbf{x}(h - Ft)^2 \\ &= 2L^{-d}\int \mathrm{d}^d\mathbf{x}\,(\nabla h)^2\phi(|\nabla h|^2) - 2L^{-d}\int \mathrm{d}^d\mathbf{x}\,(\nabla^2 h)^2. \end{aligned} \tag{5.78}$$

Provided $\phi(s)$ decays at least as $1/s$ for large arguments, i.e. $\gamma \geq 1$ in equation (5.75), the first term on the right hand side is bounded and W^2 can increase no faster than linearly in t.

Šmilauer and Vvedensky [340] have recently performed a detailed simulation study of mounding in the framework of an Arrhenius-type SOS model supplemented with step edge barriers. As a function of temperature and growth rate they observe a rather broad range of behaviours, comparable in diversity to the experimental studies. Coarsening exponents vary between $1/z \approx 0{\cdot}19$ and $1/z \approx 0{\cdot}26$, and both slope selection and power law steepening can be found. Siegert and Plischke [355] studied a somewhat different model in which the existence of selected slopes could be demonstrated directly through a measurement of the surface current [92]. They concluded that asymptotically $1/z \approx 0{\cdot}25$ in the case of isotropic step-edge barriers, but $1/z \approx 0{\cdot}18$ when anisotropy of the kind occuring on the GaAs(001) surface is included.

Interestingly, the simulations [340, 355] indicate that coarsening and steepening are *competing* processes, in the sense that coarsening is slowed down when the mounds steepen during growth. A related effect can be derived for 1D surfaces, under the assumption that the coarsening is driven purely by fluctuations [249]. Introducing a steepening exponent through the relation $u_{\max} \sim \xi^{\delta}$, one obtains the expression

$$z = 3 + 2\delta \tag{5.79}$$

for the coarsening exponent. For $\delta = 0$ (slope selection) this reduces to the well known result $z = 3$ for the 1D Kawasaki Ising model at low temperatures [356, 357, 358], while the limit $\delta \to \infty$ represents the Poisson growth of wedding cakes, where no coarsening occurs ($1/z = 0$) and the surface width increases as $W \sim t^{(1+\delta)/z} \sim \sqrt{t}$.

5.4. *The non-equilibrium chemical potential*

The conserved KPZ equation

$$\frac{\partial h}{\partial t} = -\nabla^2 \left[\nu \nabla^2 h + \frac{\lambda}{2} (\nabla h)^2 \right] + \eta \tag{5.80}$$

was proposed in 1989 by Sun, Guo and Grant [359] in a first exploration of non-KPZ universality classes. These authors were concerned with the non-equilibrium dynamics of interfaces under conditions of local volume conservation, and therefore chose the noise term η to be of the conserving type, characterized by the covariance (3.17). The equation re-emerged, equipped with nonconserving 'shot noise', in the first papers on ideal MBE [101, 132]. In both contexts the quadratic nonlinearity in equation (5.80) was written down by appealing to symmetry considerations, and to the analogy with the KPZ equation (see section 4).

A physical interpretation was suggested by Villain [20], who pointed out that the nonlinearity in equation (5.80) could be thought to arise from an inclination dependence of the *adatom density* under growth conditions; such a dependence is easily demonstrated, for example in the framework of the BCF-type theories discussed in section 5.2.1 (see section 5.4.4). Villain's picture is very close to the point of view adopted in section 3.1, where nonlinear terms of the form $\nabla^2(\nabla h)^{2n}$ were argued to represent the inclination dependence of a non-equilibrium contribution to the *adatom chemical potential* μ_{NE} (see equation (3.13)). In the notation of section 3.1, the coefficients in equation (5.80) are $\nu = \Gamma_a \sigma$ and $\lambda = -2\Gamma_a \lambda_2$.

The goal of this section is to give a precise microscopic meaning to the notion of an inclination dependent, non-equilibrium chemical potential. We will be working mostly in the context of the Arrhenius MBE model described in section 5.1.2. Besides having the advantage of a simple equilibrium dynamics [276], this model suits our purposes because, as shown in section 5.2.2, it does not allow any non-equilibrium surface current. According to the power counting arguments of section 3.3, this implies that the nonlinearity in equation (5.80) is a relevant term which governs the large-scale behaviour of the surface. We noted in section 3.3 that the role of higher-order corrections of the form $\nabla^2(\nabla h)^{2n}$ with $n \geq 2$, i.e. the consistency of keeping only the leading term in the gradient expansion (3.13), is not well understood, especially in low dimensionalities. Here we will follow the common practice and disregard this complication; some further discussion is provided in section 5.5.2.

Once the physics behind the nonequilibrium chemical potential has been elucidated for the case of growth, it is straightforward to devise other microscopic mechanisms that give rise to the same kind of effects under conditions of volume conservation, and thus to construct models that are described by the (fully) conserved KPZ equation originally envisioned by Sun *et al.* [359]. This will be addressed briefly in section 5.4.2. In section 5.4.3 we summarize what is known analytically about the properties of equation (5.80), with conserved or nonconserved noise. An application to the problem of layer-by-layer growth is briefly described in section 5.4.4.

5.4.1. *Microscopic origin in the Arrhenius model*

As a starting point, consider the change in the ensemble-averaged local height $\langle h_{\mathbf{x}} \rangle$ induced by deposition and diffusion processes. For the purpose of the present discussion, we envision an ensemble of microscopic surface configurations that

correspond to the same, slowly varying macroscopic surface shape. Owing to deposition, $\langle h_{\mathbf{x}} \rangle$ increases at a constant rate F; diffusion processes remove particles from site $\mathbf{x}$ and add particles coming from the neighbouring sites. The resulting dynamics can be written as

$$\frac{\mathrm{d}}{\mathrm{d}t}\langle h_{\mathbf{x}} \rangle = \frac{1}{2d} \sum_{n.n.} \langle R_{\mathbf{yx}} - R_{\mathbf{xy}} \rangle + F, \tag{5.81}$$

with the sum over the averaged rates including the nearest neighbour sites $\mathbf{y}$ of $\mathbf{x}$. For the standard Arrhenius model described in section 5.1.2, $R_{\mathbf{xy}} = \exp(-2K_1 n_{\mathbf{x}}/k_{\mathrm{B}}T)$, which is independent of the final site $\mathbf{y}$ (recall that K_1 is the coupling constant of the SOS Hamiltonian $\mathscr{H}_1$ in equation (5.10)). Consequently the sum on the right hand side of equation (5.81) takes the form of the lattice Laplacian of the quantity

$$M_{\mathbf{x}} \equiv \langle \exp(-2K_1 n_{\mathbf{x}}/k_{\mathrm{B}}T) \rangle, \tag{5.82}$$

and the coarse-grained equation of motion reads

$$\frac{\partial h}{\partial t} = \frac{1}{2d} \nabla^2 M + F. \tag{5.83}$$

It is clear from a comparison with the conserved interface equation (3.15) that M should be associated with the chemical potential μ (the geometric prefactor $[1 + (\nabla h)^2]^{1/2}$ in equation (3.15) does not appear in the large-scale description of SOS models; see [251, 276]). In particular, a term $\nabla^2(\nabla h)^2$ appears in the equation of motion if and only if the local value of M depends on the local surface slope.

In fact a more precise connection can be established. In (global) thermal equilibrium ($F = 0$) it can be shown that $M = \exp(-2dK_1/k_{\mathrm{B}}T)$, independent of inclination [266]. Moreover, if the surface is constrained by an inhomogeneous chemical potential $\mu_{\mathbf{x}}$ to adopt a modulated, *local* equilibrium shape, one finds

$$M_{\mathbf{x}} = \exp[-(2dK_1 - \mu_{\mathbf{x}})/k_{\mathrm{B}}T]. \tag{5.84}$$

We give here a simple proof due to Dobbs [276]. Let the total energy of a surface configuration $H = \{h_{\mathbf{x}}\}$ be given by (compare to equation (5.10))

$$\mathscr{H} = K_1 \sum_{\langle \mathbf{xy} \rangle} |h_{\mathbf{x}} - h_{\mathbf{y}}| - \sum_{\mathbf{x}} \mu_{\mathbf{x}} h_{\mathbf{x}}, \tag{5.85}$$

and let $H' = \{h'_{\mathbf{y}}\}$ denote the configuration obtained from $\{h_{\mathbf{y}}\}$ by removing a particle at site $\mathbf{x}$,

$$h'_{\mathbf{y}} = \begin{cases} h_{\mathbf{y}} - 1, & \mathbf{y} = \mathbf{x}, \\ h_{\mathbf{y}}, & \mathbf{y} \neq \mathbf{x}. \end{cases} \tag{5.86}$$

The energy difference between the two configurations is readily shown to be

$$\mathscr{H}(H') - \mathscr{H}(H) = 2K_1(n_{\mathbf{x}} - d) + \mu_{\mathbf{x}}. \tag{5.87}$$

Consequently,

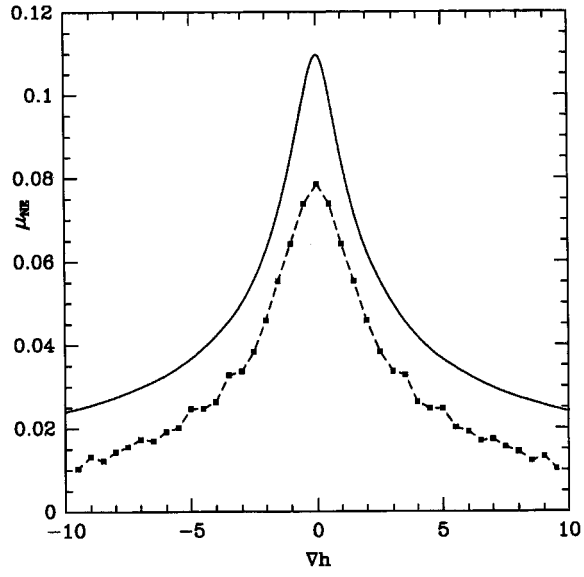

Figure 43. Inclination-dependent non-equilibrium chemical potential for the 1D Arrhenius model, at reduced inverse temperature $K_1/k_BT = 1{\cdot}15$ and deposition rate $F = 0{\cdot}01$. The symbols represent numerical results from simulations of a system of size $L = 40$, averaged over 10^7 Monte Carlo steps per site (10^5 monolayers) for each data point. The full curve is the result of the approximate analytic theory.

$$\langle \exp\{-[2K_1(n_x - d) + \mu_x]/k_BT\}\rangle = \frac{1}{Z}\sum_H \exp\{-[\mathscr{H}(H) + 2K_1(n_x - d) + \mu_x]/k_BT\}$$

$$= \left\{\sum_H \exp[-\mathscr{H}(H)/k_BT]\right\}^{-1}$$

$$\times \sum_{H'} \exp[-\mathscr{H}(H')/k_BT] = 1, \tag{5.88}$$

and equation (5.84) follows.

Turning the relation (5.84) around, we see that the quantity

$$\mu(\mathbf{x}) \equiv k_BT \ln\langle \exp(-2K_1 n_x/k_BT)\rangle + 2dK_1 \tag{5.89}$$

provides a direct measure of the local chemical potential which can be used also in a non-equilibrium situation. In figure 43 we show a measurement of the chemical potential as a function of inclination, for the 1D Arrhenius MBE model with parameters $K_1/k_BT = 1{\cdot}15$ and $F = 0{\cdot}01$. The chemical potential is seen to be increased relative to its equilibrium value $\mu = 0$, with a distinct peak at zero slope. In a slope expansion as in equation (3.13) this implies a *negative* value of λ_2, which is estimated from the data to be $\lambda_2 \approx -0{\cdot}015$. It should be no surprise that this is a small number: since μ_{NE} is induced by the growth, its scale is set by the deposition rate F. This will be made more precise shortly.

To gain some insight into the behaviour of the chemical potential, we note that (5.82) can be expressed as [360]

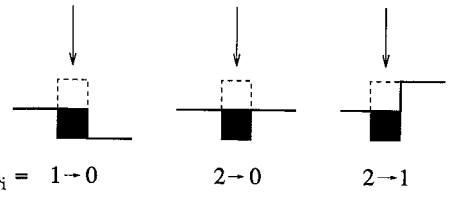

Figure 44. Changes in the local coordination numbers n_i owing to the deposition of atoms.

$$M = \sum_{n=0}^{2d} c_n \exp(-2K_1 n/k_B T), \tag{5.90}$$

where c_n is the probability that a surface atom has n lateral nearest neighbours. The c_n depend on the surface inclination even in thermal equilibrium. For example, in $d = 1$ all sites have $n = 1$ for strongly tilted surfaces, so that $c_1 \to 1$ and $c_{0,2} \to 0$ for $\nabla h \to \pm\infty$. It is only the specific linear combination (5.90) that is slope independent in equilibrium, due to the subtle constraint of detailed balance. Conversely, it is evident that virtually *any* non-equilibrium influence disrupting detailed balance will also make M a slope-dependent quantity [249].

In the case of growth, one expects that the deposition beam will create isolated adatoms and thereby increase c_0 relative to the c_n with $n > 0$. Since c_0 enters the sum (5.90) with the largest coefficient, this results in an overall increase of M, and also of the chemical potential $\mu = k_B T \ln M + 2dK_1$. On the other hand, for large slopes it is easy to see that sites with $n = d$ will dominate, thereby resetting M and μ to their equilibrium values $M = \exp(-2dK_1/k_B T)$, $\mu = 0$. Consequently, the behaviour of the non-equilibrium chemical potential depicted in figure 43, that is $\mu_{NE} > 0$, with a peak at zero inclination and $\mu_{NE} \to 0$ for large slopes, should be generally valid.

For the 1D case a simple scheme can be devised to approximately calculate the non-equilibrium chemical potential. Let g_{mn} denote the probability that deposition onto a site occupied by an atom with m lateral nearest neighbours will create an atom with n lateral nearest neighbours. Non-zero off-diagonal elements of g are g_{10} (creation of an isolated adatom on a step edge), g_{20} (creation of an adatom on a flat portion of the surface) and g_{21} (deposition below a step edge) (see figure 44). For a 1D equilibrium surface governed by the Hamiltonian $\mathcal{H}_1$ in equation (5.10), the g_{mn} are easily calculated as a function of surface inclination. To leading order in the deposition flux, the changes δc_n in the coordination number densities can then be expressed as

$$\delta c_n = F \sum_m (g_{mn} - g_{nm}), \tag{5.91}$$

which, inserted into equation (5.90), yields the changes in M and in μ. The result of this calculation is shown as the full curve in figure 43. The overall behaviour of the chemical potential is well reproduced, though the magnitude is considerably overestimated. The situation appears to be similar, in this respect, to the calculation of the slope-dependent current in section 5.2.3.

5.4.2. *Conserved non-equilibrium dynamics*

In their original work on equation (5.80) with conserving noise, Sun *et al.* [359] proposed a microscopic realization based on the restricted solid-on-solid (RSOS)

model of Kim and Kosterlitz [183]. It was subsequently pointed out by Rácz *et al.* [250] that this model in fact possesses detailed balance, and therefore cannot display the nonlinear term in equation (5.80). Rácz *et al.* [250] showed how to break detailed balance in the RSOS rule; however, in the process a non-equilibrium surface current was also generated [92]. As a consequence, the large-scale dynamics of their model contains a Laplacian term $\nu_1 \nabla^2 h$ which supersedes the effect of the nonlinearity (see section 3.3), except at a special parameter value where ν_1 is (close to) zero.

From the discussion in the preceding section it is clear how to construct a model of conserved surface dynamics that is described by the conserved KPZ equation (5.80) for *arbitrary* parameter values. We have seen that the essential effect of the deposition current in the Arrhenius MBE model is to upset the delicate balance between the terms in the sum (5.90) defining the local chemical potential, such that the conserved KPZ nonlinearity is generated in the large-scale equation of motion. Thus, the task is to break detailed balance *without* violating the symmetry of the Arrhenius model that disallows a net non-equilibrium surface current (see section 5.2.2).

It is easy to imagine non-equilibrium processes that have this effect, and that do not change the amount of mass on the surface. For example, consider a surface exposed to a beam of energetic ions. The kinetic energy provided by the beam allows particles on the surface to move to neighbouring sites without thermal activation [361, 362]. Within an Arrhenius-type model, we may suppose that an adatom is 'kicked' by the beam with probability p, and performs a thermal jump with probability $1 - p$. The total jump rate is then

$$R_{\mathbf{xy}} = p + (1 - p) \exp(-2K_1 n_{\mathbf{x}}), \tag{5.92}$$

which is still independent of the final site $\mathbf{y}$, but no longer satisfies detailed balance; the deviation from equilibrium is governed by the parameter p, the analogue of the deposition flux in the MBE case. A straightforward simulation verifies that an inclination-dependent non-equilibrium chemical potential is indeed generated [249]. Since the total volume of the solid is conserved, one therefore expects this model to be described asymptotically by the conserved KPZ equation, equation (5.80), with conserving noise.

A simpler (and computationally more efficient) rule with the same properties is obtained as follows. A site $\mathbf{x}$ is chosen at random. It is checked whether the height at any one of the neighbouring sites *exceeds* $h_{\mathbf{x}}$, by at least one lattice spacing. If so, the particle at $\mathbf{x}$ is regarded as immobile and a new site is chosen; if not, the particle at $\mathbf{x}$ is moved to a randomly chosen neighbour site. Note that, under this rule, particles incorporated into a perfect, flat singular surface are mobile. Simulation results for this rule are shown in figures 45 and 46. The exponents are in good agreement with the theoretical predictions for equation (5.80), which we describe next.

5.4.3. *Properties of the conserved Kardar–Parisi–Zhang equation*

One-loop renormalization group analyses of equation (5.80) were reported by Sun *et al.* [359] for the case of conserved noise, and by Lai and Das Sarma [121] for the case of non-conserved noise; the latter work was extended by Tang and Nattermann [122] by including the effect of a lattice pinning potential, which turns out to be irrelevant on large length scales. In the conserved case the lattice potential gives rise to a Kosterlitz–Thouless-type roughening transition in $d = 2$ [363]. A

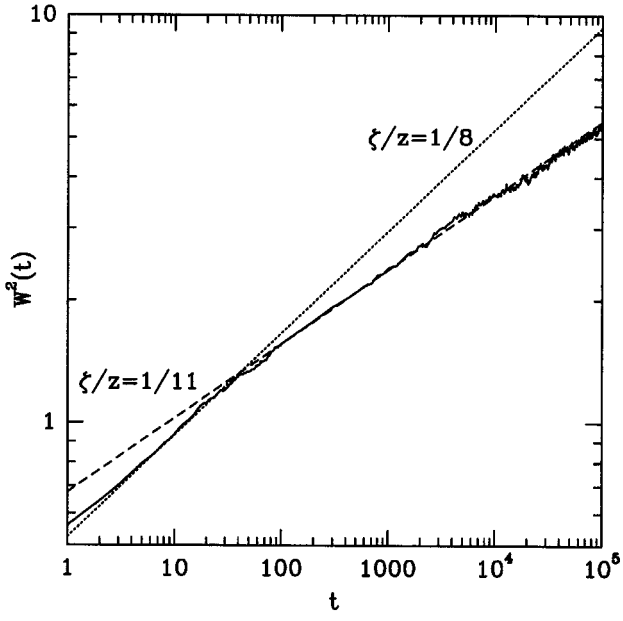

Figure 45. Simulation results for the simple symmetric non-equilibrium surface diffusion model described in the text. The full curve shows the surface width (squared) as a function of time, for a 1D surface of length $L = 2 \times 10^5$. The dotted line indicates an initial Mullins regime, with $\zeta/z = 1/8$, while the broken line $W^2 \approx 0{\cdot}68t^{2/11}$ shows the asymptotic behaviour predicted by the conserved KPZ equation (5.98).

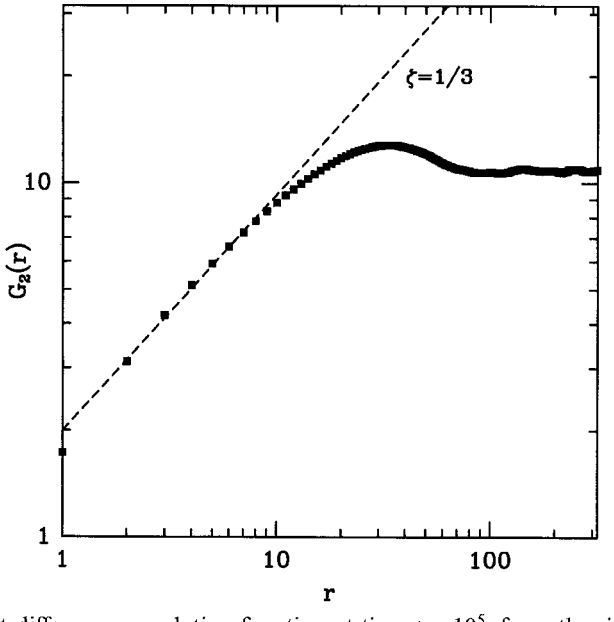

Figure 46. Height-difference correlation function at time $t = 10^5$, from the simulation shown in figure 45. The broken line indicates the predicted roughness exponent $\zeta = 1/3$ (see equation (5.97)), $G_2 \approx 2{\cdot}0r^{2/3}$.

two-loop analysis of the non-conserved case has been reported by Das Sarma and Kotlyar [364].

These calculations suggest a remarkably simple picture. We noted above in section 4.3 that the lack of coupling between the average motion of the surface, and the internal fluctuations, which is a common feature of all ideal MBE processes described by equations of the type (5.3), enforces the *exact* exponent identity $z = d + 2\zeta$ (equation (4.27)). Replacing the deposition noise η by the conserving noise η_c defined by equation (3.17) merely shifts the dimensionality $d \to d + 2$ and implies the relation

$$z = d + 2 + 2\zeta. \tag{5.93}$$

While the scale independence of the noise strength is an exact property of these equations, the one-loop calculations indicate that the coefficient λ of the nonlinearity in equation (5.80) is also invariant under rescaling, implying the second identity

$$\zeta + z = 4, \tag{5.94}$$

the analogue of the Galilean invariance relation (4.7) for the KPZ equation. The relation (5.94) was implicitly used by Villain [20] in a Flory-type estimate of the scaling exponents.

The invariance of λ is commonly believed to hold to all orders [364], though this has not been rigorously established; it is not clear what symmetry plays the role of Galilean invariance in the conventional KPZ context (see [122, 250, 359] for discussions of this point). Here we follow the common view and *assume* that λ is scale independent. This leaves us in the fortunate situation encountered previously in the treatment of the 1D KPZ equation in section 4.1: having two invariant quantities at our disposal, both exponents and scaling forms can be determined exactly, up to universal scaling functions and amplitudes [177]. Using equations (4.27) and (5.94) we obtain the exponents [20, 121]

$$\zeta = (4 - d)/3, \quad z = (8 + d)/3, \quad d \leq d_c = 4, \tag{5.95}$$

for equation (5.80) with non-conserved noise, and [359]

$$\zeta = (2 - d)/3, \quad z = (10 + d)/3, \quad d \leq d_c = 2, \tag{5.96}$$

for the conserved noise case.

Specializing to the case of conserved noise in $d = 1$ dimensions, we can further introduce universal amplitudes through the relations

$$G_2(r, t) \approx a_2(D_c/\lambda)^{2/3} r^{2/3}, \quad r \ll \xi(t), \tag{5.97}$$

for the stationary height difference correlation function (see section 3.2), and

$$W^2(L, t) \approx c_2(D_c^4/\lambda^3)^{2/11} t^{2/11}, \quad \xi(t) \ll L. \tag{5.98}$$

For the simple model described in section 5.4.2, a measurement of the average jump rate as a function of surface inclination (which is the equivalent of the quantity M defined in equation (5.82) for the Arrhenius growth model) yields the value $\lambda \approx 0{\cdot}17$ (see figure 47). Together with the prefactors of G_2 and W^2 obtained from the data in figures 45 and 46, this allows us to estimate the universal amplitude ratio

$$\mathscr{R} \equiv c_2^{11/12}/a_2 \approx 0{\cdot}47. \tag{5.99}$$

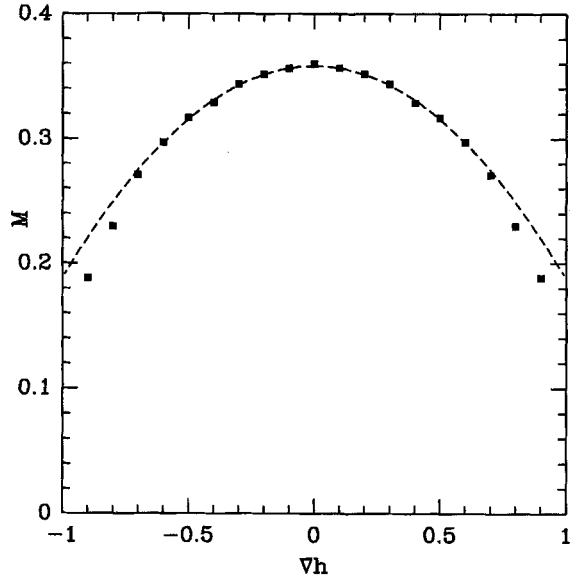

Figure 47. Average jump rate M as a function of inclination for the non-equilibrium surface diffusion model described in section 5.4.2. The data were obtained from simulations of a system of size $L = 200$; each point constitutes an average over 10^7 attempted moves per site. The broken curve is a parabolic fit $M = 0{\cdot}358 - 0{\cdot}17(\nabla h)^2$. The large-scale equation of motion for this model is, in analogy to equation (5.83), $\partial h/\partial t = (1/2)\nabla^2 M$; hence comparison with equation (5.80) shows that $\lambda \approx 0{\cdot}17$.

In view of the somewhat uncertain status of the scaling relation (5.94), it is clearly desirable to confirm the predictions (5.95) and (5.96) for the scaling exponents through a direct numerical integration of equation (5.80). Chakrabarti [365] carried out such a study for the equation with conserved noise, and found agreement with equation (5.96). For the case of non-conserved noise the numerical integration was first attempted by Tu [366] and Moser [367]. Both authors encountered severe difficulties in integrating the equation for $d = 1$, which they attributed to the large value $\zeta = 1$ of the roughness exponent (see equation (5.95)). Tu found the temporal behaviour of the width to be consistent with the prediction, $W \sim t^{1/3}$, up to a finite transition time at which the interface developed singularities and the algorithm broke down. He conjectured that the development of finite time singularities might be an intrinsic feature of the *deterministic* conserved KPZ equation (5.80) with $\eta = 0$.

This seems unlikely in view of recent analytic work by Putkaradze, Bohr and Krug [368], who show that (i) cusp-like singularities can develop in finite time, but only if the stabilizing linear term in equation (5.80) is absent, i.e. if $\nu = 0$, and (ii) the solutions remain bounded even when singularities do develop. Nevertheless, it is worth pointing out that the behaviour of the deterministic, conserved KPZ equation is less well understood (and potentially more interesting) than its non-conserved counterpart, which can be exactly linearized using the Cole–Hopf transformation [207] (see also section 4.5).

A recent numerical integration study by Kim and Das Sarma [369] did not report any stability problems, and gave the estimates $\zeta = 1{\cdot}02 \pm 0{\cdot}03$, $\zeta/z = 0{\cdot}34 \pm 0{\cdot}01$ in agreement with equation (5.95).

In $d = 2$ dimensions the equation is numerically better behaved. Tu [366] estimates that $\zeta/z = 0{\cdot}21 \pm 0{\cdot}03$ and $\zeta \approx 0{\cdot}71$, in reasonable agreement with the predictions 1/5 and 2/3, respectively. The extensive simulations of Moser [367] yield the estimate $\zeta/z = 0{\cdot}183 \pm 0{\cdot}010$, somewhat smaller than predicted, however, the deviation is attributed to a finite-time effect. Thus, at present there appears to be no compelling reason to doubt the values (5.95) of the scaling exponents (see, however, section 5.5.2).

5.4.4. *Kinetic roughening and layer-by-layer growth*

So far in this article we have been concerned with the *asymptotic*, large distance/long time behaviour of kinetically roughened surfaces. From a practical point of view, it is often more relevant to understand the early and intermediate stage of a deposition process, say, the growth of the first dozens or hundreds of monolayers. Provided the surface is close to a singular orientation, in the sense that the substrate step spacing l greatly exceeds the diffusion length l_D, this early time regime is typically *oscillatory*, that is, the surface morphology (characterized, for example, by the step density or the width) changes periodically as a function of the number of deposited layers. The oscillations can be detected using RHEED [338, 370, 371] and other techniques [372, 373], and are taken as evidence for an approximate *layer-by-layer* growth mode. In perfect layer-by-layer growth, the $(n+1)$th layer nucleates only after the nth layer has been completed. In this limit, the step density and the surface width drop to zero at integer values of the coverage θ, and reach maxima at half-integer coverages. In reality, the oscillation amplitude is reduced due to the fact that more than two layers grow simultaneously and, moreover, the amplitude decreases with time as the growth front broadens.

The connection between the damping of growth oscillations and the kinetic roughening of the surface is intuitively obvious, but a satisfactory theory that captures the basic mechanism—the 'dephasing' of spatially separated regions due to the beam fluctuations [374]—is still lacking. Cohen *et al.* [311] studied a variety of mean-field models (without lateral structure) for the time evolution of the layer coverages, and found either persistent or damped oscillations depending on the assumptions made regarding interlayer transport. Kang and Evans [253] explored the relationship between surface roughening and oscillation damping in simulations of models for low-temperature epitaxy, which include only downward funnelling and transient mobility [99] but no thermal diffusion. They observed empirically that the oscillation amplitude decays as $\exp(-CW^2)$, where W denotes the surface width and the constant $C \approx 9{\cdot}9$.

This result was subsequently explained by Bartelt and Evans [344] under the assumption that the height probability distribution $P_j = \text{Prob}\,[h = j]$ (note that $P_j = \theta_j - \theta_{j+1}$, where θ_j is the coverage of the jth layer) can be written as a shifted shape function f,

$$P_j = w^{-1} f\,[(j - \theta)/w], \tag{5.100}$$

with the normalization $\int \mathrm{d}s\, f(s) = \int \mathrm{d}s\, s^2 f(s) = 1$. The width parameter w in equation (5.100) equals the conventionally defined surface width [311]

$$W^2 = \sum_j (j - \theta)^2 P_j \tag{5.101}$$

only asymptotically for $w \to \infty$, when the discrete layer structure becomes irrelevant. The form (5.100) for the height probability distribution certainly holds in the limit of perfect layer-by-layer growth, where

$$f(s) = 1 - |s|, \quad |s| \leq 1, \tag{5.102}$$

and $w = 1$. Bartelt and Evans used the ansatz (5.100) to compute the kinematic Bragg intensity at the out-of-phase condition [253]

$$I_{\text{Bragg}} = \left[\sum_j (-1)^j P_j \right]^2. \tag{5.103}$$

For a Gaussian shape function f one obtains the simple expression

$$I_{\text{Bragg}} = 4 \cos^2 (\pi\theta) \exp (-\pi^2 w^2). \tag{5.104}$$

Thus for $w, W \to \infty$ the oscillation amplitude decays as $\exp(-CW^2)$ with $C = \pi^2 \approx 9{\cdot}87$. It can be demonstrated that the oscillatory contribution to the surface width (5.101) decays with the same leading behaviour [375].

In the context of simulations of collective diffusion models, the relationship between oscillation damping and growth conditions was first studied by Gilmer [376, 377] and subsequently explored in depth by Vvedensky and co-workers [267, 269, 272, 339]. In recent simulations, Wolf and co-workers [261, 378] discovered a power law relationship between the damping time scale θ_c (which measures the number of layers that can be grown in a layer-by-layer fashion) and the dimensionless ratio D_s/F of diffusion-to-deposition rate or, equivalently, the diffusion length $l_D \sim (D_s/F)^\gamma$ (see equation (5.23)). As an application of the considerations in earlier parts of this section, we show here how such a relationship can be derived from continuum theory. Of course, the continuum equations do not contain any growth oscillations, which are distinctly a lattice effect. However, it should have become clear from the previous discussion that the damping sets in roughly when the long wavelength contribution to the surface width becomes of the order of the monolayer thickness, since then different regions on the surface fall out of phase. Therefore, our strategy will be to compute the surface width W in the asymptotic regime, where continuum theory applies, and to extrapolate to early times in order to extract the coverage θ_c at which $W(\theta_c) \approx 1$.

The model considered by Wolf [261] is a collective diffusion model in which only isolated adatoms move (dimers are stable); there are no step edge barriers, and consequently no growth-induced surface current (compare to section 5.2.2). The appropriate large-scale description is therefore provided by the conserved KPZ equation (5.80) with non-conserved noise. The non-renormalization results mentioned in section 5.4.3 imply that the surface width can be written, up to a universal constant of order unity, as [177]

$$W \approx [(D^4/\lambda^d) t^{4-d}]^{1/(8+d)}. \tag{5.105}$$

The shot noise strength D is equal to the deposition flux F, and hence what remains is to express the nonlinear coupling λ in terms of l_D and F. This can be done using BCF theory. Note first that the non-equilibrium chemical potential μ_{NE} may be approximately identified with the (excess) density of adatoms generated by the deposition flux [20]. On a singular surface the adatom density is given by Fl_D^2/D_s (equation (5.29)), while on a vicinal surface with step spacing $l < l_D$ it is reduced to

Fl^2/D_s (equation (5.15)). The inclination dependence of this quantity can therefore be written, close to singular orientations, as

$$n(\nabla h) \approx (Fl_D^2/D_s)[1 - (l_D \nabla h/a)^2 + \mathcal{O}(|\nabla h|^4)], \tag{5.106}$$

where we have used $\nabla h \approx a/l$ (cf. section 5.2.1). This induces a current $J = -D_s \nabla n$, the divergence of which gives rise to the conserved KPZ nonlinearity with coefficient

$$\lambda \approx Fl_D^4 a^{-1}. \tag{5.107}$$

Measuring height in units of a, we can therefore rewrite equation (5.105) as

$$W \approx (\theta/\theta_c)^{(4-d)/(8+d)}, \tag{5.108}$$

with a characteristic coverage

$$\theta_c \approx l_D^{4d/(4-d)} \tag{5.109}$$

in dimensionalities $d \leq 4$. For $d > 4$ the surface does not roughen, and persistent oscillations are possible [374].

For the case of stable dimers the exponent γ in equation (5.23) is equal to $1/(2d+2)$ [299], so that equation (5.109) predicts $\theta_c \sim (D_s/F)^{1/3}$ in $d = 1$, in good agreement with the estimate $\theta_c \sim (D_s/F)^{0.33 \pm 0.01}$ obtained numerically by Brendel [378]. It thus appears, somewhat surprisingly, that the extrapolation from the asymptotic regime is able to capture the essence of the oscillation damping phenomenon. It is clear that the same strategy can be applied to other continuum equations of kinetic roughening, provided the coefficients entering the prefactor of W can be computed (see section 4.2 for a discussion in the KPZ context). Here we merely remark another interesting consequence of the continuum approach, namely the appearance of a new lateral length scale associated with the damping. Using the results of section 5.4.3 we can compute the prefactor of the stationary height difference correlation function $G_2(r, t = \infty)$, and ask at what lateral length scale r_c the relative height fluctuations become of order unity, $G_2(r = r_c, t = \infty) = 1$; equivalently, r_c equals the dynamic correlation length $\xi(t)$ at the critical coverage θ_c. One obtains

$$r_c \sim l_D^{4/(4-d)} \sim \theta_c^{1/d}, \tag{5.110}$$

which much exceeds l_D. Physically, r_c is the size of regions which oscillate in phase; in systems of lateral extent less than r_c the growth oscillations persist forever.

5.5. *The universality classes of ideal molecular beam epitaxy*

In this section we have attempted to provide microscopic derivations of the non-equilibrium contributions to the conserved growth equation (3.15), which allow us, at least in principle, to estimate their magnitude under conditions of real MBE growth. The relevance of these terms for the large-scale surface fluctuations has already been discussed in section 3.3. The emerging picture is that of a 'nested' sequence of universality classes:

(i) Under generic circumstances, the behaviour is dominated by the linear part of the non-equilibrium surface current $J_{NE}(\nabla h)$. Depending on the sign of the leading coefficient ν_1 in the gradient expansion (3.14), one obtains either Edwards–Wilkinson (EW) scaling, with logarithmic roughness in

$d = 2$ surface dimensions (see section 3.2), or unstable growth of the kind discussed in section 5.3.

(ii) If, for reasons of symmetry (or, more realistically, because asymmetric configurations such as step edges are dynamically unimportant), $J_{NE} \equiv 0$, the most relevant terms are those generated by the non-equilibrium chemical potential, equation (3.13), and one expects the surface to be described by the conserved KPZ equation with the exponents (5.95) (at the conserved KPZ fixed point the geometric nonlinearities in equation (3.15) are believed to be irrelevant [121]).

(iii) Finally, if the symmetry of the system not only prohibits non-equilibrium surface currents, but also imposes an invariance of the dynamics under arbitrary tilts, all conceivable nonlinearities are irrelevant and one is left with a surface described exactly by the noisy Mullins equation, with $\zeta = 1$ and $z = 4$ in $d = 2$ (see section 3.4).

Strictly speaking, this list does not exhaust all possibilities. For example, one should also consider the case where both $J_{NE} \equiv 0$ and $\mu_{NE} \equiv 0$ in equation (3.15), and ask what scaling behaviour results from the interplay of the geometric nonlinearities with the non-conserved shot noise [90, 91]. As was mentioned in section 3.3, this problem is difficult to control, because all geometric nonlinearities are relevant below $d = 2$. However, it is hard to imagine a situation where $\mu_{NE} \equiv 0$, except for the case of tilt invariance, which suppresses the geometric nonlinearities at the same time. Thus, for the present discussion we restrict our attention to the cases (i)–(iii).

The purpose of this section is to examine to what extent the available numerical results on ideal MBE growth are consistent with the picture sketched above. The case of unstable growth has already been dealt with in section 5.3, and will not be discussed here. A preliminary assessment of kinetic roughening *experiments* is given in section 5.6.

5.5.1. *Computer simulations*

5.5.1.1. *Limited mobility models.* A surprising result of the numerical measurement of nonequilibrium surface currents in [92] was the prediction of a crossover to Edwards–Wilkinson scaling for the Wolf–Villain (WV) model both in one and two substrate dimensions; the crossover time was estimated to be $t_c \approx 10^6$ ML in $d = 1$, and $t_c \approx 2 \times 10^4$ ML in $d = 2$. Direct numerical evidence for such a crossover has been presented in several recent studies [258, 259, 263, 379–381]. Moreover, the measurement of surface currents for a variety of limited mobility rules introduced by Das Sarma and Ghaisas [256] indicates that J_{NE} is non-zero generically for these models [382]. This is to be expected, since their dynamics, which is governed by a comparison of local coordination numbers (see section 5.1.1), does not possess any symmetries that would enforce $J_{NE} \equiv 0$; the only exception is the 1D rule DT1 (section 5.2.2). Both uphill and downhill currents have been observed [382]. The most spectacular manifestation of uphill currents and unstable growth was displayed by Šmilauer and Kotrla [263, 383] in a study of the WV model in $d = 3$ and $d = 4$ substrate dimensions.

However, clean and unambiguous EW scaling is observed in these models only when the dynamics favours downhill moves in some obvious way, through funnelling [252, 253] or an explicit suppression of upward jumps [256, 384]; inclusion of next-

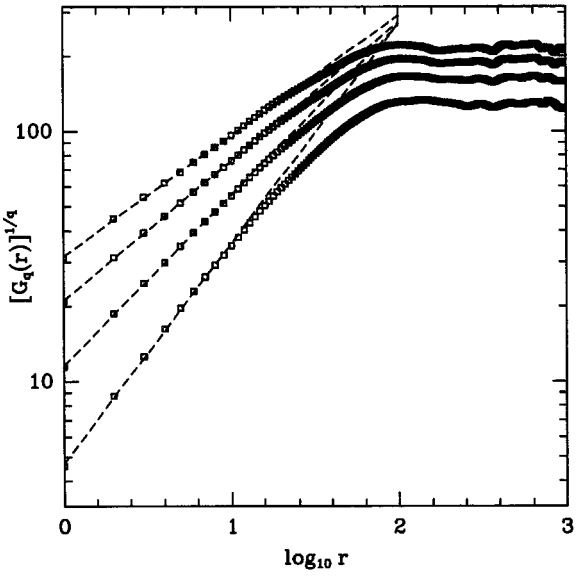

Figure 48. Generalized height difference correlation functions $G_q(r)$, defined in equation (5.111), from a simulation of the DT1 limited mobility model. From top to bottom, the data sets correspond to $q = 4$, 3, 2 and 1 [112].

nearest-neighbour interactions also seems to speed up the crossover [258, 259]. In all other cases the downhill currents are very weak, and the scaling on numerically relevant length and time scales is governed by some *effective continuum theory* that is often difficult to identify. In one dimension this effective theory would also be expected to govern the *asymptotic* behaviour of the DT1 model, which has no EW term.

Early results obtained for the surface width $W(L, t)$ in *one dimension* suggested that the effective behaviour might be described simply by the linear noisy Mullins equation [101, 132], but recent studies of the full height-difference correlation function point at a much more complex scenario [107, 108, 112]. It appears that limited mobility models in one dimension generically show anomalous scaling of correlation functions, as in equation (3.49), with exponents α and $\tilde{\zeta}$ that cannot easily be associated with continuum theories. Microscopically, the anomalous behaviour manifests itself in an extremely broad (stretched exponential) distribution of local height differences, with moments scaling according to equation (5.61). This can lead to *multiscaling* of the generalized height-difference correlation functions G_q,

$$G_q(r) = \langle |h(x + r) - h(x)|^q \rangle \sim r^{q\tilde{\zeta}_q}, \tag{5.111}$$

with q-dependent exponents $\tilde{\zeta}_q$, through the dominance of rare, large slope fluctuations for large q [112] (see figure 48). Phenomenologically, the behaviour is reminiscent of the intermittent velocity fluctuations in fully developed fluid turbulence [112, 385].

The anomalous scaling exponents are found to be distinctly *non-universal.* Schroeder [386] has investigated the effect of increasing the incorporation range in the WV model (see section 5.1.1). He finds that this dramatically decreases the value

of α in equation (3.49), while leaving the roughness exponent $\tilde{\zeta}$ essentially unchanged. Analogous, though somewhat less pronounced behaviour was reported recently for the DT model [264]. Increasing the incorporation range from 1 to 20 lattice sites changes the roughness exponent $\tilde{\zeta}$ from 0·67 to 0·76, but the step size exponent α from 0·71 to 0·13; at the same time the scaling exponents $\tilde{\zeta}_q$ in equation (5.111) become essentially independent of q. It appears, therefore, that the long wavelength fluctuations described by $\tilde{\zeta}$ are not influenced by the divergence of the short-range slope fluctuations expressed by the scaling $G_2(1, t) \sim \xi^{2\alpha}$. This suggests [107] a picture of a conventionally rough surface 'decorated' by anomalous local fluctuations, which can be eliminated by local smoothening, for example by increasing the diffusion range.

The actual, possibly universal value of the roughness exponent found in these models is close to $\tilde{\zeta} = 3/4$, a result that has been associated [107, 379] with the continuum equation

$$\frac{\partial h}{\partial t} = \nu_3 \nabla (\nabla h)^3 - \kappa \nabla^4 h + \eta, \tag{5.112}$$

which is obtained if the next-to-leading, cubic term in the gradient expansion (3.14) of J_{NE} dominates over the leading linear term. Balancing the nonlinear term in equation (5.112) against the time derivative one obtains the relation $2\zeta + z = 4$, which, together with the general exponent identity (4.27), yields [121, 256]

$$\zeta = \tilde{\zeta} = (4 - d)/4, \quad z = (4 + d)/2, \tag{5.113}$$

and hence $\zeta = 0{\cdot}75$ in $d = 1$. However, the validity of this result, and in particular its relevance for the description of microscopic growth models, must be questioned. It is easy to see [364, 369] that the cubic nonlinearity in conjunction with the noise in equation (5.112) gives rise to an effective surface diffusion current which is in fact *linear* in the imposed surface inclination, with a coefficient $\tilde{\nu}_1 \approx \nu_3 \kappa / D$. Thus, as it stands, equation (5.112) gives rise to either Edwards–Wilkinson scaling (if $\nu_3 > 0$), or to unstable growth (if $\nu_3 < 0$). Different behaviour (possibly described by equation (5.113)) can be expected only if a 'bare' Laplacian term $\nu_1 \nabla^2 h$ is added to the right hand side of equation (5.112), and the coefficient ν_1 is tuned such that $\nu_1 + \tilde{\nu}_1 = 0$. It seems unlikely that such fine tuning would take place in any 'generic' microscopic model. In addition, the association with equation (5.112) certainly cannot hold for the DT1 model, where the cubic nonlinearity is excluded by symmetry (section 5.2.2); nevertheless the measured exponent $\tilde{\zeta}$ is very similar to that of the WV model [112, 264, 382].

In three cases [121, 126, 260] the scaling behaviour of 1D limited mobility models has been reported to agree with the predictions (5.95) of the conserved KPZ equation; however, in two of these only the behaviour of the surface width was analysed, which is not sensitive to anomalous scaling [107, 382]. Indeed, a recent reanalysis [264] of the model suggested by Lai and Das Sarma [121] clearly revealed anomalous scaling, with a roughness exponent $\tilde{\zeta} \approx 0{\cdot}65$ rather than 1. For the 'local minimization' model of Kim and Das Sarma [126] (see section 3.4) the absence or presence of anomalous scaling has not been established. So far only the restricted SOS model of Kim, Park and Kim [260] has been convincingly demonstrated to conform to equation (5.95); in this model anomalous scaling is suppressed by definition, since the local slopes can only take a finite number of values.

In 2D limited mobility models the effects of anomalous scaling appear to be reduced, but still detectable [382]. Šmilauer and Kotrla [263, 379] estimate that $\alpha/z \approx 0{\cdot}05$ for the $d = 2$ WV model, as compared to $\alpha/z \approx 0{\cdot}19$ in one dimension with nearest-neighbour incorporation; in fact the increase of $G_2(1, t)$ may be only logarithmic in t [263, 381]. The roughness exponent is $\tilde{\zeta} = 0{\cdot}65 \pm 0{\cdot}03$, which supports the identification [379, 384] of the conserved KPZ equation as the preasymptotic universality class of the model. For some of the variants considered by Das Sarma and Ghaisas [256], the measured exponents are closer to the values (5.113) associated with the cubic equation (5.112) [387]. As mentioned already, the reason for the applicability of this equation needs to be clarified. Unfortunately, none of the 2D models studied so far [256] seems to possess a symmetry analogous to the 1D DT1 model, which would exclude a crossover to EW behaviour and therefore facilitate the study of the preasymptotic universality class.

5.5.1.2. *Collective diffusion models.* We have shown in this section that (i) the Arrhenius model of MBE has no net surface current, and (ii) a non-equilibrium chemical potential $\mu_{\mathrm{NE}} > 0$, quantified by the expression (5.89), is generated under growth conditions. Thus, the large-scale behaviour of this model should be governed *asymptotically* by the conserved KPZ equation (5.80) with non-conserved noise. This conclusion is supported by simulations of Wilby, Vvedensky and Zangwill [388] in dimensionalities $d = 1$, 2 and 3, though the scaling range in these simulations, especially in $d = 1$ and 3, was quite small. Moreover, these simulations evaluated only the temporal increase of the surface width, which contains no information about spatial correlations.

Recent detailed studies [257, 263, 264, 312] have clearly demonstrated the presence of anomalous scaling in the Arrhenius model, with the same nonuniversal features that were earlier found in limited mobility models. The exponent α describing the divergence of the local height gradient is found to decrease with increasing temperature and/or decreasing deposition rate [257, 263, 264]. The roughness exponent $\tilde{\zeta}$ also seems to depend somewhat on the deposition conditions. In one dimension, Siegert and Plischke [312] report $\tilde{\zeta} \approx 1{\cdot}05$ at $(F/\omega_0)\exp(E_{\mathrm{S}}/k_{\mathrm{B}}T) = 0{\cdot}05$ and $E_{\mathrm{N}}/k_{\mathrm{B}}T = 2$, while Kotrla and Šmilauer [263] obtain values in the range $\tilde{\zeta} = 0{\cdot}73$–$0{\cdot}77$ for $10^{-4} \leq (F/\omega_0)\exp(E_{\mathrm{S}}/k_{\mathrm{B}}T) \leq 10^{2}$ and $E_{\mathrm{N}}/k_{\mathrm{B}}T = 3{\cdot}5$–5, and Das Sarma *et al.* [264] estimate $\tilde{\zeta} = 0{\cdot}61$–$0{\cdot}64$ under similar conditions (see section 5.1.2 for the definition of the model parameters). The latter two sets of values are close to those cited above for the limited mobility models, suggesting that a common universality class might still exist. However, such hopes are shattered by the 2D simulation results. Despite the fact that the anomalous scaling exponent α is quite small in $d = 2$—in fact Kotrla and Šmilauer [263] observe that the divergence of the local height gradient is typically logarithmic in time, rather than a power law—the measured values of the roughness exponent ($\tilde{\zeta} = 0{\cdot}4$–$0{\cdot}47$ [263] and $\tilde{\zeta} = 0{\cdot}31$–$0{\cdot}34$ [264]) are clearly incompatible with the conserved KPZ prediction $\zeta = 2/3$, *as well as* with the limited mobility results mentioned above. Thus, despite the encouraging early results of Wilby *et al.* [388], the question of the universality class of the Arrhenius model must be considered to be open.

The behaviour of the Metropolis model, defined by the Hamiltonian (5.10) and the jump rates (5.11), can be understood completely from the consideration of the surface current [92, 312]. For $q = 1$ one observes a considerable downhill current and clean EW scaling [277]. For $q = 4$ the current is uphill and the surface is unstable [89,

312]. Finally, for $q = 2$ the symmetry argument given in section 5.2.2 implies that the surface should be governed by the linear Mullins equation, in agreement with recent simulations [312].

Among the collective diffusion simulations with detailed balance violating diffusion algorithms mentioned in section 5.1.2, we discuss here only the careful work of Pal and Landau [286]. In their model, the suppression of upward jumps would be expected to induce a downhill current. Indeed, the logarithmic roughening characteristic of the 2D EW equation is observed, though the dynamic exponent is estimated to be $z = 1{\cdot}61 \pm 0{\cdot}02$, rather than the EW value $z = 2$; it appears, however, that the data are not inconsistent with $z = 2$.

5.5.1.3. *Models with bulk defects.* If bulk defects are allowed, the surface fluctuations are asymptotically governed by the KPZ equation, as was discussed already in section 5.1.3. In the present context it is worthwhile to recall that two recent studies [262, 264] have found clear evidence of anomalous scaling in the early time behaviour of such models, including quantitative agreement of the anomalous scaling exponents with those measured for certain SOS models [262]. This observation is important because it indicates that the anomalous scaling scenario is not solely an artifact of the ideal MBE assumptions.

5.5.2. *Anomalous scaling revisited*

The conclusion from the foregoing summary of simulation results is that the overall picture of the universality classes of ideal MBE is well confirmed; however, the status of class (ii)—models without growth-induced current but with tilt-dependent dynamics—remains unclear due to the additional complication of *anomalous scaling*. The issue is not academic, since it concerns also the (possibly extended) preasymptotic behaviour of generic systems in which the growth-induced currents are small. In this section we therefore briefly review what is presently known about the nature and origin of the phenomenon.

The working definition of anomalous scaling which has been adopted in this article refers to the divergence of local height gradients with time or system size, and the related fact that height difference correlation functions do not possess a finite limit for $t \to \infty$ and $L \to \infty$. This type of behaviour can be derived for the linear growth equations of section 3.2.3, and is observed numerically in the lattice models described in the previous section. It is, however, important to realize [107] that different mechanisms lead to similar real-space phenomenologies in the two cases. This can be appreciated by considering the structure factor $S(q, t)$ defined by equation (3.24). Under ideal MBE conditions, the most general scaling form for S is

$$S(q, t) = L^{-d} q^{-z} g(q\xi(t)), \quad \text{with } \xi \sim t^{1/z}, \quad g(s \to 0) \sim s^z. \tag{5.114}$$

The q^{-z} scaling of the prefactor and the behaviour of the scaling function g for small arguments are dictated by the nonrenormalization of the noise strength D (the decoupling between the centre-of-mass motion and the internal surface dynamics; see section 4.3), which implies that $S(q, t) \sim Dt/L^d$ for $q\xi \ll 1$. In contrast, no such constraints exist for the behaviour of g at *large* arguments. In the linear theories of section 3.2, one has $g(s \to \infty) = \text{const.}$ always. Under such conditions it is easy to check that a divergence of the height gradient

$$\langle(\nabla h)^2\rangle \sim \int_0^\infty \mathrm{d}q\, q^{d+1-z} g(q\xi) \tag{5.115}$$

can occur only below the characteristic dimensionality $d_c^{(2)} = z - 2$, in which case the anomalous scaling exponents are given by $\alpha = (d_c^{(2)} - d)/2$, $\tilde{\zeta} = 1$, as in the linear theory (section 3.2.3). Consequently, anomalous scaling with $\tilde{\zeta} < 1$, as is observed in the lattice models, *cannot be explained by this scenario.* Rather, it requires a power law divergence of the scaling function $g(s)$ for large arguments, $g(s) \sim s^\phi$. Provided

$$\phi > z - 2 - d, \tag{5.116}$$

the integral in equation (5.115) will then be infrared convergent, which gives $\langle(\nabla h)^2\rangle \sim \xi^\phi$ and allows us to identify

$$\alpha = \phi/2, \quad \tilde{\zeta} = (z - d - \phi)/2 = \zeta - \alpha \tag{5.117}$$

in terms of the anomalous scaling form (3.49). Here ϕ, and therefore α, is a truly independent exponent, and $\tilde{\zeta} < 1$ because of equation (5.116). If one insists on a scaling function $\tilde{g}$ which is constant for large arguments, the scaling form (5.114) has to be decorated by an additional power of $q\xi$,

$$S(q, t) = L^{-d}(q\xi)^\phi q^{-z}\tilde{g}(q\xi), \tag{5.118}$$

which is well confirmed by simulations [107, 382] (note that in these papers a different definition of the dynamic exponent z is used); as usual, the stationary ($t \to \infty$) scaling form is obtained from equation (5.118) by replacing ξ with L. Incidentally, equation (5.118) is precisely analogous to the way in which intermittency corrections appear in fluid turbulence [389].

As was pointed out already by Schroeder *et al.* [107], it is not easy to imagine a continuum theory that would give rise to the anomalous scaling form (5.118). On the other hand, the considerations collected in this section would seem to indicate that, provided the phenomenon of anomalous scaling can be explained by continuum theory at all, it must be somehow related to the conserved KPZ equation (5.80), possibly supplemented with higher-order nonlinearities; as was mentioned in section 3.3, infinite sequences of relevant higher-order terms exist in low dimensionalities. This observation [112] was the starting point for the recent work of Bhattacharjee, Das Sarma and Kotlyar [390], who attempted a perturbative calculation of anomalous scaling exponents for the generalized, conserved KPZ equation

$$\frac{\partial h}{\partial t} = -\nabla^2\left[\nu\nabla^2 h + \sum_{n=1}^{\infty} \lambda_{2n}(\nabla h)^{2n}\right] + \eta, \tag{5.119}$$

obtained from the gradient expansion (3.13) of the non-equilibrium chemical potential. The basic idea of the calculation is that each of the higher-order nonlinearities in equation (5.119) gives rise (in $d = 1$) to a logarithmic correction to the scaling exponents (5.95). By summing the series of logarithms one obtains a power law correction with an exponent that may depend on the coefficients λ_{2n} in equation (5.119), and therefore show the desired non-universal features. Of course, an explicit computation of exponents is not possible in this scheme, and it remains to be seen if a consistent theory of anomalous scaling can be constructed along these lines. At present, the phenomenon must be regarded as one of the major open challenges in the field of kinetic roughening theory.

5.6. *Kinetic roughening experiments*

Over the past few years, an increasing number of deposition experiments have been performed with the aim of verifying the dynamic scaling scenario, and estimating the universal scaling exponents widely advertised by theoreticians. In carrying out such experiments and interpreting their results in the light of theory, one is faced with two somewhat unrelated difficulties.

First, real surfaces are immensely more complex than the theorist's mental images. They typically display a wide variety of characteristic length scales, associated for example with reconstructions, grain boundaries, defects and impurities, and it is often hard to ensure that the phenomena occurring at the scale accessible to a particular experimental technique are indeed governed by the simple processes described by theoretical models; other roughening mechanisms compete with and may supersede the purely stochastic, noise-induced roughening of interest (see for example section 5.6.2). An additional complication is the substrate roughness, which can be quite comparable to that developed kinetically during growth (see section 3.2.5).

Second, all experimental techniques that can access the microscopic and mesoscopic scales of interest are, to a larger or lesser degree, *indirect* in the sense that the interpretation of data requires additional assumptions and theoretical input. For example, in order to extract the lateral height correlations from diffuse X-ray scattering data, a model for the full height–height correlation has to be assumed [116, 117] (very recently, Salditt *et al.* [392] have proposed a method which overcomes this restriction). We have seen in section 3.2.4 that the traditional ansatz [116, 391]

$$\mathscr{C}(s) = \exp(-cs^{2\zeta}) \tag{5.120}$$

for the scaling function in equation (3.54) in *not* supported by explicit calculations within the linear theory [115]; even worse, for nonlinear growth equations no analytic information about the shape of the correlation function is available. While it is possible, under favourable circumstances, to extract the value of the roughness exponent ζ in a model-independent way [393], the estimate for the correlation length ξ has been shown to depend sensitively on the choice of the scaling function [118].

These inherent difficulties place high demands on the versatility and inventiveness of the experimental investigation. To unambiguously determine that kinetic roughening is taking place, it is crucial that the *dynamic* development of the roughness be monitored (through the increase of the surface width W or the correlation length ξ, and preferably both) in addition to its spatial characterization through the roughness exponent ζ. This requires either the use of some *in situ* technique by which the surface morphology can be observed during growth, or the preparation of a sequence of samples with different film thicknesses (that is, deposition times) that are then investigated *ex situ*. An interesting third possibility is the growth of multilayer films, where the surface configurations at various stages of the deposition process are preserved in the bulk of the film in the form of solid–solid interfaces [353, 394, 395]. In order to overcome the limitations of any particular experimental probe of surface roughness, it is essential that the same system be investigated using different, complementary techniques [396].

Some of the problems described above can be avoided by a judicious choice of the experimental system. For example, recent work on equilibrium step dynamics

[397, 398] has demonstrated the great advantage of working with 1D objects (steps), which are easier to image and manipulate, allowing for a detailed quantitative comparison between theory and experiment. It would therefore seem promising to continue the study of kinetic step roughening during growth initiated by Lagally and co-workers [309]. However, it is clear that substantial progress can be made only when the scope of existing theory is broadened to at least qualitatively take into account the effects that dominate the physics of real surfaces.

A large body of experimental work, involving both vapour deposition and ion-beam erosion ('negative growth'), has recently been reviewed by Krim and Palasantzas [17]. We refer the reader to their article for a detailed discussion of the experiments, and highlight here only some of the general conclusions. We then briefly evaluate certain ambiguities in interpreting the experiments (section 5.6.2) and describe a class of 'rapidly roughening' systems which cannot be understood within conventional theories (section 5.6.3); these last two sections are intended primarily to suggest possible directions for future theoretical research.

5.6.1. *Conserved and non-conserved growth*

First of all, the theoretical distinction between non-conservative (KPZ) and conservative (ideal MBE) growth appears to be mirrored in reality at least to the extent that vapour deposition experiments often yield exponents consistent with conservative growth equations (see below), while ion-beam erosion (which clearly violates volume conservation [202, 399]) does not (see, however, the experiment of Yang *et al.* on ion-sputtered Si(111), which shows anomalous scaling consistent with the noisy Mullins equation [114]). In one erosion experiment (Ar^+ erosion of pyrolytic graphite) scaling exponents consistent with the KPZ equation were reported [400]. For the second large class of non-conservative growth processes—the growth of amorphous films—the experimental evidence is less encouraging. While the observation of clean Edwards–Wilkinson scaling in amorphous W/Si multilayers [395] could be, optimistically, interpreted as preasymptotic KPZ behaviour, an experiment with amorphous Si designed explicitly to search for KPZ scaling [401] failed to detect any temporal increase in roughness at all.

Krim and Palasantzas [17] point out that the large majority of vapour deposition experiments yield roughness exponents in the range 0·7–1·0, squarely between the values $\zeta = 2/3$ predicted by the conserved KPZ equation (equation (5.95)), and $\zeta = 1$ associated with the noisy Mullins equation; in the latter case the actually observed, effective exponent might well be smaller than unity due to the logarithmic correction appearing at the border to the anomalous scaling regime (see section 3.2.3 and [402]). KPZ behaviour, $\zeta \approx 0{\cdot}387$ [137], is clearly ruled out. Moreover, among the experiments which monitored the temporal increase of the roughness, about half found values for the relevant exponent ratio ζ/z in the range 0·2–0·33, reasonably close to the numbers 1/5 and 1/4 predicted by the conserved KPZ and noisy Mullins equations, respectively. In the cases where ζ and ζ/z were measured independently, the estimates are consistent with the scaling relation (4.27) characteristic of conserved growth. Summarizing the experimental situation, Krim and Palasantzas conclude that *"There is considerable overlap between experimental observation for the vapour deposition systems and the predictions of the conservative growth models"* [17].

5.6.2. *Mounding versus roughening*

As has been remarked in several recent papers [332, 334, 355, 403], many of the experiments associated with conserved growth equations could be equally well interpreted within the context of the mounding instability described in section 5.3. The height difference correlation function of a mounded surface will show an apparent roughness exponent close to unity, $G_2(r) \sim r^2$, simply because most of the surface has a fixed, non-zero misorientation relative to the average; the surface width will increase as a power law in time, $W(t) \sim \xi(t) \sim t^{1/z}$ (or faster in the presence of steepening), with an exponent $1/z \approx 1/4$, and the mound spacing $\xi(t)$ may, for many purposes, look like the dynamic correlation length of the roughening process. Even the exponent identity (4.27) would be fulfilled for the mounded surface, provided $1/z = 1/4$ exactly.

In the experiments mentioned in section 5.3, the mound morphology was usually identified by direct visual inspection. It is less clear how to distinguish between a stochastically rough, and a disorderly mounded surface on the basis of statistical averages, such as height correlation functions and structure factors. We have seen in section 3.2.4 that the presence of oscillations in the spatial height correlation function is not sufficient to deduce the existence of a characteristic length scale, since oscillations can be produced also by a purely stochastic equation. This problem has been discussed in detail by Siegert and Plischke [355], who conclude that (i) the oscillations are much more pronounced in the case of mounding, but (ii) the apparent roughness exponent deduced from $G_2(r, t)$ can be considerably less than unity at finite times. A cleaner distinction may be possible by using the structure factor $S(q, t)$ (see equation (3.25)), since it is a monotonically decreasing function of q for all (known) stochastic roughening processes, but would be expected to develop a maximum in the presence of a characteristic scale [16].

In some cases the distinction between roughening and mounding appears to be merely a question of observation scale. Prior to the discovery of mounds on the GaAs(001) surface, Orr and co-workers presented a detailed STM study [404, 405] of roughening during MBE on the very same surface, and concluded that the roughening proceeds very slowly, as $W(t) \sim t^{0.04}$ [405] (see also [120]). In the light of the subsequent work, it is clear that what was in fact observed in these experiments were the *sides* of the mounds, the mounds themselves being too large to be detected in the STM images. According to the theory outlined in section 5.3.3, the sides of the mounds take on an orientation where the non-equilibrium surface current $\mathbf{J}_{\mathrm{NE}}$ has a stable zero; in the linearization around such an orientation the current therefore gives rise to an Edwards–Wilkinson term $\nu_1 \nabla^2 h$ with $\nu_1 > 0$, which implies *logarithmic* roughening, consistent with the observations [405, 120].

Nevertheless, it is puzzling that in several instances different experiments carried out on the same system under virtually identical conditions found mounding or roughening morphologies, respectively. For example, the growth of Fe on Fe(001) was first studied by He *et al.* using high resolution low energy electron diffraction (HRLEED) [406]. They extracted scaling exponents, $\zeta = 0{\cdot}79 \pm 0{\cdot}05$ and $\zeta/z = 0{\cdot}22 \pm 0{\cdot}02$, which are in excellent agreement with the scaling relation (4.27), and concluded that their system is well described by conserved equations of kinetic roughening. Recently the same system was reinvestigated by Stroscio *et al.* using STM and RHEED, and a clear case of mounding was identified [332]. Stroscio *et al.* attribute the discrepancy to the larger amount of substrate roughness present in the earlier experiment, which might somehow suppress the formation of mounds

[407]. An effect of substrate disorder was also implicated in the case of Si(111); however, there it seems to work in the opposite direction—pyramids (mounds) form on imperfect substrates, but kinetic roughness evolves if the substrate is sufficiently flat [408]. Understanding the influence of substrate roughness on unstable growth thus appears to be an important open problem.

Another set of experiments that has to be mentioned in this context is the work of Krim and co-workers involving the growth of silver on silicon and quartz substrates, perhaps the most thoroughly investigated kinetic roughening system [396, 409] and the only case where the scaling exponents ζ and z *as well as* the ratio ζ/z were determined independently [410]. As was mentioned in section 5.3, silver has a sizable step edge barrier (much larger than that of iron) and shows beautiful wedding cakes at room temperature [318]. Nevertheless, the surfaces investigated by Krim *et al.*, which were also grown at room temperature, show no sign of mounding or unstable growth [410]. Again, the different behaviour must be attributed to the substrate and the early stages of growth. Since the substrates used by Krim *et al.* are not wetted by the silver, the initial growth proceeds through the formation of 3D islands, which lead to a polycrystalline film structure; apparently the polycrystallinity is not compatible with the formation of mounds. Palasantzas and Krim [410] remarked that the dynamic correlation length $\xi(t)$ determined from their STM data was nearly equal to the grain size in the films. This indicates that the increase of ξ may be related to some bulk coarsening process, rather than to the roughening of the surface. In any case the grain size introduces an additional length scale which has to be taken into account in a proper theoretical interpretation of these experiments [411].

5.6.3. *Rapid roughening*

Above we have been concerned with situations in which the observed behaviour is consistent with kinetic roughening theories, but the assignment of the underlying mechanism is ambiguous. Here we address cases of growth-induced roughening where an explanation in terms of conventional kinetic roughening theories can be excluded from the outset, because the roughness $W(t)$ is found to increase *faster* than $t^{1/2}$, the natural 'random deposition' limit of stochastic roughening. (At least for conservative growth equations the relation (4.27) bounds the temporal increase of W, because $\zeta/z = (1/2)(1 - d/z) < 1/2$.)

This type of *rapid roughening* behaviour has been reported for a variety of semiconductor surfaces at low temperatures [120, 353, 412] and was recently reviewed by Eaglesham [401] in the context of understanding the crystalline–amorphous transition in limited thickness epitaxy [413]. In many cases the roughness increases approximately linearly with film thickness, $W(t) \sim t$, though more rapid growth laws ($W(t) \sim t^2$ or $W(t) \sim \exp(t)$ [401]) have also been observed: in the case of Si(111) [412] an initial regime of 'conventional' roughness, $W(t) \sim t^{1/4}$, is found [113]. Eaglesham and co-workers initially attributed the behaviour to the presence of step edge barriers [353]; however, as was discussed in section 5.3.3, it seems questionable whether this effect suffices. Recent investigations strongly indicate that gas phase contamination, in particular H impurities, plays a decisive role [401]; a direct relationship between the rate of roughening and the hydrogen pressure in the MBE chamber has been established [414]. Surface instability due to adsorbed impurities is a classic topic in crystal growth theory [415–417], but its consequences for the asymptotic roughening of the surface do not seem to be understood.

Rapid roughening also occurs on some metal surfaces. Fang *et al.* [418] observed $W(t) \sim t^{0.77\pm0.05}$ for deposition of Pb on Pb(110), and König [119] obtained $W(t) \sim t^{0.81\pm0.02}$ in a study of Au films on Ti buffers. In the latter case visual inspection of transmission electron micrographs revealed a distinct polycrystallinity, which moreover seemed to evolve with thickness. It seems plausible that the presence of these grain boundaries influences the roughening of the surface. We showed in section 4.6.3, in the context of the inhomogeneous KPZ equation, that the presence of quenched randomness in the lateral direction can significantly speed up the roughening process, leading typically to the 'subballistic' behaviour (4.65), which is hard to distinguish from power law scaling with exponents close to unity [212]. It remains to be seen if such considerations lead to a theory for this kind of rapid roughening.

We note, finally, that the nonlocal shadowing effects described in section 2 provide another, very natural, mechanism for rapid roughening with $W(t) \sim t$. Indeed, a linear scaling of the roughness is expected whenever the growth process generates a broad height distribution, such as the power law (2.1), in which the film thickness constitutes the only characteristic scale. Shadowing is probably the dominant mechanism in a recent AFM study of obliquely sputtered chromium films [419], where $W \sim t$ was observed. In the simulation work on oblique incidence ballistic deposition [29, 31, 32] the 'width of the active zone' is measured rather than the surface width; this quantity increases more slowly than linearly with time.

Acknowledgments

Much of this work originated from most enjoyable collaborations with Tapio Ala-Nissilä, Tomas Bohr, Harvey Dobbs, Geoff Grinstein, Tim Halpin-Healy, Mogens Jensen, Klaus Kassner, Sami Majaniemi, Mike Plischke, Martin Rost, Martin Schimschak, Martin Siegert, Kim Sneppen and Lei-Han Tang. I am particularly indebted to Paul Meakin for his contributions to the study of competitive growth processes. I am grateful to Jim Evans, Terry Hwa, Herbert Spohn, Dietrich Wolf and Andy Zangwill for sharing their insights; to Richard Ghez for introducing me to the BCF theory of crystal growth; to Uwe Klemradt, Frank König and Matthias Funke for alerting me to the subtleties of kinetic roughening experiments; and to Pavel Šmilauer for a careful reading of the manuscript. Last but not least, Reinhard Lipowsky has provided continuous guidance and encouragement while this work was in progress.

Some important ideas were developed during productive visits to Simon Fraser University, NORDITA, Helsinki University and the ITP at Santa Barbara. I also wish to thank the organizers of the recent summer schools on *Complex Systems* (Humlebæk, August 1993), *Scale Invariance, Interfaces and Non-equilibrium Dynamics* (Cambridge, UK, June 1994) and *Stochastic Processes* (Beg-Rohu, July 1995) for giving me the opportunity to deliver a number of lectures on the topics discussed here.

This review was completed in December 1995. A preliminary version was accepted in June 1995 as a Habilitation Thesis by the Heinrich-Heine-Universität in Düsseldorf.

References

[1] WITTEN, T. A., and SANDER, L. M., 1981, Diffusion limited aggregation: a kinetic critical phenomenon, *Phys. Rev. Lett.*, **47**, 1400.

[2] VICSEK, T., 1989, *Fractal Growth Phenomena* (Singapore: World Scientific).
[3] MEAKIN, P., 1988, The growth of fractal aggregates and their fractal measures, *Phase Transitions and Critical Phenomena*, Vol. 12, edited by C. Domb and J. L. Lebowitz (New York: Academic).
[4] MANDELBROT, B. B., 1982, *The Fractal Geometry of Nature* (San Francisco: W. H. Freeman).
[5] KADANOFF, L. P., 1986, Fractals—where's the physics?, *Phys. Today*, February, p. 6.
[6] BAK, P., TANG, C., and WIESENFELD, K., 1987, Self-organized criticality—an explanation of $1/f$ noise, *Phys. Rev. Lett.*, **59,** 381.
[7] GRINSTEIN, G., 1995, Generic scale invariance and self-organized criticality, *Scale Invariance, Interfaces and Non-Equilibrium Dynamics*, edited by A. J. McKane, M. Droz, J. Vannimenus and D. E. Wolf (New York: Plenum Press), p. 261.
[8] KRUG, J., and SPOHN, H., 1991, Kinetic roughening of growing surfaces, *Solids far from Equilibrium*, edited by C. Godrèche (Cambridge: Cambridge University Press), p. 479.
[9] FAMILY, F., and VICSEK, T. (editors), 1991, *Dynamics of Fractal Surfaces* (Singapore: World Scientific).
[10] MEAKIN, P., 1993, The growth of rough surfaces and interfaces, *Phys. Rep.*, **235,** 189.
[11] HALPIN-HEALY, T. J., and ZHANG, Y. C., 1995, Kinetic roughening phenomena, stochastic growth, directed polymers and all that, *Phys. Rep.*, **254,** 215.
[12] BARABÁSI, A.-L., and STANLEY, H. E., 1995, *Fractal Concepts in Surface Growth* (Cambridge: Cambridge University Press).
[13] RUDNICK, J., and BRUINSMA, R., 1994, Thin-film growth: models and morphologies, *Low Energy Ion–Surface Interactions*, edited by J. W. Rabalais (New York: John Wiley), p. 535.
[14] TANG, L.-H., 1995, Nonequilibrium surfaces, *Annual Reviews of Computational Physics II*, edited by D. Stauffer (Singapore: World Scientific), p. 137.
[15] ZANGWILL, A., 1995, Theory of growth-induced surface roughness, *Microstructural Evolution of Thin Films*, edited by H. A. Atwater and C. V. Thompson (New York: Academic).
[16] TONG, W. M., and WILLIAMS, R. S., 1994, Kinetics of surface growth: phenomenology, scaling, and mechanisms of smoothening and roughening, *Ann. Rev. Phys. Chem.*, **45,** 401.
[17] KRIM, J., and PALASANTZAS, G., 1995, Experimental observations of self-affine scaling and kinetic roughening at sub-micron lengthscales, *Int. J. mod. Phys.* B, **9,** 599.
[18] MULLINS, W. W., 1963, Solid surface morphologies governed by capillarity, *Metal Surfaces: Structure, Energetics and Kinetics*, edited by N. A. Gjostein and W. D. Robertson (Metals Park, Ohio: American Society of Metals).
[19] KARDAR, M., PARISI, G., and ZHANG, Y. C., 1986, Dynamic scaling of growing interfaces, *Phys. Rev. Lett.*, **56,** 889.
[20] VILLAIN, J., 1991, Continuum models of crystal growth from atomic beams with and without desorption, *J. Phys. (France)* I, **1,** 19.
[21] BAHR, H.-A., BAHR, U., and PETZOLD, A., 1992, 1-d deterministic crack pattern formation as a growth process with restrictions, *Europhys. Lett.*, **19,** 485.
[22] BAHR, H.-A., BAHR, U., GERBATSCH, I., PFLUGBEIL, A., VOJTA, A., and WEISS, H.-J., 1995, Fracture mechanical analysis of morphological transitions in thermal shock cracking, *Fracture Mechanics of Ceramics*, Vol. 11/12, edited by R. C. Bradt *et al.* (New York: Plenum).
[23] COUDER, Y., ARGOUL, F., ARNÉODO, A., MAURER, J., and RABAUD, M., 1990, Statistical properties of fractal dendrites and anisotropic diffusion-limited aggregates, *Phys. Rev.* A, **42,** 3499.
[24] GRAFF, D. S., and SANDER, L. M., 1993, Branch-height distribution in diffusion-limited deposition, *Phys. Rev.* E, **47,** R2273.
[25] WITTMER, J. P., CATES, M. E., JOHNER, A., and TURNER, M. S., 1996, Diffusive growth of a polymer layer by *in-situ* polymerization, *Europhys. Lett.*, **33,** 397.
[26] MEAKIN, P., RAMANLAL, P., SANDER, L. M., and BALL, R. C., 1986, Ballistic deposition on surfaces, *Phys. Rev.* A, **34,** 5091.

[27] LEAMY, H. J., GILMER, G. H., and DIRKS, A. G., 1980, The microstructure of vapor deposited thin films, *Current Topics in Materials Science*, Vol. 6, edited by E. Kaldis (New York: North-Holland), p. 309.
[28] MEAKIN, P., and KRUG, J., 1990, Columnar microstructure in three-dimensional ballistic deposition, *Europhys. Lett.*, **11,** 7.
[29] MEAKIN, P., and KRUG, J., 1992, Three-dimensional ballistic deposition at oblique incidence, *Phys. Rev.* A, **46,** 3390.
[30] KRUG, J., 1995, The columnar growth angle in obliquely evaporated thin films, *Mater. wissen. Werkstofftech.*, **26,** 22.
[31] KRUG, J., and MEAKIN, P., 1991, Columnar growth in oblique incidence ballistic deposition: faceting, noise reduction and mean-field theory, *Phys. Rev.* A, **43,** 900.
[32] KRUG, J., and MEAKIN, P., 1989, Microstructure and surface scaling in ballistic deposition at oblique incidence, *Phys. Rev.* A, **40,** 2064.
[33] MEAKIN, P., and KRUG, J., 1992, Scaling structure in simple screening models for columnar growth, *Phys. Rev.* A, **46,** 4654.
[34] MATSUSHITA, M., and MEAKIN, P., 1988, Cluster-size distribution of self-affine fractals, *Phys. Rev.* A, **37,** 3645.
[35] NAGATANI, T., 1991, Scaling structure in a simple growth model with screening: forest formation model, *J. Phys.* A, **24,** L449.
[36] GUMBEL, E. J., 1958, *Statistics of Extremes* (New York: Columbia University Press).
[37] KRUG, J., and SPOHN, H., 1988, Universality classes for deterministic surface growth, *Phys. Rev.* A, **38,** 4271.
[38] TANG, C., ALEXANDER, S., and BRUINSMA, R., 1990, Scaling theory for the growth of amorphous films, *Phys. Rev. Lett.*, **64,** 772.
[39] WESTOBY, M., 1984, The self-thinning rule, *Adv. Ecol. Res.*, **14,** 167.
[40] WHITE, J., 1981, The allometric interpretation of the self-thinning rule, *J. theor. Biol.*, **89,** 475.
[41] HARA, T., 1984, A stochastic model and the moment dynamics of the growth and size distribution in plant populations, *J. theor. Biol.*, **109,** 173.
[42] KARUNASIRI, R. P. U., BRUINSMA, R., and RUDNICK, J., 1989, Thin-film growth and the shadow instability, *Phys. Rev. Lett.*, **62,** 788.
[43] BALES, G. S., BRUINSMA, R., EKLUND, E. A., KARUNASIRI, R. P. U., RUDNICK, J., and ZANGWILL, A., 1990, Growth and erosion of thin solid films, *Science*, **249,** 264.
[44] BALES, G. S., and ZANGWILL, A., 1991, Macroscopic model for columnar growth of amorphous films by sputter deposition, *J. Vac. Sci. Technol.* A, **9,** 145.
[45] YAO, J. H., ROLAND, C., and GUO, H., 1992, Interfacial dynamics with long-range screening, *Phys. Rev.* A, **45,** 3903.
[46] KRUG, J., and MEAKIN, P., 1993, Scaling properties of the shadowing model for sputter deposition, *Phys. Rev.* E, **47,** R17.
[47] YAO, J. H., and GUO, H., 1993, Shadowing instability in three dimensions, *Phys. Rev.* E, **47,** 1007.
[48] TANG, C., and LIANG, S., 1994, Patterns and scaling properties in a ballistic deposition model, *Phys. Rev. Lett.*, **71,** 2769.
[49] LANGER, J. S., 1971, Theory of spinodal decomposition in alloys, *Ann. Phys.*, **65,** 53.
[50] ROSSI, G., 1987, Diffusion-limited aggregation without branching: a detailed analysis, *Phys. Rev.* A, **35,** 2246.
[51] ROLAND, C., and GUO, H., 1991, Interface growth with a shadow instability, *Phys. Rev. Lett.*, **66,** 2106.
[52] MEAKIN, P., 1986, Diffusion-limited surface deposition in the limit of large anisotropy, *Phys. Rev.* A, **33,** 1984.
[53] ROSSI, G., 1986, Diffusion-limited aggregation without branching, *Phys. Rev.* A, **34,** 3543.
[54] WANG, X. R., 1989, Scaling of the shortest-path aggregation, *Phys. Rev.* A, **40,** 6767.
[55] KRUG, J., KASSNER, K., MEAKIN, P., and FAMILY, F., 1993, Laplacian needle growth, *Europhys. Lett.*, **27,** 527.
[56] CATES, M. E., 1986, Diffusion-limited aggregation without branching in the continuum approximation, *Phys. Rev.* A, **34,** 5007.

[57] KASSNER, K., 1990, Solutions to the mean-field equations of branchless diffusion-limited aggregation, *Phys. Rev.* A, **42,** 3637.

[58] WITTEN, T. A., and SANDER, L. M., 1983, Diffusion-limited aggregation, *Phys. Rev.* B, **27,** 5686.

[59] FELLER, W., 1957, *An Introduction to Probability Theory and its Applications*, Vol. 1 (New York: Wiley).

[60] SCHWARZER, S., LEE, J., BUNDE, A., HAVLIN, S., ROMAN, H. E., and STANLEY, H. E., 1990, Minimum growth probability of diffusion-limited aggregates, *Phys. Rev. Lett.*, **65,** 603.

[61] BALL, R. C., and BLUMENFELD, R., 1991, Exact results on exponential screening in two-dimensional diffusion limited aggregation, *Phys. Rev.* A, **44,** R828.

[62] DURAND, E., 1966, *Electrostatique* (Paris: Masson).

[63] KRUG, J., 1995, Statistical physics of growth processes, *Scale Invariance, Interfaces and Non-Equilibrium Dynamics*, edited by A. J. McKane, M. Droz, J. Vannimenus and D. E. Wolf (New York: Plenum), p. 1.

[64] HALSEY, T. C., and LEIBIG, M., 1992, Theory of branched growth, *Phys. Rev.* A, **46,** 7793.

[65] HALSEY, T. C., 1994, Diffusion-limited aggregation as branched growth, *Phys. Rev. Lett.*, **72,** 1228.

[66] PETERS, H. P., STAUFFER, D., HÖLTES, H. P., and LOEWENICH, K., 1979, Radius, perimeter, and density profile for percolation clusters and lattice animals, *Z. Phys.* B, **34,** 399.

[67] PLISCHKE, M., and RÁCZ, Z., 1984, Active zone of growing clusters: diffusion-limited aggregation and the Eden model, *Phys. Rev. Lett.*, **53,** 415.

[68] JULLIEN, R., and BOTET, R., 1985, Scaling properties of the surface of the Eden model in $d = 2, 3, 4$, *J. Phys.* A, **18,** 2279.

[69] EDEN, M., 1958, A probabilistic model for morphogenesis, *Symposium on Information Theory in Biology* (New York: Pergamon Press), p. 359.

[70] FAMILY, F., and VICSEK, T., 1985, Scaling of the active zone in the Eden process on percolation networks and the ballistic deposition model, *J. Phys.* A, **18,** L75.

[71] VICSEK, T., CSERZÖ, M., and HORVÁTH, V. K., 1990, Self-affine growth of bacterial colonies, *Physica* A, **167,** 315.

[72] RUBIO, M. A., EDWARDS, C. A., DOUGHERTY, A., and GOLLUB, J. P., 1989, Self-affine fractal interfaces from immiscible displacement in porous media, *Phys. Rev. Lett.*, **63,** 1685.

[73] HE, S., KAHANDA, G. L. M. K. S., and WONG, P.-Z., 1992, Roughness of wetting fluid invasion fronts in porous media, *Phys. Rev. Lett.*, **69,** 3731.

[74] AMARAL, L. A. N., BARABÁSI, A.-L., BULDYREV, S. V., HARRINGTON, S. T., HAVLIN, S., SADR-LAHIJANY, R., and STANLEY, H. E., 1995, Avalanches and the directed percolation depinning model: experiments, simulations and theory, *Phys. Rev.* E, **51,** 4655.

[75] ZHANG, J., ZHANG, Y. C., ALSTROM, P., and LEVINSEN, M. T., 1992, Modeling forest fire by a paper-burning experiment, a realization of the interface growth mechanism, *Physica* A, **189,** 383.

[76] PROVATAS, N., ALA-NISSILÄ, M., GRANT, M., ELDER, K. R., and PICHÉ, L., 1995, *Phys. Rev.* E, **51,** 4232.

[77] MEDINA, E., HWA, T., KARDAR, M., and ZHANG, Y. C., 1989, Burgers equation with correlated noise: renormalization-group analysis and applications to directed polymers and interface growth, *Phys. Rev.* A, **39,** 3053.

[78] ZHANG, Y. C., 1990, Non-universal roughening of kinetic self-affine interfaces, *J. Phys. (France)*, **51,** 2129.

[79] KRUG, J., 1991, Kinetic roughening by exceptional fluctuations, *J. Phys. (France)* I, **1,** 9.

[80] LAM, C.-H., and SANDER, L. M., 1993, Exact scaling in surface growth with power-law noise, *Phys. Rev.* E, **48,** 979.

[81] CSAHÓK, Z., HONDA, K., and VICSEK, T., 1993, Dynamics of surface roughening in disordered media, *J. Phys.* A, **26,** L171.

[82] TANG, L.-H., KARDAR, M., and DHAR, D., 1995, Driven depinning in anisotropic media, *Phys. Rev. Lett.*, **74,** 920.
[83] OLAMI, Z., PROCACCIA, I., and ZEITAK, R., 1995, Interface roughening in systems with quenched disorder, *Phys. Rev.* E, **52,** 3402.
[84] AMARAL, L. A. N., BARABÁSI, A.-L., MAKSE, H. A., and STANLEY, H. E., 1995, Scaling properties of driven interfaces in disordered media, *Phys. Rev.* E, **52,** 4087.
[85] DEVILLARD, P., 1991, Interface motion in a two-dimensional Ising model with a field, *J. statist. Phys.*, **62,** 443.
[86] DIEHL, H. W., KROLL, D. M., and WAGNER, H., 1980, The interface in a Ginsburg–Landau–Wilson model: derivation of the drumhead model in the low-temperature limit, *Z. Phys.* B, **36,** 329.
[87] SPOHN, H., 1993, Interface motion in models with stochastic dynamics, *J. statist. Phys.*, **71,** 1081.
[88] GHEZ, R., and IYER, S. S., 1988, The kinetics of fast steps on crystal surfaces and its application to the molecular beam epitaxy of silicon, *IBM J. Res. Dev.*, **32,** 804.
[89] SIEGERT, M., and PLISCHKE, M., 1992, Instability in surface growth with diffusion, *Phys. Rev. Lett.*, **68,** 2035.
[90] SUN, T., and PLISCHKE, M., 1994, Dynamics of interfaces in a model for molecular-beam epitaxy, *Phys. Rev.* E, **50,** 3370.
[91] FAMILY, F., and AMAR, J. G., 1993, The morphology and evolution of the surface in epitaxial and thin film growth: a continuum model with surface diffusion, *Fractals*, **1,** 753.
[92] KRUG, J., PLISCHKE, M., and SIEGERT, M., 1993, Surface diffusion currents and the universality classes of growth, *Phys. Rev. Lett.*, **70,** 3271.
[93] KOPLIK, J., and LEVINE, H., 1985, Interface moving through a random background, *Phys. Rev.* B, **32,** 280.
[94] GRINSTEIN, G., LEE, D. H., and SACHDEV, S., 1990, Conservation laws, anisotropy, and 'self-organized criticality' in noisy nonequilibrium systems, *Phys. Rev. Lett.*, **64,** 1927.
[95] HWA, T., and KARDAR, M., 1992, Avalanches, hydrodynamics and discharge events in models of sandpiles, *Phys. Rev.* A, **45,** 7002.
[96] LIPOWSKY, R., 1985, Nonlinear growth of wetting layers, *J. Phys.* A, **18,** L585.
[97] GRANT, M., 1988, Dynamics of roughening and complete wetting, *Phys. Rev.* B, **37,** 5705.
[98] EDWARDS, S. F., and WILKINSON, D. R., 1982, The surface statistics of a granular aggregate, *Proc. R. Soc. Lond.* A, **381,** 17.
[99] EVANS, J. W., 1991, Factors mediating smoothness in epitaxial thin-film growth, *Phys. Rev.* B, **43,** 3897.
[100] GOLUBOVIĆ, L., and BRUINSMA, R., 1991, Surface diffusion and fluctuations of growing interfaces, *Phys. Rev. Lett.*, **66,** 321; 1991, *Ibid.*, Erratum, **67,** 2747.
[101] WOLF, D. E., and VILLAIN, J., 1990, Growth with surface diffusion, *Europhys. Lett.*, **13,** 389.
[102] KRUG, J., and MEAKIN, P., 1991, Kinetic roughening of Laplacian fronts, *Phys. Rev. Lett.*, **66,** 703.
[103] FOLTIN, G., OERDING, K., RÁCZ, Z., WORKMAN, R. L., and ZIA, R. K. P., 1994, Width distribution for random-walk interfaces, *Phys. Rev.* E, **50,** R639.
[104] PLISCHKE, M., RÁCZ, Z., and ZIA, R. K. P., 1994, Width distribution for curvature-driven interfaces: a study of universality, *Phys. Rev.* E, **50,** 3589.
[105] RÁCZ, Z., and PLISCHKE, M., 1994, Width distribution for $(2+1)$-dimensional growth and deposition processes, *Phys. Rev.* E, **50,** 3530.
[106] AMAR, J. G., LAM, P.-M., and FAMILY, F., 1993, Groove instabilities in surface growth with diffusion, *Phys. Rev.* E, **47,** 3242.
[107] SCHROEDER, M., SIEGERT, M., WOLF, D. E., SHORE, J. D., and PLISCHKE, M., 1993, Scaling of growing surfaces with large local slopes, *Europhys. Lett.*, **24,** 563.
[108] DAS SARMA, S., GHAISAS, S. V., and KIM, J. M., 1994, Kinetic super-roughening and anomalous dynamic scaling in nonequilibrium growth models, *Phys. Rev.* E, **49,** 122.
[109] FISHER, M. E., 1986, Interface wandering in adsorbed and bulk phases, pure and impure, *J. chem. Soc. Faraday Trans.* 2, **82,** 1569.

[110] NATTERMANN, T., and VILLAIN, J., 1988, Random-field Ising systems: a survey of current theoretical views, *Phase Transitions*, **11,** 5.
[111] LIPOWSKY, R., 1991, The conformation of membranes, *Nature*, **349,** 475.
[112] KRUG, J., 1994, Turbulent interfaces, *Phys. Rev. Lett.*, **72,** 2907.
[113] YANG, H.-N., WANG, G.-C., and LU, T.-M., 1994, Instability in low-temperature molecular beam epitaxy growth of Si/Si(111), *Phys. Rev. Lett.*, **73,** 2348.
[114] YANG, H.-N., WANG, G.-C., and LU, T.-M., 1994, Anomalous dynamic scaling on the ion-sputtered Si(111) surface, *Phys. Rev.* B, **50,** 7635.
[115] MAJANIEMI, S., ALA-NISSILÄ, T., and KRUG, J., 1996, Kinetic roughening of surfaces: derivation, solution and application of linear growth equations, *Phys. Rev.* B, **53,** 8071.
[116] SINHA, S. K., SIROTA, E. B., GAROFF, S., and STANLEY, H. B., 1988, X-ray and neutron scattering from rough surfaces, *Phys. Rev.* B, **38,** 2297.
[117] SINHA, S. K., 1994, X-ray diffuse scattering as a probe for thin film and interface structure, *J. Phys. III France*, **4,** 1543.
[118] PALASANTZAS, G., and KRIM, J., 1993, Effect of the form of the height-height correlation function on diffuse X-ray scattering from a self-affine surface, *Phys. Rev.* B, **48,** 2873.
[119] KÖNIG, F., 1995, Einfluss der Herstellungsparameter auf die Oberflächenrauhigkeit dünner Goldfilme, ermittelt aus der Streuung harter Röntgenstrahlen unter streifenden Winkeln, *KFA Jülich Report*, No. 3092.
[120] KLEMRADT, U., FUNKE, M., FROMM, B., LENGELER, B., PEISL, J., and FÖRSTER, A., 1996, Growth-induced interface roughness of GaAs/AlAs-layers studied by X-ray scattering under grazing angles. *Physica* B (in the press).
[121] LAI, Z.-W., and DAS SARMA, S., 1991, Kinetic growth with surface relaxation: continuum versus atomistic models, *Phys. Rev. Lett.*, **66,** 2348.
[122] TANG, L.-H., and NATTERMANN, T., 1991, Kinetic roughening in molecular beam epitaxy, *Phys. Rev. Lett.*, **66,** 2899.
[123] KRUG, J., and SCHIMSCHAK, M., 1995, Metastability of step flow growth in 1+1 dimensions, *J. Phys. France* I, **5,** 1065.
[124] MEAKIN, P., and DEUTCH, J. M., 1986, The formation of surfaces by diffusion limited annihilation, *J. chem. Phys.*, **85,** 2320.
[125] CAROLI, B., CAROLI, C., and ROULET, B., 1991, Instabilities of planar solidification fronts, *Solids far from Equilibrium*, edited by C. Godrèche (Cambridge: Cambridge University Press), p. 155.
[126] KIM, J. M., and DAS SARMA, S., 1994, Discrete models for conserved growth equations, *Phys. Rev. Lett.*, **72,** 2903.
[127] FAMILY, F., 1986, Scaling of rough surfaces: effects of surface diffusion, *J. Phys.* A, **19,** L441.
[128] WEEKS, J. D., and GILMER, G. H.,1979, Dynamics of crystal growth, *Adv. chem. Phys.*, **40,** 157.
[129] KRUG, J., 1989, Classification of some growth and deposition processes, *J. Phys.* A, **22,** L769.
[130] MEAKIN, P., and JULLIEN, R., 1987, Restructuring effects in the rain model for random deposition, *J. Phys. (France)*, **48,** 1651.
[131] LIU, D., and PLISCHKE, M., 1988, Universality in two- and three-dimensional growth and deposition models, *Phys. Rev.* B, **38,** 4781.
[132] DAS SARMA, S., and TAMBORENEA, P., 1991, A new universality class for kinetic growth: one dimensional molecular beam epitaxy, *Phys. Rev. Lett.*, **66,** 325.
[133] TAMBORENEA, P. I., and DAS SARMA, S., 1993, Surface diffusion-driven kinetic growth on one-dimensional substrates, *Phys. Rev.* E, **48,** 2575.
[134] KRUG, J., and SPOHN, H., 1990, Mechanism for rough-to-rough transitions in surface growth, *Phys. Rev. Lett.*, **64,** 2232.
[135] TANG, L.-H., and NATTERMANN, T., 1992, Kinetic surface roughening. I. The Kardar–Paris–Zhang equation in the weak coupling regime, *Phys. Rev.* A, **45,** 7156.
[136] ALA-NISSILÄ, T., HJELT, T., KOSTERLITZ, J. M., and VENÄLÄINEN, O., 1993, Scaling exponents for kinetic roughening in higher dimensions, *J. statist. Phys.*, **72,** 207.

[137] Ala-Nissilä, T., and Venäläinen, O., 1994, Scaling exponents for driven two-dimensional surface growth, *J. statist. Phys.*, **76,** 1083.
[138] Beccaria, M., and Curci, G., 1994, Numerical simulation of the Kardar–Parisi–Zhang equation, *Phys. Rev.* E, **50,** 4560.
[139] Sun, T., and Plischke, M., 1994, Field-theory renormalization approach to the Kardar–Parisi–Zhang equation, *Phys. Rev.* E, **49,** 5046.
[140] Frey, E., and Täuber, U. C., 1994, Two-loop renormalization group analysis of the Burgers Kardar–Parisi–Zhang equation, *Phys. Rev.* E, **50,** 1024.
[141] Sun, T., 1995, Comment on 'Two-loop renormalization-group analysis of the Burgers Kardar–Parisi–Zhang equation', *Phys. Rev.* E, **51,** 6316.
[142] Täuber, U. C., and Frey, E., 1995, Reply to "Comment on 'Two-loop renomalization-group analysis of the Burgers Kardar–Paris–Zhang equation'", *Phys. Rev.* E, **51,** 6319.
[143] Lässig, M., 1995, On the renormalization of the Kardar–Parisi–Zhang equation, *Nucl. Phys.* B, **448[FS],** 559.
[144] Newman, T. J., and Kallabis, H., 1996, Strong coupling probe for the Kardar–Parisi–Zhang equation, *J. Phys. (France)* I, **6,** 385.
[145] Doherty, J. P., Moore, M. A., Kim, J. M., and Bray, A. J., 1994, Generalizations of the Kardar–Parisi–Zhang equation, *Phys. Rev. Lett.*, **72,** 2041.
[146] Fujisaka, H., and Yamada, T., 1977, Theoretical study of a chemical turbulence, *Progr. theoret. Phys.*, **57,** 734.
[147] van Beijeren, H., Kutner, R., and Spohn, H., 1985, Excess noise for driven diffusive systems, *Phys. Rev. Lett.*, **54,** 2026.
[148] Krug, J., 1987, Scaling relation for a growing interface, *Phys. Rev.* A, **36,** 5465.
[149] Hwa, T., and Frey, E., 1991, Exact scaling function of interface growth dynamics, *Phys. Rev.* A, **44,** R7873.
[150] Schwartz, M., and Edwards, S. F., 1992, Nonlinear deposition: a new approach, *Europhys. Lett.*, **20,** 301.
[151] Bouchaud, J. P., and Cates, M., 1993, Self-consistent approach to the Kardar–Parisi–Zhang equation, *Phys. Rev.* E, **47,** 1455; 1993, *Ibid.*, Erratum, **48,** 635.
[152] Blum, T., and McKane, A. J., 1995, Improved perturbation theory for the Kardar–Parisi–Zhang equation, *Phys. Rev.* E, **52,** 4741.
[153] Moore, M. A., Blum, T., Doherty, J. P., Marsili, M., Bouchaud, J.-P., and Claudin, P., 1995, Glassy solutions of the Kardar–Parisi–Zhang equation, *Phys. Rev. Lett.*, **74,** 4257.
[154] Halpin-Healy, T., 1990, Disorder-induced roughening of diverse manifolds, *Phys. Rev.* A, **42,** 711.
[155] Nattermann T., and Leschhorn, H., 1991, Interfaces and directed polymers in disordered systems: a three-parameter renormalization group approach, *Europhys. Lett.*, **14,** 603.
[156] Stepanow, S., 1995, Towards describing the strong-coupling regime of the Kardar–Parisi–Zhang equation, *J. Phys.: condens. Matter*, **7,** L605.
[157] Tu, Y., 1994, Absence of finite upper critical dimension in the spherical Kardar–Parisi–Zhang equation, *Phys. Rev. Lett.*, **73,** 3109.
[158] Wolf, D. E. 1991, Kinetic roughening of vicinal surfaces, *Phys. Rev. Lett.*, **67**, 1783.
[159] Fisher, M. P. A., and Grinstein, G., 1992, Nonlinear transport and $1/f^{\alpha}$ noise in insulators, *Phys. Rev. Lett.*, **69,** 2322.
[160] Hwa, T., 1992, Nonequilibrium dynamics of driven line liquids, *Phys. Rev. Lett.*, **69,** 1552.
[161] Janssen, H. K., and Schmittmann, B., 1986, Field theory of long time behavior in driven diffusive systems, *Z. Phys.* B, **63,** 517.
[162] Krug, J., 1991, Boundary-induced phase transitions in driven diffusive systems, *Phys. Rev. Lett.*, **67,** 1882.
[163] Derrida, B., Evans, M. R., Hakim, V., and Pasquier, V., 1993, Exact solution of a 1D asymmetric exclusion model using a matrix formulation, *J. Phys.* A, **26,** 1493.
[164] Schütz, G., and Domany, E., 1993, Phase transitions in an exactly soluble one-dimensional exclusion process, *J. statist. Phys.*, **72,** 277.

[165] DERRIDA, B., and EVANS, M. R., 1993, Exact correlation functions in an asymmetric exclusion model with open boundaries, *J. Phys. (France)* I, **3,** 311.

[166] DERRIDA, B., EVANS, M. R., and MALLICK, K., 1995, Exact diffusion constant of a one-dimensional asymmetric exclusion model with open boundaries, *J. statist. Phys.*, **79,** 833.

[167] FORSTER, D., NELSON, D. R., and STEPHEN, M. J., 1977, Large-distance and long-time properties of a randomly stirred fluid, *Phys. Rev.* A, **16,** 732.

[168] HUSE, D. A., HENLEY, C. L., and FISHER, D. S., 1985, Huse, Henley, and Fisher respond, *Phys. Rev. Lett.*, **55,** 2924.

[169] GWA, L.-H., and SPOHN, H., 1992, Bethe solution for the dynamical-scaling exponent of the noisy Burgers equation, *Phys. Rev.* A, **46,** 844.

[170] FOGEDBY, H. C., ERIKSSON, A. B., and MIKHEEV, L. V., 1995, Continuum limit, Galilean invariance, and solitons in the quantum equivalent of the noisy Burgers equation, *Phys. Rev. Lett.*, **75,** 1883.

[171] NEERGAARD, J., and DEN NIJS, M., 1995, Crossover scaling functions in one dimensional dynamic growth models, *Phys. Rev. Lett.*, **74,** 730.

[172] KIM, D., 1995, Bethe ansatz solution for crossover scaling functions of the asymmetric XXZ chain and the Kardar–Parisi–Zhang-type growth model, *Phys. Rev.* E, **52,** 3512.

[173] TANG, L.-H., 1992, Steady-state scaling function of the (1 + 1)-dimensional single-step model, *J. statist. Phys.*, **67,** 819.

[174] KRUG, J., MEAKIN, P., and HALPIN-HEALY, T., 1992, Amplitude universality for driven interfaces and directed polymers in random media, *Phys. Rev.* A, **45,** 638.

[175] KIM, J. M., MOORE, M. A., and BRAY, A. J., 1991, Zero-temperature directed polymers in a random potential, *Phys. Rev.* A, **44,** 2345.

[176] FRIEDBERG, R., and YU, Y.-K., 1994, Replica model at low integer N for directed polymers in (1 + 1) dimensions, *Phys. Rev.* E, **49,** 4157.

[177] AMAR, J. G., and FAMILY, F., 1992, Universality in surface growth: scaling functions and amplitude ratios, *Phys. Rev.* A, **45,** 5378.

[178] KRUG, J., and MEAKIN, P., 1990, Universal finite size effects in the rate of growth processes, *J. Phys.* A, **23,** L987.

[179] KRUG, J., and TANG, L.-H., 1994, Disorder-induced unbinding in confined geometries, *Phys. Rev.* E, **50,** 104.

[180] KRUG, J., 1991, $1/f$ noise for driven interfaces, *Phys. Rev.* A, **44,** R801.

[181] SANDER, L. M., and YAN, H., 1991, Temporal characteristics in nonequilibrium surface-growth models, *Phys. Rev.* A, **44,** 4885.

[182] DERRIDA, B., EVANS, M. R., and MUKAMEL, D., 1993, Exact diffusion constant for one-dimensional asymmetric exclusion models, *J. Phys.* A, **26,** 4911.

[183] KIM, J. M., and KOSTERLITZ, J. M., 1989, Growth in a restricted solid-on-solid model, *Phys. Rev. Lett.*, **62,** 2289.

[184] SIVASHINSKY, G. I., 1983, Instabilities, pattern formation, and turbulence in flames, *Ann. Rev. Fluid Mech.*, **15,** 179.

[185] MISBAH, C., MÜLLER-KRUMBHAAR, H., and TEMKIN, D. E., 1991, Interface structure at large supercooling, *J. Phys. (France)* I, **1,** 585.

[186] BENA, I., MISBAH, C., and VALANCE, A., 1993, Nonlinear evolution of a terrace edge during step-flow growth, *Phys. Rev.* B, **47,** 7408.

[187] KARMA, A., and MISBAH, C., 1993, Competition between noise and determinism in step flow growth, *Phys. Rev. Lett.*, **71,** 3810.

[188] LAQUEY, R. E., MAHAJAN, S. M., RUTHERFORD, P. H., and TANG, W. M., 1975, Nonlinear saturation of the trapped-ion mode, *Phys. Rev. Lett.* **34,** 391.

[189] KURAMOTO, Y., 1984, *Chemical Oscillations, Waves, and Turbulence* (Berlin: Springer).

[190] YAKHOT, V., 1981, Large-scale properties of unstable systems governed by the Kuramoto–Sivashinksi (*sic*) equation, *Phys. Rev.* A, **24,** 642.

[191] CUERNO, R., and LAURITSEN, K. B., 1995, Renormalization group analysis of a noisy Kuramoto–Sivashinsky equation, *Phys. Rev.* E, **52,** 4853.

[192] ZALESKI, S., 1989, A stochastic model for the large scale dynamics of some fluctuating interfaces, *Physica* D, **34,** 427.

[193] SNEPPEN, K., KRUG, J., JENSEN, M. H., JAYAPRAKASH, C., and BOHR, T., 1992, Dynamic scaling and crossover analysis for the Kuramoto–Sivashinsky equation, *Phys. Rev.* A, **46,** R7351.
[194] L'VOV, V. S., LEBEDEV, V. V., PATON, M., and PROCACCIA, I., 1993, Proof of scale invariant solutions in the Kardar–Parisi–Zhang and Kuramoto–Sivashinsky equations in 1 + 1 dimensions: analytical and numerical results, *Nonlinearity*, **6,** 25.
[195] CHOW, C., and HWA, T., 1995, Defect-mediated stability: an effective hydrodynamic theory of spatiotemporal chaos, *Physica* D, **84,** 494.
[196] PROCACCIA, I., JENSEN, M. H., L'VOV, V. S., SNEPPEN, K., and ZEITAK, R., 1992, Surface roughening and the long-wavelength properties of the Kuramoto–Sivashinsky equation, *Phys. Rev.* A, **46,** 3220.
[197] JAYAPRAKASH, C., HAYOT, F., and PANDIT, R., 1993, Universal properties of the two-dimensional Kuramoto–Sivashinsky equation, *Phys. Rev. Lett.*, **71,** 12.
[198] L'VOV, V. S., and PROCACCIA, I., 1992, Comparison of scale invariant solutions of the Kuramoto–Sivashinsky and Kardar–Parisi–Zhang equations in d dimensions, *Phys. Rev. Lett.*, **69,** 3543.
[199] L'VOV, V. S., and LEBEDEV, V. V., 1993, Interaction locality and scaling solution in $d + 1$ KPZ and KS models, *Europhys. Lett.*, **22,** 419.
[200] L'VOV, V., and PROCACCIA, I., 1994, Comment on 'Universal properties of the two-dimensional Kuramoto–Sivashinsky equation', *Phys. Rev. Lett.*, **72,** 307.
[201] JAYAPRAKASH, C., HAYOT, F., and PANDIT, R., 1994, Jayaprakash, Hayot, and Pandit reply, *Phys. Rev. Lett.*, **72,** 308.
[202] ROST, M., and KRUG, J., 1995, Anisotropic Kuramoto–Sivashinsky equation for surface growth and erosion, *Phys. Rev. Lett.*, **75,** 3894.
[203] BOHR, T., GRINSTEIN, G., JAYAPRAKASH, C., JENSEN, M. H., and MUKAMEL, D., 1992, Chaotic interface dynamics: a model with turbulent behavior, *Phys. Rev.* A, **46,** 4791.
[204] BOHR, T., GRINSTEIN, G., JAYAPRAKASH, C., JENSEN, M. H., KRUG, J., and MUKAMEL, D., 1992, Turbulence, power laws and Galilean invariance, *Physica* D, **59,** 177.
[205] ROST, M., and KRUG, J., 1995, A particle model for the Kuramoto–Sivashinsky equation, *Physica* D, **88,** 1.
[206] BOHR, T., and PIKOVSKY, A., 1993, Anomalous diffusion in the Kuramoto–Sivashinsky equation, *Phys. Rev. Lett.*, **70,** 2892.
[207] BURGERS, J. M., 1974, *The Nonlinear Diffusion Equation* (Dordrecht: Reidel).
[208] SCHULMAN, L. S., 1981, *Techniques and Applications of Path Integration* (New York: Wiley).
[209] ROUX, S., HANSEN, A., and HINRICHSEN, E. L., 1991, A direct mapping between Eden growth model and directed polymers in random media, *J. Phys.* A, **24,** L295.
[210] TANG, L.-H., KERTÉSZ, J., and WOLF, D. E., 1991, Kinetic roughening with power-law waiting time distribution, *J. Phys.* A, **25,** L1193.
[211] TANG, L.-H., 1992, Waiting-time formulation of surface growth and mapping to directed polymers in a random medium, *Growth Patterns in Physical Sciences and Biology*, edited by E. Louis, L. M. Sander, P. Meakin and J. M. Garcia-Ruiz (New York: Plenum).
[212] KRUG, J., and HALPIN-HEALY, T., 1993, Directed polymers in the presence of columnar disorder, *J. Phys. (France)* I, **3,** 2179.
[213] FORGACS, G., LIPOWSKY, R., and NIEUWENHUIZEN, TH. M., 1991, The behavior of interfaces in ordered and disordered systems, *Phase Transitions and Critical Phenomena,* Vol. 14, edited by C. Domb and J. L. Lebowitz (London: Academic Press).
[214] EVANS, M. R., and DERRIDA, B., 1992, Improved bounds for the transition temperature of directed polymers in a finite-dimensional random medium, *J. statist. Phys.*, **69,** 427.
[215] FISHER, D. S., and HUSE, D. A., 1991, Directed paths in a random potential, *Phys. Rev.* B, **43,** 10728.
[216] SCHULTZ, U., VILLAIN, J., BRÉZIN, E., and ORLAND, H., 1988, Thermal fluctuations in some random field models, *J. statist. Phys.*, **51,** 1.
[217] HWA, T., and FISHER, D. S., 1994, Anomalous fluctuations of directed polymers in random media, *Phys. Rev.* B, **49,** 3136.

[218] WOLF, D. E., and TANG, L.-H., 1990, Inhomogeneous growth processes, *Phys. Rev. Lett.*, **65,** 1591.

[219] JANOWSKY, S. A., and LEBOWITZ, J. L., 1992, Finite-size effects and shock fluctuations in the asymmetric simple-exclusion process, *Phys. Rev.* A, **45,** 618.

[220] KANDEL, D., and MUKAMEL, D., 1992, Defects, interface profile and phase transitions in growth models, *Europhys. Lett.*, **20,** 325.

[221] KANDEL, D., GERSHINSKY, G., MUKAMEL, D., and DERRIDA, B., 1993, Phase transitions induced by a defect in a growing interface model, *Physica Scripta* T, **49B,** 622.

[222] DERRIDA, B., LEBOWITZ, J. L., SPEER, E. R., and SPOHN, H., 1991, Dynamics of an anchored Toom interface, *J. Phys.* A, **24,** 4805.

[223] KARDAR, M., 1985, Depinning by quenched randomness, *Phys. Rev. Lett.*, **55,** 2235.

[224] ZAPOTOCKY, M., and HALPIN-HEALY, T., 1991, Comment on 'Depinning due to quenched randomness', *Phys. Rev. Lett.*, **67,** 3463.

[225] WUTTKE, J., and LIPOWSKY, R., 1991, Universality classes for wetting in two-dimensional random bond systems, *Phys. Rev.* B, **44,** 13042.

[226] TANG, L.-H. AND LYUKSYUTOV, I. F., 1993, Directed polymer localization in a disordered medium, *Phys. Rev. Lett.*, **71,** 2745.

[227] BALENTS, L., and KARDAR, M., 1994, Disorder-induced unbinding of a flux line from an extended defect, *Phys. Rev.* B, **49,** 13030.

[228] KINZELBACH, H., and LÄSSIG, M., 1995, Depinning in a random medium, *J. Phys.* A, **28,** 6536.

[229] HWA, T., and NATTERMANN, T., 1995, Disorder-induced depinning transition, *Phys. Rev.* B, **51,** 455.

[230] KOLOMEISKY, E. B., and STRALEY, J. P., 1995, Line-delocalization transitions in the presence of quenched disorder, *Phys. Rev.* B, **51,** 8030.

[231] NATTERMANN, T., and LIPOWSKY, R., 1988, Vortex behavior in high-T_c superconductors with disorder, *Phys. Rev. Lett.*, **61,** 2508.

[232] TANG, L.-H., private communication.

[233] BURTON, W. K., CABRERA, N., and FRANK, F. C., 1951, The growth of crystals and the equilibrium structure of their surfaces, *Phil. Trans. R. Soc. (Lond.)* A, **243,** 299.

[234] KRUG, J., 1992, Kinetic roughening in the presence of quenched random phases, *Surface Disordering: Growth, Roughening and Phase Transitions*, edited by R. Jullien, J. Kertész, P. Meakin and D. E. Wolf (Commack, NY: Nova Science), p. 177.

[235] KRUG, J., 1995, Driven interfaces with phase disorder, *Phys. Rev. Lett.*, **75,** 1795.

[236] NATTERMANN, T., and RENZ, W., 1989, Diffusion in a random catalytic environment, polymers in random media, and stochastically growing interfaces, *Phys. Rev.* A, **40,** 4675.

[237] CATES, M. E., and BALL, R. C., 1988, Statistics of a polymer in a random potential, with implications for a nonlinear interfacial growth model, *J. Phys. (France)*, **49,** 2009.

[238] HANSEN, A., HINRICHSEN, E. L., and ROUX, S., 1993, Non-directed polymers in a random medium, *J. Phys. (France)* I, **3,** 1569.

[239] EBELING, W., ENGEL, A., ESSER, B., and FEISTEL, R., 1984, Diffusion and reaction in random media and models of evolution processes, *J. statist. Phys.*, **37,** 369.

[240] BECKER, V., and JANSSEN, H. K., 1992, Speeding-up of fluctuations in driven diffusive systems with quenched disorder, *Europhys. Lett.*, **19,** 13.

[241] ARSENIN, I., HALPIN-HEALY, T., and KRUG, J., 1994, Competing effects of point versus columnar disorder on the roughening of directed polymers in random media, *Phys. Rev.* E, **49,** R3561.

[242] SZNITMAN, A.-S., 1996, Brownian confinement and pinning in a Poissonian potential, *Probab. Theor. rel. Fields*, **105,** 1.

[243] BARABÁSI, A.-L., ARAUJO, M., and STANLEY, H. E., 1992, Three-dimensional Toom model: connection to the anisotropic Kardar–Parisi–Zhang equation, *Phys. Rev. Lett.*, **68,** 3729.

[244] KRUG, J., SOCOLAR, J. E. S., and GRINSTEIN, G., 1992, Surface fluctuations and criticality in a class of one-dimensional sandpile models, *Phys. Rev.* A, **46,** R4479.

[245] DEVILLARD, P., and SPOHN, H., 1992, Universality class of interface growth with reflection symmetry, *J. statist. Phys.*, **66,** 1089.
[246] PACZUSKI, M., BARMA, M., MAJUMDAR, S. N., and HWA, T., 1992, Fluctuations of a nonequilibrium interface, *Phys. Rev. Lett.*, **69,** 2735.
[247] KRUG, J., and SOCOLAR, J. E. S., 1992, Comment on 'Scalings of growing self-organized surfaces', *Phys. Rev. Lett.*, **68,** 722.
[248] FORREST, B. M., and TANG, L.-H., 1990, Surface roughening in a hypercube-stacking model, *Phys. Rev. Lett.*, **64,** 1405.
[249] KRUG, J., 1996, Nonequilibrium surface dynamics with volume conservation, *Nonequilibrium Statistical Physics in One Dimension*, edited by V. Privman, (Cambridge: Cambridge University Press) (in the press).
[250] RÁCZ, Z., SIEGERT, M., LIU, D., and PLISCHKE, M., 1991, Scaling properties of driven interfaces: symmetries, conservation laws and the role of constraints, *Phys. Rev.* A, **43,** 5275.
[251] KRUG, J., and DOBBS, H. T., 1994, Current-induced faceting of crystal surfaces, *Phys. Rev. Lett.*, **73,** 1947.
[252] KANG, H. C., and EVANS, J. W., 1992, Scaling analysis of surface roughness in simple models for molecular-beam epitaxy, *Surf. Sci.*, **269/270,** 784.
[253] KANG, H. C., and EVANS, J. W., 1992, Scaling analysis of surface roughness and Bragg oscillation decay in models for low-temperature epitaxial growth, *Surf. Sci.*, **271,** 321.
[254] PARK, H., PROVATA, A., and REDNER, S., 1991, Interface growth with competing surface currents, *J. Phys.* A, **24,** L1391.
[255] LAM, P.-M., and FAMILY, F., 1991, Surface growth in a model of molecular-beam epitaxy with correlated noise, *Phys. Rev.* A, **44,** 4854.
[256] DAS SARMA, S., and GHAISAS, S. V., 1992, Solid-on-solid rules and models for nonequilibrium growth in $2+1$ dimensions, *Phys. Rev. Lett.*, **69,** 3762.
[257] LANCZYCKI, C. J., and DAS SARMA, S., 1994, Nonequilibrium influence of upward atomic mobility in one-dimensional molecular-beam epitaxy, *Phys. Rev.* E, **50,** 213.
[258] RYU, C. S., and KIM, I.-M., 1995, Crossover behaviors in a molecular-beam epitaxial-growth model *Phys. Rev.* E, **51,** 3069.
[259] RYU, C. S., and KIM, I.-M., 1995, Solid-on-solid model with next-nearest-neighbor interaction for epitaxial growth, *Phys. Rev.* E, **52,** 2424.
[260] KIM, Y., PARK, D. K., and KIM, J. M., 1994, Conserved growth in a restricted solid-on-solid model, *J. Phys.* A, **27,** L533.
[261] WOLF, D. E., 1995, Computer simulation of molecular beam epitaxy, *Scale Invariance, Interfaces and Non-Equilibrium Dynamics*, edited by A. J. McKane, M. Droz, J. Vannimenus and D. E. Wolf (New York: Plenum Press), p. 215.
[262] SCHIMSCHAK, M., and KRUG, J., 1995, Bulk defects and surface roughening in epitaxial growth, *Phys. Rev.* B, **52,** 8550.
[263] KOTRLA, M., and ŠMILAUER, P., 1996, Nonuniversality in models of epitaxial growth, *Phys. Rev.* B, **53,** 13 777.
[264] DAS SARMA, S., LANCZYCKI, C. J., KOTLYAR, R., and GHAISAS, S. V., 1996, Scale invariance and dynamical correlations in growth models of molecular beam epitaxy, *Phys. Rev.* E, **53,** 359.
[265] BONZEL, H. P., 1976, Surface diffusion of metals—a comparison of intrinsic and mass transfer measurements, *CRC crit. Rev. solid St. Sci.*, **6,** 171.
[266] GILMER, G. H., and BENNEMA, P., 1972, Simulation of crystal growth with surface diffusion, *J. appl. Phys.*, **43,** 1347.
[267] CLARKE, S., and VVEDENSKY, D. D., 1987, Origin of reflection high-energy electron-diffraction intensity oscillations during molecular-beam epitaxy: a computational modeling approach, *Phys. Rev. Lett.*, **58,** 2235.
[268] VVEDENSKY, D. D., and CLARKE, S., 1990, Recovery kinetics during interrupted epitaxial growth, *Surf. Sci.*, **225,** 373.
[269] CLARKE, S., WILBY, M. R., and VVEDENSKY, D. D., 1991, Theory of homoepitaxy on Si(001). I. Kinetics during growth, *Surf. Sci.*, **255,** 91.
[270] DAS SARMA, S., 1990, Numerical studies of epitaxial kinetics: what can a computer simulation tell us about nonequilibrium crystal growth? *J. Vac. Sci. Technol.* A, **8,** 2714.

[271] ŠMILAUER, P., WILBY, M. R., and VVEDENSKY, D. D., 1993, Morphology of singular and vicinal metal surfaces sputtered at different temperatures, *Surf. Sci. Lett.*, **291,** L733.

[272] ŠMILAUER, P., WILBY, M. R., and VVEDENSKY, D. D., 1993, Reentrant layer-by-layer growth: a numerical study, *Phys. Rev.* B, **47,** 4119.

[273] VVEDENSKY, D. D., ZANGWILL, A., LUSE, C. N., and WILBY, M. R., 1993, Stochastic equations of motion for epitaxial growth, *Phys. Rev.* E, **48,** 852.

[274] JOHNSON, M. D., ORME, C., HUNT, A. W., GRAFF, D., SUDIJONO, J., SANDER, L. M., and ORR, B. G., 1994, Stable and unstable growth in molecular beam epitaxy, *Phys. Rev. Lett.*, **72,** 116.

[275] BIHAM, O., and KARIMI, M., Model for diffusion and island growth in metal monolayers (preprint).

[276] KRUG, J., DOBBS, H. T., and MAJANIEMI, S., 1995, Adatom mobility for the solid-on-solid model, *Z. Phys.* B, **97,** 281.

[277] SIEGERT, M., and PLISCHKE, M., 1993, Scaling behavior of driven solid-on-solid models with diffusion, *J. Phys. (France)* I, **3,** 1371.

[278] PLISCHKE, M., and SIEGERT, M., 1992, Comment on 'Kinetic phase diagram for crystal growth: a (1 + 1)-dimensional model', *Phys. Rev. Lett.*, **68,** 2854.

[279] WEEKS, J. D., 1980, The roughening transition, *Ordering in Strongly Fluctuating Condensed Matter Systems,* edited by T. Riste (New York: Plenum Press), p. 293.

[280] PHILLIPS, R., and CHRZAN, D. C., 1991, Kinetic phase diagram for crystal growth: a (1 + 1)-dimensional model, *Phys. Rev. Lett.*, **67,** 220.

[281] SCHWOEBEL, R. L., and SHIPSEY, E. J., 1966, Step motion on crystal surfaces, *J. appl. Phys.*, **37,** 3682.

[282] SCHWOEBEL, R. L., 1969, Step motion on crystal surfaces. II, *J. appl. Phys.*, **40,** 614.

[283] EHRLICH, G., and HUDDA, F. G., 1966, Atomic view of surface self-diffusion: tungsten on tungsten, *J. chem. Phys.*, **44,** 1039.

[284] WANG, S.-C., and TSONG, T. T., 1982, Measurement of the barrier height of the reflective W(110) plane boundaries in surface diffusion of single atoms, *Surf. Sci.*, **121,** 85.

[285] WANG, S. C., and EHRLICH, G., 1993, Adatom motion to lattice steps: a direct view, *Phys. Rev. Lett.*, **70,** 41.

[286] PAL, S., and LANDAU, D. P., 1994, Monte Carlo simulation and dynamic scaling of surfaces in MBE growth, *Phys. Rev.* B, **49,** 10597.

[287] YAN, H., 1992, Kinetic growth with surface diffusion: the scaling aspect, *Phys. Rev. Lett.*, **68,** 3048.

[288] KESSLER, D., LEVINE, H., and SANDER, L. M., 1992, Molecular-beam epitaxial growth and surface diffusion, *Phys. Rev. Lett.*, **69,** 100.

[289] SARGENT, R. B., 1990, Effects of surface diffusion on thin-film morphology: a computer study, *Modeling of Optical Thin Films II,* edited by M. R. Jacobson, Proc. SPIE, Vol. 1324, p. 13.

[290] MARMORKOS, I. K., and DAS SARMA, S., 1990, Kinetic simulation of molecular beam epitaxial growth dynamics, *Surf. Sci. Lett.*, **237,** L411.

[291] MARMORKOS, I. K., and DAS SARMA S., 1992, Atomistic numerical study of molecular beam epitaxial growth kinetics, *Phys. Rev.* B, **45,** 11262.

[292] PELLEGRINI, Y. P., and JULLIEN, R., 1991, Kinetic roughening phase transition in surface growth: numerical study and mean field approach, *Phys. Rev.* A, **43,** 920.

[293] DAS SARMA, S., LANCZYCKI, C. J., GHAISAS, S. V., and KIM, J. M., 1994, Defect formation and crossover behavior in the dynamic scaling properties of molecular-beam epitaxy, *Phys. Rev.* B, **49,** 10693.

[294] KESSLER, D. A., 1992, Continuum modeling of growing films, *Abstracts of the 1992 Fall Meeting of the Materials Research Society*, p. 150.

[295] DOERING, C. R., HORSTHEMKE, W., and RIORDAN, J., 1994, Nonequilibrium fluctuation-induced transport, *Phys. Rev. Lett.*, **72,** 2984.

[296] BÜTTIKER, M., 1987, Transport as a consequence of state-dependent diffusion, *Z. Phys.* B, **68,** 161.

[297] LANDAUER, R., 1988, Motion out of noisy states, *J. statist. Phys.*, **53,** 233.

[298] MARKOV, I., 1994, Kinetics of surfactant-mediated epitaxial growth, *Phys. Rev.* B, **50,** 11271.
[299] VILLAIN, J., PIMPINELLI, A., TANG, L., and WOLF, D., 1992, Terrace sizes in molecular beam epitaxy, *J. Phys. (France)* I, **2,** 2107.
[300] SIEGERT, M., and PLISCHKE, M., 1994, Slope selection and coarsening in molecular beam epitaxy, *Phys. Rev. Lett.*, **73,** 1517.
[301] MYERS-BEAGHTON, A. K., and VVEDENSKY, D. D., 1990, Nonlinear equation for diffusion and adatom interactions during epitaxial growth on vicinal surfaces, *Phys. Rev.* B, **42,** 5544.
[302] MYERS-BEAGHTON, A. K., and VVEDENSKY, D. D., 1991, Generalized Burton–Cabrera–Frank theory for growth and equilibration on stepped surfaces, *Phys. Rev.* A, **44,** 2457.
[303] FUENZALIDA, V., 1991, Cluster-size distribution during epitaxial growth from the vapor on strongly misoriented surfaces, *Phys. Rev.* B, **44,** 10835.
[304] VILLAIN, J., PIMPINELLI, A., and WOLF, D., 1992, Layer by layer growth in molecular beam epitaxy, *Comments condens. matter Phys.*, **16,** 1.
[305] GHEZ, R., COHEN, H. G., and KELLER, J. B., 1993, The stability of growing or evaporating crystals, *J. appl. Phys.*, **73,** 3685.
[306] KELLER, J. B., COHEN, H. G., and MERCHANT, G. J., 1993, The stability of rapidly growing or evaporating crystals, *J. appl. Phys.*, **73,** 3694.
[307] SIEGERT, M., 1995, Non-equilibrium ordering dynamics and pattern formation, *Scale Invariance, Interfaces and Non-Equilibrium Dynamics*, edited by A. J. McKane, M. Droz, J. Vannimenus and D. E. Wolf, (New York: Plenum), p. 165.
[308] BALES, G. S., and ZANGWILL, A., 1990, Morphological instability of a terrace edge during step-flow growth, *Phys. Rev.* B, **41,** 5500.
[309] WU, F., JALOVIAR, S. G., SAVAGE, D. E., and LAGALLY, M. G., 1993, Roughening of steps during homepitaxial growth on Si(001) *Phys. Rev. Lett.*, **71,** 4190.
[310] ELKINANI, I., and VILLAIN, J., 1994, Growth roughness and instabilities due to the Schwoebel effect: a one-dimensional model, *J. Phys. (France)* I, **4,** 949.
[311] COHEN, P. I., PETRICH, G. S., PUKITE, P. R., WHALEY, G. J., and ARROTT, A. S., 1989, Birth–death models of epitaxy. I. Diffraction oscillations from low index surfaces, *Surf. Sci.*, **216,** 222.
[312] SIEGERT, M., and PLISCHKE, M., 1994, Solid-on-solid models of molecular beam epitaxy, *Phys. Rev.* E, **50,** 917.
[313] PLISCHKE, M., private communication.
[314] SHORE, J. D., private communication.
[315] HEY, R., WASSERMEIER, M., BEHREND, J., DÄWERITZ, L., PLOOG, K., and RAIDT, H., 1995, Morphological instabilities on exactly oriented and on vicinal GaAs(001) surfaces during molecular beam epitaxy, *J. Cryst. Growth*, **154,** 1.
[316] LEE, N.-E., CAHILL, D. G., and GREENE, J. E., 1996, Surface roughening during low-temperature Si epitaxial growth on singular versus vicinal Si(001) substrates, *Phys. Rev.* B, **53,** 7876.
[317] BOTT, M., MICHELY, T., and COMSA, G., 1992, The homoepitaxial growth of Pt on Pt(111) studied with STM, *Surf. Sci.*, **272,** 161.
[318] VRIJMOETH, J., VAN DER VEGT, H. A., MEYER, J. A., VLIEG, E., and BEHM, R. J., 1994, Surfactant-induced layer-by-layer growth of Ag on Ag(111): origins and side effects, *Phys. Rev. Lett.*, **72,** 3843.
[319] MEYER G., WOLLSCHLÄGER, J., and HENZLER, M., 1990, Epitaxial growth of thin copper layers on Cu(111) studied by high-resolution low-energy-electron-diffraction, *Surf. Sci.*, **231,** 64.
[320] HENZLER, M., 1993, LEED from epitaxial surfaces, *Surf. Sci.*, **298,** 369.
[321] ALBRECHT, M., FRITZSCHE, H., and GRADMANN, U., 1993, Kinetic facetting in homoepitaxy of Fe(110) on Fe(110), *Surf. Sci.*, **294,** 1.
[322] AMMER, CH., SCHAEFER, T., TEICHERT, CH., MEINEL, K., and KLAUA, M., 1994, The multilayer growth mode in the epitaxy of Ag on Ag(111) analysed by SPALEED, *Surf. Sci.*, **307,** 570.
[323] VVEDENSKY, D. D., 1994, New slant on epitaxial growth, *Phys. World,* March, page 30.

[324] SMITH, G. W., PIDDUCK, A. J., WHITEHOUSE, C. R., GLASPER, J. L., AND SPOWART, J., 1993, Real-time laser-light scattering studies of surface topography development during GaAs MBE growth, *J. Cryst. Growth*, **127,** 966.

[325] ORME, C., JOHNSON, M. D., SUDIJONO, J. L., LEUNG, K. T., and ORR, B. G., 1994, Large scale surface structure formed during GaAS(001) homoepitaxy, *Appl. Phys. Lett.*, **64,** 860.

[326] ORME, C., JOHNSON, M. D., LEUNG, K.-T., ORR, B. G., ŠMILAUER, P., and VVEDENSKY, D., 1995, Studies of large scale unstable growth formed during GaAs(001) homoepitaxy, *J. Cryst. Growth*, **150,** 128.

[327] COTTA, M. A., HAMM, R. A., STALEY, CHU, S. N. G., HARRIOTT, L. R., PANISH, M. B., and TEMKIN, H., 1993, Kinetic surface roughening in molecular beam epitaxy of InP, *Phys. Rev. Lett.*, **70,** 4106.

[328] COTTA, M. A., HAMM, R. A., CHU, S. N. G., HARRIOTT, L. R., and TEMKIN, H., 1994, Lateral thickness modulation of InGaAs/InP quantum wells grown by metalorganic molecular beam epitaxy, *J. appl. Phys.*, **75,** 630.

[329] VAN NOSTRAND, J. E., CHEY, S. J., HASAN, M.-A., CAHILL, D. G., and GREENE, J. E., 1995, Surface morphology during multilayer epitaxial growth of Ge(001), *Phys. Rev. Lett.*, **74,** 1127.

[330] VAN NOSTRAND, J. E., CHEY, S. J., and CAHILL, D. G., 1995, Surface roughness and pattern formation during homoepitaxial growth of Ge(001) at low temperature, *J. Vac. Sci. Technol.* B, **13,** 1816.

[331] THÜRMER, K., KOCH, R., WEBER, M., and RIEDER, K. H., 1995, Dynamic evolution of pyramid structures during growth of epitaxial Fe(001) films, *Phys. Rev. Lett.*, **75,** 1767.

[332] STROSCIO, J. A., PIERCE, D. T., STILES, M., ZANGWILL, A., and SANDER, L. M., 1995, Coarsening of unstable surface features during Fe(001) homoepitaxy, *Phys. Rev. Lett.*, **75,** 4246.

[333] YANG, H.-N., WANG, G. C., LU, T. M., 1995, Formation of facets and pyramidlike structures in molecular-beam-epitaxy growth of Si on a singular Si(111) surface, *Phys. Rev.* B, **51,** 14293.

[334] ERNST, H.-J., FABRE, F., FOLKERTS, R., and LAPUJOULADE, J., 1994, Observation of a growth instability during low temperature molecular beam epitaxy, *Phys. Rev. Lett.*, **72,** 112.

[335] ERNST, H.-J., FABRE, F., FOLKERTS, R., and LAPUJOULADE, J., 1994, Kinetics of growth of Cu on Cu(001), *J. Vac. Sci. Technol.* A, **12,** 1809.

[336] LIAU, Z. L., and ZEIGER, H. J., 1990, Surface energy-induced mass-transport phenomenon in annealing of etched compound semiconductor structures: Theoretical modeling and experimental confirmation, *J. appl. Phys.*, **67,** 2434.

[337] JOHNSON, M. D., SUDIJONO, J., HUNT, A. W., and ORR, B. G., 1994, Growth mode evolution during homoepitaxy of GaAs(001), *Appl. Phys. Lett.*, **64,** 484.

[338] NEAVE, J. H., DOBSON, P. J. and JOYCE, B. A., 1985, Reflection high-energy electron diffraction oscillations from vicinal surfaces—a new approach to surface diffusion measurements, *Appl. Phys. Lett.*, **47,** 100.

[339] ŠMILAUER, P., and VVEDENSKY, D. D., 1993, Step edge barriers on GaAs(001), *Phys. Rev.* B, **48,** 17603.

[340] ŠMILAUER, P., and VVEDENSKY, D. D., 1995, Coarsening and slope evolution during unstable epitaxial growth, *Phys. Rev.* B, **52,** 14263.

[341] ŠMILAUER, P., private communication.

[342] MEYER, J. A., VRIJMOETH, J., VAN DER VEGT, H. A., VLIEG, E., and BEHM, R. J., 1995, Importance of the additional step-edge barrier in determining film morphology during epitaxial growth, *Phys. Rev.* B, **51,** 14790.

[343] ŠMILAUER, P., and HARRIS, S., 1995, Determination of step-edge barriers to interlayer transport from surface morphology during the initial stages of homoepitaxial growth, *Phys. Rev.* B, **51,** 14798.

[344] BARTELT, M. C., and EVANS, J. W., 1995, Transition to multilayer kinetic roughening for Metal(100) homoepitaxy, *Phys. Rev. Lett.*, **75,** 4250.

[345] STROSCIO, J. A., PIERCE, D. T., and DRAGOSET, R. A., 1993, Homoepitaxial growth of iron and a real space view of reflection-high-energy-electron-diffraction, *Phys. Rev. Lett.*, **70,** 3615.
[346] STOLTZE, P., 1994, Simulation of surface defects, *J. Phys.: condens. Matter*, **6,** 9495.
[347] MERIKOSKI, J., and ALA-NISSILÄ, T., 1995, Diffusion processes and growth on stepped metal surfaces, *Phys. Rev.* B, **52,** R8715.
[348] BRAY, A. J., 1994, Theory of phase ordering kinetics, *Adv. Phys.*, **43,** 357.
[349] GOLUBOVIĆ, L., and KARUNASIRI, R. P. U., 1991, Spinodal decomposition of the interface in nonlinear Edwards–Wilkinson model, *Phys. Rev. Lett.*, **66,** 3156.
[350] LIU, F., and METIU, H., 1993, Dynamics of phase separation of crystal surfaces, *Phys. Rev.* B, **48,** 5808.
[351] HUNT, A. W., ORME, C., WILLIAMS, D. R. M., ORR, B. G., and SANDER, L. M., 1994, Instabilities in MBE growth, *Europhys. Lett.*, **27,** 611.
[352] LANGER, J. S., 1991, An introduction to the kinetics of first-order phase transitions, *Solids far from Equilibrium,* edited by C. Godrèche (Cambridge: Cambridge University Press), p. 297.
[353] EAGLESHAM, D. J., and GILMER, G. H., 1992, Roughening during Si deposition at low temperatures, *Surface Disordering: Growth, Roughening and Phase Transitions*, edited by R. Jullien, J. Kertész, P. Meakin and D. E. Wolf (New York: Nova Science), p. 69.
[354] ROST, M., private communication.
[355] SIEGERT, M., and PLISCHKE, M., 1996, Formation of pyramids and mounds in molecular beam epitaxy, *Phys. Rev.* E, **53,** 307.
[356] KAWAKATSU, T., and MUNAKATA, T., 1985, Kink dynamics in a one dimensional conserved TDGL system, *Prog. theor. Phys.*, **74,** 11.
[357] CORNELL, S. J., KASKI, K., and STINCHCOMBE, R. B., 1991, Domain scaling and glassy dynamics in a one-dimensional Kawasaki Ising model, *Phys. Rev.* B, **44,** 12263.
[358] MAJUMDAR, S. N., HUSE, D. A., and LUBACHEVSKY, B. D., 1994, Growth of long-range correlations after a quench in conserved-order-parameter systems, *Phys. Rev. Lett.*, **73,** 182.
[359] SUN, T., GUO, H., and GRANT, M., 1989, Dynamics of driven interfaces with a conservation law, *Phys. Rev.* A, **40,** 6763.
[360] LUSE, C. N., ZANGWILL, A., VVEDENSKY, D. D., and WILBY, M. R., 1992, Adatom mobility on vicinal surfaces during epitaxial growth, *Surf. Sci. Lett.*, **274,** L535.
[361] CAVAILLÉ, J. Y., and DRECHSLER, M., 1978, Surface self-diffusion by ion impact, *Surf. Sci.*, **75,** 342.
[362] STRICKLAND, B., and ROLAND, C., 1995, Low-temperature growth and ion-assisted deposition, *Phys. Rev.* B, **51,** 5061.
[363] SUN, T., MORIN, B., GUO, H., and GRANT, M., 1992, Roughening transition of a driven interface with a conservation law, *Surface Disordering: Growth, Roughening and Phase Transitions*, edited by R. Jullien, J. Kertész, P. Meakin and D. E. Wolf (New York: Nova Science), p. 45.
[364] DAS SARMA, S., and KOTLYAR, R., 1994, Dynamical renormalization group analysis of fourth-order conserved growth nonlinearities, *Phys. Rev.* E, **50,** R4275.
[365] CHAKRABARTI, A., 1990, Computer simulation of stochastically growing interfaces with a conservation law, *J. Phys.* A, **23,** L919.
[366] TU, Y., 1992, Instability in a continuum kinetic-growth model with surface relaxation, *Phys. Rev.* A, **46,** R729.
[367] MOSER, K., 1993, Stochastische Differentialgleichungen für rauhe Oberflächen, Doctoral Thesis, University of Cologne.
[368] PUTKARADZE, V., BOHR, T., and KRUG, J., 1995, Global estimates for the solutions of the noiseless conserved Kardar–Parisi–Zhang equation, NBI preprint No. 95-04.
[369] KIM, J. M., and DAS SARMA, S., 1995, Dynamical universality of the nonlinear conserved current equation for growing interfaces, *Phys. Rev.* E, **51,** 1889.
[370] VAN HOVE, J. M., LENT, C. S., PUKITE, P. R., and COHEN, P. I., 1983, Damped oscillations in reflection high energy electron diffraction during GaAs MBE, *J. Vac. Sci. Technol.* B, **1,** 741.
[371] LARSEN, P. K., and DOBSON, P. J., (editors), 1988, *Reflection High-Energy Electron Diffraction and Reflection Imaging of Surfaces* (New York: Plenum).

[372] VLIEG, E., DENIER VAN DER GON, A. W., VAN DER VEEN, J. F., MACDONALD, J. E., and NORRIS, C., 1988, Surface X-ray scattering during crystal growth: Ge on Ge(111), *Phys. Rev. Lett.*, **61,** 2241.

[373] ERNST, H.-J., FABRE, F., and LAPUJOULADE, J., 1992, Growth of Cu on Cu(100), *Surf. Sci.*, **275,** L682.

[374] GRINSTEIN, G., MUKAMEL, D., SEIDIN, R., and BENNETT, C. H., 1993, Temporally periodic phases and kinetic roughening, *Phys. Rev. Lett.*, **70,** 3607.

[375] DOBBS, H. T., private communication.

[376] GILMER, G. H., 1978, Simulation of 2D nucleation and crystal growth, *Faraday Symp.*, **12,** 59.

[377] GILMER, G. H., 1980, Transients in the rate of crystal growth, *J. Cryst. Growth*, **49,** 465.

[378] BRENDEL, L., 1994, Fluktuationsschwächung in Wachstumsmodellen für Molekularstrahlepitaxie, Diploma Thesis, University of Duisburg.

[379] ŠMILAUER, P., and KOTRLA, M., 1994, Crossover effects in the Wolf–Villain model of epitaxial growth in 1 + 1 and 2 + 1 dimensions, *Phys. Rev.* B, **49,** 5769.

[380] PARK, K., KAHNG, B., and KIM, S. S., 1994, Surface dynamics of the Wolf–Villain model for epitaxial growth in 1 + 1 dimensions, *Physica* A, **210,** 146.

[381] SIEGERT, M., 1996, Determining exponents in models of kinetic surface roughening, *Phys. Rev.* E, **53,** 3209.

[382] PLISCHKE, M., SHORE, J. D., SCHROEDER, M., SIEGERT, M., and WOLF, D. E., 1993, Comment on 'Solid-on-solid rules and models for nonequilibrium growth in 2 + 1 dimensions', *Phys. Rev. Lett.*, **71,** 2509.

[383] ŠMILAUER, P., and KOTRLA, M., 1994, Kinetic roughening in growth models with diffusion in higher dimensions, *Europhys. Lett.*, **27,** 261.

[384] KOTRLA, M., LEVI, A. C., and ŠMILAUER, P., 1992, Roughness and nonlinearities in (2 + 1)-dimensional growth models with diffusion, *Europhys. Lett.*, **20,** 25.

[385] KRUG, J., 1995, Turbulence and generic scale invariance, *Modern Quantum Field Theory II*, edited by S. R. Das, G. Mandal, S. Mukhi and S. R. Wadia (Singapore: World Scientific), p. 141.

[386] SCHROEDER, M., 1993, Modelle mit Bezug zum epitaktischen Kristallwachstum, Diploma Thesis, University of Duisburg.

[387] DAS SARMA, S., and GHAISAS, S. V., 1993, Das Sarma and Ghaisas reply, *Phys. Rev. Lett.*, **71,** 2510.

[388] WILBY, M. R., VVEDENSKY, D. D., and ZANGWILL, A., 1993, Scaling in a solid-on-solid model of epitaxial growth, *Phys. Rev.* B, **46,** 12896; 1993, *Ibid.*, Erratum, **47,** 16068.

[389] NELKIN, M., 1974, Turbulence, critical fluctuations and intermittency, *Phys. Rev.* A, **9,** 388.

[390] BHATTACHARJEE, J. K., DAS SARMA, S., and KOTLYAR, R., 1996, Infrared singularities in interface growth models, *Phys. Rev.* E, **53,** R1313.

[391] WEBER, W., and LENGELER, B., 1992, Diffuse scattering of hard X-rays from rough surfaces, *Phys. Rev.* B, **46,** 7953.

[392] SALDITT, T., METZGER, T. H., PEISL, J., REINKER, B., MOSKE, M., and SAMWER, K., 1995, Determination of the height–height correlation function of rough surfaces from diffuse X-ray scattering, *Europhys. Lett.*, **32,** 331.

[393] SALDITT, T., METZGER, T. H., BRANDT, CH., KLEMRADT, U., and PEISL, J., 1995, Determination of the static scaling exponent of self-affine interfaces by nonspecular X-ray scattering, *Phys. Rev.* B, **51,** 5617.

[394] MILLER, D. J., GRAY, K. E., KAMPWIRTH, R. T., and MURDUCK, J. M., 1992, Studies of growth instabilities and roughening in sputtered NbN films using a multilayer decoration technique, *Europhys. Lett.*, **19,** 27.

[395] SALDITT, T., METZGER, T. H., and PEISL, J., 1994, Kinetic roughness of amorphous multilayers studied by diffuse X-ray scattering, *Phys. Rev. Lett.*, **73,** 2228.

[396] CHIARELLO, R., PANELLA, V., KRIM, J., and THOMPSON, C., 1991, X-ray reflectivity and adsorption isotherm study of fractal scaling in vapor-deposited films, *Phys. Rev. Lett.*, **67,** 3408.

[397] GIESEN-SEIBERT, M., JENTJENS, R., POENSGEN, M., and IBACH, H., 1993, Time dependence of step fluctuations on vicinal Cu(119) surfaces investigated by tunneling microscopy, *Phys. Rev. Lett.*, **71,** 3521.

[398] BARTELT, N. C., GOLDBERG, J. L., EINSTEIN, T. L., and WILLIAMS, E. D., 1993, Brownian motion of steps on Si(111), *Phys. Rev.* B, **48,** 15453.

[399] CUERNO, R., and BARABÁSI, A.-L., 1995, Dynamic scaling of ion sputtered surfaces, *Phys. Rev. Lett.*, **74,** 4746.

[400] EKLUND, E. A., SNYDER, E. J., and WILLIAMS, R. S., 1993, Correlation from randomness: quantitative analysis of ion etched graphite surfaces using the scanning tunneling microscope, *Surf. Sci.*, **285,** 157.

[401] EAGLESHAM, D. J., 1995, Semiconductor molecular-beam epitaxy at low temperatures, *J. appl. Phys.*, **77,** 3597.

[402] YANG, H.-N., and LU, T.-M., 1995, Inconsistency between height-height correlation and power-spectrum functions of scale invariant surfaces for roughness exponent $\alpha \sim 1$, *Phys. Rev.* B, **51,** 2479.

[403] ZENG, H., and VIDALI, G., 1995, Measurement of growth kinetics in a heteroepitaxial system: Pb on Cu(100), *Phys. Rev. Lett.*, **74,** 582.

[404] SUDIJONO, J., JOHNSON, M. D., SNYDER, C. W., ELOWITZ, M. B., and ORR, B. G., 1992, Surface evolution during molecular-beam-epitaxy deposition of GaAs, *Phys. Rev. Lett.*, **69,** 2811.

[405] JOHNSON, M. D., SUDIJONO, J., HUNT, A. W., and ORR, B. G., 1993, The dynamical transition to step-flow growth during molecular-beam epitaxy of GaAs(001), *Surf. Sci.*, **298,** 392.

[406] HE, Y.-L., YANG, H.-N., LU, T.-M., and WANG, G.-C., 1992, Measurement of dynamic scaling from epitaxial growth front: Fe film on Fe(001), *Phys. Rev. Lett.*, **69,** 3770.

[407] ZANGWILL, A., private communication.

[408] YANG, H.-N., WANG, G.-C., and LU, T.-M., 1995, Formation of facets and pyramidlike structures in molecular-beam-epitaxy growth of Si on a singular Si(111) surface, *Phys. Rev.* B, **51,** 14293.

[409] THOMPSON, C., PALASANTZAS, G., FENG, Y. P., SINHA, S. K., and KRIM, J., 1994, X-ray reflectivity study of the growth kinetics of vapor-deposited silver films, *Phys. Rev.* B, **49,** 4902.

[410] PALASANTZAS, G., and KRIM, J., 1994, Scanning tunneling microscopy study of the thick film limit of kinetic roughening, *Phys. Rev. Lett.*, **73,** 3564.

[411] PALASANTZAS, G., 1994, Finite-size effects on self-affine fractal surfaces due to domains, *Phys. Rev.* B, **49,** 10544.

[412] CHEVRIER, J., CRUZ, A., PINTO, N., BERBEZIER, I., and DERRIEN, J., 1994, Influence of kinetic roughening on the epitaxial growth of silicon, *J. Phys. (France)* I, **4,** 1309.

[413] EAGLESHAM, D. J., GOSSMANN, H.-J., and CERULLO, M., 1990, Limiting thickness h_{epi} for epitaxial growth and room-temperature Si growth on Si(100), *Phys. Rev. Lett.*, **65,** 1227.

[414] ADAMS, D. P., YALISOVE, S. M., and EAGLESHAM, D. J., 1993, Effect of hydrogen on surface roughening during Si homoepitaxial growth, *Appl. Phys. Lett.*, **63,** 3571.

[415] CABRERA, N., and VERMILYEA, D. A., 1958, The growth of crystals from solution, *Growth and Perfection of Crystals*, edited by R. Doremus, B. Roberts and D. Turnbull (New York: Wiley), p. 393.

[416] V.D. EERDEN, J. P., and MÜLLER-KRUMBHAAR, H., 1986, Dynamic coarsening of crystal surfaces by formation of macrosteps, *Phys. Rev. Lett.*, **57,** 2431.

[417] KANDEL, D., and WEEKS, J. D., 1994, Theory of impurity-induced step bunching, *Phys. Rev.* B, **49,** 5554.

[418] FANG, K., LU, T.-M., and WANG, G.-C., 1994, Roughening and faceting in a Pb thin film growing on the Pb(110) surface, *Phys. Rev.* B, **49,** 8331.

[419] LE BELLAC, D., NIKLASSON, G. A., and GRANQVIST, C. G., 1995, Scaling of surface roughness in obliquely sputtered chromium films, *Europhys. Lett.*, **32,** 155.